Syntheses, Characterization, and Stimuli-Responsive Luminescence Behaviors of Ternary Lanthanide(III) Tris-(β-diketonate) Complexes Based on Terpyridyl-Imidazole Ligands

A Thesis

Submitted for the Degree of

Doctor of Philosophy (Science)

of

Jadavpur University

by

Toushique Ahmed

DEPARTMENT OF CHEMISTRY

JADAVPUR UNIVERSITY

JADAVPUR, KOLKATA-700032

INDIA

2025

যাদবপুর বিশ্ববিদ্যালয়
কলকাতা-৭০০০৩২, ভারত

*JADAVPUR UNIVERSITY
KOLKATA-700 032, INDIA

FACULTY OF SCIENCE: DEPARTMENT OF CHEMISTRY : INORGANIC CHEMISTRY SECTION

CERTIFICATE FROM THE SUPERVISOR

This is to certify that the thesis entitled **"Syntheses, Characterization, and Stimuli-Responsive Luminescence Behaviors of Ternary Lanthanide(III) Tris-(β-diketonate) Complexes Based on Terpyridyl-Imidazole Ligands"** Submitted by Sri **Toushique Ahmed** who got his name registered on **25.09.2019** for the award of Ph. D. (Science) Degree of Jadavpur University, is absolutely based upon his own work under the supervision of **Prof. Sujoy Baitalik** and that neither this thesis nor any part of it has been submitted for either any degree /diploma or any other academic award anywhere before.

Sujoy Baitalik 11/09/2025

(Signature of the Supervisor with date and official seal)

Professor Sujoy Baitalik
Department of Chemistry
Jadavpur University
Kolkata- 700 032, India

দূরভাষ: ২৪১৪-৬৬৬৬/৬১৯৪/৬৬৪৩/৬৪৯৫/৬৪৪৩ প্রসারণ: ২৪৬৯ Website:www.jadavpur.edu Phone:2414-6666/6194/6643/6495/6443 Extn.2469
দূরবার্তা: (৯১)-০৩৩-২৪১৪-৬৪১৪/৬২১০/২৪১৩-৭১২১ E-mail : hod@chemistry.jdvu.ac.in Fax: (91)-033-2414-6414/6210/2413-7121

Dedicated

to

My Family

& Well-wishers

"Don't read success stories, you will only get a message. Read failure stories, you will get some ideas to achieve success"

…Dr. APJ Abdul Kalam

PREFACE

The work encompassed in the thesis entitled "Syntheses, Characterization, and Stimuli-Responsive Luminescence Behaviors of Ternary Lanthanide(III) Tris-(β-diketonate) Complexes Based on Terpyridyl-Imidazole Ligands" has been carried out in the Department of Chemistry of Jadavpur University during the period between 2019 and 2025. The thesis is comprised of six chapters.

Chapter 1 describes a brief review on the design and syntheses of various lanthanide(III) complexes and their photophysical behaviors in general and luminescence characteristics in particular. Special attention has been paid on the design and syntheses of ternary lanthanide(III) tris-(β-diketonate) complexes and their stimuli-responsive luminescence behaviors. Finally, the objective and scope of this thesis have been demonstrated at the end of the chapter.

Chapter 2 comprises the design of four ternary lanthanide tris-(β-diketonate) complexes of the form, [Ln(tta)$_3$(tpy-HImzphen)], where Ln=La, Eu, Sm, Tb, and their thorough characterization by standard analytical tools and spectroscopic techniques, including single-crystal X-ray diffraction analysis. The photophysical behaviors of all the complexes were thoroughly investigated via absorption and both steady-state and time-resolved emission spectroscopic techniques. The introduction of the terpyridyl-based ancillary ligand into the Ln(tta)$_3$ moieties led us to observe four distinctive luminescence responses, when inspected at both room temperature and 77 K. Finally, attempts have also been made to decipher the role of the said ligand on the photophysical, and in particular on the luminescence characteristics of the complexes.

Chapter 3 deals with detailed thermosensing and thermochromic behaviors of the [Eu(tta)$_3$(tpy-HImzphen)] complex as presented in chapter 2. The complex acts as an excellent thermosensor in terms of both luminescence intensity ratio and lifetime values within the temperature range of 273-343 K. The dual emissive nature of the complex led to remarkable thermochromism (red at 268 K, violet at 303 K, and blue at 343 K). Additionally, various emitting colors, apart from its characteristic red emission, were

observed from the said complex upon varying the nature of the solvents. Finally, amalgamating the thermochromic and solvatochromic features of the complex, single-component white light emission was achieved at 283 K. At the end, a plausible energy transfer mechanism has been proposed, counting on the role of low-lying ligand-to-metal charge transfer (LMCT) state as the quencher of the Eu^{III}-centered emission.

Chapter 4 comprises of syntheses, characterization and thorough investigation of the photophysical properties of a new array of ternary Ln^{III} complexes of the type $[Ln(hfa)_3(tpy\text{-}HImzphen)]$, where Ln=La, Eu, Sm, Tb. Incorporation of tpy-HImzphen ligand onto the Ln-hfa moiety results in a bathochromic shift of the absorption spectral window of the complexes into the visible region. Detailed steady-state and time-resolved emission spectroscopic measurements at both RT and 77K indicate four distinctive behaviors viz. huge red-shift of the ligand-centered peak for La^{III}; almost complete energy transfer for Eu^{III}; very little energy transfer for Sm^{III}, and reverse energy transfer in case of Tb^{III}. The Eu^{III}-complex exhibits excellent thermosensing behavior in solution as well as when doped in poly(methyl methacrylate) (PMMA) matrix. The thermosensitive luminescence response in solution was further utilized to mimic Set-Reset Flip-flop Boolean logic operation.

Syntheses and characterization of a new array of four homobimetallic Ln^{III}-complexes (where Ln=La, Eu, Sm, Tb) derived from 2-thenoyltrifluoroacetonate (tta) as antenna and a heteroditopic terpyridine-phenanthroline (phen-Hbzim-tpy) type bridging ligand, are reported in **Chapter 5**. Room temperature photophysical properties and temperature-dependent luminescence spectral behaviors of the complexes together with phen-Hbzim-tpy ligand, have been thoroughly investigated. The phen-Hbzim-tpy ligand is found to be thermally activated delayed fluorescence (TADF)-active. All the four complexes act as efficient thermosensors via their luminescence thermometric attributes. The La-complex could not sustain the TADF phenomenon, whereas the rest of the complexes displayed remarkable thermochromism via coupling of this TADF and their respective dual-emissive characteristics. Attempts have also been made to comprehend the synergy among the lowest triplet states of both the ligands and the lowest emissive states of the corresponding Ln^{III} ions, which is believed to be responsible for the observed

photophysical and temperature-dependent luminescence spectral behaviors of the complexes.

Chapter 6 encompasses the design of an analogous series of ternary homobimetallic Ln^{III} complexes replacing tta with hexafluoroacetylacetonate (hfa). After the successful characterization of the complexes, detailed photophysical properties were explored. Substantial improvements in the absorption, emission quantum yield, lifetime, and sensitization efficiency were noticed upon the replacement of the antenna ligand. In fact, unlike the previous case, all four complexes were found to display the TADF behavior, exploiting which excellent thermosensing and thermochromic properties were observed. Apart from this TADF-assisted thermochromism, the luminescence spectral characteristics of the complexes were found to be well-dependent on solvent polarity and excitation wavelength. Finally, tuning of emitting colors across the entire VIBGYOR region, as well as room temperature single-component white light emission, was achieved upon the appropriate exercise of the said three stimuli on the complexes.

ACKNOWLEDGEMENTS

I want to acknowledge those people who played direct or indirect roles toward the successful completion of my thesis.

First and foremost, I would like to express my sincere gratitude to my supervisor, Professor Sujoy Baitalik, without whom this journey would have been impossible. I greatly benefited from his experience and resourceful insight during the critical times. His hard work and dedication toward research would inspire me a lot. His guidance is an unforgettable and lifelong lesson for me.

I am very much thankful to the Department of Chemistry of Jadavpur University for providing me with all sorts of facilities needed to carry out my research work. I would like to thank the present Dean, Faculty Council of Science, Prof. Mahammad Ali, and the Head of the department, Prof. Kajal Krishna Rajak, and the Section-in-charge, Prof. Partha Roy for providing the departmental and laboratory facilities. I also extend my heartfelt gratitude to all the faculty members and non-teaching staffs of this department for their help and cooperative attitudes.

I would especially like to acknowledge Dr. Bibhuti Bhusan Show, Prof. Chittaranjan Sinha, Prof. Subrata Mukhopadhayay, Prof. Jnan Prakash Naskar, Prof. Mahammad Ali, Dr. Tapan Kumar Mondal for their kind cooperation and constant encouragement throughout my journey of research. I would also convey my gratitude to Dr. Papu Biswas from IIEST, Shibpur for serving as the 'Subject Expert' of my Research Advisory Committee (RAC).

I am grateful to CSIR for awarding me JRF and SRF fellowships for five years to carry out my research work smoothly.

I would like to acknowledge DST for providing the Time-Resolved Nanosecond Spectrofluorimeter in PURSE programme to the Department of Chemistry, Jadavpur University.

I also want to express my heartfelt regards and a lot of thanks to my former lab-mates Dr. Manoranjan Bar, Dr. Poulami Pal, Dr. Animesh Paul, Dr. Shruti Mukherjee, Dr. Amit Chakraborty, Dr. Papri Mondal, Dr. Anik Sahoo, and Dr. Tanusree Ganguly for

their continuous help and support. The passionate and helping attitudes from my present lab-mates Soumi Das, Sohini Bhattacharya, Raju Biswas, and Tuhin Abedin, deserve my heartfelt gratitude. All the moments we spent together both inside and outside of the laboratory became a memory to cherish for the rest of my life. I find myself fortunate enough to get an opportunity to work with this friendly research group.

This journey would have been incomplete without the unconditional love, unwavering support, and endless encouragement from my family members, who always kept me in their prayers and were a part of this journey alongside me in every way. I am really blessed to have such a wonderful and supportive family.

I must acknowledge all of those friends and well-wishers who never refrained from offering me mental and research support in various crises throughout these years. I would especially like to convey my heartfelt gratitude to Angshuman (JNCASR, Bengaluru), Atin (IISER Kolkata), Suvendu (IACS, Kolkata), Subhojit (IACS, Kolkata), Riaz da (JU), Nahid (IISER Pune), Satyajit (CU, Kolkata), Anik (CSMCRI, Bhavnagar), Shalini (IIT Bombay), Diptam (IACS, Kolkata), Dimitra di (JU), and Moishilee di (JU). I am also indebted to Sudip (TIFR Hyderabad), Indranil (CU, Kolkata), and Debolina (CU, Kolkata) for always standing by me. Now I am expressing my sincere apology since I have failed to mention everyone personally.

And last but not least, I would like to thank the Almighty for his blessing throughout this entire journey.

Toushique Ahmed 11/09/'25

(Toushique Ahmed)
Department of Chemistry
Inorganic Chemistry Section
Jadavpur University
Kolkata-700032, India

CONTENTS

List of Publications

Chapter 1

General Introduction and Brief Review on Luminescent Lanthanide(III) Tris-(β-Diketonate) Complexes and Objective and Scope of the Present Work

1.1. General Introduction

The appropriate design of various coordination complexes comprising of trivalent lanthanide ions (Ln^{III}) has always been a matter of interest for chemists due to their fascinating optical and magnetic properties.[1-9] Both of these properties come from the f-electrons present in the Ln^{III} ions. The optical properties in general and the luminescence properties in particular in the lanthanide complex are generated from the electronic transitions within their f-shells, called intra-configurational f-f transitions. It is well-known that the f-electrons are effectively shielded by the $5s^2$ and $5p^6$ subshells. This shielding leaves barely a chance for the coordinated ligand to perturb the electronic configuration of the Ln^{III} ion. That is why each Ln^{III} ion offers some unique, environment-independent, and well-defined luminescence attributes from their resulting complexes, viz. characteristic atom-like sharp emission and long excited-state lifetime. These distinctive luminescence features paved the way for Ln^{III} complexes to be suitable in a wide range of applications like magnetic resonance imaging (MRI), light harvesting materials, sensors for temperature, pressure, pH, or any analyte and biomedical assays.[10-23]

Despite having such intriguing luminescence attributes, unfortunately, the f-f intra-configurational transitions in the Ln^{III} ions are both spin and parity-forbidden, resulting in very low absorption coefficients (<10 M^{-1} cm^{-1}), which in turn yields very weak luminescence upon direct Ln^{III} excitation. To bypass this hurdle, high light-absorbing organic chromophores (>10,000 M^{-1} cm^{-1}) are coordinated with the Ln^{III} ion. The chelating ligand absorbs the energy and transfers it to the coordinated Ln^{III} ion, resulting in enhanced luminescence. This indirect sensitization is referred to as the 'antenna effect' (Figure 1.1).[1-9]

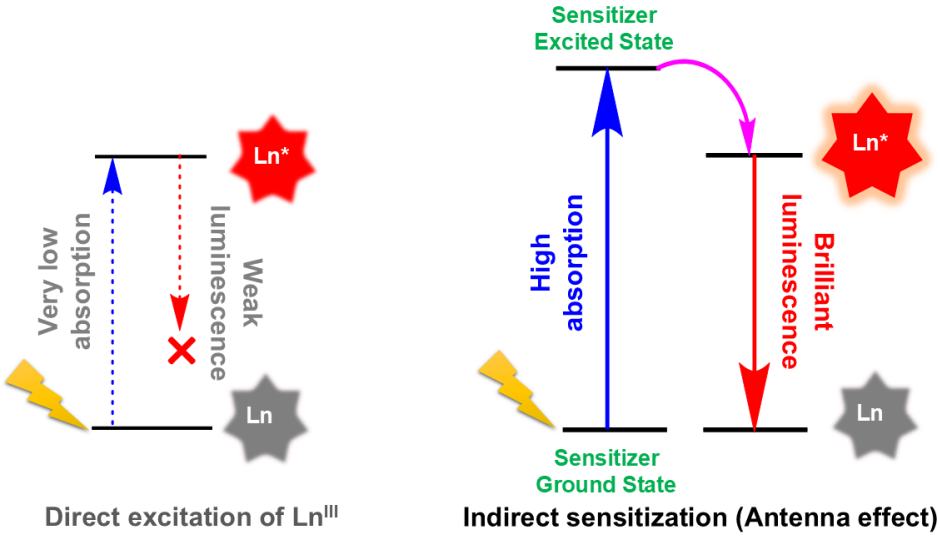

Figure 1.1. Indirect sensitization of Ln^{III} ions (Antenna effect).

Accordingly, substantial attention has already been paid for the design and syntheses of various antenna ligands, e.g., N- or O-containing chelating ligands, cryptates, polyaminocarboxylates, cyclams, podands, as well as β-diketonates.[24-41] From the literature survey, it appears that most of the earlier reports regarding Ln^{III} luminescence are mainly comprised of macrocycles, helicates, supramolecules, coordination polymers, metal-organic frameworks (Ln-MOFs), etc. By contrast, Ln^{III}-based discrete luminescent complexes are relatively less explored. Among the pyridine-based ligands, 2,2'-bipyridine (bpy) and 1,10-phenanthroline (phen) have been frequently employed for sensitization of the Ln^{III} ion. By contrast, the 2,2':6',2''–terpyridine (tpy) type ligands have been less explored in spite of their favourable structural attributes. In the present dissertation, we have employed terpyridine coordination motifs covalently connected with other aromatic as well as hetero-aromatic moieties for effective sensitization of lanthanide ions. We have employed the terpyridine ligands for the synthesis of wide variety of monometallic as well as bimetallic complexes using different trivalent lanthanide ions. Following synthesis, all the complexes have been thoroughly characterized by standard analytical tools and spectroscopic techniques including single crystallography for representative complexes. The photophysical properties of the complexes have been studied in detail using absorption and both steady state and time-resolved emission spectroscopic techniques. In conjunction with experimental demonstration, theoretical calculations employing density functional theory (DFT) and time-dependent density functional theory (TD-DFT) were executed to visualize the electronic structure of representative ligand for the appropriate assignment of the spectral bands.

The photophysical properties of the lanthanide complexes could also be altered in the presence of various external stimuli, viz. excitation wavelength, solvent, temperature, pressure, pH, to name a few.[22,42-48] The stimuli-responsive behaviors have been examined in detail via multiple optical channels and spectroscopic techniques. The stimuli-responsive luminescence spectral response was utilized to generate various color emitting materials which could be potential building blocks for the display devices. Some of the designed complexes also function as efficient sensors of temperature, which in turn could be employed in molecular luminescence thermometry. Additionally, the Ln^{III}-based discrete complexes are doped in polymer matrices to extricate their stimuli-responsive luminescence attributes for real practical applications.

1.2. Background Information about Lanthanide (III) Luminescence

In 1942, Weismann first observed the lanthanide(III) complexes (Eu, Sm, and Tb) display luminescence via absorption of light by another constituent within the complex framework.[49] This observation laid the foundation of 'antenna effect' offered by the 'other constituent' for a fruitful Ln^{III} sensitization. In 1964, Melby et al. synthesized various Ln^{III} complexes, where they also observed that light absorption takes place by the organic constituent and subsequent energy transfer takes place to the coordinated Ln^{III} ion.[50] Nevertheless, this indirect photosensitization of Ln^{III} ions or the antenna effect phenomenon needed some time to be able to draw the attention of the concerned community. Since the late 1970s, the world has finally become familiar with this indirect Ln^{III} sensitization via the antenna effect of the coordinated ligands. Since then, numerous dedicated efforts have been made to date to design various antenna ligands.

1.3. Overview of Lanthanide (III) Photophysics

The word 'lanthanides', which encompasses lanthanum ($_{57}La$) and 14 subsequent elements altogether, originally came from the Greek word 'lanthaneien', which means 'lying hidden'. All of the lanthanides possess very similar chemical properties owing to their common +3 oxidation state. However, considerable differences take place in displaying their luminescence features. Except for the La^{III} and Lu^{III}, all of the lanthanides have their own characteristic emissive signatures, viz. Ce^{III} and Gd^{III} emit in the ultraviolet region; Sm^{III} (emits orange color), Eu^{III} (red), Tb^{III} (green), Dy^{III} (orange), and Tm^{III} (blue) emit in the visible domain. On the other hand, Nd^{III}, Er^{III}, and Yb^{III} display emission in the NIR region. Some of less discussed Ln^{III} ions like Pr^{III} and Ho^{III} also have their characteristic emission in this NIR domain. Design and synthesis of various antenna molecules started in the late 1970s by different researchers across the globe. Latva et al first noticed in 1997 that all the coordinated organic constituents cannot yield an effective Ln^{III} sensitization. Rather, it very much depends on the energy gap between the excited state of the organic chromophore attached to a Ln^{III} ion and the emissive state of that particular Ln^{III} ion.[51] This observation further led to a deeper insight into the intramolecular or intercomponent energy transfer mechanism for the luminescent Ln^{III} complexes. But the most well-accepted mechanism was proposed by Whan and Crosby.[52] They proposed that the sensitization process involves three consecutive steps, viz. (i) spin and parity (Laporte)-allowed light absorption by the organic chromophoric ligand with high molar absorption coefficient (ε>10000 M^{-1} cm^{-1}) and excitation to its first singlet excited state ($S_0 \rightarrow S_1$), followed by (ii) rapid intersystem crossing

(ISC) to the first triplet excited state ($S_1 \rightarrow T_1$) of the ligand and finally, (iii) transferring the absorbed energy to the lowest emissive state of the central Ln^{III} ion ($T_1 \rightarrow Ln^*$). The singlet state lifetime is too short for this indirect lanthanide sensitization, although a few such instances are also reported.[53-56]

Some empirical rules are evolved thereafter and found to be quite useful in elucidating the quantitative aspect for the occurrence of the energy transfer process. The first one is the Reinhoudt's rule, which indicates that the required energy gap between the S_1 and T_1 ($\Delta E_{S1\text{-}T1}$) of a ligand should be >5000 cm^{-1} for the ISC process to be operative.[57] Secondly, for effective execution of the antenna effect via the 'Dexter exchange' pathway,[58] it is postulated that the ligand T_1 should be at least ~2500-4000 cm^{-1} higher than the position of Ln*.[59] It is to be noted that following the rules of Latva et al, if the value of $\Delta E_{S1\text{-}T1}$ becomes <1800 cm^{-1}, reverse or back energy transfer takes place from Ln* to ligand T_1 instead of an effective Ln^{III} sensitization.[51,60-63] The emitting excited states (Ln*) of all the trivalent lanthanide ions (except La^{III} and Lu^{III}, as they are not subjected to such f-f transitions) are well-defined, and their values are independent of the chelating ligand or surrounding environment. For example, the values of the lowest emissive states (Ln*) for Eu^{III} ($^5D_0$), Sm^{III} ($^4G_{5/2}$), and Tb^{III} ($^5D_4$) have already been estimated to be ~17300, ~17900, and ~20500 cm^{-1}, respectively.[64-66] The energy of the S_1 state of the ligand could be estimated from the onset of its absorption spectral profile.[67-69] The strategy to estimate the energy of the T_1 state of the ligand is quite interesting. The ligand is first allowed to coordinate with Gd^{III} salt, and the resulting complex is then subjected to emit at liquid nitrogen temperature (77K). It is to be noted that the excited state energy of Gd^{III} resides at ~32750 cm^{-1}, while the value of the T_1 states of the common antenna ligands usually lie within the range of ~20000-25000 cm^{-1}. Hence, the ligands are unable to sensitize Gd^{III}; rather, the only option left for it is to get deactivated from its T_1 state. The observed emission maxima indicate the transition from the lowest triplet state of the ligand (T_1).[67-73] Hence, all the above-mentioned criteria should be borne in mind while designing suitable antenna ligands for the synthesis of highly luminescent Ln^{III} complexes (Figure 1.2).

1.4. Developments in the Design of Antenna Ligands: Binary Ln^{III} Complexes

Regarding the Ln^{III}-sensitization, it appears that oxygen donor containing negatively charged chelating ligands, viz. acyclic or macrocyclic ligands, were primarily employed for

this purpose. The acyclic ligands incorporate anions like carboxylates, naphthalates, aminophosphonates, acetonates, phosphinates, polyaminocarboxylates, to name a few.[24-32,74-83] On the other hand, the cyclic ligands encompass cyclens, diazapolyoxabicyclic ligands, cryptands, azocycloalkanes, podands, helicates, etc.[33-41,84-100] The main motive of choosing such design protocol was to protect the Ln^{III} ion from being coordinated to solvent or water molecules, which could affect the desired luminescence properties of the Ln^{III} complexes. These resulting Ln^{III} complexes were water soluble, thereby immediately drew attention to various bio-applications.

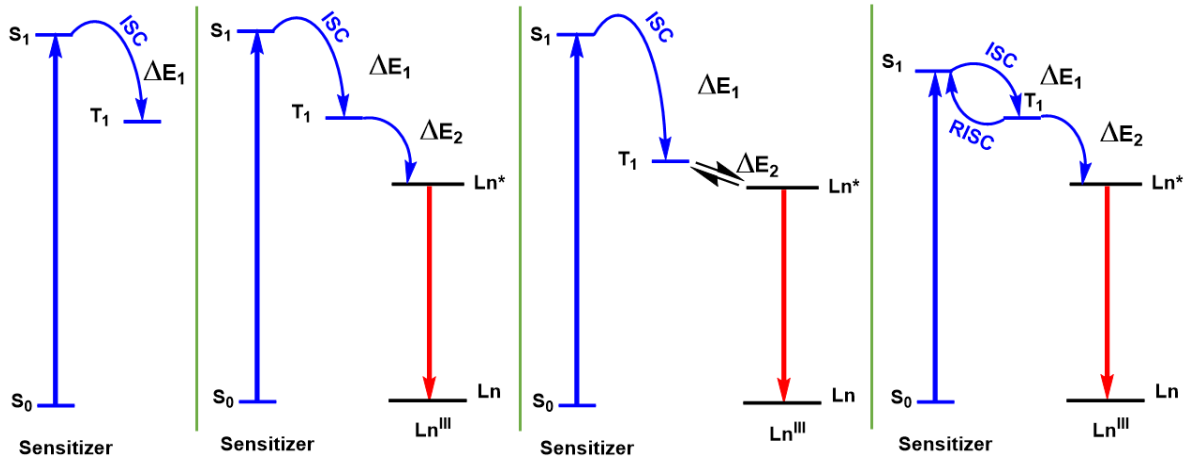

Figure 1.2. Possible energy transfer pathways within a sensitizer and its coordinated Ln^{III} ion.

1.5. Ln-tris(β-diketonate) Complexes: the 'rose with thorns'

An already reported class of sensitizers suddenly gained attention at ~2000, with a new spirit and immediately became one of the most explored domains regarding lanthanide sensitization. Within a very short span of time, various groups across the globe were actively engaged in the design and thoroughly investigate the photophysical behaviors of a specific class of complexes, lanthanide(III) tris-β-diketonate assembly. The simplest β-diketonate is acetylacetonate (acac). Eventually, it was found that replacing the high-energy oscillating C-H bonds with more rigid and low-vibrating C-F bonds results in the prevention of energy dissipation, and at the same time, it can lower the triplet energy level of the corresponding β-diketonate. Because of the cumulative effect of these two factors, the extent of energy transfer from the β-diketonate to the coordinated lanthanide(III) ion gets significantly improved.[61] Since then, various tailoring agendas on the structure of β-diketonate have been

taken to improve their sensitizing ability.[70,101-109] Consequently, numerous β-diketonate molecules were found to be designed and explored with regard to lanthanide(III) luminescence e.g., trifluoroacetylacetonate (tfaa), hexafluoroacetylacetonate (hfa), benzoyltrifluoroacetonate (btfa), dibenzoylmethane (dbm), 2-thenoyltrifluoroacetylacetonate (tta), trifluorofurylacetonate (tfa), etc (Figure 1.3). Singh and colleagues have accumulated this diversity very explicitly in one of their review articles.[110]

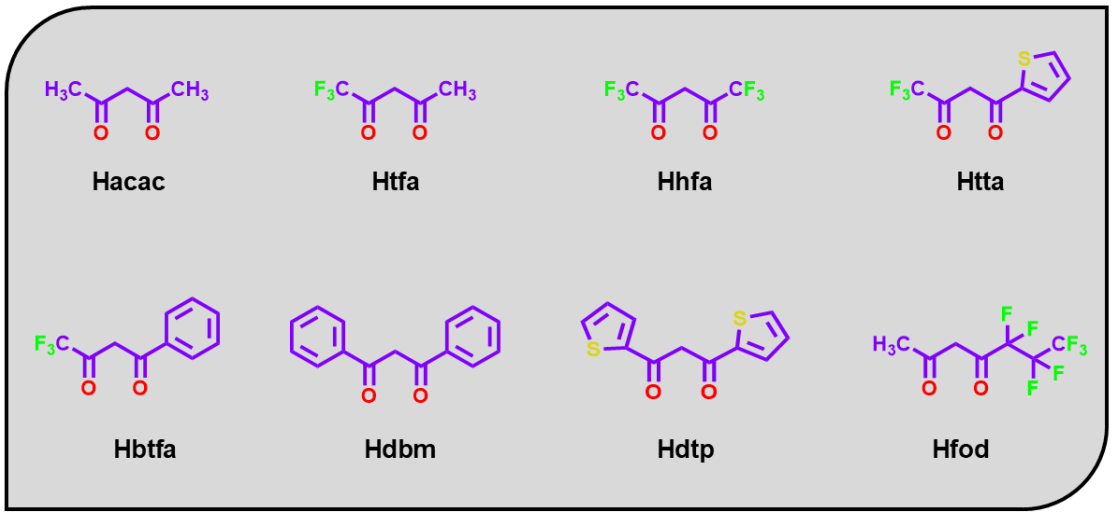

Figure 1.3. Chemical structures of some common β-diketonate ligands.

But, even after the substitutions with CF_3- moiety or aryl groups in the β-diketonate ligand framework, the maximum desired sensitized luminescence from Ln^{III} ions was still to be achieved. It is because the Ln^{III} ions can't help coordinate the water or solvent molecules to fulfill their high coordination number. As a result, a considerable portion of the transferred energy is utilized to vibrate the high-energy oscillators like the O-H bond, which in turn induces a detrimental impact on the radiative deactivation. Hence, it needed further development. To circumvent this problem, neutral and high-energy-absorbing chromophores were brought into play. This incoming ligand, mostly comprised of O- or N-containing polyaromatic motifs, was termed an ancillary ligand. The ancillary ligand is supposed to replace the already coordinated water or solvent molecules, resulting in improved luminescence characteristics in terms of quantum yield or lifetime. This new assembly was referred to as the ternary lanthanide tris-β-diketonate complex.

It is noteworthy to mention that the ancillary ligands could also directly coordinate with the Ln^{III} ions, forming a binary assembly that can also exhibit fluorescence. However, the resulting complexes counter an unwanted problem of solubility. This very problem is also

noticed to be resolved in the ternary complexes, which offer excellent solubility in solvents with a wide range of polarity.

1.6. Introduction of the Ancillary Ligands

As soon as the motivation for designing ternary assemblies was established, various groups across the globe devoted their research interests to designing different types of ternary mononuclear as well as dinuclear complexes comprising diverse ancillary ligands. The ancillary ligands employed for this purpose mainly encompass N-, O-, or both N, O-containing polyaromatic and heterocyclic organic moieties that can bind in mono-, bi-, or tridentate fashion (Figure 1.4). It is noteworthy to mention that the incoming ancillary ligands may assist in improving the photophysical characteristics not only via replacing the quencher molecules coordinated with the corresponding Ln^{III} ions but also by serving as another sensitizer or second antenna molecules for the Ln^{III} ions of the ternary assembly.

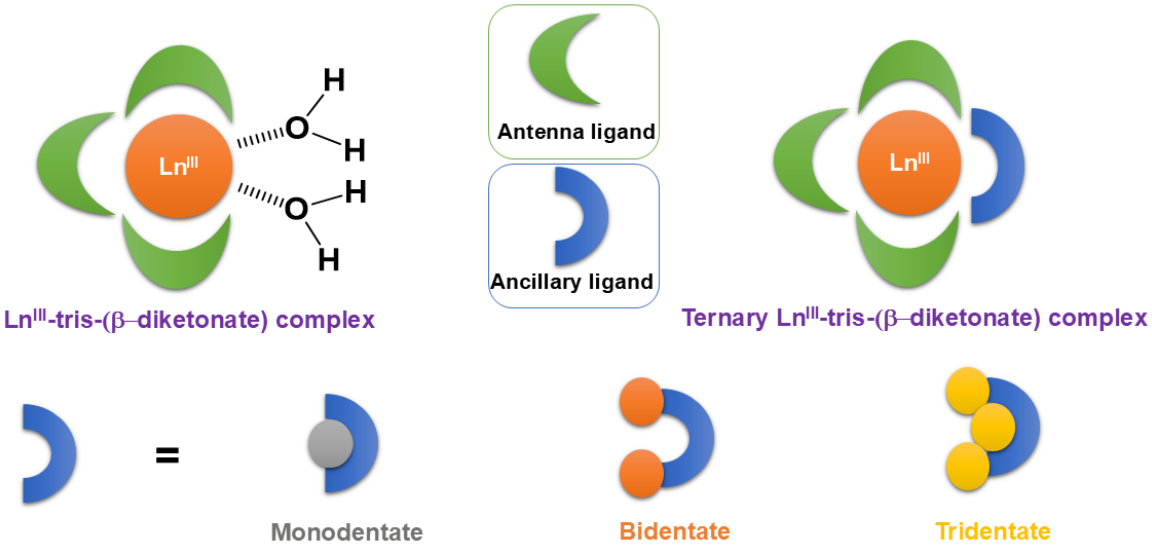

Figure 1.4. Schematic representation of Ln^{III} tris-(β-diketonate) complex and its ternary Ln^{III} tris-(β-diketonate) complex comprising mono-, bi-, and tridentate ligands.

1.6.1. Monodentate Ancillary Ligand

Iftikhar and coworkers synthesized a series of ternary Ln^{III}-complexes comprising of La^{III}, Sm^{III}, Eu^{III}, and Tb^{III} ions and upon employing hexafluoroacetylacetonate (hfa) as an antenna ligand as well as pyrazole as the ancillary ligand (Scheme 1.1).[111,112] From the single

crystal structures, it was observed that the Ln^{III} ions are surrounded by two pyrazole ligands and three hfa ligands, making them eight-coordinate complexes.

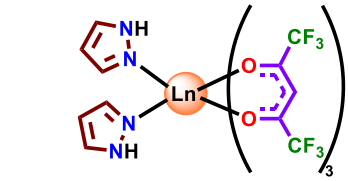

$Ln(hfa)_3(Pyrazole)_2$; Ln= La, Eu, Sm, Tb

Scheme 1.1

In another set of works, they introduced indazole as the ancillary ligand (Scheme 1.2).[113-115] The crystal structures of the resulting complexes showed that the La, Sm, and Eu complexes are nine-coordinate owing to the incorporation of three indazole ligands. On the other hand, probably due to the size factor, the Tb-ion accommodates only two indazole units, forming an eight-coordinate assembly.

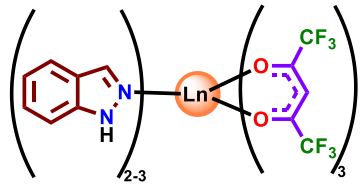

$Ln(hfa)_3(Indazole)_{2\text{-}3}$; Ln= La, Eu, Sm, Tb

Scheme 1.2

Hasegawa et al. designed a number of eight-coordinated Eu-tris-hfa complexes by utilizing triphenylphosphine oxide (TPPO) itself and its methyl, trimethyl, and phenoxy derivatives as the ancillary ligands (Scheme 1.3). They found that the complex with the phenoxy-derived ligand offered the highest quantum yield than the others. This was attributed to effect of the reduction of geometrical symmetry around the Eu^{III} ion in the said complex.[116]

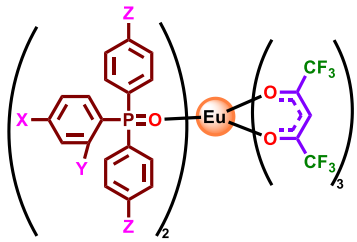

X, Y, Z = H $Eu(hfa)_3(TPPO)_2$
X = CH_3, Y, Z = H $Eu(hfa)_3(TPPO\text{-}Me)_2$
X, Z = CH_3, Y = H $Eu(hfa)_3(TPPO\text{-}3Me)_2$
X, Z = H, Y= 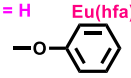 $Eu(hfa)_3(TPPO\text{-}OPh)_2$

Scheme 1.3

In another set of work, they introduced chrysene in the phosphine oxide ligand (DPCO) (Scheme 1.4). This said ligand was found to participate in the ligand-to-metal-charge-transfer (LMCT) process via the luminescence quenching in the resulting Eu-complex upon elevation of temperature.[117]

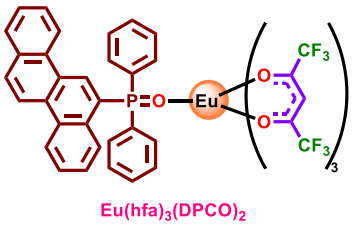

$Eu(hfa)_3(DPCO)_2$

Scheme 1.4

The said group also designed a series of Tb-complexes based on substituted phosphine oxide ligands (Scheme 1.5). They executed temperature dependent emission spectral measurements. The outcomes of the measurements indicate that the complexes exhibit thermally assisted back energy transfer to ligands. It is to noted that this is the first report wherein the Tb-hfa complex exhibits thermosensing behaviors via ligand-assisted back energy transfer process.[118]

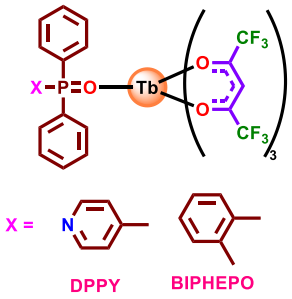

Scheme 1.5

Labella et al. utilized 4,4'-bipyridine N-oxide (bipyMO) and pyrazine N-oxide (pyrzMO) as the monodentate ancillary ligands to synthesize two series of Eu-complexes together with tta, dbm, btfa, and hfa as the antenna ligands and thoroughly investigated their photophysical properties (Scheme 1.6). The results of the experiments indicated that the pyrzMO-based complexes exhibit a higher extent of non-radiative deactivation than that of the bipyMO-based complexes. They also explored the temperature-dependent luminescence spectral behaviors of the complexes. The outcomes of the experiments suggest that both back energy transfer from Eu^{III} to the antenna, as well as the involvement of LMCT, are operative

in case of the tta and dbm series. On the other hand, only the LMCT factor is active for the btfa and hfa series, as their higher triplet level position could rule out the chance of back energy transfer.[119]

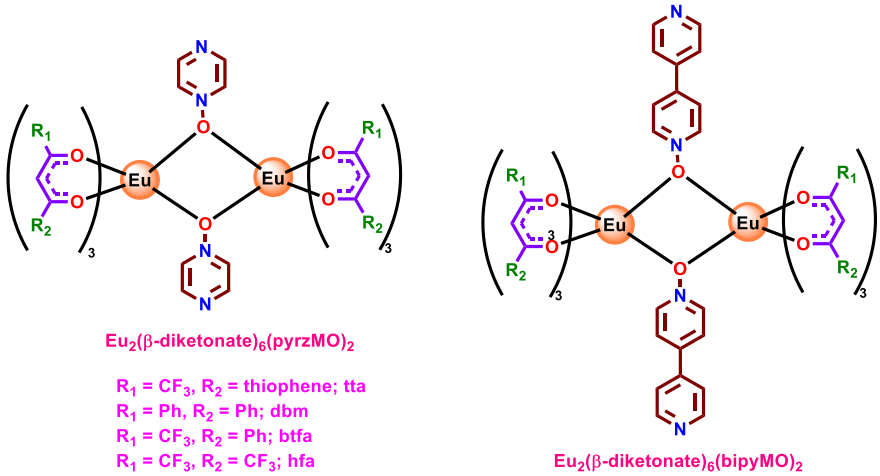

Scheme 1.6

1.6.2. Bidentate Ancillary Ligand

Hasegawa and co-workers designed a ternary Sm-hfa complex comprising phenanthroline as the ancillary ligand (Scheme 1.7). They investigated the solvent effect upon considering acetone, acetonitrile, and pyridine. The asymmetrical nine-coordinated structure in pyridine $Sm(hfa)_3(phen)_2(py)$ was believed to be responsible for enhanced emission characteristics of the said complex as compared to that in the rest of the solvents.[120]

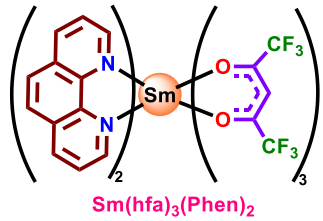

Scheme 1.7

In another work, the said group designed a photochromic Eu-hfa complex with an O-containing bidentate ligand, which can exist both in open and closed chain conformations (Scheme 1.8).[121]

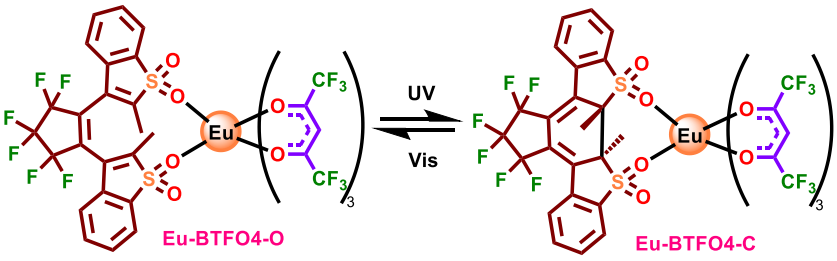

Scheme 1.8

They also synthesized two Eu-complexes with oxo-linked bidentate phosphine oxide ligands and thoroughly investigated their solvent-dependent luminescence spectral behaviors in toluene, chloroform, acetone, and DMF (Scheme 1.9).[122]

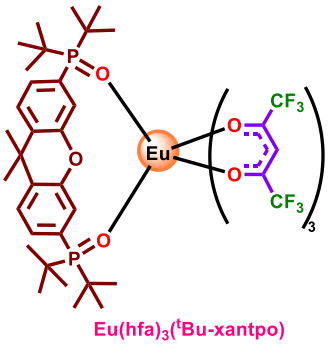

Scheme 1.9

Teotonio et al. reported another TPPO-based ternary Eu-complex where they kept tta as the antenna ligand and investigated its photoluminescence as well as triboluminescence properties (Scheme 1.10).[68]

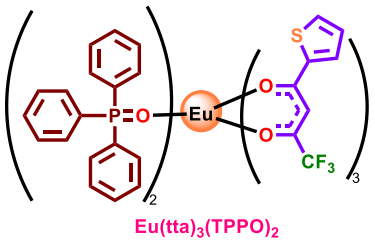

Scheme 1.10

Robertson et al. synthesized two tris-hfa complexes of Eu(III) and Tb(III) comprising a phosphine oxide-based bidentate ancillary ligand (DPEPO) and studied their photophysical

behaviors (Scheme 1.11). The total photoluminescence quantum yield of the Eu-complex was estimated to be as high as 0.8.[123]

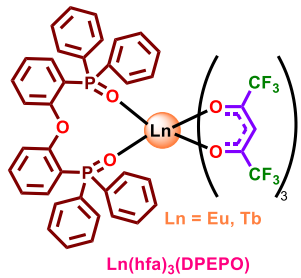

Scheme 1.11

Vaidyanathan et al. designed a number of 1,10-phenanthroline based ligands upon incorporating different substitutions on the phenanthroline moiety and utilized them for the synthesis of Eu-tris-tta type complexes (Scheme 1.12).[124-126] The resulting complexes exhibited bright red luminescence. They proposed that the ancillary ligands also act as the antenna molecule together with tta. An efficient energy transfer from the ligand to Eu^{III} is found to take place in almost all the complexes.

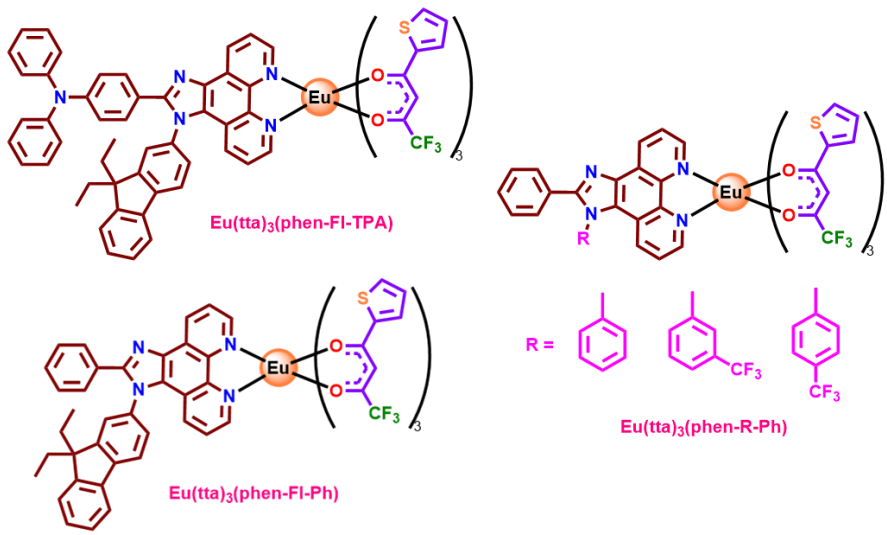

Scheme 1.12

In a following work, they also employed a diphenylamine-functionalized phenanthroline-based ancillary ligand to design a ternary Eu-tris-tta complex (Scheme 1.13).[127] In contrast to the previous case, inefficient energy transfer was noticed herein. On the other hand, this partial energy migration led to the attainment of single-component white

light emission in solution as well as when conjugated with an LED (395 nm). This was the first report of single-component white light emission from discrete lanthanide(III) complexes.

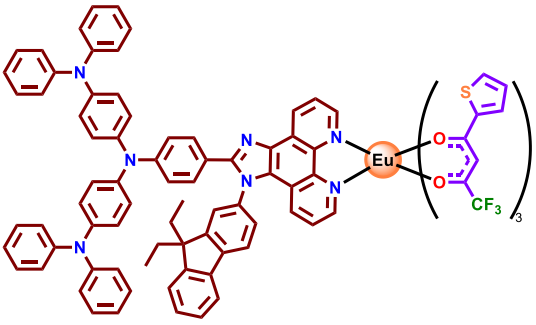

$Eu(tta)_3(phen\text{-}FI\text{-}TPA\text{-}DPA)$

Scheme 1.13

In another work, the same group designed a series of imidazo-bipyridyl-based ancillary ligands with phenyl (Ph), naphthyl (Np), and triphenylamine (TPA) substitution in the ligand framework (Scheme 1.14). The photophysical properties of all the complexes were thoroughly investigated in solution, thin film, as well as in the solid state. The Eu-tta complex with TPA-substitution was found to exhibit inefficient energy transfer from ligand to the Eu(III) unit. But at the same time, the complex exhibits excellent temperature sensitivity as demonstrated by temperature-dependent emission spectral measurements.[128]

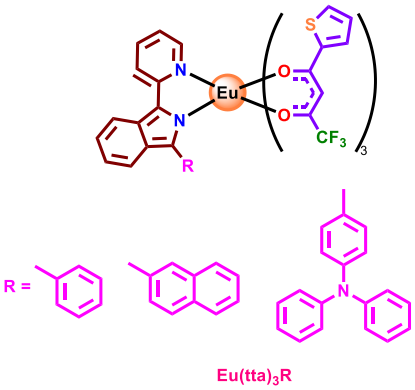

$Eu(tta)_3R$

Scheme 1.14

Gallardo and coworkers designed another thiadiazole-functionalized phenanthroline-based ancillary ligand to synthesize Eu-tris-tta type complex (Scheme 1.15). The single crystal X-ray structure indicated that the ligand was coordinating in a bidentate fashion via the phenanthroline moiety, making an eight-coordinate assembly around the Eu^{III} ion. They also executed detailed studies on its photophysical and electrochemical behaviors, where they

found that the complex exhibits brilliant red luminescence both in the solution and solid state.[129]

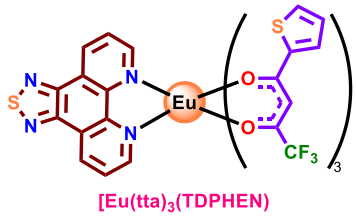

[Eu(tta)$_3$(TDPHEN)

Scheme 1.15

Zucchi et al. reported another type of ternary Eu(tta)$_3$ complex by employing a dicarbazolyl-based phenanthroline unit as the ancillary ligand and thoroughly characterized by standard analytical tools including single crystal X-ray diffraction analysis (Scheme 1.16). Interestingly, the complex exhibited excellent (bright red) luminescence both in solution and solid state, even after being excited by visible light.[130]

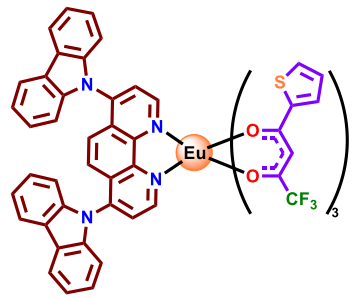

Scheme 1.16

Li et al. designed two series of ternary Eu-complexes comprising of four phenanthroline-based ligands with increased conjugation. One class comprises of tta, while the other based on dbm derivatives (Scheme 1.17). The single-crystal structures from both series revealed the existence of face-to-face intermolecular π-π stacking owing to the large conjugation planes. They also found a correlation among the quantum yield and the structure of the ancillary ligands in all the eight complexes. It is observed that the energy of the emitting triplet state become lower with increase in the conjugation in the ligand within the complex framework.[131]

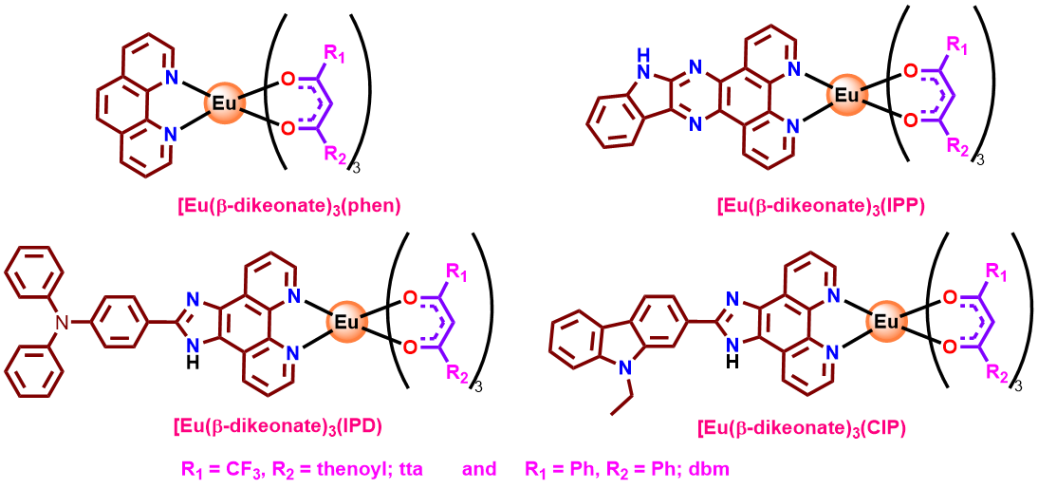

Scheme 1.17

Yuqing Zhao designed a series of substituted phenanthroline ligands with low triplet energy levels and utilized those for the design of ternary Eu^{III} tris-tta complexes (Scheme 1.18). The resulting Eu^{III} tris-tta complexes induce back energy transfer to the ancillary ligands. They demonstrated that this sort of energy dissipation, which they termed as 'the triplet trap', could be prevented in the presence of F^- ion, as the latter upon interaction with the ligands, essentially elevates their triplet energy levels.[132]

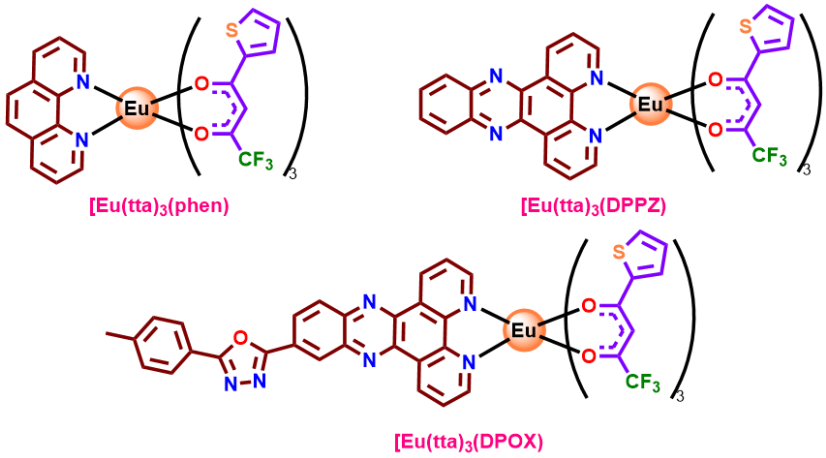

Scheme 1.18

Tsaryuk et al. reported two series of Eu- and Tb-tris-tfa complexes comprising bipyridine and phenanthroline as the ancillary ligands (Scheme 1.19). They observed that the photoluminescence responses of all complexes at 77 K significantly improved as compared to those at 295 K. The observed emission quenching at elevated temperatures was attributed to the thermally assisted and LMCT-mediated back energy transfer to ligand for Tb^{III} and Eu^{III},

respectively. They also found that the extent of luminescence quenching via the LMCT state is most prominent when the said state exists near the ligand triplet state.[63]

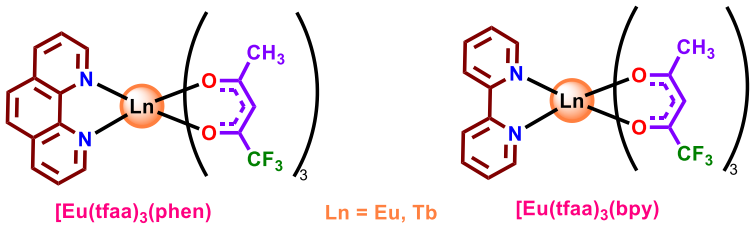

Scheme 1.19

Grachova et al. synthesized a pyridyl-derived pyridazine-based ligand (dppn) to design a series of Ln-tris-tta complexes (Scheme 1.20). The UV-visible absorption spectral characteristics of the complexes suggested that the dppn ligand is capable to sensitize the Ln^{III} ions along with tta itself. The Eu- and Sm-complexes were found to exhibit intense Ln^{III}-centered emission in their solid state.[133]

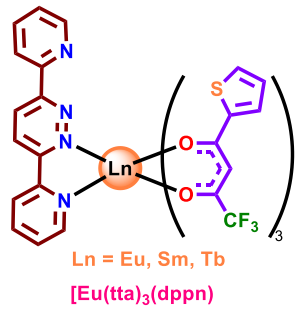

Scheme 1.20

Apart from the N, N-bidentate ancillary ligands, some groups also synthesized and reported N, O-based ligands. Huang et al. prepared a mono N-oxide derivative of 2,2'-bipyridine (Obpy) and explored the electroluminescence behavior of its resulting Eu-tris-tta complex (Scheme 1.21).[134]

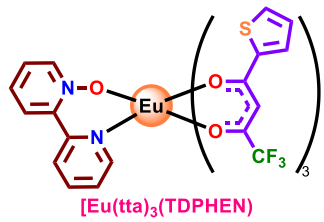

Scheme 1.21

Wang et al. synthesized 2'-pyridyl derivatives of benzoxazole (PBO), benzimidazole (PBI), and benzothiazole (PBT) and coordinated them to Eu-tris-tta moiety (Scheme 1.22). The photoluminescence and electroluminescence behaviors of the complexes were thoroughly studied. It was observed that the complex containing the benzoxazole (N, O)-based ligand exhibited the highest quantum yield among the three complexes.[135]

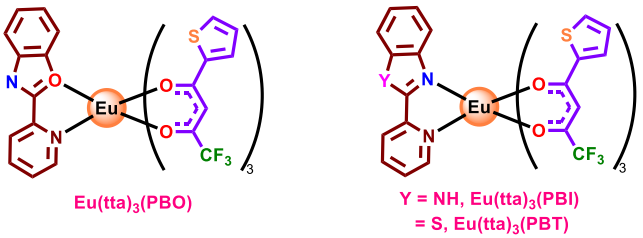

Scheme 1.22

Swavey et al. introduced 2,2'-bipyrimidine (bpm) as the ancillary ligand along with tta and tfa motifs to design two binuclear ternary Eu-tris-(β-diketonate) complexes, whose eight-coordinate arrangements were revealed from their single crystal structures (Scheme 1.23).[136]

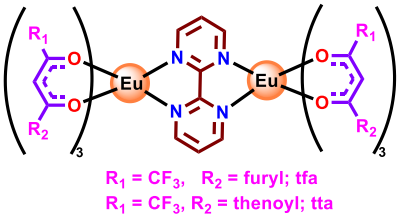

Scheme 1.23

In another work, they synthesized a polyazine-based ancillary ligand (dpp) which was coordinated to two Eu(tta)$_3$ units, resulting in the formation of another ternary binuclear Ln^{III}-complex (Scheme 1.24).[137] In both of these works, they explored the temperature-dependent emission spectral behaviors of the newly synthesized complexes, where the Eu^{III}-centered emission intensities were found to systematically decrease with rising temperature.

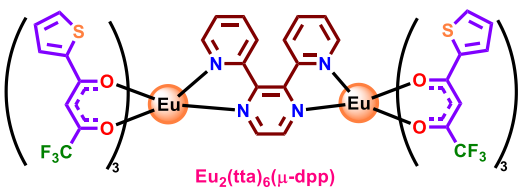

Scheme 1.24

Do et al. utilized dbm and tta as the antenna ligand and reported the single crystal structures of a couple of ternary binuclear Eu(III)-complexes comprising bpm as the ancillary ligand (Scheme 1.25). They thoroughly explored the photophysical and electroluminescence behaviors of the newly synthesized complexes.[138]

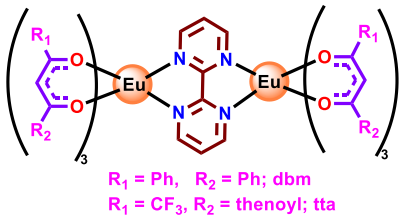

Scheme 1.25

Zucchi et al. reported a series of binuclear Ln^{III} (Sm, Eu, and Tb) complexes comprising bipyrimidine (bpm) as the ancillary ligand and acac as the antenna ligand (Scheme 1.26). They also fabricated OLEDs via doping the complexes where they observed white electroluminescence from the Eu-complex.[139]

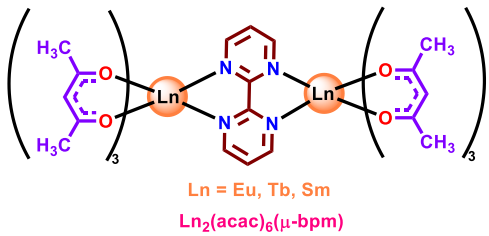

Scheme 1.26

They also reported another ternary dinuclear Sm-tta complex, where the Sm^{III}-centered emission was observed upon excitation with a wide range of wavelengths spanning from UV (250 nm) to visible (500 nm) domain (Scheme 1.27).[140]

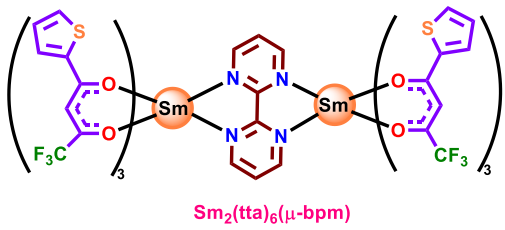

Scheme 1.27

Vaidyanathan and coworkers functionalized a phenanthroline moiety with a spacer and substituted it with fluorene and phenyl groups. The two newly synthesized ligands were employed to design two Eu-tris-tta-based dinuclear complexes (Scheme 1.28). The photophysical investigations revealed that both of these ligands acted as efficient sensitizers for Eu^{III}. Additionally, the sensitizing efficiency of the fluorene-based ligand was found to be greater (η_{sens}=92%) relative to that of the phenyl-based ligand (η_{sens}=85%).[141]

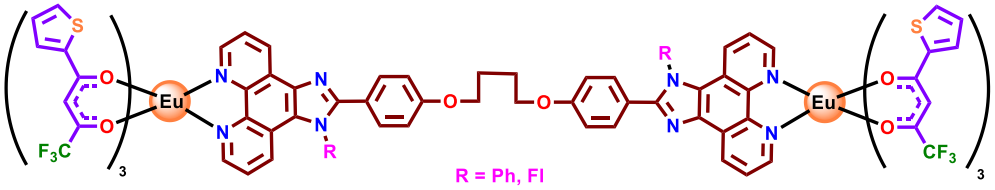

Scheme 1.28

1.6.3. Tridentate Ancillary Ligand

Accorsi et al. synthesized chloro- and carbazole-appended terpyridyl-based ligands to design respective ternary Eu(III) and Tb(III) complexes in combination with dbm as the antenna ligand (Scheme 1.29).[142]

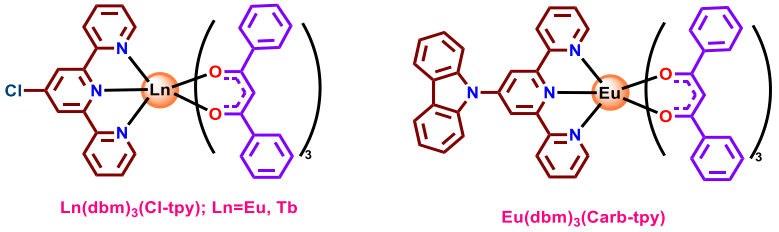

Scheme 1.29

Zheng et al. designed a ternary complex assembly via coupling an $Eu(hfa)_3$ unit with a triazine-based ancillary ligand (tptz) and characterized by single-crystal X-ray diffraction (Scheme 1.30). The photophysical investigation of this nona-coordinated complex revealed a high quantum yield value (Φ=0.6), which they believed to be could be due to cumulative energy transfer efficacy of both hfa and tptz ligands.[143]

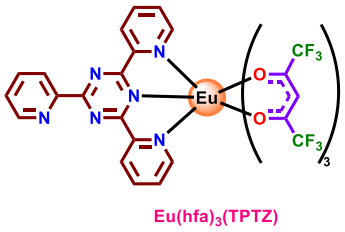

Scheme 1.30

Holliday and coworkers developed a pyrazole-pyridine-based ancillary ligand which they utilized to synthesize a series of Eu(III)-complexes employing hfa, tta, and btfa as the antenna ligands (Scheme 1.31). The single crystal structure of the Eu-hfa complex revealed a low local symmetry around Eu^{III} ion which in turn is responsible for its enhanced photoluminescence properties.[144]

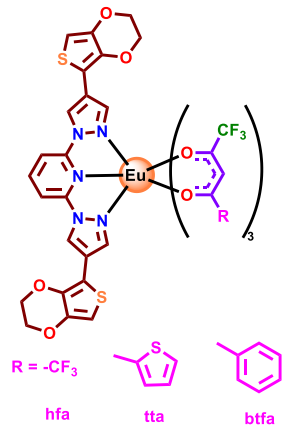

Scheme 1.31

Hasegawa et al. designed a tridentate O-donor phosphine oxide-based ligand (TPPM) and synthesized its Eu(III) and Sm(III) complexes with hfa as the antenna ligand (Scheme 1.32). The single crystal structure of $Eu(hfa)_3(TPPM)$ depicted the existence of a C-H/O H-bonding between the aliphatic H atom of the ligand and the coordinated water and/or acetone molecule. This interaction, despite being present at the outer coordination sphere of the Eu^{III} ion, leads to a slight alteration in the Eu^{III}-centered emission pattern in the said complex.[145]

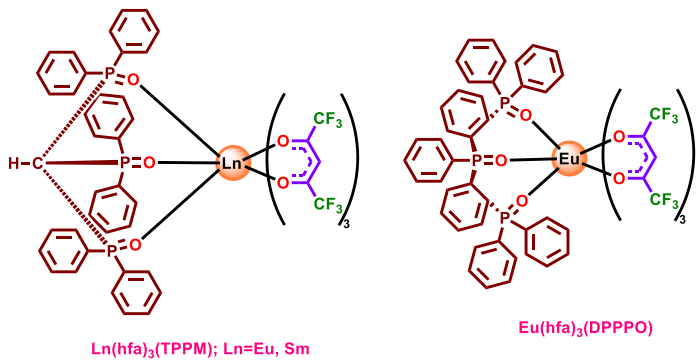

Scheme 1.32

Zhang et al. reported a dipyrazolyltriazine-based ternary Eu(III)-tris-tta complex {$Eu(tta)_3(dpbt)$}, where the absorption spectral window of the complex was found to extend up to 460 nm (Scheme 1.33). They demonstrated that the energy transfer occurred via the

singlet state of the ancillary ligand, contrary to most of the hitherto reported cases wherein the energy transfer takes place via the triplet state. This was the first report of lanthanide sensitization via the singlet pathway in a visible-light excited Eu^{III}-complex.[146]

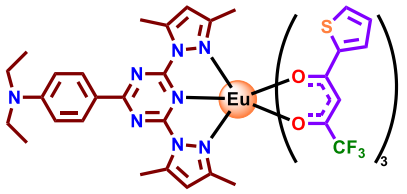

$Eu(tta)_3(dpbt)$

Scheme 1.33

In their subsequent work, they introduced a 2,6-dimethyl substitution on the N,N-diethylaniline moiety of the aforementioned ligand and synthesized its Eu(III)-tris-tta complex {$Eu(tta)_3(dmpbt)$}. The absorption spectral window of the resulting complex was found to extend even more in the visible region (up to 490 nm) (Scheme 1.34).[147]

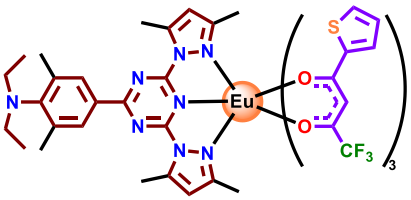

$Eu(tta)_3(dmbpt)$

Scheme 1.34

Zheng et al. reported a number of Eu(III) and Tb(III) complexes with tptz as the ancillary ligand and dbm, tta, ta, btfa as the antenna ligands (Scheme 1.35). The structures of these complexes were established by single-crystal X-ray diffraction studies. The photophysical investigations of these complexes led them to assume that the bulky tptz ligand induced a shielding effect on the coordinated Ln^{III} ions, which prevents the solvent quenching of lanthanide-centered emission.[148]

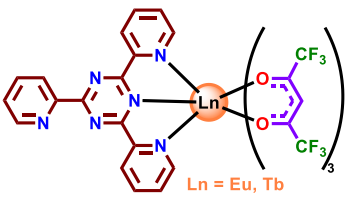

R_1 = Ph; R_2 = Ph : dbm
R_1 = CF_3; R_2 = thenoyl : tta
R_1 = Ph; R_2 = CH_3 : ba
R_1 = Ph; R_2 = CF_3 : btfa

$Eu(hfa)_3(TPTZ)$

Scheme 1.35

You et al. synthesized a chiral terpyridyl-type ligand to design two chiral ternary Eu(III)-complexes comprising tta and btfa as the antenna ligands (Scheme 1.36). The structures of both complexes were established by single-crystal X-ray diffraction studies. They assumed that the difference in crystal polarities between these two complexes was responsible for the distinction in their chiral optical properties, like triboluminescence, non-linear optical (NLO) properties, and ferroelectric behaviors.[149]

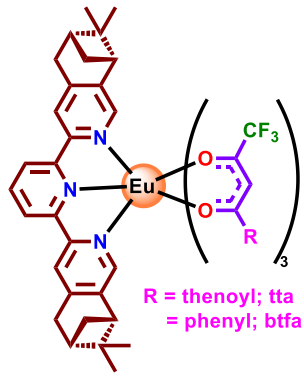

Scheme 1.36

Bian et al. designed two series of 1,10-phenanthroline- and 2,2'-bipyridine-based tridentate ligands and explored the electroluminescence properties of Eu(III)-tris-tta complexes (Scheme 1.37). Their findings suggest that the tridentate ligands could impart higher stability in resulting complexes which in turn leads to enhanced electroluminescence properties in the resulting complexes.[150]

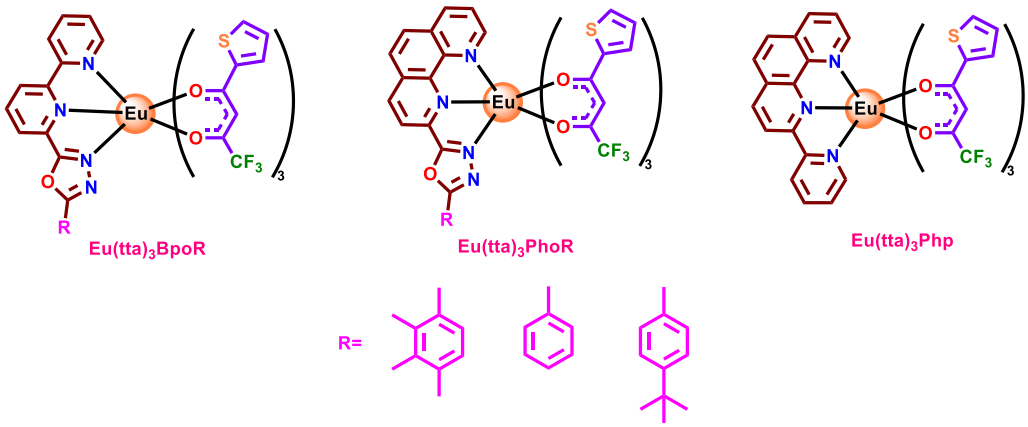

Scheme 1.37

Patra et al. prepared another terpyridyl-derived ancillary ligand, which they utilized to design an Eu(III)-tta-based ternary complex (Scheme 1.38). The said complex was found to

be highly pH-sensitive and acted as a luminescence sensor for anions in the physiological pH domain. Moreover, the complex strongly binds with CT-DNA and BSA, which were visualized via multiple optical channel and spectroscopic techniques.[151]

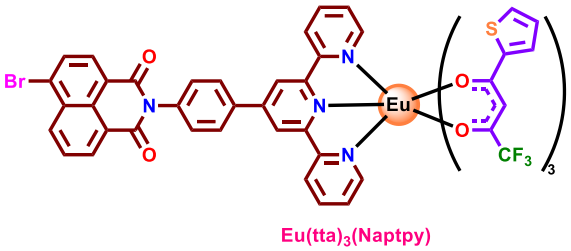

$Eu(tta)_3(Naptpy)$

Scheme 1.38

In another work, the said group designed furyl, 2-thienyl, and pyrolyl derivatives of terpyridine and utilized the ligands to synthesize their respective Eu(III) and Tb(III) complexes upon incorporating tta antenna ligand (Scheme 1.39). All the complexes were structurally characterized by X-ray crystallography and detailed investigations on their photophysical properties were executed.[152]

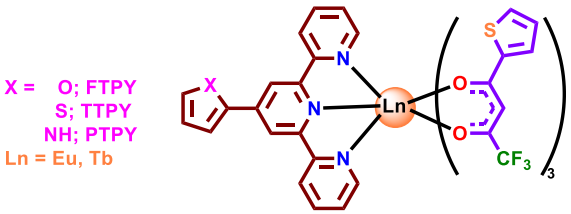

Scheme 1.39

The same group also designed a homoditopic piperazine-phenyl-derived terpyridyl ligand to synthesize a homobimetallic Eu(III)-tris-tta complex (Scheme 1.40). Herein, the ancillary ligand acts as the second antenna ligand. This dual antennae-sensitized Eu(III)-luminescence was utilized in pH sensing, binding with DNA and BSA, and cell imaging.[153]

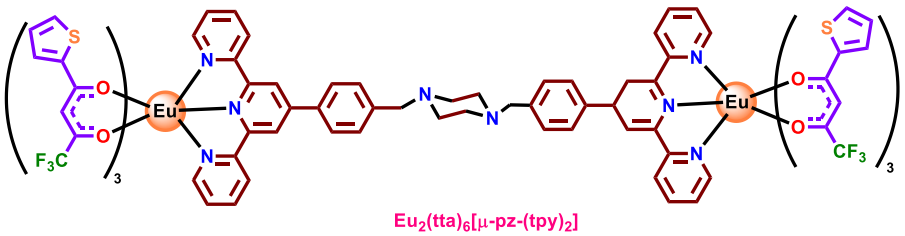

$Eu_2(tta)_6[\mu\text{-pz-}(tpy)_2]$

Scheme 1.40

Labella et al. reported two homobimetallic Eu(III) and La(III) complexes comprised of a pyridyl-N-oxide-derived terpyridyl ligand (pyterpyNO) and tta as the antenna ligand and thoroughly studied their photophysical properties (Scheme 1.41).[154]

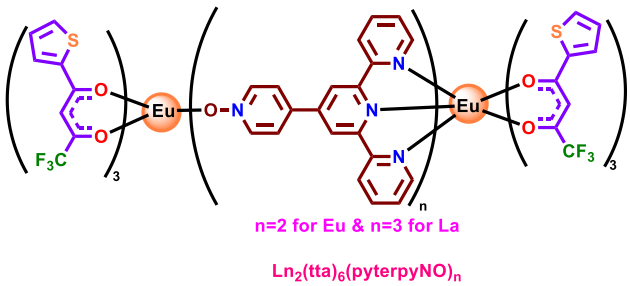

Scheme 1.41

1.7. Doping of the Ln^{III} complexes into Polymer Matrices

In order to extricate the practical utility of remarkable luminescence properties offered by these lanthanide(III) complexes, researchers from the concerned community considered doping them into polymer films, viz., poly(methyl methacrylate) (PMMA), polyvinyl alcohol (PVA), polyurethane (PU), etc. The criteria for choosing such polymers are associated with their optically transparent nature, as well as their high mechanical and optical stability. PMMA is the most widely used polymer in this regard owing to its low cost and ease of preparation. Besides, this polymer is optically transparent above 250 nm. It is also noteworthy to mention that two different strategies have been adopted to bring a materialistic approach to the solution-state luminescence properties of Ln^{III}-complexes. One involved the embedding of Ln-tris-(β-diketonate) assemblies where the carbonyl groups of PMMA coordinate with the Ln^{III} ions, replacing the already coordinated water or solvent molecules. Consequently, the luminescence properties were improved due to the elimination of quencher molecules. The other strategy comprises of doping the coordinatively saturated Ln^{III}-complexes into the polymer matrix. Here also the photophysical behaviors of the complexes are usually enhanced by suppressing the non-radiative deactivations via imposing rigidity from the polymer matrix.

Robertson et al. synthesized a series of Eu-complexes with a bidentate phosphine oxide-based ancillary ligand and five different fluorinated β-diketonates (Scheme 1.42). The photoluminescence investigations of these complexes, upon doping them into PMMA, revealed very high quantum yields (Φ_{rel}=0.26-0.85). The value of 0.85 was believed to be the highest among the related hitherto reported cases.[155]

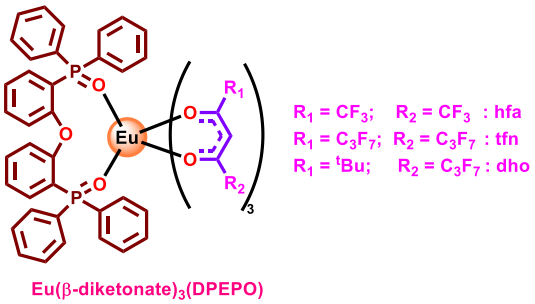

Scheme 1.42

Reddy et al. embedded another ternary Eu(III)-tris-(β-diketonate) complex of type $Eu(CPFHP)_3(DDXPO)$ into PMMA in various proportions, viz. 2.5, 7.5, 10, and 15% (Scheme 1.43). The corresponding Φ_{rel} values were found to alter between 0.79 and 0.84. From the absorption spectral characteristics of the composites, they surmised that both the organic chromophore and PMMA polymer absorbed light, which in turn resulted in such a high luminescence quantum yield.[156]

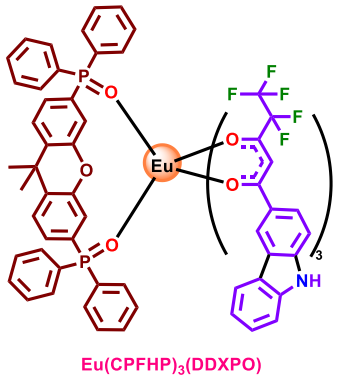

Scheme 1.43

Zucchhi et al. doped an Eu(III)-complex containing tta and a phenanthroline-based ancillary ligand into PMMA (Scheme 1.44). The resulting composite material was found to

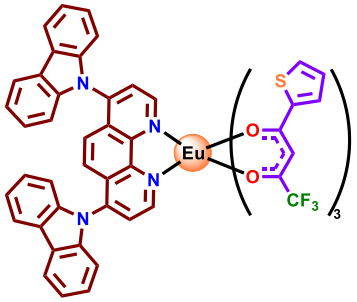

Scheme 1.44

be air-stable for at least a few weeks. Besides, brilliant red emission was achieved upon excitation over a wide range of wavelengths (250-560 nm). The absolute quantum yield of this material was estimated to be as high as 0.80.[130]

Yan et al. designed a new fluorinated and indone-based β-diketonate ligand (5,6-DTFI) to synthesize its corresponding Eu(III) tris-complex and ternary Eu(III) complex with 1,10-phenanthroline (phen) (Scheme 1.45). They embedded both complexes into PMMA. The photophysical investigations demonstrated that PMMA not only acts as a co-sensitizer but also played a better role than phen in enhancing the Eu-centered luminescence.[108]

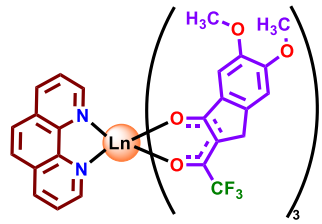

$Ln(5,6\text{-}DTFI)_3(Phen)$; Ln= Eu, Sm

Scheme 1.45

Iftikhar and coworkers doped a ternary Sm(III) complex of type $\{Sm(hfa)_3(Hind)_3\}$ into PMMA and noticed enhancement in its quantum yield and lifetime values as compared to those in solution state (Scheme 1.46).[157]

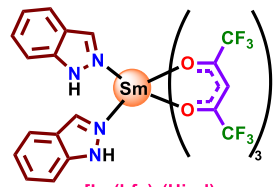

$[Ln(hfa)_3(Hind)_3$

Scheme 1.46

The said group also embedded Sm(III), Eu(III), and Tb(III)-complexes with dbm and another bidentate ancillary ligand, impy onto PMMA and observed significant improvement in their luminescence spectral features (Scheme 1.47).[158]

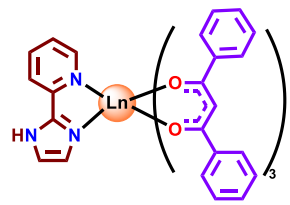

$Ln(dbm)_3(impy)$; Ln= Eu, Sm, Tb

Scheme 1.47

Vaidyanathan et al. doped a series of Eu(III)-tris-tta complexes comprising three phenanthroline-based ancillary ligands into PMMA (Scheme 1.48). The quantum yield values of the hybrid thin films were estimated to be as high as 0.76.[159]

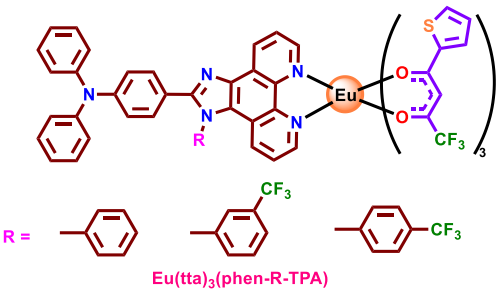

Scheme 1.48

Wang et al. designed four new β-diketonate ligands to synthesize an array of bipyrimidine (bpm)-bridged homobimetallic ternary Eu^{III}-complexes (Scheme 1.49). All the complexes were also doped into PMMA. One of the said complexes is found to exhibit remarkably high values of lifetime (0.946 ms) and quantum yield (0.72).[160]

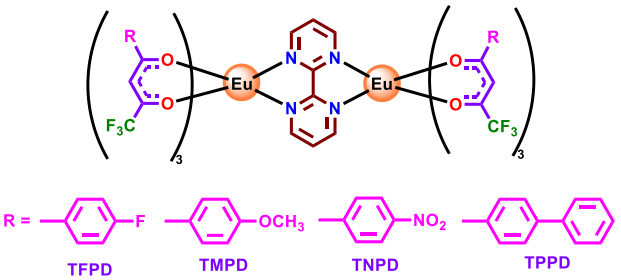

Scheme 1.49

Brito et al. prepared a thin film of PMMA upon co-doping $[Eu(tta)_3(H_2O)_2]$ and $[Tb(acac)_3(H_2O)_3]$. The photo-stability co-dopped species was found to be enhanced relative to those of the individual species (Scheme 1.50). PMMA acted as a co-sensitizer here, resulting in improved photophysical properties. Moreover, the emitting colors of the film could be fine-tuned by adjusting both composition and excitation wavelength between the two primary colors, viz. red and green.[161]

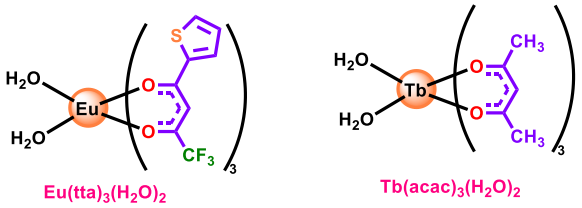

Scheme 1.50

Some other groups have also reported various type of such thin hybrid films embedded with Ln^{III}-based discrete molecules and thoroughly investigated their photophysical and in particular their emission spectral characteristics and summarized their results in several review articles.[162,163]

1.8. Stimuli-Responsive Photophysical Behaviors of Ln^{III} Complexes in Solution and Polymer Matrix

After exploration of the characteristics of diverse antenna ligands as well as ancillary ligands for effective sensitization of the lanthanide ions, the researchers from this community are now interested on further modulation of their photophysical, in particular their luminescence spectral characteristics, in presence of diverse external stimuli. The primary motive is to utilize the unique and well-defined luminescence properties in sensing applications. The lanthanide complexes are now being widely utilized for sensing of pressure, temperature, different analytes, pH, to name a few. Besides, the luminescence behaviors are also found to be well-dependent on stimuli like current, solvent, and excitation wavelength. Consequently, the Ln^{III}-based complexes are capable to generate several emitting colors, including white light, holding prospects for applications as various light-harvesting materials. The stimuli-responsive behaviors of discrete Ln^{III} complexes have mostly been explored in their solution states, although a few reports are now available in the literature wherein the thin hybrid films containing such Ln^{III} complexes have been investigated (Figure 1.5).

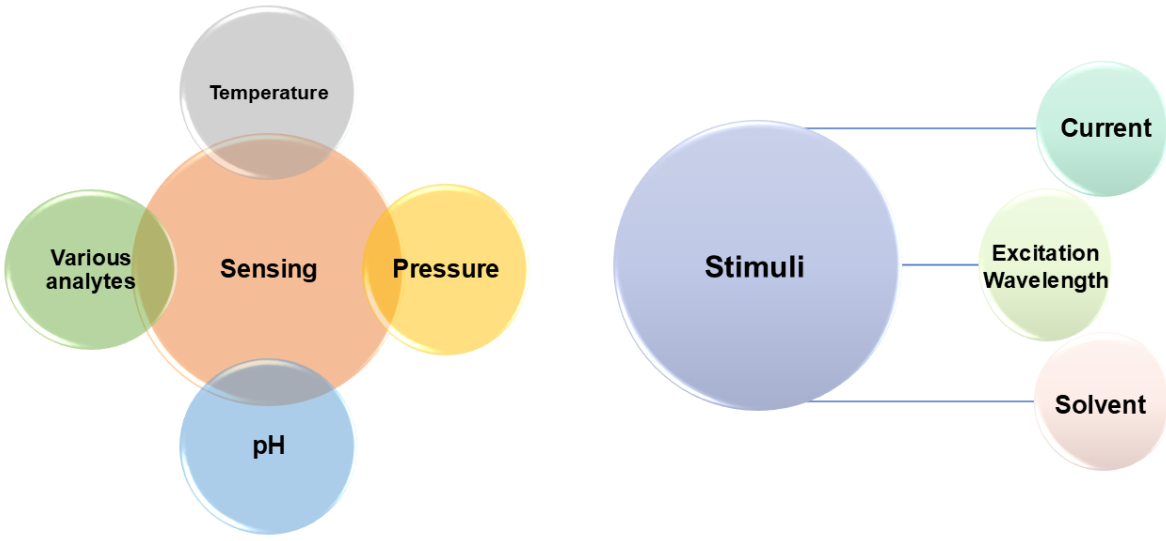

Figure 1.5. Various Stimuli for the Luminescence Properties of Ln^{III}-based Discrete Molecules.

Among the different stimuli, temperature has been mostly employed for the Ln^{III} complexes. Eventually, the temperature-dependent luminescence spectral behaviors of these Ln^{III} complexes were further utilized in luminescence thermometry. This opened up a broader window in the thermosensing domain as sensing the temperature with utmost accuracy has always been a matter of urgency, as far as the significance of temperature in biological and industrial sectors is concerned. Immediately after the thermosensing ability of Ln^{III} complexes had been established, it started outplaying the traditional thermosensors owing to their several advantageous attributes like thermostability, photostability, non-invasive (non-contact) nature, high resolution in the nanoscale domain, and functionality even in strong electromagnetic fields. However, the literature suggests that, primarily, the Ln^{III}-based coordination polymers and metal-organic frameworks were mostly utilized for this purpose. By contrast, Ln^{III}-based discrete molecules have been far less explored, while terpyridyl-derived ligand-based reports are even more sparse. Over the preceding couple of decades, various thermometric parameters have been employed to execute and assess the efficacy of luminescence thermometry using the Ln^{III} complexes. Luminescent intensity ratio (LIR) and excited state lifetime are the two frontrunners in this regard, followed by area ratio, quantum yield, bandwidth, emission intensity, etc. From these thermometric parameters, the thermosensing efficacy of a molecule has been determined by estimating two quantitative parameters, viz., temperature sensitivity and temperature resolution. The last two parameters are often applied to visualize the efficacy of a thermosensor. A comparison of the thermosensing efficacy of several Ln^{III}-based discrete thermosensors is depicted in tabular form (Table 0).

Apart from temperature, solvents also play a crucial role in the luminescence spectral outcomes of Ln^{III} complexes. Hasegawa et al. noticed that the emission spectral properties of $Sm(hfa)_3(phen)_2$ complex differs when the measurements are carried out in three different solvents, such as acetone, acetonitrile, and pyridine (Scheme 1.51). To be more specific, the electric dipole transition intensity as well as the radiative rate constant of the said complex

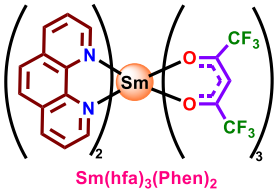

Scheme 1.51

were found to be much higher in pyridine relative to other two solvents. The X-ray crystal structures of the complex in all three solvents indicated that the formation of an asymmetrical nine-coordinate structure, $Sm(hfa)_3(phen)(py)$ in pyridine might be the plausible reason for enhanced luminescence properties as compared to the symmetrical 10-coordinate structures in both acetone and acetonitrile.[120]

In subsequent work of the same group, the luminescence properties of a number of Eu(III)-tris-hfa complexes comprising phosphine oxide-based ligands were also found to be well dependent on the nature of the solvents (Scheme 1.52).[122,164]

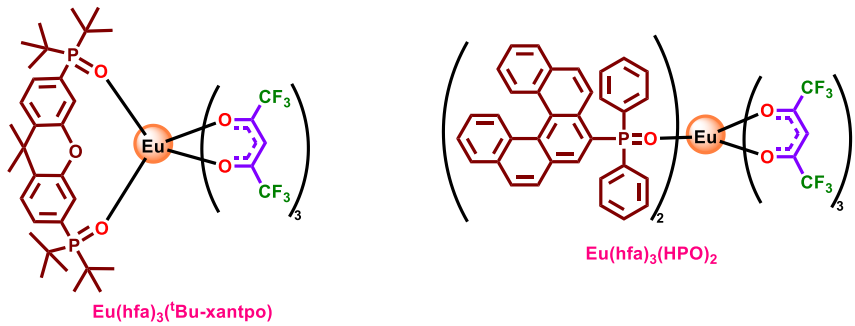

Scheme 1.52

Iftikhar et al. investigated the solvent-dependence luminescence spectral behaviors of $Eu(acac)_3(pyz)_2$ and $Sm(acac)_3(pyz)_2$ (pyz=pyrazine) complexes in both non-coordinating (chloroform) as well as coordinating solvents (ethanol and methanol) (Scheme 1.53). They found that the electric dipole transition intensities and quantum yields are higher in chloroform than in ethanol and methanol for both complexes. The poor luminescence responses in ethanol and methanol were attributed to non-radiative deactivation via high-energy O-H oscillators, along with quenching of the ligand triplet state via dipole-dipole coupling among the ligands and the solvent molecules.[165]

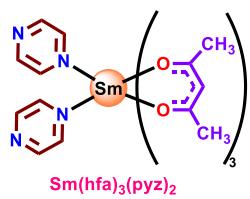

Scheme 1.53

Vaidyanathan et al. investigated the solvent-dependent luminescence spectral responses of some Eu(III)-tris-tta complexes containing N-based bidentate ligands, where in

each case both the ligand- as well as Eu-centered emission signals were observed (Scheme 1.54).[128,166] They also found that the quantum yield and lifetime of the Eu-centered emission are higher in less polar or non-polar solvents relative to that of the polar solvents. The ligand-centered emission peaks underwent a red-shift upon increasing the polarity of the solvents. They surmised that the dipole of the ligand's excited state is higher in polar solvents, which in turn, leads to such shifting of the emission peaks.

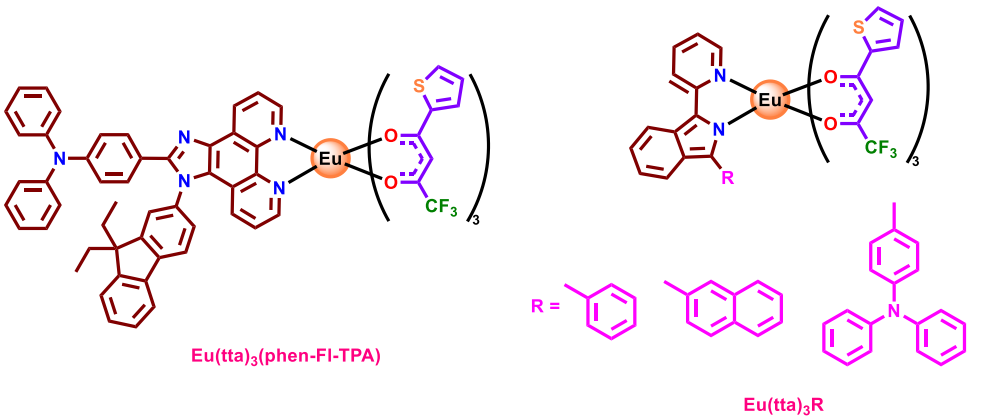

Scheme 1.54

Ward and co-workers observed three types of luminescence (red, green, and blue) from an Eu^{III} complex with a naphthalimide-derived macrocyclic ligand (Scheme 1.55). They utilized its solvent-dependent luminescence behaviors and accomplished white light emission by maintaining the appropriate ratio of acetonitrile and water.[45]

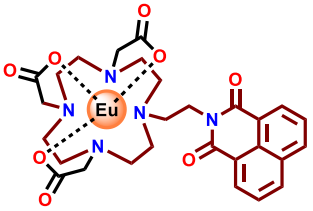

Scheme 1.55

Kitchen and co-workers synthesized a dual-emissive Eu^{III} complex with another type of naphthalimide-based ligand (Scheme 1.56). The naphthalimide-based fluorophore exhibits blue emission, while the respective Eu(III) complex displays red emission. They also tuned the extent of these two emission intensities by changing the excitation wavelengths, which resulted in an alteration of overall emission colors from red to blue, including white light.[42]

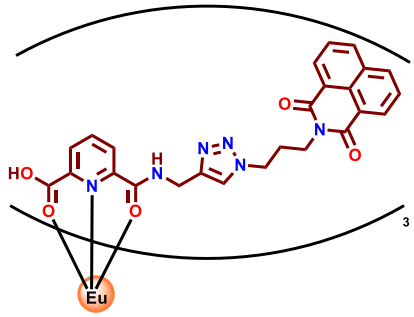

Scheme 1.56

The stimuli-responsive behaviors of the complexes are also studied in their solid state, especially upon being doped in a polymer matrix. Wong et al. designed and synthesized a ternary Eu(III)-tris-tta complex upon coordinating with a pyridazine-triazine-based tridentate ancillary ligand (Scheme 1.57**)**. They accomplished white electroluminescence from the said complex in its solid state upon judicious mixing of ligand-centered bluish-green emission and Eu-centered red emission.[44]

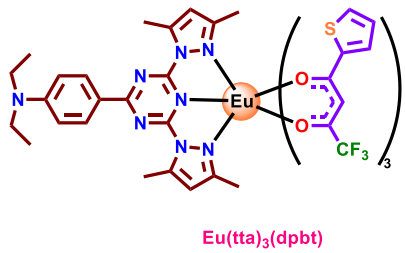

$Eu(tta)_3(dpbt)$

Scheme 1.57

Raithby and co-workers synthesized Eu^{III}- and Tb^{III}-based tris-hfa complexes comprising a benzimidazole-based ligand and doped them onto a poly(urethane) (PU) matrix (Scheme 1.58). While the Eu-complex showed brilliant red photoluminescence both in solution and thin films of PU, the Tb complex displayed near white light emission in solution as well as in thin films owing to the presence of its ligand-centered emission. Moreover, the Eu complex exhibits excellent tuneable electroluminescence (from blue to magenta), and at

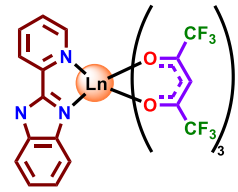

$[Ln(hfa)_3(Py\text{-}Im)$; Ln=Eu, Tb

Scheme 1.58

the same time, the said complex acted as a sensitizer to improve the electroluminescence performance of a red-emitting iridium complex.[167]

Singh and co-workers doped $Eu(dbm)_3(phen)$ complex into the PMMA matrix and investigated the temperature-dependent luminescence spectral properties of the hybrid film (Scheme 1.59). The relative temperature sensitivity of the said film was estimated to be 1.75 % K^{-1} within the temperature domain of 50-318 K.[43]

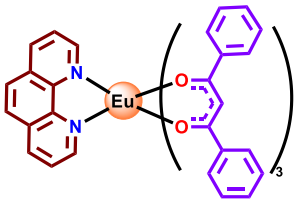

$[Eu(dbm)_3(phen)]$

Scheme 1.59

In another work, they investigated the effect of temperature on the photoluminescence behaviors of $Eu(tta)_3(phen)$ complex where the average relative temperature sensitivity was estimated to be 3.67 $\%K^{-1}$ in the temperature domain of 50-305 K (Scheme 1.60). They also doped the same complex into PVA and found that the relative temperature sensitivity of the film reaches up to 6.5 $\%K^{-1}$ within the temperature domain of 305-340 K.[168]

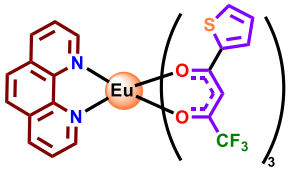

$[Eu(tta)_3(phen)]$

Scheme 1.60

Lapaev and co-workers prepared a 20 mm-thick vitrified film of a ternary Eu(III) complex, sandwiching it between two quartz plates by melting (Scheme 1.61). The said film

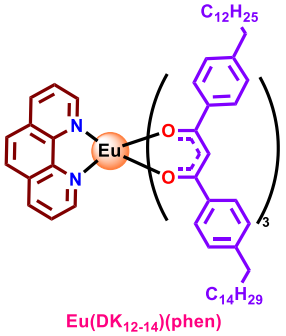

$Eu(DK_{12\text{-}14})(phen)$

Scheme 1.61

was found to exhibit temperature-dependent luminescence as well as lifetime upon monitoring at 611 nm within the temperature range of 270-370 K. The highest value of relative temperature sensitivity was observed to be 0.27 % K^{-1} at 370 K.[169]

1.9. Objective and Scope of the Work

A thorough survey of literature reveals that ligands possessing oxygen donor(s) were primarily utilized for sensitization of the Ln(III) ions. A wide variety of such ligands together with their binary Ln(III) complexes were designed by various researchers across the globe. These complexes were usually soluble in water, and this specificity led them to be utilized in various bio-applications. As soon as the development of this topic gets started with nitrogen donor(s) ligands, an unwanted drawback of insolubility of the complexes in most of the organic solvents arises. Contemporarily, an earlier reported class of Ln^{III} sensitizers has started to gain attention again, which could circumvent this problem. This class is referred to as the β-diketonates. Consequently, these β-diketonates were employed to synthesize diverse lanthanide(III) tris-β-diketonate complexes. Substantial efforts were devoted for the design of suitable Ln(III) complexes with enhanced photophysical properties, in particular their luminescence characteristics. Eventually, it was found that replacing the high-energy oscillating C-H bonds with more rigid C-F bonds could lead to an improvement in the sensitization efficacy in the resulting lanthanide complexes. However, the higher coordination tendency of the Ln^{III} ions often invites the surrounding water or solvent molecules to coordinate, which in turn induces the non-radiative deactivation of the excited state upon light irradiation. As a result, the highest luminescence is still to be achieved. To overcome the lacuna, the concept of an ancillary ligand was introduced. This sort of ligand not only replaces the quencher molecules but also can act as another sensitizer to the Ln(III), provided they meet the criteria of relevant excited state energy levels. Upon literature survey, it appears that most of the ligands employed for this purpose are either monodentate or bidentate in nature. Surprisingly, the tridentate terpyridine-type are found to be far less explored in spite of their several favourable structural attributes. This set our first major objective of utilizing terpyridine coordinating motif for the design of luminescent Ln(III) complexes in combination with diverse β-diketonate ligands.

To meet our objective, we designed four new series of ternary monometallic as well as homobimetallic Ln^{III} complexes (Ln=La, Eu, Sm, and Tb) comprising two terpyridyl-based ancillary ligands and two different fluorinated β-diketonate ligands as antennas (Figure 1.6).

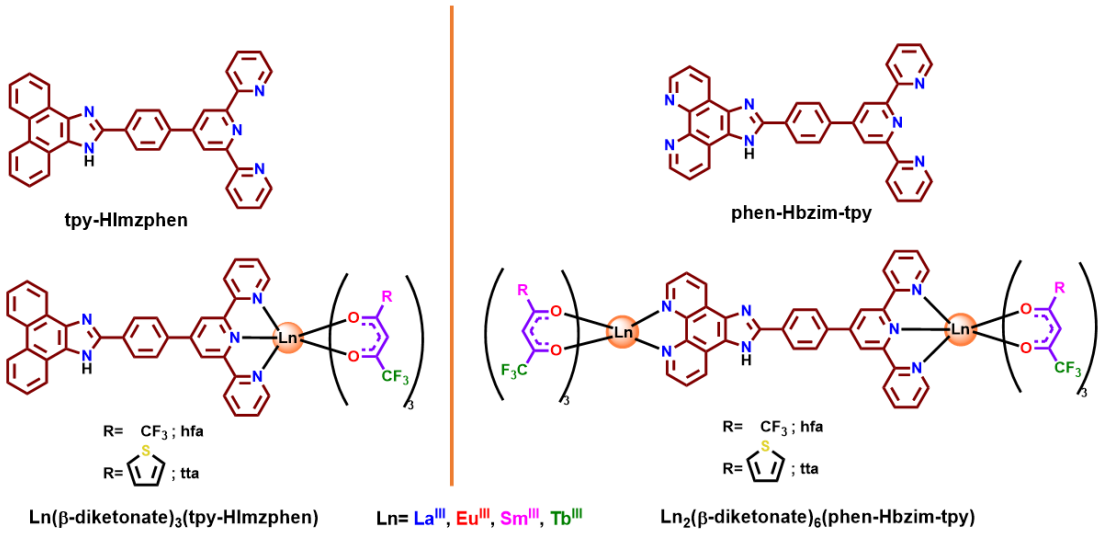

Figure 1.6. Chemical structures of the ligands and their ternary Ln^{III} (β-diketonate) complexes.

The first ligand, 2-(4-[2,2′:6′,2″]Terpyridin-4′-yl-phenyl)-1*H*-phenanthro[9,10-*d*] imidazole, abbreviated as tpy-HImzphen, was synthesized via refluxing a mixture of 4′-(*p*formylphenyl)-2,2′:6′,2″-terpyridine (tpy-PhCHO) and 9,10-phenanthrenedione in a 1:1 molar ratio in the presence of excess ammonium acetate in acetic acid medium. The second ligand, 2-(4-(2,6-di(pyridin-2-yl)pyridine-4-yl)phenyl)-1*H*-imidazole[4,5-f][1,10] phenanthroline (phen-Hbzim-tpy) is actually a heteroditopic ligand comprising of both terpyridine and phenanthroline coordinating motif, which was prepared following the same process, except employing 1,10-phenanthroline-5,6-dione in place of 9,10-phenanthrenedione. After synthesis, thorough characterization of the complexes will be carried out via Fourier Transform infrared (FT-IR) spectroscopy, ^{1}H muclear magnetic resonance (NMR) spectroscopy, matrix-assisted laser desorption ionization-time of flight (MALDI-TOF) mass spectrometry, high resolution mass spectrometry (HRMS), thermogravimetric analysis (TGA), powdered X-ray diffraction (PXRD), and in some cases single crystal X-ray diffraction analysis. Following synthesis and characterizations, detailed investigations on photophysical behaviors of the all the complexes will be executed via absorption, and both steady-state and time-resolved emission spectroscopic measurements.

As mentioned earlier, an ancillary ligand can also take part in the Ln^{III} sensitization depending on its triplet energy level. In fact, in such ternary assemblies, the extent as well as direction of energy transfer is very much dependent on the energy level of the ancillary ligand, despite anchoring a suitable antenna ligand. For example, the Tb(III) complexes often encounter back energy transfer to the ancillary ligand owing to its high-lying emissive ($^{5}D_4$)

level; the Sm^{III} complexes often experience poor Ln^{III}-centered luminescence as it is very prone to multi-phonon relaxation due to the low energy gap between its own emissive and ground state (~7500 cm^{-1}); in the Eu(III)-complexes, on the other hand, involvement of ligand-to-metal-charge-transfer (LMCT) state results in substantial energy dissipation from the lowest emissive level of Eu^{III} ($^5D_0$). To this end, our main objective will be to employ the proposed terpyridyl-imidazole based ancillary ligands for effective sensitization of the coordinated Ln(III) ions.

We have already pointed out that sensing of temperature with utmost accuracy has always been a matter of importance, as far as the significance of temperature in biological and industrial sectors is concerned. Among the different stimuli, temperature has been frequently employed for the Ln^{III} complexes for modulation of their emission spectral responses. Eventually, the temperature-dependent luminescence spectral behaviors of these Ln^{III} complexes were further utilized in luminescence thermometry. We will be interested to thoroughly investigate the thermosensing behaviors of the designed Ln^{III} complexes via luminescence thermometry. The literature data indicate that the Eu^{III} complexes has been mostly employed for this purpose and thereafter the Tb^{III}. Sm^{III} has been used in very few cases, while La^{III} is hardly found to be utilized. Moreover, in most of the reported cases, only the Ln^{III}-centered luminescence responses have been taken into consideration for this purpose. But monitoring the alteration of both ligand- as well as Ln^{III}-centered luminescence responses could shed light onto the mechanistic aspect of the temperature-dependent luminescence phenomena (Figure 1.7). In other words, one can understand the process that involves thermo-assisted back energy transfer from Ln^{III} to ligand (which is quite common for the Tb^{III}-complexes) or low-lying ligand-to-metal charge transfer (LMCT)-mediated back

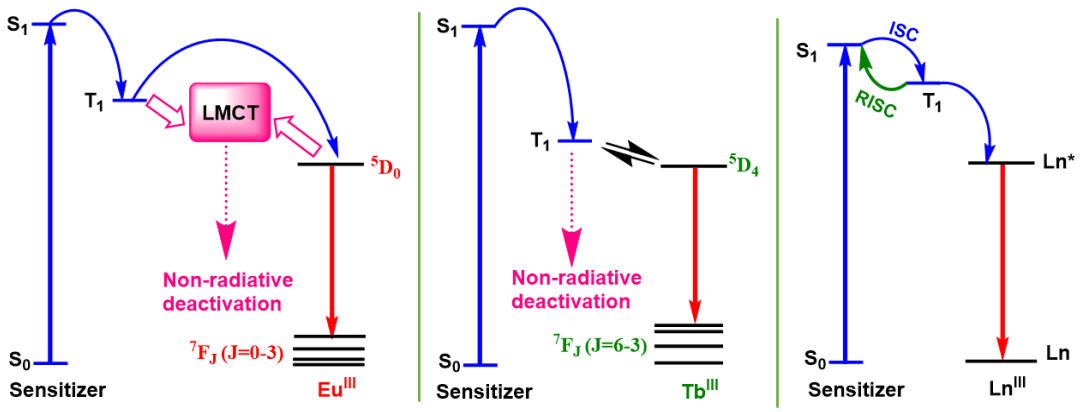

Figure 1.7. Schematic representation of various temperature-induced energy transfer pathways within the Ln^{III} complexes.

energy transfer from Ln^{III} to ligand (which applies to the Eu^{III}-complexes) or the occurrence of thermally activated back energy transfer (TADF). It is of interest to note that appropriate tuning of both the ligand as well as the Ln^{III}-centered emission could lead to the occurrence of remarkable thermochromism. The thermosensing ability of the present complexes is also investigated in a thin hybrid film for probable practical utility. Apart from temperature, other stimuli, like solvent or excitation wavelength, were also employed to modulate the luminescence spectral responses of the present Ln^{III} complexes, which in turn result in the generation of various emitting colors apart from the characteristic colors of the respective Ln^{III} ions (Figure 1.8).

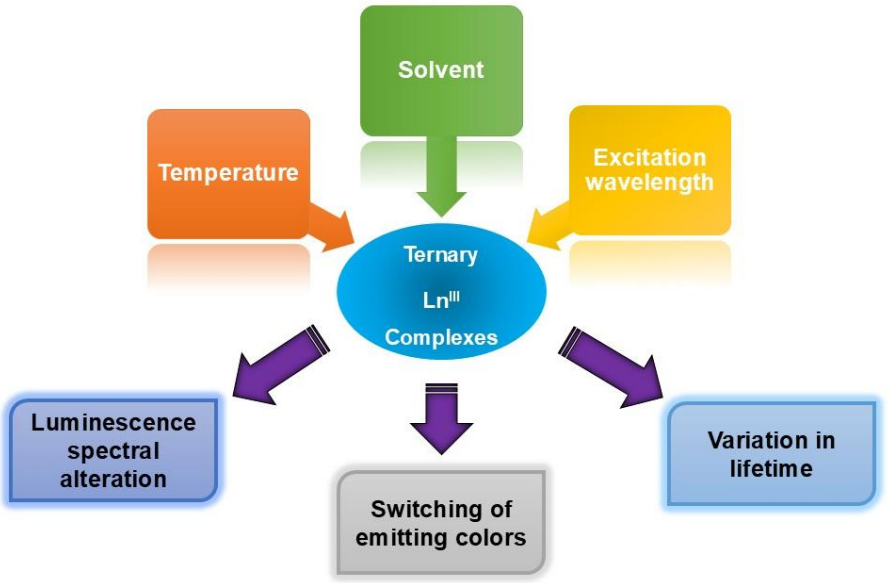

Figure 1.8. Schematic representation of stimuli-responsive luminescence behaviors of ternary Ln^{III}-based complexes.

Chapter 2-6 demonstrates the execution of the above-mentioned objectives via related investigations. Chapter 2 deals with the synthesis of four ternary lanthanide tris-(β-diketonate) complexes of the form, $[Ln(tta)_3(tpy\text{-}HImzphen)]$, where Ln=La, Eu, Sm, Tb. All the four complexes are fully characterized by standard analytical tools and spectroscopic techniques, including single-crystal X-ray diffraction analysis. The photophysical behaviors of the complexes were thoroughly investigated via absorption and both steady-state and time-resolved emission spectroscopic techniques. The incorporation of the terpyridyl-imidazole based ancillary ligand into the $Ln(tta)_3$ moieties leads to the generation of four distinctive luminescence responses, when inspected at both room temperature and 77 K. In the end,

attempts are made to decipher the role of the said ligand on the photophysical, in particular luminescence spectral behaviors of the complexes.

The thermosensing and thermochromic behaviors of the [Eu(tta)$_3$(tpy-HImzphen)] complex have been thoroughly investigated in Chapter 3. The complex acts as an excellent thermosensor in terms of both luminescence intensity ratio (S_m=5.78 %K^{-1}, T_m=343 K, δT=0.012 K) and lifetime values (S_m=3.36 %K^{-1}, T_m=333 K, δT=0.009 K) within the temperature range of 273-343 K. The dual emissive nature of the complex leads to remarkable thermochromism (red at 268 K, violet at 303 K, and blue at 343 K) within the said temperature domain. Moreover, various emitting colors, apart from its characteristic red emission, are observed upon varying the nature of the solvents. Finally, amalgamating these thermochromic and solvatochromic features of the complex, single-component white light emission is achieved at 283 K. At the end, a plausible energy transfer mechanism has also been proposed elucidating the role of low-lying ligand-to-metal charge transfer (LMCT) state for observed quenching of the Eu^{III}-centered emission.

Chapter 3 deals with the design, syntheses, and characterization of a new array of ternary Ln^{III} complexes of the type [Ln(hfa)$_3$(tpy-HImzphen)], where Ln=La^{III}, Eu^{III}, Sm^{III}, Tb. The absorption spectroscopic investigation reveals that incorporation of tpy-HImzphen ligand onto the Ln-hfa moiety results in a bathochromic shift of the absorption spectral window of the complexes into the visible region (onset at ~450 nm). The steady-state and time-resolved emission spectral behaviors at both RT and at 77K indicate four distinctive behaviors upon incorporation of tpy-HImzphen onto the Ln(hfa)$_3$ motifs, viz. huge red-shift of the ligand-centered peak for La^{III}; almost complete energy transfer for Eu^{III}; very little energy transfer for Sm^{III}, and reverse energy transfer in case of Tb^{III}. Additionally, the Eu^{III}-complex exhibits excellent thermosensing behavior in solution as well as when doped in poly(methyl methacrylate) (PMMA) matrix. The thermosensitive luminescence response was further utilized to mimic the operation of Set-Reset Flip-flop Boolean logic.

Syntheses and characterization of a new array of four homobimetallic Ln^{III}-complexes (where Ln=La, Eu, Sm, Tb) derived from a heteroditopic terpyridine-phenanthroline (phen-Hbzim-tpy) bridge together with tta as the antenna ligand are reported in Chapter 5. Detailed investigations on room temperature photophysical properties as well as temperature-dependent luminescence spectral behaviors of complexes, together with the free phen-Hbzim-tpy ligand, have been thoroughly investigated. Interestingly, the phen-Hbzim-tpy bridging ligand is found to display thermally activated delayed fluorescence (TADF). All the four

complexes act as efficient thermosensors as evidenced by their favourable luminescence thermometric attributes. The La(III) complex cannot sustain the TADF phenomenon, while the rest of the complexes displayed remarkable thermochromism via coupling of TADF and respective dual-emission characteristics. Finally, attempts have been made to understand the synergy among the lowest triplet states of both the ligands and the lowest emissive states of the respective Ln^{III} ions, which is believed to be responsible for the observed photophysical and temperature-dependent luminescence spectral behaviors of the complexes.

Chapter 6 deals with the synthesis of an analogous series of ternary homobimetallic Ln^{III} complexes upon replacing tta with hfa. Following synthesis, thorough characterization of the complexes have been done via standard analytical tools and spectroscopic techniques. Detailed investigations on the phtophysical properties are also conducted. Substantial improvement in the absorption and emission spectral characterises (viz. quantum yield and lifetime), and sensitization efficiency are noticed upon replacement of the antenna ligand from tta to hfa. In contrary to the previous bimetallic series, all the four complexes herein are found to display the TADF behavior. Furthermore, the complexes display excellent thermosensing and thermochromic properties. Apart from TADF-assisted thermochromism, the luminescence spectral characteristics of the complexes are found to be well-dependent on the polarity of the solvent as well as on the excitation wavelength. Finally, tuning of emitting colors across the entire VIBGYOR region, as well as room temperature single-component white light emission, is achieved upon the appropriate interplay of said three stimuli on the complexes.

1.10. References

1. Bünzli, J.-C. G. On the Design of Highly Luminescent Lanthanide Complexes. *Coord. Chem. Rev.* **2015**, *293*, 19–47.
2. Hasegawa, Y.; Wada, Y.; Yanagida, S. Strategies for the Design of Luminescent Lanthanide(III) Complexes and Their Photonic Applications. *J. Photochem. Photobiol., C* **2004**, *5*, 183–202.
3. Armelao, L.; Quici, S.; Barigelletti, F.; Accorsi, G.; Bottaro, G.; Cavazzini, M.; Tondello, E. Design of Luminescent Lanthanide Complexes: From Molecules to Highly Efficient Photo-Emitting Materials. *Coord. Chem. Rev.* **2010**, *254*, 487–505.
4. Parker, D.; Fradgley, J. D.; Wong, K.-L. The Design of Responsive Luminescent Lanthanide Probes and Sensors. *Chem. Soc. Rev.* **2021**, *50*, 8193–8213.

5. Swavey, S.; Swavey, R. Dinuclear and Polynuclear Lanthanide Coordination Complexes Containing Polyazine Ligands: Synthesis and Luminescent Properties. *Coord. Chem. Rev.* **2009**, *253*, 2627–2638.
6. Feng, J.; Zhang, H. Hybrid Materials Based on Lanthanide Organic Complexes: A Review. *Chem. Soc. Rev.* **2013**, *42*, 387–410.
7. Reddy, M. L. P.; Sivakumar, S. Lanthanide Benzoates: A Versatile Building Block for the Construction of Efficient Light Emitting Materials. *Dalton Trans.* **2013**, *42*, 2663–2678.
8. Binnemans, K. Lanthanide-based Luminescent Hybrid Materials. *Chem. Rev.* **2009**, *109*, 4283–4374.
9. de Sá, G. F.; Malta, O. L.; de Mello Donegá, C.; Simas, A. M.; Longo, R. L.; Santa-Cruz, P. A.; da Silva, E. F., Jr. Spectroscopic Properties and Design of Highly Luminescent Lanthanide Coordination Complexes. *Coord. Chem. Rev.* **2000**, *196*, 165–195.
10. Li, P.; Li, H. Recent Progress in the Lanthanide-Complexes Based Luminescent Hybrid Materials. *Coord. Chem. Rev.* **2021**, *441*, 213988–214004.
11. Wei, C.; Ma, L.; Wei, H.; Liu, Z.; Bian, Z.; Huang, C. Advances in Luminescent Lanthanide Complexes and Applications. *Sci. China Technol. Sci.* **2018**, *61*, 1265–1285.
12. Montgomery, C. P.; Murray, B. S.; New, E. J.; Pal, R.; Parker, D. Cell-Penetrating Metal Complex Optical Probes: Targeted and Responsive Systems Based on Lanthanide Luminescence. *Acc. Chem. Res.* **2009**, *42*, 925–937.
13. Aulsebrook, M. L.; Graham, B.; Grace, M. R.; Tuck, K. L. Lanthanide Complexes for Luminescence-Based Sensing of Low Molecular Weight Analytes. *Coord. Chem. Rev.* **2018**, *375*, 191–220.
14. Wu, N.; Bo, C.; Guo, S. Luminescent Ln-MOFs for Chemical Sensing Application on Biomolecules. *ACS Sens.* **2024**, *9*, 4402–4424.
15. Matulionyte, M.; Skripka, A.; Ramos-Guerra, A.; Benayas, A.; Vetrone, F. The Coming of Age of Neodymium: Redefining Its Role in Rare Earth Doped Nanoparticles. *Chem. Rev.* **2023**, *123*, 515–554.
16. Mohanto, S.; Biswas, A.; Gholap, A. D.; Wahab, S.; Bhunia, A.; Nag, S.; Ahmed, M. G. Potential Biomedical Applications of Terbium-Based Nanoparticles (TbNPs): A Review on Recent Advancement. *ACS Biomater. Sci. Eng.* **2024**, *10*, 2703–2724.

17. Alexander, C.; Guo, Z.; Glover, P. B.; Faulkner, S.; Pikramenou, Z. Luminescent Lanthanides in Biorelated Applications: From Molecules to Nanoparticles and Diagnostic Probes to Therapeutics. *Chem. Rev.* **2025**, *125*, 2269–2370.
18. Bodman, S. E.; Butler, S. J. Advances in Anion Binding and Sensing Using Luminescent Lanthanide Complexes. *Chem. Sci.* **2021**, *12*, 2716–2734.
19. Sun, G.; Xie, Y.; Sun, L.; Zhang, H. Lanthanide Upconversion and Downshifting Luminescence for Biomolecules Detection. *Nanoscale Horiz* **2021**, *6*, 766–780.
20. Prodi, L.; Rampazzo, E.; Rastrelli, F.; Speghini, A.; Zaccheroni, N. Imaging Agents Based on Lanthanide Doped Nanoparticles. *Chem. Soc. Rev.* **2015**, *44*, 4922–4952.
21. Amoroso, A. J.; Pope, S. J. A. Using Lanthanide Ions in Molecular Bioimaging. *Chem. Soc. Rev.* **2015**, *44*, 4723–4742.
22. Su, L.; Liu, X.; Niu, Q.; Li, Z. Photoresponsive Lanthanide Luminescent Materials. *J. Mater. Chem. C* **2024**, *12*, 10759–10774.
23. Sun, S.; Zhao, Y.; Wang, J.; Pei, R. Lanthanide-Based MOFs: Synthesis Approaches and Applications in Cancer Diagnosis and Therapy. *J. Mater. Chem. B Mater. Biol. Med.* **2022**, *10*, 9535–9564.
24. Sinha, S. P. 2, 2′-Dipyridyl complexes of rare earths—III: Change in Fluorescence Intensities of Europium and Terbium Chelates on Ligand Substitution. *J. Inorg. Nucl. Chem.* **1966**, *28*, 189–193.
25. Brittain, H. G.; Richardson, F. S. pH Dependence of Circularly Polarized Emission and Total Emission from Europium (III)/L-malic Acid and Europium (III)/L-Malic Acid/Terbium (III) Complexes in Water and Water-d_2 Solutions. *Inorg. Chem.* **1976**, *15*, 1507–1511.
26. Salama, S.; Richardson, F. S. Spectroscopic Studies of Lanthanide Ion Binding to Multidentate Ligands in Aqueous Solution. 1. Malic Acid. *Inorg. Chem.* **1980**, *19*, 629–634.
27. Holz, R. C.; Meister, G. E.; Horrocks Jr, W. D. Spectroscopic characterization of a series of europium (III) amino phosphonate complexes in solution. *Inorg. Chem.*, **1990**, *29*, 5183–5189.
28. Xu, Y. Y.; Hemmilä, I. A. Analytical Application of the Co-Fluorescence Effect in Detection of Europium, Terbium, Samarium and Dysprosium with Time-Resolved Fluorimetry. *Talanta* **1992**, *39*, 759–763.

29. Werts, M. H. V.; Hofstraat, J. W.; Geurts, F. A. J.; Verhoeven, J. W. Fluorescein and Eosin as Sensitizing Chromophores in Near-Infrared Luminescent Ytterbium(III), Neodymium(III) and Erbium(III) Chelates. *Chem. Phys. Lett.* **1997**, *276*, 196–201.
30. Magennis, S. W.; Parsons, S.; Pikramenou, Z.; Corval, A.; Derek Woollins, J. Imidodiphosphinate Ligands as Antenna Units in Luminescent Lanthanide Complexes. *Chem. Commun.* **1999**, 1, 61–62.
31. Cooper, M. E.; Sammes, P. G. Synthesis and Spectral Properties of a New Luminescent Europium(III) Terpyridyl Chelate. *J. Chem. Soc., Perkin Trans. 2* **2000**, 8, 1695–1700.
32. Chen, J.; Selvin, P. R. Synthesis of 7-Amino-4-Trifluoromethyl-2-(1H)-Quinolinone and Its Use as an Antenna Molecule for Luminescent Europium Polyaminocarboxylates Chelates. *J. Photochem. Photobiol. A Chem.* **2000**, *135*, 27–32.
33. Parker, D.; Senanayake, K.; Gareth Williams, J. A. Luminescent Chemosensors for pH, Halide and Hydroxide Ions Based on Kinetically Stable, Macrocyclic Europium–Phenanthridinium Conjugates. *Chem. Commun.* **1997**, 18, 1777–1778.
34. Sabbatini, N.; Dellonte, S.; Ciano, M.; Bonazzi, A.; Balzani, V. Spectroscopic and Photophysical Properties of the Europium (III) Cryptate [Eu3+⊂ 2.2. 1]. *Chem. Phys. Lett.*, **1984**, *107*, 212–216.
35. Sabbatini, N.; Guardigli, M.; Mecati, A.; Balzani, V.; Ungaro, R.; Ghidini, E.; Casnati, A.; Pochini, A. Encapsulation of Lanthanide Ions in Calixarene Receptors. A Strongly Luminescent Terbium(3+) Complex. *J. Chem. Soc., Chem. Commun.* **1990**, *12*, 878–879.
36. Lehn, J. M.; Mathis, G. Energy Transfer Luminescence of Europium(II1) and Terbium(1Ir) Cryptates of Macrobicyclic Polypyridine Ligand. *Angew. Chem. Int. Ed.* **1987**, *26*, 266–267.
37. Piguet, C.; Williams, A. F.; Bernardinelli, G.; Buenzli, J. C. G. Structural and Photophysical Properties of Lanthanide Complexes with Planar Aromatic Tridentate Nitrogen Ligands as Luminescent Building Blocks for Triple-Helical Structures. *Inorg. Chem.* **1993**, *32*, 4139–4149.
38. Elhabiri, M.; Scopelliti, R.; Bünzli, J.-C. G.; Piguet, C. The First Lanthanide-Containing Helicates Self-Assembled in Water. *Chem. Commun.* **1998**, 21, 2347–2348.
39. Zucchi, G.; Scopelliti, R.; Pittet, P.-A.; Bünzli, J.-C. G.; Rogers, R. D. Structural and Photophysical Behaviour of Lanthanide Complexes with a Tetraazacyclododecane Featuring Carbamoyl Pendant Arms. *J. Chem. Soc., Dalton Trans.* **1999**, 6, 931–938.

40. Petoud, S.; Cohen, S. M.; Bünzli, J.-C. G.; Raymond, K. N. Stable Lanthanide Luminescence Agents Highly Emissive in Aqueous Solution: Multidentate 2-Hydroxyisophthalamide Complexes of Sm(3+), Eu(3+), Tb(3+), Dy(3+). *J. Am. Chem. Soc.* **2003**, *125*, 13324–13325.
41. Samuel, A. P. S.; Moore, E. G.; Melchior, M.; Xu, J.; Raymond, K. N. Water-Soluble 2-Hydroxyisophthalamides for Sensitization of Lanthanide Luminescence. *Inorg. Chem.* **2008**, *47*, 7535–7544.
42. O'Neil, A. T.; Chalard, A.; Malmström, J.; Kitchen, J. A. White Light and Colour-Tunable Emission from a Single Component Europium-1,8-Naphthalimide Thin Film. *Dalton Trans.* **2023**, *52*, 2255–2261.
43. Shahi, P. K.; Singh, A. K.; Rai, S. B.; Ullrich, B. Lanthanide Complexes for Temperature Sensing, UV Light Detection, and Laser Applications. *Sens. Actuators A Phys.* **2015**, *222*, 255–261.
44. Law, G.-L.; Wong, K.-L.; Tam, H.-L.; Cheah, K.-W.; Wong, W.-T. White OLED with a Single-Component Europium Complex. *Inorg. Chem.* **2009**, *48*, 10492–10494
45. Shelton, A. H.; Sazanovich, I. V.; Weinstein, J. A.; Ward, M. D. Controllable Three-Component Luminescence from a 1,8-Naphthalimide/Eu(III) Complex: White Light Emission from a Single Molecule. *Chem. Commun.* **2012**, *48*, 2749–2751.
46. Chen, J.; Xie, Z.; Meng, L.; Hu, Z.; Kuang, X.; Xie, Y.; Lu, C.-Z. Luminescence Tunable Europium and Samarium Complexes: Reversible on/off Switching and White-Light Emission. *Inorg. Chem.* **2020**, *59*, 6963–6977.
47. Su, Q.-Q.; Bao, S.-S.; Huang, X.-D.; Teng, Q.; Ma, X.-F.; Qin, Y.-H.; Zheng, L.-M. Stimuli-Responsive Lanthanide–Dianthracene Frameworks: Lanthanide-Dependent Photocycloaddition Reaction and Photophysical Properties. *Cryst. Growth Des.* **2024**, *24*, 10314–10325.
48. Huang, W.; Pan, F.; Liu, Y.; Huang, S.; Li, Y.; Yong, J.; Li, Y.; Kirillov, A. M.; Wu, D. An Efficient Blue-Emissive Metal-Organic Framework (MOF) for Lanthanide-Encapsulated Multicolor and Stimuli-Responsive Luminescence. *Inorg. Chem.* **2017**, *56*, 6362–6370.
49. Weissman, S. I. Intramolecular Energy Transfer the Fluorescence of Complexes of Europium. *J. Chem. Phys.* **1942**, *10*, 214–217.
50. Melby, L. R.; Rose, N. J.; Abramson, E.; Caris, J. C. Synthesis and Fluorescence of Some Trivalent Lanthanide Complexes. *J. Am. Chem. Soc.* **1964**, *86*, 5117–5125.

51. Latva, M.; Takalo, H.; Mukkala, V. M.; Matachescu, C.; Rodríguez-Ubis, J. C.; Kankare, J. Correlation between the lowest triplet state energy level of the ligand and lanthanide(III) luminescence quantum yield. *J. Lumin.* **1997**, *75*, 149–169.
52. Crosby, G. A.; Whan, R. E.; Alire, R. M. Intramolecular Energy Transfer in Rare Earth Chelates. Role of the Triplet State. *J. Chem. Phys.* **1961**, *34*, 743–748.
53. Fu, L.-M.; Wen, X.-F.; Ai, X.-C.; Sun, Y.; Wu, Y.-S.; Zhang, J.-P.; Wang, Y. Efficient Two-Photon-Sensitized Luminescence of a Europium(III) Complex. *Angew. Chem. Int. Ed.* **2005**, *44*, 747–750.
54. Ma, Y.; Wang, Y. Recent Advances in the Sensitized Luminescence of Organic Europium Complexes. *Coord. Chem. Rev.* **2010**, *254*, 972–990.
55. Miyazaki, S.; Miyata, K.; Sakamoto, H.; Suzue, F.; Kitagawa, Y.; Hasegawa, Y.; Onda, K. Dual Energy Transfer Pathways from an Antenna Ligand to Lanthanide Ion in Trivalent Europium Complexes with Phosphine-Oxide Bridges. *J. Phys. Chem. A* **2020**, *124*, 6601–6606.
56. Manzur, J.; Fuentealba, P.; Gil, Y.; Pérez-Obando, J.; Morales Alfaro, J.; Vega Carvallo, A. I.; Aravena, D.; Santana, R. C. de; Carneiro Neto, A. N.; Spodine, E. Tuning the Emission of Homometallic Dy^{III}, Tb^{III}, and Eu^{III} 1-D Coordination Polymers with 2,6-Di(1H-1,2,4-Triazole-1-Yl-Methyl)-4-R-Phenoxo Ligands: Sensitization through the Singlet State. *Inorg. Chem.* **2023**, *62*, 19195–19207.
57. Steemers, F. J.; Verboom, W.; Reinhoudt, D. N.; van der Tol, E. B.; Verhoeven, J. W. New Sensitizer-Modified Calix[4]Arenes Enabling near-UV Excitation of Complexed Luminescent Lanthanide Ions. *J. Am. Chem. Soc.* **1995**, *117*, 9408–9414.
58. Mara, M. W.; Tatum, D. S.; March, A. M.; Doumy, G.; Moore, E. G.; Raymond, K. N. Energy Transfer from Antenna Ligand to Europium(III) Followed Using Ultrafast Optical and X-Ray Spectroscopy. *J. Am. Chem. Soc.* **2019**, *141*, 11071–11081.
59. Comby, S.; Imbert, D.; Chauvin, A.-S.; Bünzli, J.-C. G.; Charbonnière, L. J.; Ziessel, R. F. Influence of Anionic Functions on the Coordination and Photophysical Properties of Lanthanide(III) Complexes with Tridentate Bipyridines. *Inorg. Chem.* **2004**, *43*, 7369–7379.
60. Samuel, A. P. S.; Xu, J.; Raymond, K. N. Predicting Efficient Antenna Ligands for Tb(III) Emission. *Inorg. Chem.* **2009**, *48*, 687–698.

61. Zheng, Y.; Lin, J.; Liang, Y.; Lin, Q.; Yu, Y.; Meng, Q.; Zhou, Y.; Wang, S.; Wang, H.; Zhang, H. A comparative study on the electroluminescence properties of some terbium b-diketonate complexes. *J. Mater. Chem.*, **2001**, 11, 2615–2619.
62. Souza, A. S.; Nunes, L. A.; Felinto, M. C. F. C.; Brito, H. F.; Malta, O. L. On the Quenching of Trivalent Terbium Luminescence by Ligand Low Lying Triplet State Energy and the Role of the $^7F_5$ Level: The $[Tb(tta)_3(H_2O)_2]$ Case. *J. Lumin.* **2015**, *167*, 167–171.
63. Zhuravlev, K. P.; Tsaryuk, V. I.; Kudryashova, V. A. Photoluminescence of Europium and Terbium Trifluoroacetylacetonates. Participation of LMCT State in Processes of the Energy Transfer to Eu^{3+} Ion. *J. Fluor. Chem.* **2018**, *212*, 137–143.
64. De Shazer, L. G.; Dieke, G. H. Spectra and Energy Levels of Eu^{3+} In $LaCl_3$. *J. Chem. Phys.* **1963**, *38*, 2190–2199.
65. Yan, B.; Song, Y. S. Spectroscopic Study on the Photophysical Properties of Lanthanide Complexes with 2,2′-Bipyridine-N,N′-Dioxide. *J. Fluoresc.* **2004**, *14*, 289-294.
66. Horrocks, W. D., Jr.; Albin, M. Lanthanide Ion Luminescence in Coordination Chemistry and Biochemistry. In Progress in Inorganic Chemistry; Lippard, S. J., Ed.; 1984.
67. Sivakumar, S.; Reddy, M. L. P.; Bright Green Luminescent Molecular Terbium Plastic Materials Derived from 3,5-Bis(Perfluorobenzyloxy)Benzoate. *J. Mater. Chem.* **2012**, *22*, 10852–10859.
68. Teotonio, E. E.; Fett, G. M.; Brito, H. F.; Faustino, W. M.; de Sá, G. F.; Felinto, M. C. F.; Santos, R. H. Evaluation of Intramolecular Energy Transfer Process in the Lanthanide(III) Bis-and Tris-(TTA) Complexes: Photoluminescent and Triboluminescent Behavior. *J. Lumin.* **2008**, *128*, 190–198.
69. He, Y.; Liu, L.; Zhang, Z.; Fu, G.; Lü, X.; Wong, W.-K.; Jones, R. A. A Tris-Diketonate-Eu(III) Complex with the Brominated 2,2′-Bpy Ancillary Ligand Doped in PMMA for High Color-Purity Red Luminescence. *Inorg. Chem. Commun.* **2016**, *64*, 13–15.
70. Shi, J.; Hou, Y.; Chu, W.; Shi, X.; Gu, H.; Wang, B.; Sun, Z. Crystal Structure and Highly Luminescent Properties Studies of Bis-β-Diketonate Lanthanide Complexes. *Inorg. Chem.* **2013**, *52*, 5013–5022.
71. Feng, J.; Yu, J.-B.; Song, S.-Y.; Sun, L.-N.; Fan, W.-Q.; Guo, X.-M.; Dang, S.; Zhang, H.-J. Near-Infrared Luminescent Xerogel Materials Covalently Bonded with Ternary

Lanthanide [Er(III), Nd(III), Yb(III), Sm(III)] Complexes. *Dalton Trans.* **2009**, 13, 2406–2414.

72. An, B.-L.; Gong, M.-L.; Li, M.-X.; Zhang, J.-M. Synthesis, Structure and Luminescence Properties of Samarium (III) and Dysprosium (III) Complexes with a New Tridentate Organic Ligand. *J. Mol. Struct.* **2004**, *687*, 1–6.
73. Bassett, A. P.; Magennis, S. W.; Glover, P. B.; Lewis, D. J.; Spencer, N.; Parsons, S.; Williams, R. M.; De Cola, L.; Pikramenou, Z. Highly Luminescent, Triple- and Quadruple-Stranded, Dinuclear Eu, Nd, and Sm(III) Lanthanide Complexes Based on Bis-Diketonate Ligands. *J. Am. Chem. Soc.* **2004**, *126*, 9413–9424.
74. Brittain, H. G. Intermolecular Energy Transfer between Lanthanide Complexes in Aqueous Solution. 1. Transfer from Terbium(III) to Europium(III) Complexes of Pyridinecarboxylic Acids. *Inorg. Chem.* **1978**, *17*, 2762–2766.
75. Brittain, H. G. Circularly polarized luminescence studies of the optical activity induced in the europium (III) chelate of 4, 4, 4-trifluoro-1-(2-thienyl) butane-1, 3-dionate through adduct formation with cinchona alkaloids. *J. Chem. Soc., Dalton Trans.*, **1980**, *12*, 2369–2373.
76. Horrocks Jr, W. D.; Sudnick, D. R. Lanthanide ion probes of structure in biology. Laser-induced luminescence decay constants provide a direct measure of the number of metal-coordinated water molecules. *J. Am. Chem. Soc.*, **1979**, *101*, 334–340.
77. Frey, S. T.; Chang, C. A.; Carvalho, J. F.; Varadarajan, A.; Schultze, L. M.; Pounds, K. L.; Horrocks, W. D., Jr. Characterization of Lanthanide Complexes with a Series of Amide-Based Macrocycles, Potential MRI Contrast Agents, Using Eu^{3+} Luminescence Spectroscopy and Molecular Mechanics. *Inorg. Chem.* **1994**, *33*, 2882–2889.
78. Xu, Y.-Y.; Hemmilä, I. A. Co-Fluorescence Enhancement System Based on Pivaloyltrifluoroacetone and Yttrium for the Simultaneous Detection of Europium, Terbium, Samarium and Dysprosium. *Anal. Chim. Acta* **1992**, *256*, 9–16.
79. Werts, M. H. V.; Jukes, R. T. F.; Verhoeven, J. W. The Emission Spectrum and the Radiative Lifetime of Eu^{3+} in Luminescent Lanthanide Complexes. *Phys. Chem. Chem. Phys.* **2002**, *4*, 1542–1548.
80. Bassett, A. P.; Van Deun, R.; Nockemann, P.; Glover, P. B.; Kariuki, B. M.; Van Hecke, K.; Van Meervelt, L.; Pikramenou, Z. Long-Lived Near-Infrared Luminescent Lanthanide Complexes of Imidodiphosphinate "Shell" Ligands. *Inorg. Chem.* **2005**, *44*, 6140–6142.

81. Dadabhoy, A.; Faulkner, S.; Sammes, P. G. Small Singlet–Triplet Energy Gap of Acridone Enables Longer Wavelength Sensitisation of Europium(III) Luminescence. *J. Chem. Soc., Perkin Trans. 2* **2000**, 12, 2359–2360.
82. Dadabhoy, A.; Faulkner, S.; Sammes, P. G. Long Wavelength Sensitizers for Europium(III) Luminescence Based on Acridone Derivatives. *J Chem Soc Perkin Trans 2* **2002**, 2, 348–357.
83. Mürner, H.-R.; Chassat, E.; Thummel, R. P.; Bünzli, J.-C. G. Strong Enhancement of the Lanthanide-Centred Luminescence in Complexes with 4-Alkylated 2,2′;6′,2″-Terpyridines. *J. Chem. Soc., Dalton Trans.* **2000**, 16, 2809–2816.
84. Parker, D. Taking Advantage of the pH and pO_2 Sensitivity of a Luminescent Macrocyclic Terbium Phenanthridyl Complex. *Chem. Commun.* **1998**, 2, 245–246.
85. Gunnlaugsson, T. Luminescent Europium Tetraazamacrocyclic Complexes with Wide Range pH Sensitivity. *Chem. Commun.* **1998**, 4, 511–512.
86. Gunnlaugsson, T.; Mac Dónail, D. A.; Parker, D. Luminescent Molecular Logic Gates: The Two-Input Inhibit (INH) Function. *Chem. Commun.* **2000**, 1, 93–94.
87. Prodi, L.; Maestri, M.; Balzani, V.; Lehn, J. M.; Roth, C. Luminescence Properties of Cryptate Europium (III) Complexes Incorporating Heterocyclic N-oxide Groups. *Chem. Phys. Lett.*, **1991**, *180*, 45–50.
88. Prodi, L.; Maestri, M.; Ziessel, R.; Balzani, V. 1991. Luminescent Eu^{3+}, Tb^{3+}, and Gd^{3+} Complexes of a Branched-Triazacyclononane Ligand Containing Three 2, 2'-Bipyridine Units. *Inorg. Chem.*, *30*, 3798–3802.
89. Ziessel, R.; Maestri, M.; Prodi, L.; Balzani, V.; van Dorsselaer, A.; Dinuclear Eu^{3+}, Tb^{3+}, and Gd^{3+} Complexes of a Branched Hezaazacyclooctadecane Ligand Containing Six 2, 2'-Bipyridine Pendant Units. *Inorg. Chem.*, **1993**, *32*, 1237–1241.
90. Saudan, C.; Ceroni, P.; Vicinelli, V.; Maestri, M.; Balzani, V.; Gorka, M.; Lee, S.-K.; van Heyst, J.; Vögtle, F. Cyclam-Based Dendrimers as Ligands for Lanthanide Ions. *Dalton Trans.* **2004**, 10, 1597–1600.
91. Balzani, V.; Berghmans, E.; Lehn, J. M.; Sabbatini, N.; Terörde, R.; Ziessel, R. Luminescence Properties of Eu3+ Complexes of Tripode and Tetrapode Ligands Containing 2,2'-Bipyridine Units. *Helv. Chim. Acta.* **1990**, *73*, 2083–2089.
92. Sabbatini, N.; Guardigli, M.; Manet, I.; Bolletta, F.; Ziessel, R. Synthesis and Luminescence of Lanthanide Complexes of a Branched Macrocyclic Ligand Containing

2,2'-Bipyridine and 9-Methyl-1,10-Phenanthroline Subunits. *Inorg. Chem.* **1994**, *33*, 955–959.

93. Lehn, J. M.; Pietraszkiewicz, M.; Karpiuk, J. Synthesis and Properties of Acyclic and Cryptate Europium(III) Complexes Incorporating the 3,3′-Biisoquinoline 2,2′-Dioxide Unit. *Helv. Chim. Acta.* **1990**, *73*, 106–111.
94. Paul-Roth, C. O.; Lehn, J.-M.; Guilhem, J.; Pascard, C. Synthesis, Characterization, and Structural Properties of Luminescent Lanthanide Complexes. *Helv. Chim. Acta* **1995**, *78*, 1895–1903.
95. Sabbatini, N.; Guardigli, M.; Lehn, J.-M.; Mathis, G. Luminescence of Lanthanide Cryptates: Effects of Phosphate and Iodide Anions. *J. Alloys Compd.* **1992**, *180*, 363–367.
96. Sabbatini, N.; Guardigli, M.; Lehn, J.-M. Luminescent Lanthanide Complexes as Photochemical Supramolecular Devices. *Coord. Chem. Rev.* **1993**, *123*, 201–228.
97. Piguet, C.; Williams, A. F.; Bernardinelli, G. The First Self-Assembled Dinuclear Triple-Helical Lanthanide Complex: Synthesis and Structure. *Angew. Chem., Int. Ed. Engl.* **1992**, *31*, 1622–1624.
98. Elhabiri, M.; Scopelliti, R.; Bünzli, J.-C. G.; Piguet, C. Lanthanide Helicates Self-Assembled in Water: A New Class of Highly Stable and Luminescent Dimetallic Carboxylates. *J. Am. Chem. Soc.* **1999**, *121*, 10747–10762.
99. Petoud, S.; Bünzli, J.-C. G.; Glanzman, T.; Piguet, C.; Xiang, Q.; Thummel, R. P.; Influence of Charge-Transfer States on the Eu (III) Luminescence in Mononuclear Triple Helical Complexes with Tridentate Aromatic Ligands. *J. Lumin.*, **1999**, *82*, 69–79.
100. Le Saulnier, L.; Varbanov, S.; Scopelliti, R.; Elhabiri, M.; Bünzli, J.-C. G. Lanthanide Complexes with a P-Tert-Butylcalix[4]Arene Fitted with Phosphinoyl Pendant Arms. *J. Chem. Soc., Dalton Trans.* **1999**, 22, 3919–3925.
101. Freund, C.; Porzio, W.; Giovanella, U.; Vignali, F.; Pasini, M.; Destri, S.; Mech, A.; Di Pietro, S.; Di Bari, L.; Mineo, P. Thiophene Based Europium β-Diketonate Complexes: Effect of the Ligand Structure on the Emission Quantum Yield. *Inorg. Chem.* **2011**, *50*, 5417–5429.
102. Räsänen, M.; Takalo, H.; Rosenberg, J.; Mäkelä, J.; Haapakka, K.; Kankare, J. Study on Photophysical Properties of Eu(III) Complexes with Aromatic β-Diketones – Role of Charge Transfer States in the Energy Migration. *J. Lumin.* **2014**, *146*, 211–217.

103. Bala, M.; Kumar, S.; Taxak, V. B.; Boora, P.; Khatkar, S. P. Synthesis, Photoluminescent Features and Intramolecular Energy Transfer Mechanism of Europium (III) Complexes with Fluorinate β-Diketone Ligand and Auxiliary Ligands. *J. Fluor. Chem.* **2015**, *178*, 6–13.
104. Li, H.-Y.; Wu, J.; Huang, W.; Zhou, Y.-H.; Li, H.-R.; Zheng, Y.-X.; Zuo, J.-L. Synthesis and Photoluminescent Properties of Five Homodinuclear Lanthanide (Ln^{3+}=Eu^{3+}, Sm^{3+}, Er^{3+}, Yb^{3+}, Pr^{3+}) Complexes. *J. Photochem. Photobiol. A Chem.* **2009**, *208*, 110–116.
105. Baker, M. H.; Dorweiler, J. D.; Ley, A. N.; Pike, R. D.; Berry, S. M. Structure and Emission Spectra of Dinuclear Lanthanide(III) β-Diketonate Complexes with a Bridging 2,2′-Bipyrimidine Ligand. *Polyhedron* **2009**, *28*, 188–194.
106. Irfanullah, M.; Iftikhar, K. Hypersensitivity in the Luminescence and 4f-4f Absorption Properties of Mono- and Dinuclear Eu^{III} and Er^{III} Complexes Based on Fluorinated β-Diketone and Diimine/ Bis-Diimine Ligands. *J. Fluoresc.* **2011**, *21*, 81–93.
107. Hou, Y.; Shi, J.; Chu, W.; Sun, Z. Synthesis, Crystal Structure, and near-IR Luminescent Properties of Lanthanide Bis(B-diketonate) Complexes. *Eur. J. Inorg. Chem.* **2013**, *2013*, 3063–3069.
108. Li, W.; Yan, P.; Hou, G.; Li, H.; Li, G. Efficient Red Emission from PMMA Films Doped with 5,6-DTFI Europium(III) Complexes: Synthesis, Structure and Photophysical Properties. *Dalton Trans.* **2013**, *42*, 11537–11547.
109. Bortoluzzi, M.; Reolon, A.; Castro, J.; Enrichi, F.; Albertin, G.; Bragato, C. The Conjugate Base of Methyl 3-Oxobutanoate as an Antenna Ligand in Visible-Emitting Photoluminescent Lanthanide Complexes. *RSC Adv.* **2016**, *6*, 32727–32739.
110. Nehra, K.; Dalal, A.; Hooda, A.; Bhagwan, S.; Saini, R. K.; Mari, B.; Kumar, S.; Singh, D. Lanthanides β-Diketonate Complexes as Energy-Efficient Emissive Materials: A Review. *J. Mol. Struct.* **2022**, *1249*, 131531.
111. Ahmed, Z.; Ahmed Dar, W.; Iftikhar, K. Synthesis and Luminescence Study of a Highly Volatile Sm(III) Complex. *Inorganica Chim. Acta* **2012**, *392*, 446–453.
112. Ahmed, Z.; Iftikhar, K. Sensitization of Visible and NIR Emitting Lanthanide(III) Ions in Noncentrosymmetric Complexes of Hexafluoroacetylacetone and Unsubstituted Monodentate Pyrazole. *J. Phys. Chem. A* **2013**, *117*, 11183–11201.
113. Ahmed, Z.; Iftikhar, K. Efficient Layers of Emitting Ternary Lanthanide Complexes for Fabricating Red, Green, and Yellow OLEDs. *Inorg. Chem.* **2015**, *54*, 11209–11225.

114. Ahmed, Z.; Iftikhar, K. Red, Orange-Red and near-Infrared Light Emitting Ternary Lanthanide Tris β-Diketonate Complexes with Distorted C4v Geometrical Structures. *Dalton Trans.* **2019**, *48*, 4973–4986.
115. Ahmed, Z.; Mahiya, K.; Iftikhar, K. Structures and Pure Near-Infrared Photophysics of Erbium and Ytterbium(III) Complexes Incorporating Fluorinated β-Diketone and Neutral Unidentate Ligands. *New J Chem* **2020**, *44*, 13172–13181.
116. Hasegawa, Y.; Ohkubo, T.; Nakanishi, T.; Kobayashi, A.; Kato, M.; Seki, T.; Ito, H.; Fushimi, K. Effect of Ligand Polarization on Asymmetric Structural Formation for Strongly Luminescent Lanthanide Complexes: Effect of Ligand Polarization on Luminescent Lanthanide Complexes. *Eur. J. Inorg. Chem.* **2013**, *2013*, 5911–5918.
117. Kitagawa, Y.; Kumagai, M.; Nakanishi, T.; Fushimi, K.; Hasegawa, Y. The Role of π-f Orbital Interactions in Eu(III) Complexes for an Effective Molecular Luminescent Thermometer. *Inorg. Chem.* **2020**, *59*, 5865–5871.
118. Yamamoto, M.; Kitagawa, Y.; Nakanishi, T.; Fushimi, K.; Hasegawa, Y. Ligand-Assisted Back Energy Transfer in Luminescent TbIII Complexes for Thermosensing Properties. *Chem. Eur. J.* **2018**, *24*, 17719–17726.
119. Bellucci, L.; Bottaro, G.; Labella, L.; Causin, V.; Marchetti, F.; Samaritani, S.; Dell'Amico, D. B.; Armelao, L. Composition-Thermometric Properties Correlations in Homodinuclear Eu^{3+} Luminescent Complexes. *Inorg. Chem.* **2020**, *59*, 18156–18167.
120. Hasegawa, Y.; Tsuruoka, S.-I.; Yoshida, T.; Kawai, H.; Kawai, T. Enhanced Deep-Red Luminescence of Tris(Hexafluoroacetylacetonato)Samarium(III) Complex with Phenanthroline in Solution by Control of Ligand Coordination. *J. Phys. Chem. A* **2008**, *112*, 803–807.
121. Nakagawa, T.; Hasegawa, Y.; Kawai, T. Nondestructive Luminescence Intensity Readout of a Photochromic Lanthanide(III) Complex. *Chem. Commun.* **2009**, *37*, 5630–5632.
122. Miyata, K.; Nakanishi, T.; Fushimi, K.; Hasegawa, Y. Solvent-Dependent Luminescence of Eight-Coordinated Eu(III) Complexes with Bidentate Phosphine Oxide. *J. Photochem. Photobiol. A Chem.* **2012**, *235*, 35–39.
123. Congiu, M.; Alamiry, M.; Moudam, O.; Ciorba, S.; Richardson, P. R.; Maron, L.; Jones, A. C.; Richards, B. S.; Robertson, N. Preparation and Photophysical Studies of $[Ln(hfac)_3DPEPO]$, Ln = Eu, Tb, Yb, Nd, Gd; Interpretation of Total Photoluminescence Quantum Yields. *Dalton Trans.* **2013**, *42*, 13537–13545.

124. Rajamouli, B.; Sood, P.; Giri, S.; Krishnan, V.; Sivakumar, V. A Dual-characteristic Bidentate Ligand for a Ternary Mononuclear Europium(III) Molecular Complex – Synthesis, Photophysical, Electrochemical, and Theoretical Study. *Eur. J. Inorg. Chem.* **2016**, *2016*, 3900–3911.
125. Rajamouli, B.; Devi, R.; Mohanty, A.; Krishnan, V.; Vaidyanathan, S. Effects of Electron-Withdrawing Groups in Imidazole-Phenanthroline Ligands and Their Influence on the Photophysical Properties of Eu^{III} Complexes for White Light-Emitting Diodes. *New J Chem.* **2017**, *41*, 9826–9839.
126. Boddula, R.; Vaidyanathan, S. White Light Emissive Bipolar Ligand and Their Eu^{III} Complex for White/Red Light Emitting Diodes. *J. Photochem. Photobiol. A Chem.* **2017**, *347*, 26–40.
127. Boddula, R.; Singh, K.; Giri, S.; Vaidyanathan, S. Controlled Energy Transfer from a Ligand to an EuIII Ion: A Unique Strategy to Obtain Bright-White-Light Emission and Its Versatile Applications. *Inorg. Chem.* **2017**, *56*, 10127–10130.
128. Singh, K.; Boddula, R.; Vaidyanathan, S. Versatile Luminescent Europium(III)-β-Diketonate-Imidazo-Bipyridyl Complexes Intended for White LEDs: A Detailed Photophysical and Theoretical Study. *Inorg. Chem.* **2017**, *56*, 9376–9390.
129. Gallardo, H.; Conte, G.; Tuzimoto, P.; Bortoluzzi, A.; Peralta, R. A.; Neves, A. Synthesis, Crystal Structure and Luminescent Properties of New Tris-β-Diketonate Eu(III) Complex with Thiadiazolophenanthroline Derivative Ligand. *Inorg. Chem. Commun.* **2008**, *11*, 1292–1296.
130. Zucchi, G.; Murugesan, V.; Tondelier, D.; Aldakov, D.; Jeon, T.; Yang, F.; Thuéry, P.; Ephritikhine, M.; Geffroy, B. Solution, Solid State, and Film Properties of a Structurally Characterized Highly Luminescent Molecular Europium Plastic Material Excitable with Visible Light. *Inorg. Chem.* **2011**, *50*, 4851–4856.
131. Li, X.; Zhang, D.; Li, J. Emission "Off-On" Effect from Europium Complexes Triggered by AcO Anion: Synthesis, Characterization and Sensing Performance. *Spectrochim. Acta A Mol. Biomol. Spectrosc.* **2014**, *127*, 1–9.
132. Zhao, Y. Constructing Triplet Trap in Eu(III) Complexes and Corresponding Application for Halogen Fluorescent Optical Sensing. *Spectrochim. Acta A Mol. Biomol. Spectrosc.* **2020**, *233*, 118172.
133. Khistiaeva, V. V.; Melnikov, A. S.; Slavova, S. O.; Sizov, V. V.; Starova, G. L.; Koshevoy, I. O.; Grachova, E. V. Heteroleptic β-Diketonate Ln(III) Complexes

Decorated with Pyridyl Substituted Pyridazine Ligands: Synthesis, Structure and Luminescence Properties. *Inorg. Chem. Front.* **2018**, *5*, 3015–3027.

134. Zhu, X.-H.; Wang, L.-H.; Ru, J.; Huang, W.; Fang, J.-F.; Ma, D.-G. An Efficient Electroluminescent (2,2'-bipyridine mono N-oxide) Europium(III) β-diketonate Complex. *J. Mater. Chem.* **2004**, *14*, 2732-2734.
135. Gao, L.-H.; Guan, M.; Wang, K.-Z.; Jin, L.-P.; Huang, C.-H. A Comparative Study of the Optical and Electroluminescent Properties of Eu^{III} Complexes with TTA and 2-(2′-pyridyl)Azoles: The Crystal Structure of $[Eu(TTA)_3(PBO)]$. *Eur. J. Inorg. Chem.* **2006**, *2006*, 3731–3737.
136. Swavey, S.; Krause, J. A.; Collins, D.; D'Cunha, D.; Fratini, A. X-Ray Structure and Temperature Dependent Luminescent Properties of Two Bimetallic Europium Complexes. *Polyhedron* **2008**, *27*, 1061–1069.
137. Viviani, S.; Fratini, A.; Swavey, S. The Effect of the Lanthanide Contraction on Coordination with the Polyazine Bridging Ligand 2,3-Bis(2-Pyridyl)Pyrazine (Dpp). *Inorg. Chem. Commun.* **2012**, *24*, 29–31.
138. Jang, H.; Shin, C.-H.; Jung, B.-J.; Kim, D.-H.; Shim, H.-K.; Do, Y. Synthesis and Characterization of Dinuclear Europium Complexes Showing Pure Red Electroluminescence. *Eur. J. Inorg. Chem.* **2006**, *2006*, 718–725.
139. Zucchi, G.; Jeon, T.; Tondelier, D.; Aldakov, D.; Thuéry, P.; Ephritikhine, M.; Geffroy, B. White Electroluminescence of Lanthanide Complexes Resulting from Exciplex Formation. *J. Mater. Chem.* **2010**, *20*, 2114.
140. Zucchi, G.; Le Goff, X. F. Magneto-Structural and Photophysical Investigations on a Dinuclear Sm(III) Complex Featuring 2,2′-Bipyrimidine. *Inorganica Chim. Acta* **2012**, *380*, 354–357.
141. Boddula, R.; Vaidyanathan, S. Bi-Nuclear Luminescent Europium(III) Molecular Complexes for White Light Emitting Diodes: Experimental and Theoretical Study. *Inorganica Chim. Acta* **2019**, *494*, 141–153.
142. Accorsi, G.; Armaroli, N.; Cardinali, F.; Wang, D.; Zheng, Y. Synthesis and Photoluminescence Properties of Heteroleptic Eu^{3+}, Tb^{3+} and Tm^{3+} Complexes. *J. Alloys Compd.* **2009**, *485*, 119–123.
143. De Silva, C. R.; Wang, R.; Zheng, Z. Highly Luminescent Eu(III) Complexes with 2,4,6-Tri(2-Pyridyl)-1,3,5-Triazine Ligand: Synthesis, Structural Characterization, and Photoluminescence Studies. *Polyhedron* **2006**, *25*, 3449–3455.

144. Stanley, J. M.; Zhu, X.; Yang, X.; Holliday, B. J. Europium Complexes of a Novel Ethylenedioxythiophene-Derivatized Bis(Pyrazolyl)Pyridine Ligand Exhibiting Efficient Lanthanide Sensitization. *Inorg. Chem.* **2010**, *49*, 2035–2037.

145. Kuramochi, Y.; Nakagawa, T.; Yokoo, T.; Yuasa, J.; Kawai, T.; Hasegawa, Y. Eu(III) Emission Band Changes Caused by Peripheral C-H/O Hydrogen Bonding. *Dalton Trans.* **2012**, *41*, 6634–6640.

146. Yang, C.; Fu, L.-M.; Wang, Y.; Zhang, J.-P.; Wong, W.-T.; Ai, X.-C.; Qiao, Y.-F.; Zou, B.-S.; Gui, L.-L. A Highly Luminescent Europium Complex Showing Visible-Light-Sensitized Red Emission: Direct Observation of the Singlet Pathway. *Angew. Chem. Int. Ed.* **2004**, *43*, 5010–5013.

147. Hao, R.; Li, M.; Wang, Y.; Zhang, J.; Ma, Y.; Fu, L.; Wen, X.; Wu, Y.; Ai, X.; Zhang, S.; Wei, Y. A Europium Complex with Excellent Two-photon-sensitized Luminescence Properties. *Adv. Funct. Mater.* **2007**, *17*, 3663–3669.

148. De Silva, C. R.; Maeyer, J. R.; Dawson, A.; Zheng, Z. Adducts of Lanthanide β-Diketonates with 2,4,6-Tri(2-Pyridyl)-1,3,5-Triazine: Synthesis, Structural Characterization, and Photoluminescence Studies. *Polyhedron* **2007**, *26*, 1229–1238.

149. Li, D.-P.; Li, C.-H.; Wang, J.; Kang, L.-C.; Wu, T.; Li, Y.-Z.; You, X.-Z. Synthesis and Physical Properties of Two Chiral Terpyridyl Europium(III) Complexes with Distinct Crystal Polarity. *Eur. J. Inorg. Chem.* **2009**, *2009*, 4844–4849.

150. Chen, Z.; Ding, F.; Hao, F.; Guan, M.; Bian, Z.; Ding, B.; Huang, C. Synthesis and Electroluminescent Property of Novel Europium Complexes with Oxadiazole Substituted 1,10-Phenanthroline and 2,2'-Bipyridine ligands. *New J. Chem.* **2010**, *34*, 487–494

151. Gupta, K.; Patra, A. K. A Luminescent pH-responsive Ternary Europium(III) Complex of β-diketonates and Terpyridine Derivatives as Sensitizing Antennae – Photophysical Aspects, Anion Sensing, and Biological Interactions: *Eur. J. Inorg. Chem.* **2018**, *2018*, 1882–1890.

152. Abbas, Z.; Dasari, S.; Beltrán-Leiva, M. J.; Cantero-López, P.; Páez-Hernández, D.; Arratia-Pérez, R.; Butcher, R. J.; Patra, A. K. Luminescent Europium(III) and Terbium(III) Complexes of β-Diketonate and Substituted Terpyridine Ligands: Synthesis, Crystal Structures and Elucidation of Energy Transfer Pathways. *New J Chem* **2019**, *43*, 15139–15152.

153. Yadav, U.; Verma, M.; Abbas, Z.; Sivakumar, S.; Patra, A. K. An Emissive Dual-Sensitized Bimetallic Eu_2^{III}-Bioprobe: Design Strategy, Biological Interactions, and Nucleolus Staining Studies. *New J Chem* **2022**, *46*, 16007–16018.
154. Fioravanti, L.; Bellucci, L.; Armelao, L.; Bottaro, G.; Marchetti, F.; Pineider, F.; Poneti, G.; Samaritani, S.; Labella, L. Stoichiometrically Controlled Assembly of Lanthanide Molecular Complexes of the Heteroditopic Divergent Ligand 4'-(4-Pyridyl)-2,2':6',2″-Terpyridine N-Oxide in Hypodentate or Bridging Coordination Modes. Structural, Magnetic, and Photoluminescence Studies. *Inorg. Chem.* **2022**, *61*, 265–278.
155. Moudam, O.; Rowan, B. C.; Alamiry, M.; Richardson, P.; Richards, B. S.; Jones, A. C.; Robertson, N. Europium Complexes with High Total Photoluminescence Quantum Yields in Solution and in PMMA. *Chem. Commun.* **2009**, 43, 6649–6651.
156. Raj, D. B. A.; Francis, B.; Reddy, M. L. P.; Butorac, R. R.; Lynch, V. M.; Cowley, A. H. Highly Luminescent Poly(Methyl Methacrylate)-Incorporated Europium Complex Supported by a Carbazole-Based Fluorinated β-Diketonate Ligand and a 4,5-Bis(Diphenylphosphino)-9,9-Dimethylxanthene Oxide Co-Ligand. *Inorg. Chem.* **2010**, *49*, 9055–9063.
157. Iftikhar, K.; Hasan, N. Syntheses, Crystal Structure and Photophysical Properties of [Sm(Dbm)3(Impy)] and $[Tb(dbm)_3(Impy)]$ and Their Hybrid Films. *New J Chem* **2019**, *43*, 4391–4405.
158. Hasan, N.; Iftikhar, K. Synthesis, Crystal Structure and Photoluminescence Studies of $[Eu(dbm)_3(Impy)]$ and Its Polymer-Based Hybrid Film. *New J Chem* **2019**, *43*, 2479–2489.
159. Boddula, R.; Tagare, J.; Singh, K.; Vaidyanathan, S. White Light-Emissive Europium Complexes and Their Versatile Applications. *Mater. Chem. Front.* **2021**, *5*, 3159–3175.
160. Wang, H.; Wan, Y.; Du, H.; Lyu, H.; Wang, D. Preparation and Photoluminescent Behaviors of Bipyrimidine Bridged Dinuclear Eu (III) Complexes and Their PMMA Polymer Films. *J. Lumin.* **2022**, *244*, 118703.
161. Kai, J.; Felinto, M. C. F. C.; Nunes, L. A. O.; Malta, O. L.; Brito, H. F. Intermolecular energy transfer and photostability of luminescence-tuneable multicolour PMMA films doped with lanthanide–β-diketonate complexes. *J. Mater. Chem.*, **2011**, *21*, 3796.
162. Kuriki, K.; Koike, Y.; Okamoto, Y. Plastic Optical Fiber Lasers and Amplifiers Containing Lanthanide Complexes. *Chem. Rev.* **2002**, *102*, 2347–2356.

163. Carlos, L. D.; Ferreira, R. A. S.; de Zea Bermudez, V.; Julián-López, B.; Escribano, P. Progress on Lanthanide-Based Organic-Inorganic Hybrid Phosphors. *Chem. Soc. Rev.* **2011**, *40*, 536–549.

164. Kitagawa, Y.; Ohno, R.; Nakanishi, T.; Fushimi, K.; Hasegawa, Y. Solvent-Dependent Dual-Luminescence Properties of a Europium Complex with Helical π-Conjugated Ligands. *Photochem. Photobiol. Sci.* **2017**, *16*, 683–689.

165. Dar, W. A.; Iftikhar, K. Phase Controlled Colour Tuning of Samarium and Europium Complexes and Excellent Photostability of Their PVA Encapsulated Materials. Structural Elucidation, Photophysical Parameters and the Energy Transfer Mechanism in the Eu^{3+} Complex by Sparkle/PM3 Calculations. *Dalton Trans.* **2016**, *45*, 8956–8971.

166. Rajamouli, B.; Sood, P.; Giri, S.; Krishnan, V.; Sivakumar, V. A Dual-characteristic Bidentate Ligand for a Ternary Mononuclear Europium(III) Molecular Complex – Synthesis, Photophysical, Electrochemical, and Theoretical Study: *Eur. J. Inorg. Chem.* **2016**, *2016*, 3900–3911.

167. Ilmi, R.; Khan, M. S.; Li, Z.; Zhou, L.; Wong, W.-Y.; Marken, F.; Raithby, P. R. Utilization of Ternary Europium Complex for Organic Electroluminescent Devices and as a Sensitizer to Improve Electroluminescence of Red-Emitting Iridium Complex. *Inorg. Chem.* **2019**, *58*, 8316–8331.

168. Shahi, P. K.; Singh, A. K.; Singh, S. K.; Rai, S. B.; Ullrich, B. Revelation of the Technological Versatility of the $Eu(TTA)_3Phen$ Complex by Demonstrating Energy Harvesting, Ultraviolet Light Detection, Temperature Sensing, and Laser Applications. *ACS Appl. Mater. Interfaces* **2015**, *7*, 18231–18239.

169. Lapaev, D. V.; Nikiforov, V. G.; Lobkov, V. S.; Knyazev, A. A.; Ziyatdinova, R. M.; Galyametdinov, Y. G. A Vitrified Film of an Anisometric Europium(III) β-Diketonate Complex with a Low Melting Point as a Reusable Luminescent Temperature Probe with Excellent Sensitivity in the Range of 270–370 K. *J. Mater. Chem. C Mater. Opt. Electron. Devices* **2020**, *8*, 6273–6280.

****

Chapter 2

Synthesis, characterization, luminescence properties and deciphering the role of terpyridyl-imidazole based ligand on dissimilar luminescence sensitization of ternary lanthanide(III) tris-(β-diketonate) complexes

2.1. Introduction

Appropriate design of trivalent lanthanide complexes is of pivotal importance for the development of potential light harvesting materials by taking advantage of their fascinating photo-luminescence properties.[1-4] The lanthanide complexes exhibit typical narrow monochromatic emission (high colour purity) together with large pseudo-Stokes shift and long excited-state lifetimes which make them fundamentally distinctive from other regular fluorescent probes. This is because of the presence of deep-seated 4f electrons, which remain unperturbed in presence of external ligand field. These properties make the lanthanide complexes as potential building blocks in diverse field of applications such as in laser sources, luminescent sensors, bio-imaging, drug delivery and medical diagnosis, to name a few.[5-15] But because of the symmetry forbidden characteristics of intra-configurational f-f transitions, the lanthanide complexes usually exhibit very weak luminescence which is the major deterrent for their potential light harvesting applications.[16,17] Several strategies have been adopted to overcome the discrepancies as well as to improve the luminescence characteristics of the lanthanides.[1,2]

Among the different strategies, anchoring of judicially chosen light harvesting organic chromophore with high molar absorption coefficients (ε>10000 M^{-1} cm^{-1}) could circumvent this problem.[6,18] The light absorbed by the organic chromophore could in turn excite the lanthanide core. This 'antenna effect' offers an indirect sensitization of the Ln^{III} ion and often provides substantial enhancement of luminescence intensity, quantum yield and lifetime.[4,8,19-21] Thus, tailored design of appropriate ligands could give rise to lanthanide complexes with enhanced luminescence characteristics.[22-23] It is worth-mentioning that the ligand(s) being employed should possess appropriate singlet and triplet energy levels that should match with the lowest excited state of corresponding trivalent lanthanide ion in accordance to Reinhoult's and Latva's empirical rules.[1,2,24] The photoluminescence generated from the trivalent lanthanide ions is proportional to the efficacy of energy transfer from the antenna/sensitizer ligand. In this regard, β-diketonate ligands have been widely employed as these ligands not only provide charge balance to the metal ions but also sensitize the lanthanide center creating innocent coordination environment.[25] Additionally, one can modulate the energy levels of the β-diketonates upon substitution of appropriate moiety or by incorporating another chromophoric segment to cater the need.[25-27] In spite of presenting themselves as one of the best candidates for effective sensitization of the lanthanide ions, it has been noted that the β-

diketonate ligands lack selectivity towards lanthanide ions in terms of sensitization, thereby only yield a monochromatic luminescence as anticipated for the respective lanthanides.[1-4]

The primary objective of the present work is to utilize polypyridine-based ancillary ligand in combination with β-diketonates to modulate the photophysics in general and luminescence characteristics in particular of the resulting lanthanide complexes. Presently, we have squeezed our interest on three lanthanide ions (viz., Eu^{III}, Sm^{III}, Tb^{III}) along with La^{III} itself in terms of having facility to measure the photophysical properties in the visible domain. Upon going through the literature, it appears that among the polypyridines, bidentate bipyridine-type chelating units are mostly employed for the designing of mixed-ligand lanthanide complexes.[28-36] By contrast, the systems comprising of tridentate terpyridine-type chelating motif together with β-diketonate are relatively sparse.[16,37-41] Our research group has been working since last one decade on the design and synthesis of a wide variety of terpyridine-type ligands covalently coupled with both electron-pushing and electron withdrawing groups as well as by incorporating different types of aromatic and heteroaromatic moieties.[42,44,46] We also thoroughly investigated ground- and excited state photophysical and electrochemical behaviours of 4d and 5d metals {mainly Ru(II) and Os(II}.[43,45,47-49] After careful scrutiny of the structure as well as the absorption and emission spectral behaviors, we anticipated that one of our previously reported terpyridyl-imidazole-based receptors, viz. 2-(4-[2,2′:6′,2″]Terpyridin-4′-yl-phenyl)-1*H*-phenanthro[9,10-*d*] imidazole (tpy-HImzphen) might be a good choice to serve our need. The said terpyridine ligand coupled with phenyl-phenanthro-imidazole spacer appropriately adjusts its excited state energy position so that effective sensitization of the lanthanide core could be feasible. Additionally, we have chosen 2-thenoyltrifluoroacetone (Htta) as a favourable β-diketonate, because of the presence of low-energy C-F bonds, which induce rigidity and thereby limit the non-radiative deactivation of Ln^{III} excited state energy as compared to high-energy oscillators, viz. C–H, N-H, O-H bonds.[18,50]

Herein, we report synthesis of four lanthanide complexes of the form, $Ln(tta)_3$(tpy-HImzphen) (Ln = La^{III}, Eu^{III}, Sm^{III}, and Tb^{III}) and their thorough characterization via standard analytical tools including single crystal X-ray diffraction. The photophysical properties of all the complexes were thoroughly investigated via absorption and both steady state and time-resolved emission spectroscopic techniques at room temperature and 77K to understand the deactivation dynamics of the excited states as well as to elucidate the distinctive luminescence responses of the lanthanide complexes.

2.2. Experimental Section

2.2.1. Materials. 2-Theonyltrifluoroacetone (Htta) and all the lanthanide salt containing either chloride or nitrate counter anions were purchased from Merck. The ligand precursor, 4′-(*p*-formyl phenyl)-2,2′:6′,2″-terpyridine (tpy-PhCHO) and 9,10-phenanthrenedione were synthesized by following the reported literature method.[51] All the photophysical measurements were carried out in dry and decontaminated solvents. We purified and distilled the solvents following standard literature procedures.[52]

2.2.2. Synthesis of the Ligand (tpy-HImdzphen). The ligand was synthesized by following our reported literature procedure (Scheme 2.1).[44] A mixture of 4′-(*p*-formylphenyl)-2,2′:6′,2″-terpyridine (tpy-PhCHO) (337 mg, 1.0 mmol), 9,10-phenanthrenedione (230 mg, 1.1 mmol), and ammonium acetate (1.6 g, 20 mmol) is refluxed in acetic acid and produces a pale-yellow solution, which upon pouring into an ice-water mixture, produces a pale-yellow solid. The solid is collected by filtration, washed several times with water, and upon recrystallization from a chloroform-methanol (1:1) mixture, produces a light yellow crystalline solid (370 mg, 0.70 mmol, yield 70%). ^{1}H NMR (DMSO-d_6, 500 MHz, δ/ppm) = 13.60 (s, 1H, NH(imidazole), 8.86 (d, 2H, J = 8.5 Hz, H_9), 8.82 (s, 2H, H_9), 8.79 (d, 2H, J = 4.0 Hz, H_6), 8.69 (d, 2H, J = 8.0, H_3), 8.60 (d, 2H, J = 8.0 Hz, H_{12}), 8.53 (d, 2H, J = 8.0 Hz, H_8), 8.20 (d, 2H, J = 8.5 Hz, H_7), 8.05 (t, 2H, J = 7.5 Hz, H_4), 7.75 (t, 2H, J = 7.5 Hz, H_{11}), 7.65 (t, 2H, J = 7.7 Hz, H_{10}), 7.54 (t, 2H, J = 6.0 Hz, H_5). ESI-MS: m/z 525.51 ([tpy-HImdzphen+H]$^+$). Elemental analysis: Anal. Calcd for $C_{36}H_{23}N_5$: C, 82.26; H, 4.41; N, 13.32. Found: C, 82.18; H, 4.44; N, 13.29.

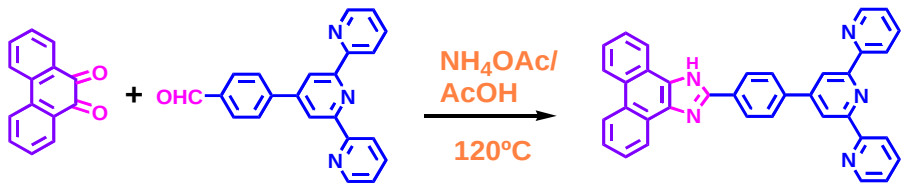

Scheme 2.1. Synthesis of the Ligand (tpy-HImdzphen)

2.2.3. Synthesis of $Ln(tta)_3(H_2O)_2$. All the four lanthanide precursors of the type, $Ln(tta)_3(H_2O)_2$, Ln^{III}= La^{III}, Eu^{III}, Sm^{III}, and Tb^{III} are synthesized by following the reported literature procedure (Scheme 2.2).[53] 2-theonyltrifluoroacetone (333 mg, 1.5mM) is dissolved in ethanol-water mixture (1:1, v/v) and kept for a few minutes after adding 1.5 mM aqueous solution of NaOH. $LnCl_3 \cdot xH_2O$ (x=6 or 7) is then added to the mixture and stirred for 2h at

60ºC. A white crystalline product was found, which was then filtered and dried in a vacuum desiccator for 2d.

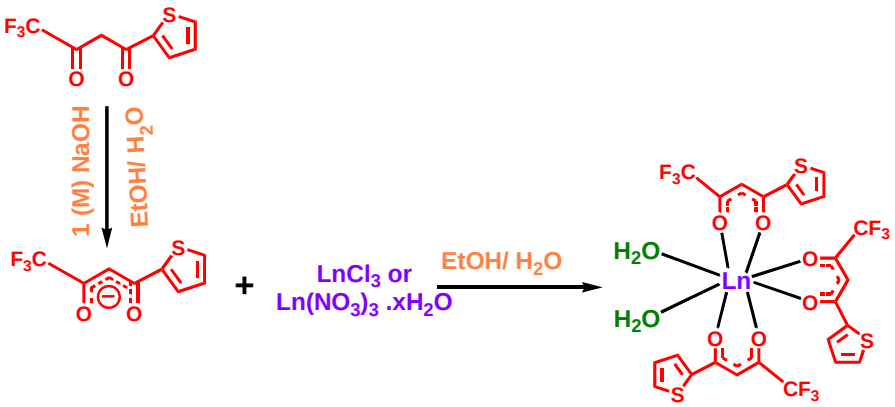

Scheme 2.2. Synthesis of the Ln^{III} Precursors, $Ln(tta)_3(H_2O)_2$ [Ln=La, Eu, Sm, Tb]

$La(tta)_3(H_2O)_2$ $LaCl_3 \cdot 7H_2O$ (186 mg, 0.5 mmol). Yield 235 mg (28 %). FT-IR: υ (in cm^{-1}) =1610, 3360. Anal. Calcd for $C_{24}H_{16}F_9S_3O_8La$: C, 34.38; H, 1.92. Found: C, 34.26; H, 1.86. ^{1}H NMR (DMSO-d_6, 400 MHz, δ/ppm): 8.02 (d, 3H, H_2; J = 8.00 Hz), 7.97 (d, 3H, H_4; J = 8.00 Hz), 7.25 (t, 3H, H_3; J = 4.36 Hz), 6.40 (s, 3H, H_1 methine).

$Eu(tta)_3(H_2O)_2$ $EuCl_3 \cdot 6H_2O$ (183 mg, 0.5 mmol). Yield 252 mg (30 %). FT-IR: υ (in cm^{-1}) =1603, 3351. Anal. Calcd for $C_{24}H_{16}F_9S_3O_8Eu$: C, 33.85; H, 1.89. Found: C, 33.78; H, 1.84. ^{1}H NMR (DMSO-d_6, 400 MHz, δ/ppm): 8.00 (d, 3H, H_2; J = 4.80 Hz), 7.95 (d, 3H, H_4; J = 3.92 Hz), 7.24 (t, 3H, H_3; J = 4.84 Hz), 1.10 (s, 3H, H_1 methine).

$Sm(tta)_3(H_2O)_2$ $SmCl_3 \cdot 6H_2O$ (182 mg, 0.5 mmol). Yield 216 mg (25 %). FT-IR: υ (in cm^{-1}) =1602, 3353. Anal. Calcd for $C_{24}H_{16}F_9S_3O_8Sm$: C, 33.92; H, 1.90; Found: C, 33.86; H, 1.83. ^{1}H NMR (DMSO-d_6, 400 MHz, δ/ppm): 8.13 (s, 3H, H_1 methine), 7.55 (s, 3H, H_2), 7.32 (s, 3H, H_3), 7.21 (t, 3H, H_4; J = 4.56 Hz).

$Tb(tta)_3(H_2O)_2$ $TbCl_3 \cdot 6H_2O$ (187 mg, 0.5 mmol). Yield 227 mg (26 %). FT-IR: υ (in cm^{-1}) =1601, 3400. Anal. Calcd for $C_{24}H_{16}F_9S_3O_8Tb$: C, 33.58; H, 1.88. Found: C, 33.55; H, 1.81. ^{1}H NMR (DMSO-d_6, 400 MHz, δ/ppm): 95.97 (s, 3H, H_1 methine), 29.14 (s, 3H, H_2), 12.22 (s, 3H, H_3), 6.65 (s, 3H, H_4).

2.2.4. Synthesis of the Lanthanide Complexes, $Ln(tta)_3$(tpy-HImzphen). A general synthetic protocol has been adopted for the synthesis of all the four lanthanide complexes, $Ln(tta)_3$**(**tpy-HImzphen**)**, Ln^{III}=La^{III} (**1**), Eu^{III} (**2**), Sm^{III} (**3**), and Tb^{III} (**4**) (Scheme 2.3). To a stirred suspension of tpy-HImzphen (20 mg, 0.038 mmol) in a chloroform-methanol (1:1 v/v) mixture, equimolar amount of respective $Ln(tta)_3(H_2O)_2$ precursor complex is added and

stirred magnetically for 6h at 60ºC. The resulting mixture is vacuum dried and then dissolved in a small amount (~5 mL) of dichloromethane and layered with hexane. After keeping for a few hours, the microcrystalline solid that deposited was filtered and then dried in vacuum desiccators.

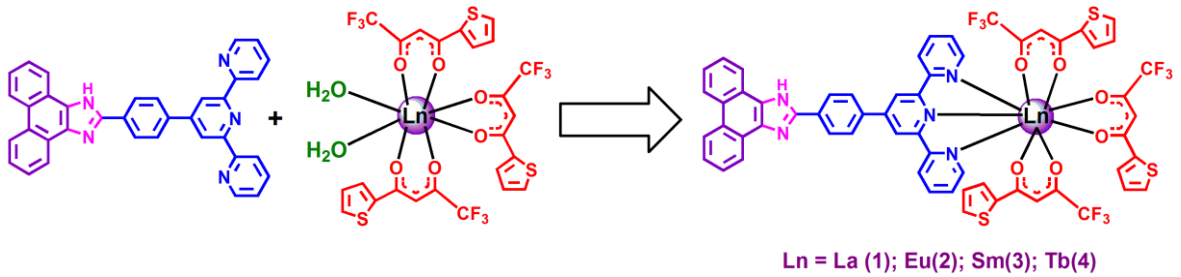

Scheme 2.3. The tpy-HImzphen Ligand, Lanthanide Precursors and Four Lanthanide Complexes Ln(tta)$_3$(tpy-HImzphen) (1-4) under Present Study

La(tta)$_3$(tpy-HImzphen) (1) La(tta)$_3$(H$_2$O)$_2$ (32 mg, 0.038 mmol); Yield: 36 mg (72%). Anal. Calcd. for $C_{60}H_{35}F_9S_3O_6N_5La$: C, 54.26; H, 2.66; N, 5.27. Found: C, 54.17; H, 2.56; N, 5.21. FT-IR: υ (in cm^{-1}) = 1535, 1605, 3250. MALDI-TOF (DCTB, positive mode): *m/z* = 1106.17 (100 %) [M-tta]$^+$. ^{1}H NMR (DMSO-d_6, 400 MHz, δ/ppm): 13.66 (s, 1H, NH(imidazole), 8.88 (d, 2H, *J* = 5.48 Hz, H$_{12}$), 8.85 (s, 2H, H$_9$), 8.81 (d, 2H, *J* = 5.3 Hz, H$_8$), 8.72 (d, 2H, *J* = 8.3 Hz, H$_5$), 8.63 (t, 2H, *J* = 8.0 Hz, H$_{15}$), 8.56 (d, 2H, *J* = 8.3 Hz, H$_{11}$), 8.22 (d, 2H, *J* = 7.4 Hz, H$_{10}$), 8.06 (d, 2H, *J* = 5.9 Hz, H$_6$), 7.80 (m, 6H; H$_2$, H$_4$), 7.74 (d, 2H, *J* = 8.0 Hz, H$_{14}$), 7.67 (d, 2H, *J* = 8.0 Hz, H$_{13}$), 7.56 (t, 2H, *J* = 6.0 Hz, H$_7$), 7.12 (t, 3H, *J* = 4.0 Hz, H$_3$), 6.18 (s, 3H, H$_1$ methine).

Eu(tta)$_3$(tpy-HImzphen) (2) Eu(tta)$_3$(H$_2$O)$_2$ (33 mg, 0.038 mmol); Yield: 37 mg (75%). Anal. Calcd for $C_{60}H_{35}F_9S_3O_6N_5Eu$: C, 53.74; H, 2.63; N, 5.22. Found: C, 53.67; H, 2.58; N, 5.18. FT-IR: υ (in cm^{-1}) = 1534, 1607, 3105. MALDI-TOF (DCTB, positive mode): *m/z* = 1120.143 (100%) [M-tta]$^+$ ^{1}H NMR (DMSO-d_6, 400 MHz, δ/ppm): 13.66 (s, 1H, NH(imidazole), 8.85 (s, 2H, H$_{12}$), 8.81 (d, 2H, *J* = 8.0 Hz, H$_9$), 8.78 (t, 2H, *J* = 4.0 Hz, H$_8$), 8.70 (t, 2H, *J* = 8.0, H$_5$), 8.63 (t, 2H, *J* = 8.0 Hz, H15), 8.55 (d, 2H, *J* = 8.0 Hz, H$_{11}$), 8.22 (d, 2H, *J* = 8.0 Hz, H$_{10}$), 8.06 (d, 2H, *J* = 8.0 Hz, H$_6$), 7.66 (d, 2H, *J* = 4.0 Hz, H$_{14}$), 7.56 (m, 2H, H$_{13}$), 7.44 (s, 2H, H$_7$), 7.36 (s, 3H, H$_4$), 6.48 (s, 3H, H$_3$), 6.36 (s, 3H, H$_2$), 4.51 (s, 3H, H$_1$ methine).

Sm(tta)$_3$(tpy-HImzphen) (3) Sm(tta)$_3$(H$_2$O)$_2$ (32 mg, 0.038 mmol); Yield: 31 mg (63%). Anal. Calcd for $C_{60}H_{35}F_9S_3O_6N_5Sm$: C, 53.80; H, 2.63; N, 5.23. Found: C, 53.72; H, 2.54; N, 5.18. FT-IR: υ (in cm^{-1}) = 1536, 1609, 3080. MALDI-TOF (DCTB, positive mode):

m/z= 1118.18 (100%) $[M\text{-tta}]^+$ ^{1}H NMR (DMSO-d_6, 400 MHz, δ/ppm): 13.66 (s, 1H, NH(imidazole), 8.85 (s, 2H, H_{12}), 8.82 (m, 2H, H_9), 8.78 (s, 2H, H_8), 8.70 (s, 2H, H_5), 8.63 (t, 2H, *J* = 8.0 Hz, H_{15}), 8.56 (d, 2H, *J* = 8.0 Hz, H_{11}), 8.22 (d, 2H, *J* = 8.0 Hz, H_{10}), 8.13 (s, 3H, H_1 methine), 8.06 (d, 2H, *J* = 8.0 Hz, H_6), 7.85 (t, 2H, *J* = 4.0 Hz, H_{14}), 7.77 (d, 2H, *J* = 8.0 Hz, H_{13}), 7.67 (d, 2H, *J* = 4.0 Hz, H_7), 7.55 (t, 3H, *J* = 6.44 Hz, H_2), 7.32 (s, 3H, H_3), 7.21 (s, 3H, H_4).

Tb(tta)$_3$(tpy-HImzphen) (4) $Tb(tta)_3(H_2O)_2$ (33 mg, 0.038 mmol); Yield: 33 mg (67%). Anal. Calcd for $C_{60}H_{35}F_9S_3O_6N_5Tb$: C, 53.46; H, 2.62; N, 5.20. Found: C, 53.36; H, 2.57; N, 5.13. FT-IR: υ (in cm^{-1}) = 1538, 1607, 3104. MALDI-TOF (DCTB, positive mode): *m/z*= 1126.01 (100%) $[M\text{-tta}]^+$. ^{1}H NMR (DMSO-d_6, 400 MHz, δ/ppm): 95.20 (s, 3H, H_1 methine), 29.00 (s, 3H, H_2), 13.76 (s, 1H, NH(imidazole), 12.16 (s, 3H, H_3), 8.97 (m, 2H, H_{12}), 8.95 (s, 2H, H_9), 8.86 (d, 2H, *J* = 4.52 Hz, H_8), 8.79 (d, 2H, *J* = 8.0Hz, H_5), 8.73 (d, 2H, *J* = 8.0 Hz, H15), 8.65 (d, 2H, *J* = 8.0 Hz, H_{11}), 8.32 (d, 2H, *J* = 8.0 Hz, H_{10}), 8.08 (t, 2H, *J* = 8.0 Hz, H_6), 7.84 (m, 2H, H_{14}), 7.72 (m, 2H, H_{13}), 7.58 (m, 2H, H_7), 6.58 (s, 3H, H_4).

2.2.5. Instruments and Physical Methods. Infrared spectra of the complexes were recorded in the range 4000-400 cm^{-1} with a PerkinElmer FT-IR spectrometer (spectrum two) with the samples following the attenuated total reflectance (ATR) technique. MALDI was performed on a Bruker Daltonics Autoflex Speed MALDI-TOF system (GT0263G201) using *trans*-2-[3-(4-*tert*-Butylphenyl)-2-methyl-2-propenylidene]malononitrile (DCTB) as the matrix. NMR spectra of the compounds were acquired in DMSO-d_6 on a Bruker 400 MHz spectrometer using tetramethylsilane (TMS) as an internal standard, and the data were analyzed by Mestre Nova software. Thermogravimetric Analysis (TGA) was executed in a PerkinElmer Thermogravimetric Analyzer (TGA 4000) instrument in a N_2 atmosphere between 30 °C and 800 °C at a heating rate of 10 °C min^{-1}. UV-vis absorption spectra of the complexes were recorded with a Shimadzu UV 1800 spectrometer. Steady-state luminescence spectra were recorded from a Horiba Fluoromax-4 spectrofluorimeter. Luminescence lifetime measurements were carried out by using time–correlated single photon counting (TCSPC) as well as multi-channel scaling (MCS) set up from Horiba (Deltaflex), and the luminescence decay data were analyzed by using Eztime software. Spectrophotometric titrations and solvatochromic studies were carried out with the compounds having concentration in the order ~10^{-5} M. The relative quantum yield at room temperature was measured for all the four complexes (**1-4**) in dichloromethane solvent, using

quinine sulfate in 1N H_2SO_4 (η=1.338, Φ = 0.546) as reference for the system. In this regard, we have utilized a general equation 2.1[54] for the calculation of quantum yield:

$$\frac{\Phi_s}{\Phi r} = \frac{A_r \eta_s^2 I_s}{A_s \eta_r^2 I_r} \quad \text{.. (2.1)}$$

where 'r' represents the reference and 's' the sample. 'A' implies the absorbance at the excitation wavelength, whereas 'I' is the integrated luminescence intensity, and 'η' represents the refractive index of the solution. The refractive index is supposed to be equivalent to that of the pure solvent (η = 1.424 for dichloromethane). The single-crystal X-ray diffraction data of complex **5** were collected on a Bruker AXS SMART APEX CCD diffractometer. Data were integrated using CrysAlis^{Pro} software with a narrow frame algorithm. Data were subsequently corrected for absorption by the program SCALE3 ABSPACK scaling algorithm. All the structures were solved by the direct methods in SHELXTL[55a] and refined by the full-matrix least-squares method on F^2 (SHELXL-2014)[55b] using the Olex-2 software.[55c] All the non-hydrogen atoms were refined with anisotropic thermal parameters. All the hydrogen atoms were included in idealized positions, and a riding model was used. All the mean plane analyses and crystallographic figures have been generated using the DIAMOND software (version 3.2k).[55d] In addition, some disordered solvent molecules were present in complex **5**. We could not solve the disorder of the solvent molecules properly due to the weak residual Q peaks. So, the Olex-2 mask program was applied to remove the disordered solvent molecules. The possible masked electron counts for void volumes are calculated as 58, which is assigned to be two acetonitrile (2x19) and two water molecules (2x10).

2.3. Results and Discussion

2.3.1. Synthesis and Characterization. All the four Ln^{III} complexes were synthesized in a straightforward manner upon refluxing a 1:1 molar ratio of the terpyridyl-imidazole ligand with respective lanthanide precursor, $Ln(tta)_3(H_2O)_2$, in chloroform-methanol (1:1 v/v) mixture. The complexes were finally purified upon diffusing hexane to their dichloromethane solutions at ambient temperature, and the products were obtained in reasonably good yields. All these complexes were thoroughly characterized by elemental analysis, FT-IR spectroscopy, ^1H NMR spectroscopy, matrix-assisted laser desorption

ionization-time of flight (MALDI-TOF) mass spectrometry, and thermogravimetric analysis. A structure of an in situ-generated complex is also determined via single-crystal X-ray diffraction analysis.

2.3.2. FT-IR Spectra. IR spectra of the complexes (**1-4**) together with the lanthanide precursors and the tpy-HImzphen ligand were acquired, and related spectra as well as selected stretching frequencies of the complexes are presented in Figure 2.1 and Table 2.1. The ligand shows a peak at ~1583 cm^{-1} due to C=N stretching of the pyridine moieties and a characteristic peak at ~3180 cm^{-1} for imidazole N-H stretch. All the lanthanide precursors, $Ln(tta)_3(H_2O)_2$ display a characteristic C=O stretching at ~1602 cm^{-1} and a broad hump within the spectral domain of 3351-3400 cm^{-1} due to coordinated water molecule. Upon complexation, the C=O stretching frequency moves to 1605-1609 cm^{-1}, and the broad peak due to OH stretching within 3351-3400 cm^{-1} of the coordinated water disappears. Additionally, two new peaks were generated within the spectral range of 1534-1538 cm^{-1} (for C=N stretch) and 3080-3250 cm^{-1} due to the imidazole N-H moiety in the complexes.[32]

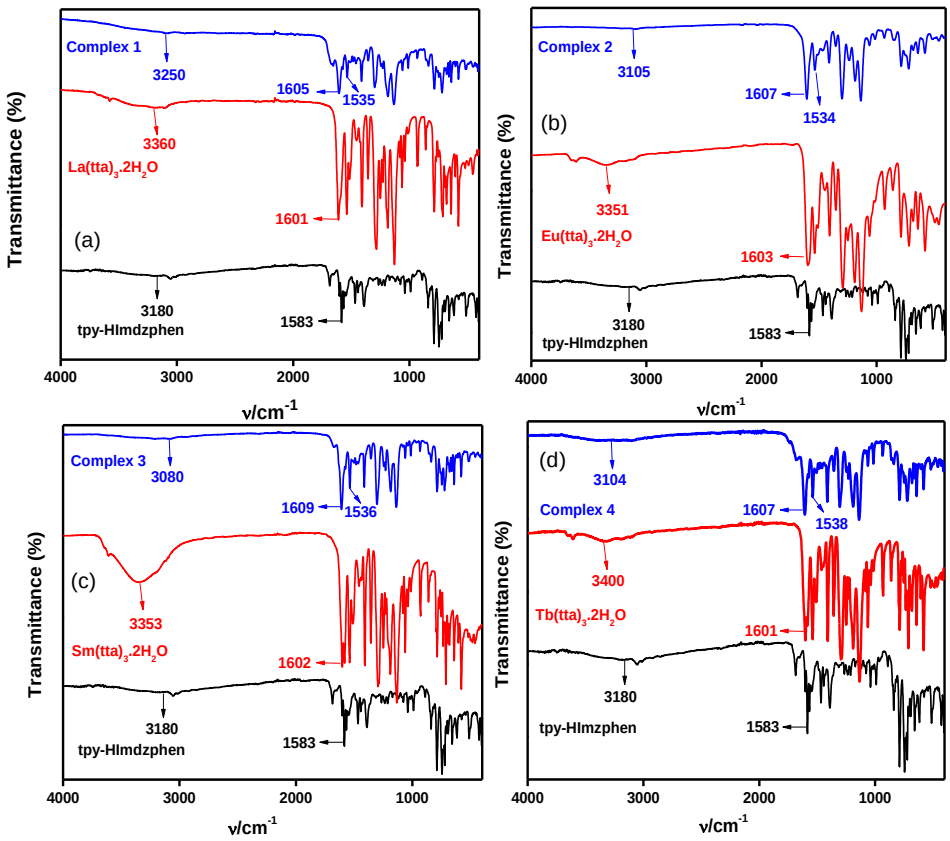

Figure 2.1. FT-IR spectra of tpy-Himzphen, all four precursors $Ln(tta)_3(H_2O)_2$ and all four complexes, $Ln(tta)_3$tpy-HImzphen (**1-4**).

Table 2.1. Stretching Frequencies of Selected Groups in Their FT-IR Spectra

Complex	$\nu_{C=O}$	$\nu_{C=N}$	ν_{N-H}	ν_{OH}
Tpy-HImdzphen	-	1583	3180	-
$La(tta)_3(H_2O)_2$	1601	-	-	3360
Complex **1**	1605	1535	3250	-
$Eu(tta)_3(H_2O)_2$	1603	-	-	3351
Complex **2**	1607	1534	3105	-
$Sm(tta)_3(H_2O)_2$	1602	-	-	3353
Complex **3**	1609	1536	3080	-
$Tb(tta)_3(H_2O)_2$	1601	-	-	3400
Complex **4**	1607	1538	3104	-

2.3.3. ^{1}H NMR Spectra. The ^{1}H NMR spectra of all the four complexes along with their tris(β-diketonate) precursors and terpyridyl-imidazole ligand were recorded in DMSO-d_6. ^{1}H NMR spectra of all the four complexes together with tentative assignments of all the proton resonances are presented in Figures 2.2-2.5 and Table 2.2. Upon coordination of the $La(tta)_3(H_2O)_2$ precursor, the protons associated with tta moiety are found to move towards up-field region in the resulting complex (Figure 2.2c). Tpy-HImzphen protons, on the other hand, undergo only minor up-field shift accompanied with change in the multiplicity of the signals compared with its free form.[44] The protons in the remaining complexes (**2**, **3,** and **4**) experience unpredictable paramagnetic shifts together with the change in multiplicity. The tpy-HImzphen protons in these complexes also don't experience remarkable alteration in their chemical shift values. By contrast, the protons associated with the tta moieties experience a notable paramagnetic up-field shift as shown in Figures 2.3-2.5. The effect is quite marked with Tb^{III} complex (Figure 2.5) relative to Eu^{III}- and Sm^{III} complexes (Figures 2.3 and 2.4, respectively).

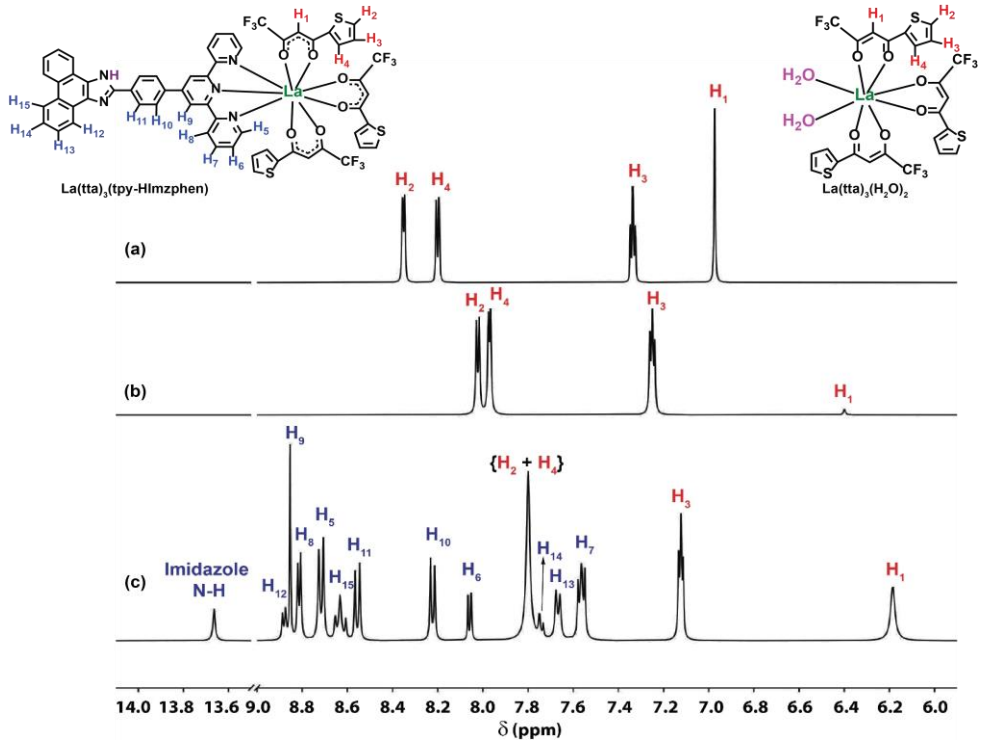

Figure 2.2. 400 MHz ^{1}H NMR spectra of Htta (a), La(tta)$_3$(H$_2$O)$_2$ (b) and La(tta)$_3$(tpy-HImzphen) (**1**) (c) in DMSO-d_6.

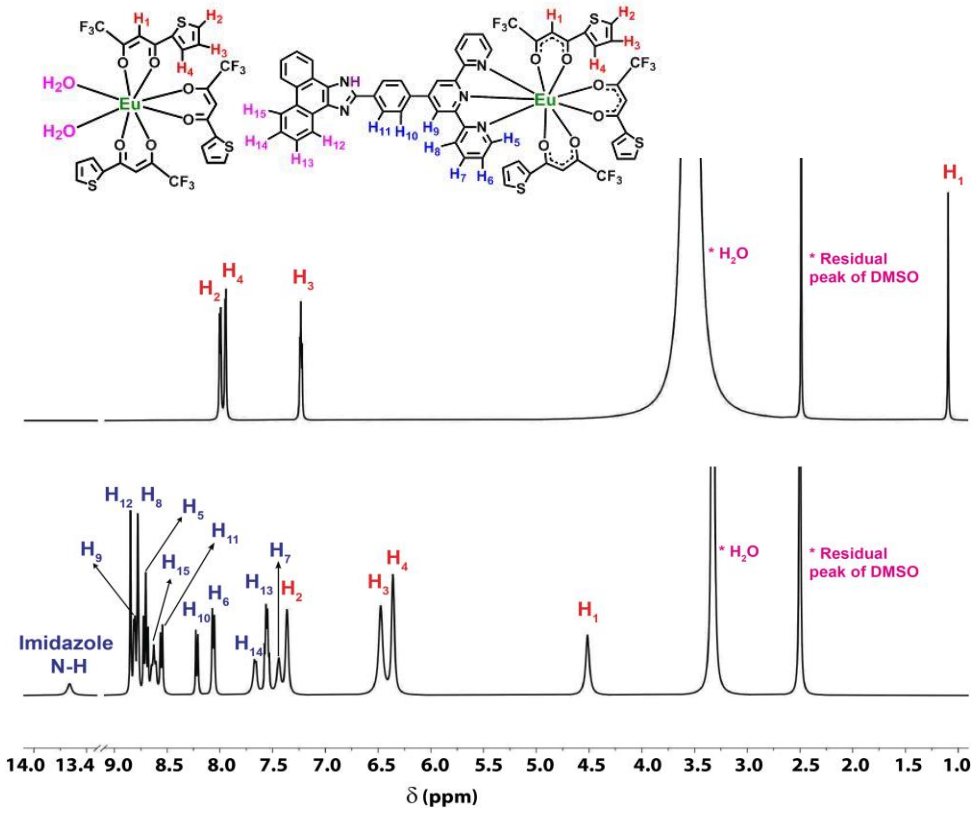

Figure 2.3. 400 MHz ^{1}H NMR spectra of Eu(tta)$_3$(H$_2$O)$_2$ (top) and Eu(tta)$_3$(tpy-HImzphen) (**2**) (bottom) in DMSO-d_6.

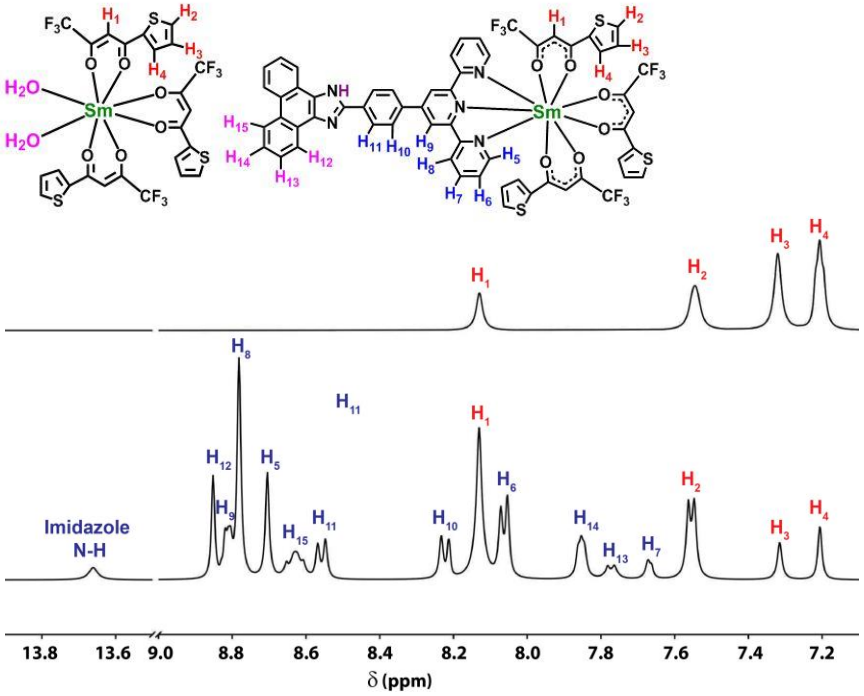

Figure 2.4. 400 MHz ^{1}H NMR spectra of $Sm(tta)_3(H_2O)_2$ (top) and $Sm(tta)_3$(tpy-HImzphen) (**3**) (bottom) in DMSO-d_6.

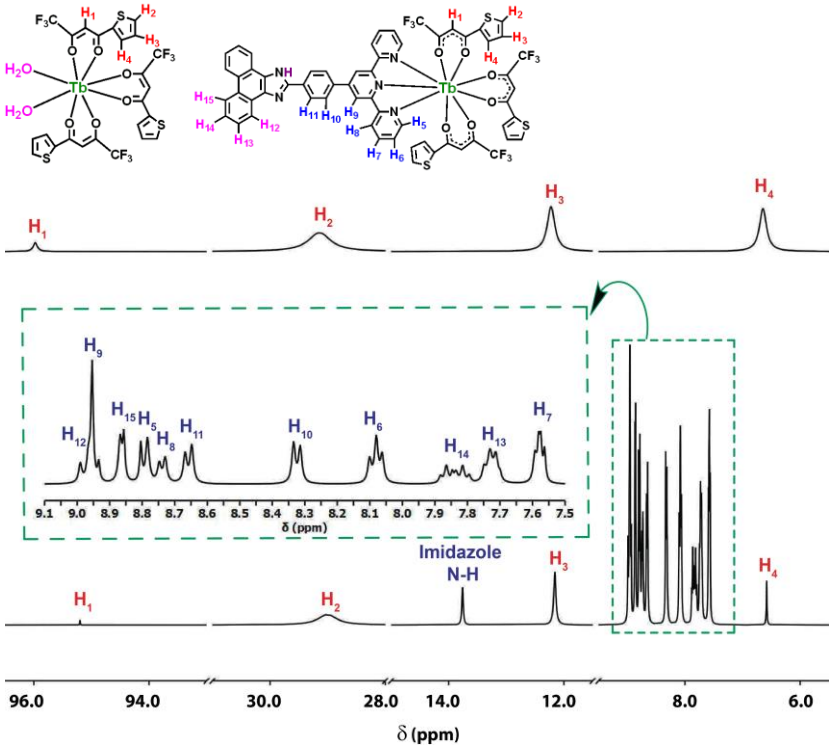

Figure 2.5. 400 MHz ^{1}H NMR spectra of $Tb(tta)_3(H_2O)_2$ (top) and [$Tb(tta)_3$(tpy-HImzphen)] (**4**) (bottom) in DMSO-d_6.

Table 2.2. Chemical Shifts of the Protons of All the Four Complexes in DMSO-d_6

Proton	Chemical shift (ppm) of Lanthanide complexes (**1-4**) {*J* = Hz}			
	1	**2**	**3**	**4**
H_1 (methine)	6.18 (s, 3H)	4.51 (s, 3H)	8.13 (s, 3H)	95.20 (s, 3H)
H_2	~7.80 (m, 3H)	6.36 (s, 3H)	7.55 (t, 3H, *J* = 6.44 Hz)	29.00 (s, 3H)
H_3	7.12 (t, 3H, *J* = 4.0 Hz)	6.48 (s, 3H)	7.32 (s, 3H)	12.16 (s, 3H)
H_4	~7.80 (m, 3H)	7.36 (s, 3H)	7.21 (s, 3H)	6.58 (s, 3H)
H_5	8.72 (d, 2H, *J* = 8.3 Hz)	8.70 (t, 2H, *J* = 8.0)	8.70 (s, 2H)	8.79 (d, 2H, *J* = 8.0)
H_6	8.06 (d, 2H, *J* = 5.9 Hz)	8.06 (d, 2H, *J* = 8.0 Hz)	8.06 (d, 2H, *J* = 8.0 Hz)	8.08 (t, 2H, *J* = 8.0 Hz)
H_7	7.56 (t, 2H, *J* = 6.0 Hz)	7.44 (s, 2H)	7.67 (d, 2H, *J* = 4.0 Hz)	7.58 (m, 2H)
H_8	8.81 (d, 2H, *J* = 5.3 Hz)	8.78 (t, 2H, *J* = 4.0 Hz)	8.78 (s, 2H)	8.86 (d, 2H, *J* = 4.52 Hz)
H_9	8.85 (s, 2H)	8.81 (d, 2H, *J* = 8.0 Hz)	8.82 (m, 2H)	8.95 (s, 2H)
H_{10}	8.22 (d, 2H, *J* = 7.4 Hz)	8.22 (d, 2H, *J* = 8.0 Hz)	8.22 (d, 2H, *J* = 8.0 Hz)	8.32 (d, 2H, *J* = 8.0 Hz)
H_{11}	8.56 (d, 2H, *J* = 8.3 Hz)	8.55 (d, 2H, *J* = 8.0 Hz)	8.56 (d, 2H, *J* = 8.0 Hz)	8.65 (d, 2H, *J* = 8.0 Hz)
H_{12}	8.88 (d, 2H, *J* = 5.48 Hz)	8.85 (s, 2H)	8.85 (s, 2H)	8.97 (m, 2H)
H_{13}	7.67 (d, 2H, *J* = 8.0 Hz)	7.56 (m, 2H)	7.77 (d, 2H, *J* = 8.0 Hz)	7.72 (m, 2H)
H_{14}	7.74 (d, 2H, *J* = 8.0 Hz)	7.66 (d, 2H, *J* = 4.0 Hz)	7.85 (t, 2H, *J* = 4.0 Hz)	7.84 (m, 2H)
H_{15}	8.63 (t, 2H, *J* = 8.0 Hz)	8.63 (t, 2H, *J* = 8.0 Hz)	8.63 (t, 2H, *J* = 8.0 Hz)	8.73 (d, 2H, *J* = 8.0 Hz)
Imidazole-NH	13.66 (s, 1H)	13.66 (s, 1H)	13.66 (s, 1H)	13.76 (s, 1H)

2.3.4. Mass Spectra. Matrix-assisted laser desorption ionization time of flight mass spectra (MALDI-TOF MS) of all the four complexes are recorded in dichloromethane to further confirm the structure of the complexes in the solution phase. The mass spectra for all four complexes (**1-4**) together with the experimental and simulated isotopic distribution pattern are presented in Figures 2.6-2.9. Good correlation between experimental and simulated isotopic pattern is observed for all cases. Each of the four complexes displays one intense peak with its *m/z* value spanning in the range of 1106.17-1126.01. Additionally, the separation between successive lines in both the experimental and simulated isotopic pattern is found to be 1.0 Da and thus corresponds to the mono-positive cations of the type, $[\{Ln(tta)_3(tpy\text{-}HImzphen)\}\text{-}(tta)]^+$ or $[M\text{-}tta]^+$.[24]

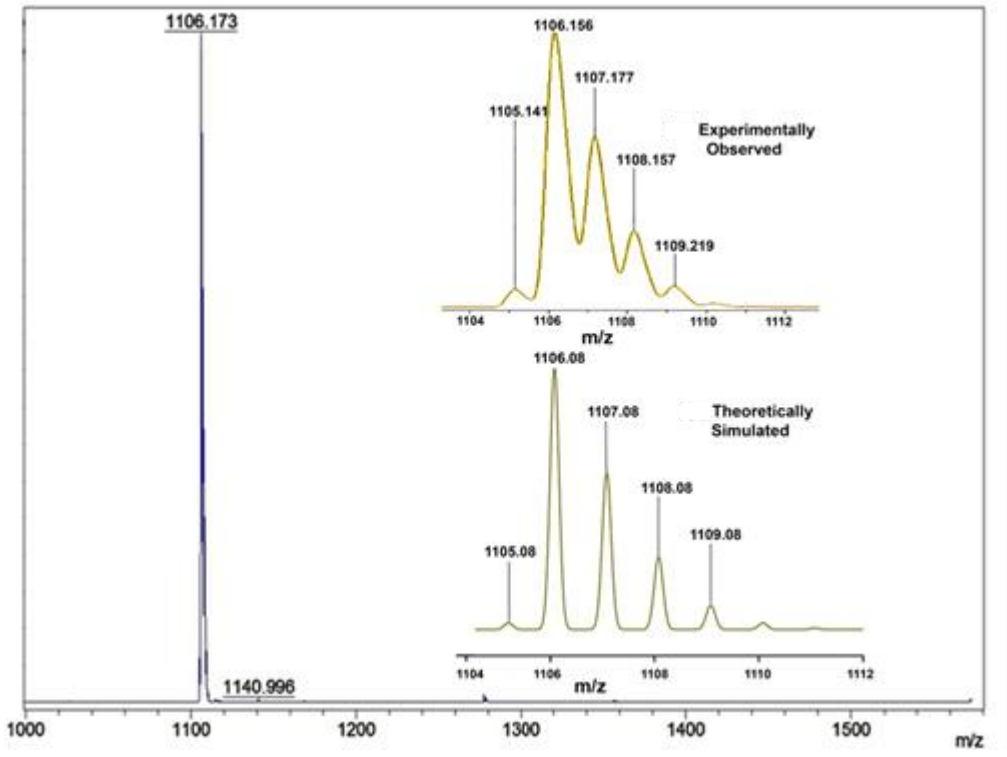

Figure 2.6. MALDI-TOF-MS of La(tta)$_3$tpy-HImzphen (**1**) in dichloromethane solution (positive mode). Upper right portion shows the experimentally observed isotopic distribution pattern and the lower right portion shows the simulated isotopic distribution pattern.

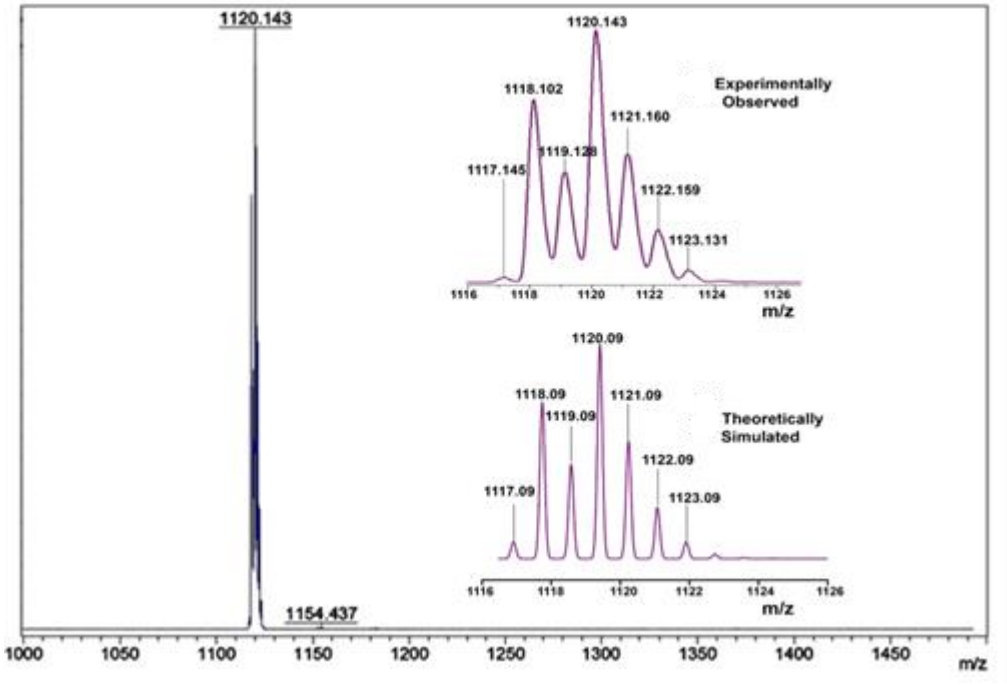

Figure 2.7. MALDI-TOF-MS of Eu(tta)$_3$tpy-HImzphen (**2**) in dichloromethane solution (positive mode). Upper right portion shows the experimentally observed isotopic distribution pattern and the lower right portion shows the simulated isotopic distribution pattern.

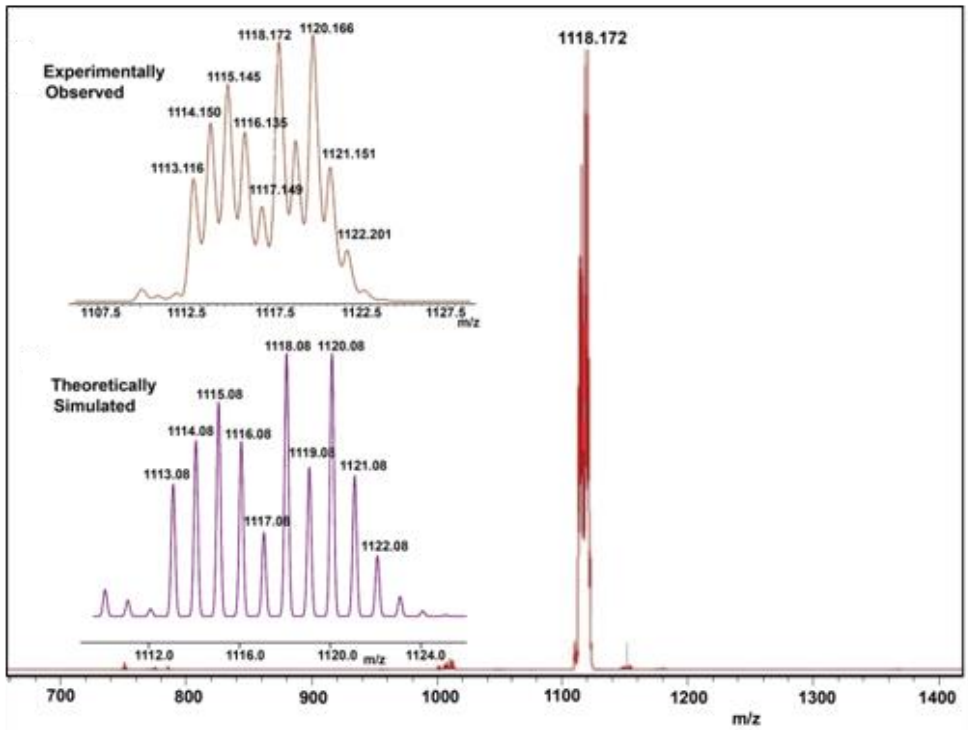

Figure 2.8. MALDI-TOF-MS of Sm(tta)$_3$tpy-HImzphen (**3**) in dichloromethane solution (positive mode). Upper left portion shows the experimentally observed isotopic distribution pattern and the lower left portion shows the simulated isotopic distribution pattern.

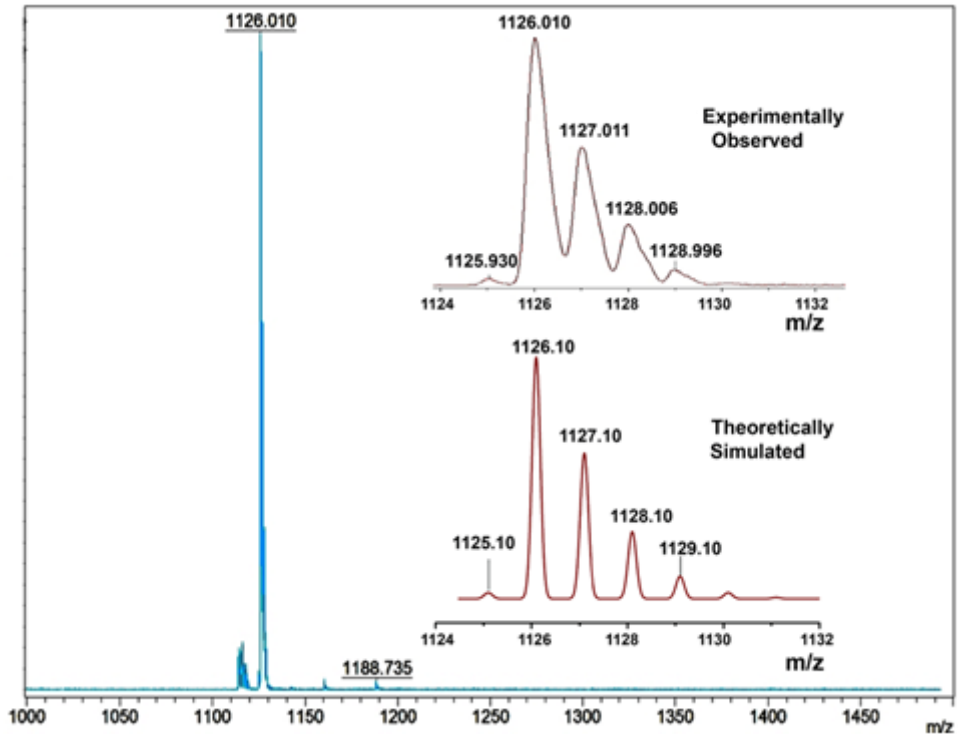

Figure 2.9. MALDI-TOF-MS of Tb(tta)$_3$tpy-HImzphen (**4**) in dichloromethane solution (positive mode). Upper right portion shows the experimentally observed isotopic distribution pattern and the lower right portion shows the simulated isotopic distribution pattern.

2.3.5. Thermal Stability of the Complexes. In order to investigate the thermal stability of the complexes, we also performed their thermogravimetric analysis in nitrogen atmosphere within the temperature range of 30-800°C and at a heating rate of 10 °C/m. All of the four complexes exhibit nearly similar pattern in terms of both decomposition and weight loss (Figure 2.10). The complexes showed a minor weight loss at ~190 °C and two major weight loss at ~290 °C and ~555 °C but do not show any weight loss at ~100 °C unlike their respective metal precursors (Figure 2.10a), which recommends that the complexes are amorphous in nature and lacks any coordinated or lattice-trapped water molecule. The minor weight loss at ~190 °C may be attributed to the loss of moisture within the sample. At the onset temperature of ~290 °C, major decomposition starts and continues up to ~400 °C (up to ~50% weight loss), which can be ascribed to loss of ancillary ligand and tta moieties. The second major weight loss starts at ~555 °C and continues thereafter, probably because of the formation of the metal oxides. Notably, in cases of the respective $Ln(tta)_3(H_2O)_2$ precursors, the major decomposition starts at ~250 °C (Figure 2.10a). Hence, it can be concluded that the complexes are more thermally stable than their corresponding metal precursors and have adequate thermal stability up to ~300 °C.

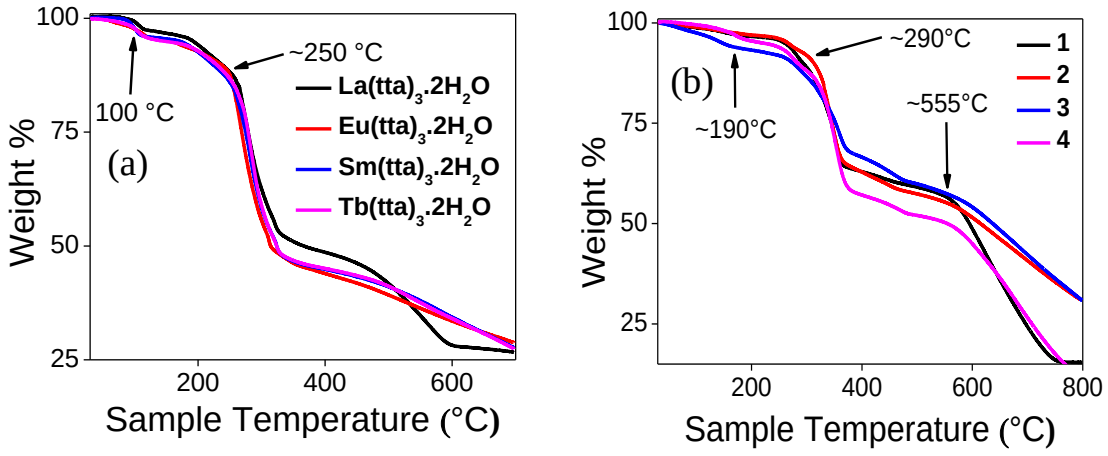

Figure 2.10. Thermogravimetric analysis of all four metal precursors $Ln(tta)_3(H_2O)_2$ (a) and their corresponding complexes **1-4** (b).

2.3.6. X-ray Crystallography. We were curious to know the unambiguous structure of the synthesized complexes through single-crystal X-ray crystallography. Despite numerous sincere efforts, we were unable to obtain suitable single crystals from the synthesized complexes. Hence, we performed an in-situ one-pot synthesis of a terbium complex by

stirring a stoichiometric mixture of $TbCl_3 \cdot 6H_2O$ and tpy-HImzphen in a chloroform-methanol mixture (1:1, v/v) followed by the addition of Htta and triethylamine at RT. The mixture was evaporated to dryness and dissolved in a small chloroform/acetonitrile mixture (1:1 v/v), and allowed the solution for slow evaporation for crystallization. Eventually, yellow-colored single crystals suitable for X-ray crystallography were obtained after ~7 days.

The compound $[Tb(tta)_2(H_2O)(tpy\text{-}HImzphen)](Cl)$ (**5**) crystallizes in C2/c space group in monoclinic system. The asymmetric unit possesses the full molecular structure. The solid-state structure of the complex is presented in Figure 2.11, while the crystallographic

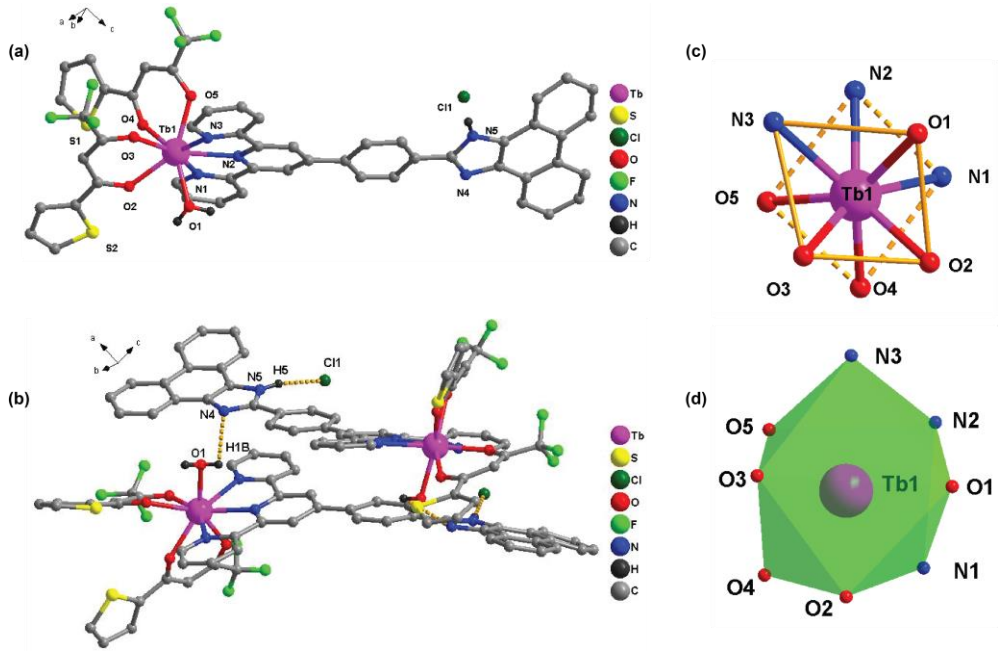

Figure 2.11. (a) The solid-state molecular structure of complex **5** (some H atoms are omitted for clarity), (b) intermolecular hydrogen bonding interaction between two head-to-tail fashioned complex cations with partial-atom labelling scheme, (c) square anti-prism geometry around tb^{III} ion, and (d) coordination polyhedra for the lanthanide core.

parameters are presented in Table 2.3. A few specific bond distances and angles of **5** were provided in Table 2.4. The structural analysis of the complex cation shows that the terpyridine motif of the terpyridyl-imidazole ligands is coordinated to the Tb^{III} ion in a tridentate fashion, two β-diketonate units of $[tta]^{-1}$ are bonded in a bidentate manner as usual, and one water molecule is also coordinated to Tb^{III}, completing the eight-coordination site and depicted distorted square antiprism geometry. The Tb-N bond lengths range from 2.495(9) to 2.533(10)Å, whereas the Tb-O bond lengths range from 2.279(7) to 2.378Å. The variation of Tb-O bond lengths reveals that a better overlap takes place between the tta^- and

Table 2.3. Crystallographic Parameters for 5

Compound	**5**
CCDC Number	2255186
Empirical formula	$C_{52}H_{34}ClF_6N_5O_5S_2Tb$
Formula weight ($gmol^{-1}$)	1181.34
Temperature (K)	108.0
Crystal system	Monoclinic
Space group	C2/c
Unit cell lengths (Å)	a= 10.9321(3)
	b = 25.1480(7)
	c = 40.0049(11)
Unit cell angles (°)	α= 90
	β = 93.586(2)
	γ = 90
Volume ($Å^3$)	10976.6(5)
Z	8
Density (calculated)	1.430
μ(mm^{-1})	8.086
F(000)	4712.0
Crystal size (mm)	0.16 × 0.12 × 0.09
2θ range for data collection (°)	4.426 to 136.824
Reflections collected	117779
Index ranges	$-12 \leq h \leq 12, -29 \leq k \leq 30, -48 \leq l \leq 47$
Independent reflections	9791 [Rint = 0.1652, Rsigma = 0.0776]
Data/Restraints/Parameter	9791/13/640
Goodness-of-fit on F^2	1.165
Final R indices [I>2sigma(I)]	R1 = 0.1276, wR2 = 0.2638

Tb^{III} ion compared with the water molecule. The bite angles around Tb^{III} centre varies between 64.9 and 152.3°.

It is evident the ligand structure exhibits a strained poly-aromatic system. The phenanthrene moiety is nearly coplanar with imidazole unit, whereas the three pyridine rings remain almost in another plane. The dihedral angle between the two planes is 31.36°. Moreover, an intermolecular hydrogen bonding is noticed between the hydrogen atom of coordinated water molecule and imidazole nitrogen of another moiety [N4-H5B, 2.68 Å; N4-H5B-O5, 74.83°] which may be responsible for eight-coordinated bis-tta coordination over desired nine-coordinated tris-tta coordination.

Table 2.4. Selected Bond Angles and Bond Distances

Selected Bond distances (Å)		Selected Bond Angles (θ)	
Tb1-O4	2.378(8)	O4-Tb1-N2	136.9(3)
Tb1-O3	2.279(7)	O4-Tb1-N1	135.6(3)
Tb1-O5	2.330(9)	O4-Tb1-N3	82.7(3)
Tb1-O2	2.340(8)	O3-Tb1-O4	73.2(3)
Tb1-O1	2.322(9)	O3-Tb1-O5	103.6(3)
Tb1-N3	2.495(9)	O3-Tb1-O2	82.8(3)
Tb1-N2	2.503(8)	O3-Tb1-O1	86.3(3)
Tb1-N1	2.533(10)	O3-Tb1-N2	142.8(3)
		O3-Tb1-N1	78.0(3)
		O3-Tb1-N3	152.3(3)
		O5-Tb1-O4	73.7(3)
		O5-Tb1-O2	140.0(3)
		O5-Tb1-N2	74.4(3)
		O5-Tb1-N1	81.3(3)
		O5-Tb1-N3	81.9(3)
		O2-Tb1-O4	70.6(3)
		O2-Tb1-N2	123.2(3)
		O2-Tb1-N1	137.8(3)
		O2-Tb1-N3	76.4(3)
		O1-Tb1-O4	139.0(3)
		O1-Tb1-O5	146.9(3)
		O1-Tb1-O2	71.8(3)
		O1-Tb1-N2	78.9(3)
		O1-Tb1-N1	69.8(3)
		O1-Tb1-N3	104.0(3)
		N2-Tb1-N1	65.0(3)
		N3-Tb1-N2	64.9(3)
		N3-Tb1-N1	129.7(3)
Hydrogen Bond			
N4-H5B	2.68	N4-H5B-O5	74.83
H5-Cl1	2.29	N5-H5-Cl1	163.55

2.3.7. Photophysical Properties. The absorption and emission spectra of the complexes together with the terpyridyl-imidazole ligand are acquired in DCM and related spectral profiles are presented in Figures 2.12 and 2.13, while the spectral data are

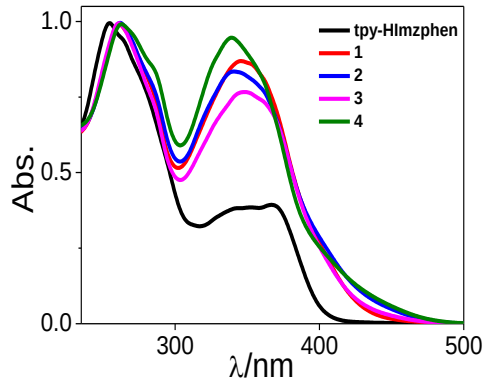

Figure 2.12. Normalized UV-vis absorption spectra of complexes **1-4** along with **tpy-HImzphen** in dry DCM.

summarized in Table 2.5. The absorption peak at 370 nm for the ligand is attributed to intra-ligand charge transfer transition (ILCT), while the peak at 265 nm is due to π-π* transitions of the aromatic and heteroaromatic moieties in the ligand (Figure 2.12). Upon complexation, the lowest energy absorption peak of the ligand underwent a hypsochromic shift, the extent of which depends upon the type of lanthanide ion, while the short wavelength peak remained practically unaffected.

Table 2.5. Photophysical Properties of tpy-HImzphen and Complexes 1-4 in RT and 77K

	Compounds	Absorption, λ_{max}/nm (ε/$M^{-1}cm^{-1}$)($\times10^4$)	λ_{max}		Lifetime (τ)	Quantum Yield (Φ_{rel}/%)
			Ligand centred	Metal centred		
RT	**tpy-HImzphen**	254(6.5), 343(2.52), 370 (2.6)	446	-	2.3 ns	-
	1	261(7.44), 343(6.45)	505	-	2.8 ns	78
	2	261(9.7), 341(8.15)	446	580, 593, 614, 652	507 μs	10
	3	261(8.47), 345(6.55)	447	565, 598, 646	73 μs	3.2
	4	262(7.34), 339(7.05)	446	-	1.9 ns	12
77K	**1**	-	458	-	2.36 ns	-
	2	-	429	579, 593, 614, 652	643 μs	-
	3	-	433	562, 597, 644	77 μs	-
	4	-	433	490, 545, 585, 620	621 μs	-

The free ligand shows a broad emission peak at 446 nm.[44] In case of La^{III} complex (**1**), the said peak shifts to 505 nm but no emission peak due to intra- configurational f-f transition is observed as La^{III} possesses no f-electron (Figure 2.13a). The Eu^{III} complex (**2**), on the other hand, displays characteristic emission peaks at 579, 592, 614 and 652 nm because of intra-configurational $^5D_0 \rightarrow {}^7F_0$, $^5D_0 \rightarrow {}^7F_1$, $^5D_0 \rightarrow {}^7F_2$, and $^5D_0 \rightarrow {}^7F_3$ transition, respectively (Figure 2.13c). The peak at 614 nm due to $^5D_0 \rightarrow {}^7F_2$ transition is the most intense among the four, because of its electric dipole (ED) character. In addition to its characteristic Eu^{III}-centered emissions, **2** also exhibits weak ligand-centered emission at 445 nm, probably because of incomplete energy transfer from the ligand to the Eu^{III} center. In case of Sm^{III} complex (**3**), the ligand-centered emission peak at 446 nm is found to be predominant, while the intensities of the Sm^{III}-centered peaks at 564 ($^5G_{5/2} \rightarrow {}^5H_{5/2}$), 598 ($^5G_{5/2} \rightarrow {}^5H_{7/2}$), and 646 nm ($^5G_{5/2} \rightarrow {}^5H_{9/2}$) are very weak, suggesting the extent of energy transfer between tpy-HImzphen ligand and Sm^{III} center is very small (Figure 2.13e). The Tb^{III}-complex (**4**), on the other hand, exhibits only ligand-centered emission at 446 nm with no signature of characteristic emission

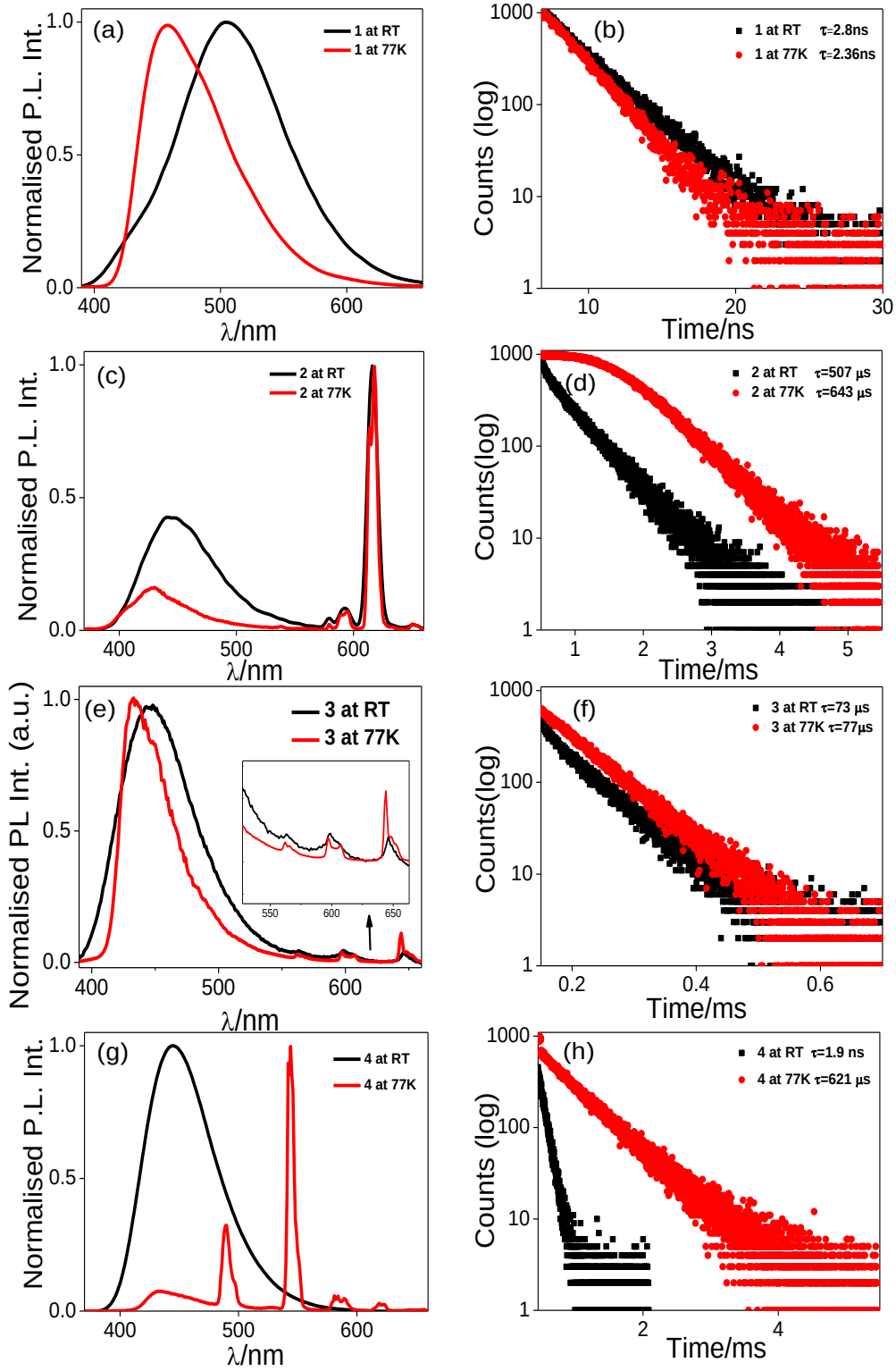

Figure 2.13. Luminescence spectra (a, c, e, g)] and lifetime decay plots (b, d, f, h) of **1-4** at both RT and 77 K.

peaks for Tb^{III} center ($^5D_4 \rightarrow {}^7F_{J,\ J=6\text{-}3}$) (Figure 2.13g). This is probably due to back energy transfer from Tb^{III} center to the ancillary ligand. The relative quantum yield (Φ) of the complexes (**1-4**) along with four $Ln(tta)_3(H_2O)_2$ precursors, are estimated in DCM by using quinine sulfate as the standard. The value of Φ ranges between 3.2% and 78%, depending upon the nature of lanthanide ion (Table 2.5). It is to be noted that the quantum yield of La and Tb-complexes are primarily due to ligand fluorescence, while for Eu-and Sm-complexes is the summation of both lanthanide-centered as well as residual ligand-centered emission.

The emission lifetimes of the compounds, acquired in DCM by time correlated single photon counting (TCSPC) or multi-channel scaling (MCS) methods, are also provided in Table 2.5. All the compounds exhibit mono-exponential decay as shown in Figures 2.13(b,d,f,h). The ligand and complexes **1** and **4** possess RT lifetimes within the domain of 1.9-2.8 ns, while **2** and **3** are long-lived, having lifetimes in the microsecond domain (73-507 μs; Table 2.5). The observed lifetimes suggest that emission in complexes **1** and **4** is primarily due to radiative deactivation of ligand-centered excited states, while for **2** and **3**, it is because of f-f transitions of the respective lanthanide metal.

In order to understand the deactivation dynamics of the excited states of the lanthanide complexes, we also recorded their steady-state luminescence spectra as well as lifetimes at 77 K. Associated data as well as spectra are provided in Table 2.5 and Figure 2.13. No significant change is observed for the La-complex (**1**) as expected. The ligand-centred emission peak undergoes only a small blue shift from 470 to 458 nm with almost no change in its lifetime upon cooling down to 77K (Figures 2.13a and 2.13b). For the Eu^{III}-complex (**2**), a remarkable increase in emission intensity of the peak at 614 nm (Figure 2.13c), as well as in lifetime (507 μs→ 643μs) is observed on passing from RT to 77K (Figure 2.13d). The Sm^{III}-complex (**3)** follows the same trend as that of the Eu^{III} (**2**), albeit to a small extent. The characteristic f-f transition peaks at ~562 nm, 597 nm, and 644 nm get enhanced to some extent along with a small increase in lifetime (73 μs→77 μs) (Figures 2.13e and 2.13f). The effect of lowering of temperature is most prominent in case of the Tb^{III}-complex (**4**). The characteristic f-f transition peaks for $^5D_4 \rightarrow {}^7F_{6\text{-}3}$ manifolds, which were absent at RT owing to the thermally-assisted metal to ligand back energy transfer, are restored at 77K (Figure 2.13g). The observed luminescence lifetime (τ=621 μs) also confirms that the decay is lanthanide metal-centric (Figure 2.13h).

2.3.8. Photophysics of *in-situ* Generated Lanthanide(III) Complexes. All the four lanthanide complexes (**1-4**) could also be generated *in situ* upon incremental addition of respective lanthanide precursor {Ln(tta)$_3$(H$_2$O)$_2$} to the DCM solution of tpy-HImzphen. The progress of the formation of the complexes was monitored through the change in absorption, and both steady-state and time-resolved emission spectroscopy (Figures 2.14-2.17). The absorbance of both ILCT and π-π* absorption bands of the ligand gradually increases in intensity with continued addition of the respective lanthanide precursor, and spectral saturation occurs upon addition of ~1 equiv. of {Ln(tta)$_3$(H$_2$O)$_2$}, indicating the formation of 1:1 complexes of the type, Ln(tta)$_3$(tpy-HImzphen). It is to be noted that broad overlapping bands within the domain of 330-370 nm coalesce to a single band with its maximum at ~340 nm.

In the emission side, gradual quenching of emission intensity takes place in all cases and spectral saturation also occurs upon addition of 1.2 equiv of {Ln(tta)$_3$(H$_2$O)$_2$}. In case of La^{III}, the ligand-centered emission gets gradually quenched together with red-shift of the maximum from 446 nm to 505 nm upon saturation (Figure 2.14b). With Eu(tta)$_3$(H$_2$O)$_2$, systematic quenching of the ligand-centered emission together with concomitant emergence of the peaks at 579, 592, 614 and 652 nm due to $^5D_0 \rightarrow {}^7F_{J\ (J=0\text{-}3)}$ transitions are observed (Figure 2.15b). The spectral profile for Sm^{III} is very similar to that of Eu^{III}, except the intensities of the newly generated characteristic emission peaks for Sm^{III} (564, 598 and 646 nm) are less (Figure 2.16b). In contrast to both Eu^{III} and Sm^{III}, no signature of characteristic emission peaks for Tb^{III} is visible during quenching of ligand-centred emission (Figure 2.17b).

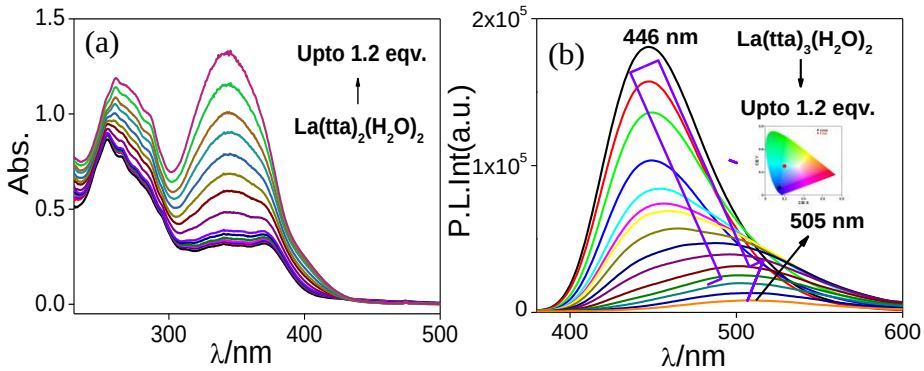

Figure 2.14. Changes in (a) absorption and (b) photoluminescence spectra (λ_{ex}=370nm) of ligand tpy-HImzphen upon incremental addition of La(tta)$_3$(H$_2$O)$_2$ in dry dichloromethane at RT. The inset shows the change of emitting color during titration.

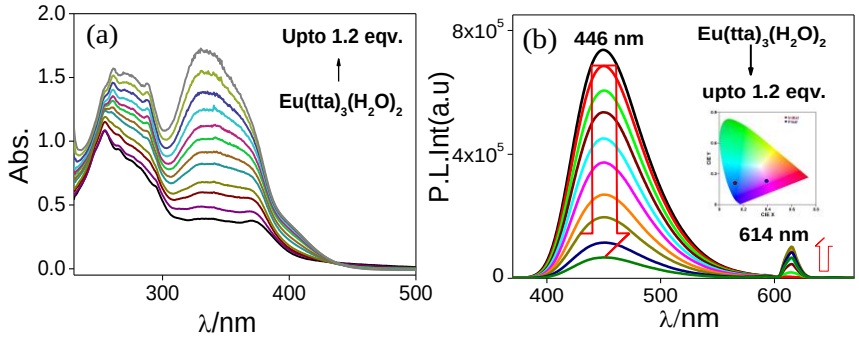

Figure 2.15. Changes in (a) absorption and (b) photoluminescence spectra (λ_{ex}=370nm) of ligand tpy-HImzphen upon incremental addition of $Eu(tta)_3(H_2O)_2$ in dry dichloromethane at RT. The inset shows the change of emitting color during titration.

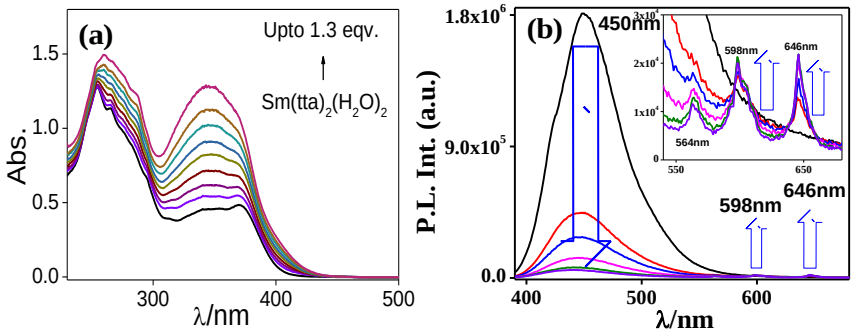

Figure 2.16. Changes in (a) absorption and (b) photoluminescence spectra (λ_{ex}=370nm) of ligand tpy-HImzphen upon incremental addition of $Sm(tta)_3(H_2O)_2$ in dry dichloromethane at RT.

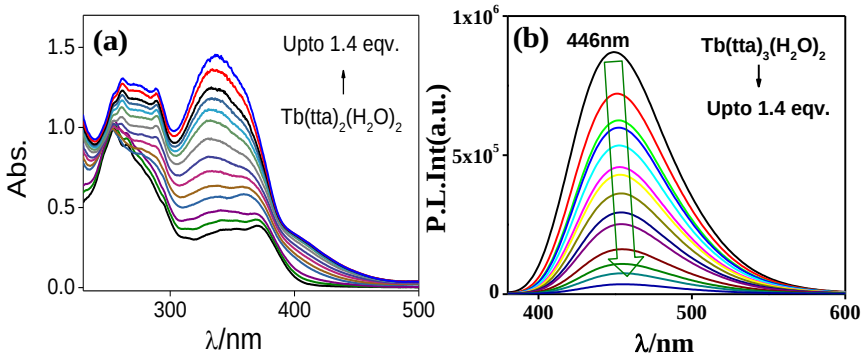

Figure 2.17. Changes in (a) absorption and (b) photoluminescence spectra (λ_{ex}=370nm) of ligand tpy-HImzphen upon incremental addition of $Tb(tta)_3(H_2O)_2$ in dry dichloromethane at RT.

We also overlaid the absorption spectra of the isolated complexes with those of the in-situ generated products at saturation (Figure 2.18). Additionally, we provided the overlaid absorption spectra for the chromophore, lanthanide precursor, and synthesized complex, as well as the in situ generated complex (all four set in Figure 2.19). It is also observed that the

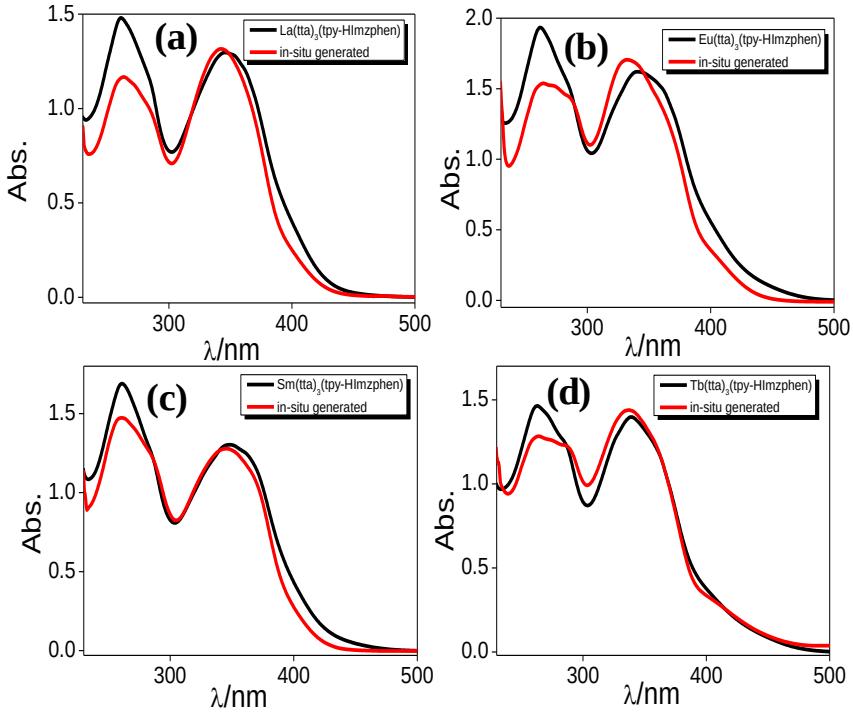

Figure 2.18. Overlayed UV-vis spectra of isolated as well as in situ generated complex for all four cases: (a) La^{III}; (b) Eu^{III}; (c) Sm^{III}; (d) Tb^{III}.

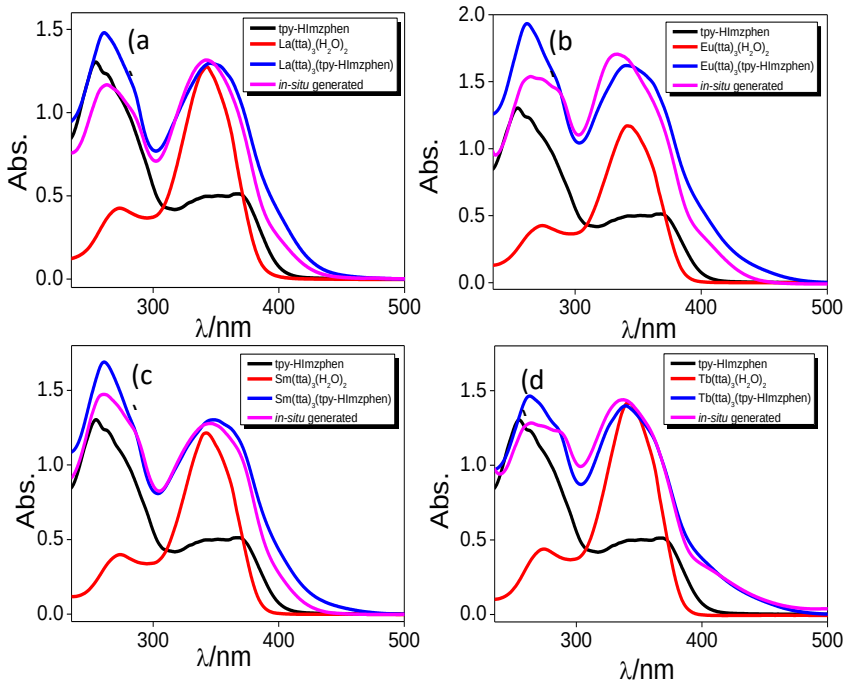

Figure 2.19. Overlayed UV-vis spectra of the chromophore tpy-HImzphen, Ln-tta precursor, isolated complex as well as in-situ generated complex for all four cases: (a) La^{III}; (b) Eu^{III}; (c) Sm^{III}; (d) Tb^{III}.

lifetime values at the end of every titration closely resemble that of the respective isolated complex as displayed in Figure 2.20. Close similarity of the spectral pattern clearly indicates a 1:1 complex of lanthanide precursor $\{Ln(tta)_3(H_2O)_2$ and tpy-HImzphen.

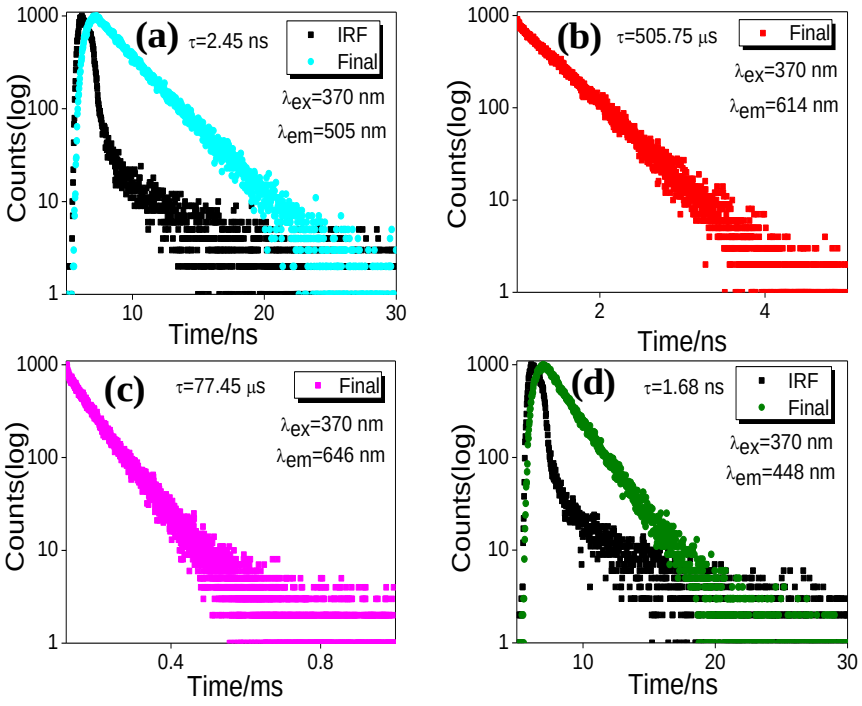

Figure 2.20. Excited state decay profiles at the end of each titration for all four cases: (a) La^{III}; (b) Eu^{III}; (c) Sm^{III}; (d) Tb^{III}.

2.3.9. Elucidation of the Distinctive Responses of Four Lanthanide Complexes. Since the 4f-4f transitions are both spin and parity (Laporte) forbidden, direct excitation of the Ln^{III} centers leads to very weak absorption (ε<10 L M^{-1} cm^{-1}).[32,33,56-57] To circumvent this disadvantage, light-harvesting organic chromophores with a high molar absorption coefficient (ε>10000 L M^{-1} cm^{-1}) are introduced here to indirectly sensitize the central lanthanide ion (antenna effect) for achieving characteristic 4f-4f emission.[6,17,18-22] The most well-accepted energy transfer mechanism for this sort of sensitization involves three steps, viz. Laporte and spin-allowed ligand absorption and excitation to the first excited state ($S_0 \rightarrow S_1$), followed by rapid intersystem crossing to the ligand triplet state ($S_1 \rightarrow T_1$) and finally transferring the energy from the triplet level of the ligand to the emitting level of the lanthanide metal ion ($T_1 \rightarrow Ln^*$).[1-3,24] The efficacy of the last step critically depends on the relative positions of both the triplet level of the ligand (T_1) and the lanthanide emitting level (Ln*). The singlet

state lifetime is too short for this energy transfer yet this mechanism is also operative.[56,57] It has been observed that both β-diketonate ligands as well as π-conjugated organic ligands could effectively sensitize the lanthanide core.[35,58,59]

It is well-known that the lowest-lying emitting excited level of Eu^{III}($^5D_0$), Sm^{III} ($^4G_{5/2}$), and Tb^{III} ($^5D_4$) resides at ~17264, 17900, and 20500 cm^{-1}, respectively. In order to achieve effective sensitization, it is postulated that the energy gap between S_1 and T_1 of the ligand should be ~5000 cm^{-1} (for effective ISC), while the energy gap between the T_1 level of ligand and lowest emitting level of lanthanide metal ion (Ln*) should be maintained within 2500-4000 cm^{-1}.[2] Now, we estimated the singlet-state energy level of our ancillary tpy-HImzphen ligand to be ~27027 cm^{-1} from its absorption spectrum,[60,61] whereas the triplet-state energy level of the same is ~20534 cm^{-1}, obtained from 77K phosphorescence spectrum of its Gd^{III}-analogue (Figure 2.21).[62-65] This positioning of the triplet-state energy level of the

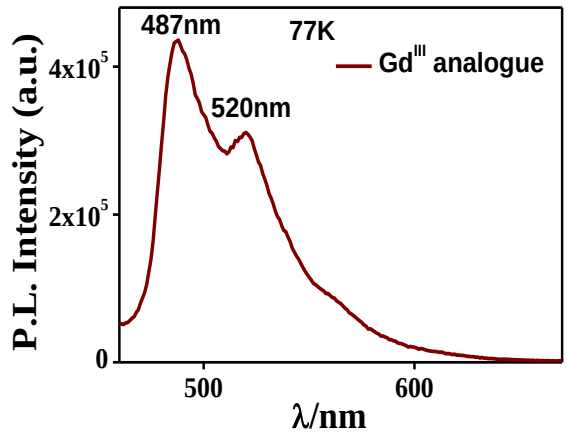

Figure 2.21. Photoluminescence spectrum of Gd^{III}-complex at 77K.

ligand is responsible for the observed variation of the photophysical properties of the complexes (**1-4**) compared to their metal precursors $Ln(tta)_3.2H_2O$. Consequently, we observed only a ligand-centred emission and lifetime value in the case of La^{III} ion as expected. In case of **2**, energy transfer from tpy-HImzphen to Eu^{III}-centre takes place quite efficiently, although it is not as substantial as could be expected from favourable thermodynamic parameters (well-matching of the $\Delta E(T_1 \rightarrow Ln^*)$. Although substantial energy transfer is taking place from tpy-HImzphen→Eu^{III}, it is not as great as could be expected from its favourable energy difference, $\Delta E(T_1 \rightarrow Ln^*)$. We are not very sure about the actual reason for this. But upon going through the literature on the luminescence characteristics of

the related lanthanide complexes, we surmise the involvement of closely associated low-lying ligand-to-metal charge transfer (LMCT) state is a distinct possibility.[13,66-69] In case of **3**, the relative intensity of the induced dipole transition for Sm^{III} at 646 nm ($^5G_{5/2}\rightarrow{}^5H_{9/2}$) together with its lifetime is much less than that of Eu^{III} ion. Here also, the extent of energy transfer is much less than one could anticipate. This could again be attributed to the presence of nearby low-lying LMCT state along with multi-phonon relaxation as reported in earlier literature.[2,69] The $\Delta E(T_1\rightarrow Ln^*)$ gap in case of Tb^{III} ion is practically zero and it is anticipated that back energy transfer from the emitting level of the lanthanide metal ion to the triplet energy level of the ligand(s) ($Ln^*\rightarrow T_1$) is taking place wherein $\Delta E(T_1\rightarrow Ln^*)$ value is less than 1800 cm^{-1}. An energy level diagram showing distinctive responses of the four lanthanide complexes is presented below (Scheme 2.4).[2,70-72]

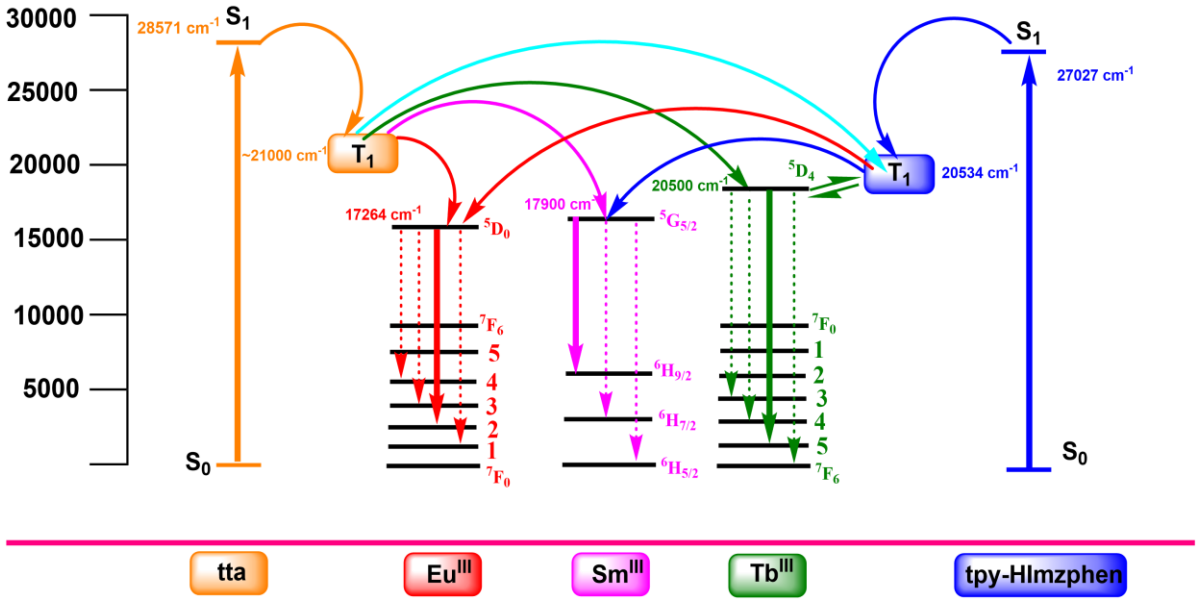

Scheme 2.4. Tentative Energy Transfer Mechanism for the Lanthanide Complexes

2.4. Conclusion

The primary objective of this work is to incorporate a terpyridyl-imidazole based tridentate ligand into β-diketonate lanthanide(III) core for improvement of the photophysical and particularly the luminescence characteristics of the resulting lanthanide complexes. To fulfill our objective, we synthesized four ternary lanthanide tris-(β-diketonate) complexes of the type, $[Ln(tta)_3(tpy\text{-}HImzphen)]$, where $Ln=La^{III}$, Eu^{III}, Sm^{III}, and Tb^{III}; tta=(2-theonyltrifluoro acetonate) and tpy-HImzphen=terpyridyl-imidazole based ligand, and thoroughly

characterized them by standard analytical tools, including single crystal X-ray diffraction. Herein, we restricted our interest to the above-mentioned four lanthanide ions in terms of having our facility to measure the photophysical properties in the visible domain. The photophysical properties of all the complexes were thoroughly investigated via absorption and both steady state and time-resolved emission spectroscopic techniques. The emission spectral measurements were carried out in at both room temperature and 77K to understand the deactivation dynamics of the excited states as well as to elucidate the distinctive luminescence responses of the lanthanide complexes. La^{III}-complex (**1**) exhibits only ligand-centred emission as expected as it does not possess any f-electron. For Eu^{III} (**2**), efficient energy transfer takes place from tpy-HImzphen to Eu^{III} centre which is reflected in its characteristic emission spectrum peaks due to intraconfigurational $^5D_0 \rightarrow {}^7F_{J\ (J=0-3)}$ transitions with concomitant diminution of ligand-centered emission. The spectral profile for Sm^{III} is very similar to that of Eu^{III}, except the intensities of its characteristic emission peaks are much less because of lesser extent of tpy-HImzphen→Sm^{III} energy transfer. In contrast to both Eu^{III} and Sm^{III}, no characteristic emission due to $^5D_4 \rightarrow {}^7F_{J\ (J=6-3)}$ transitions are observed for Tb^{III} at RT probably because of Tb^{III}→ tpy-HImzphen back energy transfer. The effect of lowering of temperature to 77K is most prominent in case of Tb^{III} complex (**4**) wherein the characteristic emission peaks due to $^5D_4 \rightarrow {}^7F_{J\ (J\ =\ 6-3)}$ transitions are observed for Tb^{III}-center during systematic quenching of ligand-centred emission peak at ~446 nm. Thus, the present terpyridyl-imidazole ligand by virtue of its suitable positioning of the triplet-state energy level is able to sensitize the lanthanide core quite efficiently and the extent of sensitization in turn depends upon the nature of the lanthanide ion.

2.5. References

1. Bünzli, J. C.; Piguet, C. Taking Advantage of Luminescent Lanthanide Ions. *Chem. Soc. Rev.* **2005**, *34*, 1048–1077.
2. Bünzli, J. C.; Eliseeva, S. V. Basics of Lanthanide Photophysics. *Lanthanide luminescence.* **2010**, 1–45.
3. Parker, D.; Fradgley, J. D.; Wong, K.-L. The Design of Responsive Luminescent Lanthanide Probes and Sensors. *Chem. Soc. Rev.* **2021**, *50*, 8193–8213.
4. D'Aléo, A.; Pointillart, F.; Ouahab, L.; Andraud, C.; Maury, O. Charge Transfer Excited States Sensitization of Lanthanide Emitting from the Visible to the Near-Infra-Red. *Coord. Chem. Rev.* **2012**, *256*, 1604–1620.

5. Eliseeva, S. V.; Bünzli, J. C. Lanthanide Luminescence for Functional Materials and Bio-Sciences. *Chem. Soc. Rev*. **2010**, *39*, 189–227.
6. Hasegawa, Y.; Kitagawa, Y.; Nakanishi, T. Effective Photosensitized, Electrosensitized, and Mechanosensitized Luminescence of Lanthanide Complexes. *NPG Asia Mater.* **2018**, *10*, 52–70.
7. Zwier, J. M.; Bazin, H.; Lamarque, L.; Mathis, G. Luminescent Lanthanide Cryptates: From the Bench to the Bedside. *Inorg. Chem.* **2014**, *53*, 1854–1866.
8. Hasegawa, Y.; Wada, Y.; Yanagida, S. Strategies for the Design of Luminescent Lanthanide(III) Complexes and Their Photonic Applications. *J. Photochem. Photobiol., C* **2004**, *5*, 183–202.
9. Aulsebrook, M. L.; Graham, B.; Grace, M. R.; Tuck, K. L. Lanthanide Complexes for Luminescence-Based Sensing of Low Molecular Weight Analytes. *Coord. Chem. Rev.* **2018**, *375*, 191–220.
10. Fradgley, J. D.; Starck, M.; Laget, M.; Bourrier, E.; Dupuis, E.; Lamarque, L.; Trinquet, E.; Zwier, J. M.; Parker, D. Targeted pH Switched Europium Complexes Monitoring Receptor Internalisation in Living Cells. *Chem. Commun.* **2021**, *57*, 5814–5817.
11. Giraud, M.; Andreiadis, E. S.; Fisyuk, A. S.; Demadrille, R.; Pécaut, J.; Imbert, D.; Mazzanti, M. Efficient Sensitization of Lanthanide Luminescence by Tetrazole-Based Polydentate Ligands. *Inorg. Chem.* **2008**, *47*, 3952–3954.
12. Hemmilä, I.; Laitala, V. Progress in Lanthanides as Luminescent Probes. J. Fluoresc. 2005, 15, 529–542.
13. Sabbatini, N.; Guardigli, M.; Lehn, J.-M. Luminescent Lanthanide Complexes as Photochemical Supramolecular Devices. *Coord. Chem. Rev.* **1993**, *123*, 201–228.
14. Xu, J.; Corneillie, T. M.; Moore, E. G.; Law, G. L.; Butlin, N. G.; Raymond, K. N. Octadentate Cages of Tb(III) 2-hydroxyisophthalamides: A New Standard for Luminescent Lanthanide Labels. *J. Am. Chem. Soc.* **2011**, *133*, 19900-19910.
15. Fradgley, J. D.; Frawley, A. T.; Pal, R.; Parker, D. Striking Solvent Dependence of Total Emission and Circularly Polarised Luminescence in Coordinatively Saturated Chiral Europium Complexes: Solvation Significantly Perturbs the Ligand Field. *Phys. Chem. Chem. Phys.* **2021**, *23*, 11479–11487.
16. Abbas, Z.; Dasari, S.; Beltrán-Leiva, M. J.; Cantero-López, P.; Páez-Hernández, D.; Arratia-Pérez, R.; Butcher, R. J.; Patra, A. K. Luminescent Europium(III) and

Terbium(III) Complexes of β-diketonate and Substituted Terpyridine Ligands: Synthesis, Crystal Structures and Elucidation of Energy Transfer Pathways. *New J. Chem.* **2019**, *43*, 15139–15152.

17. Devi, R.; Vaidyanathan, S. Narrow Band Red Emitting Europium Complexes and Their Application in Smart White LEDs and Vapoluminescent Sensors. *Dalton Trans.* **2020**, *49*, 6205–6219.
18. Stanley, J. M.; Zhu, X.; Yang, X.; Holliday, B. J. Europium Complexes of A Novel Ethylene Dioxythiophene-Derivatized Bis (Pyrazolyl) Pyridine Ligand Exhibiting Efficient Lanthanide Sensitization. *Inorg. Chem*. **2010**, *49*, 2035–2037.
19. Moore, E. G.; Samuel, A. P. S.; Raymond, K. N. From Antenna to Assay: Lessons Learned in Lanthanide Luminescence. *Acc. Chem. Res.* **2009**, *42*, 542–552.
20. Alpha, B.; Ballardini, R.; Balzani, V.; Lehn, J.-M.; Perathoner, S.; Sabbatini, N. Antenna Effect in Luminescent Lanthanide Cryptates: A Photophysical Study. *Photochem. Photobiol.* **1990**, *52*, 299–306.
21. Ge, P.; Selvin, P. R. Carbostyril Derivatives as Antenna Molecules for Luminescent Lanthanide Chelates. *Bioconjug. Chem.* **2004**, *15*, 1088–1094.
22. Singh, K.; Boddula, R.; Vaidyanathan, S. Versatile Luminescent Europium (III)-β-Diketonate-Imidazo-Bipyridyl Complexes Intended for White LEDs: A Detailed Photophysical and Theoretical Study. *Inorg. Chem.* **2017**, *56*, 9376–9390.
23. SeethaLekshmi, S.; Ramya, A.R.; Reddy, M.L.P.; Varughese, S. Lanthanide Complex-derived White-light Emitting Solids: A Survey on Design Strategies. *J. Photochem. Photobiol., C* **2017**, *33*, 109–131.
24. Khistiaeva, V. V.; Melnikov, A. S.; Slavova, S. O.; Sizov, V. V.; Starova, G. L.; Koshevoy, I. O.; Grachova, E. V. Heteroleptic β-diketonate Ln(III) Complexes Decorated with Pyridyl Substituted Pyridazine Ligands: Synthesis, Structure and Luminescence Properties. *Inorg. Chem. Front*. **2018**, *5*, 3015–3027.
25. Nehra, K.; Dalal, A.; Hooda, A.; Bhagwan, S.; Saini, R. K.; Mari, B.; Kumar, S.; Singh, D. Lanthanides β-diketonate Complexes as Energy-efficient Emissive Materials: A Review. *J. Mol. Struct.* **2022**, *1249*, 131531.
26. Hasegawa, Y.; Wada, Y.; Yanagida, S. Strategies for the Design of Luminescent Lanthanide(III) Complexes and Their Photonic Applications. *J. Photochem. Photobiol. C: Photochem. Rev.* **2004**, *5*, 183–202.

27. Galán, L. A.; Reid, B. L.; Stagni, S.; Sobolev, A. N.; Skelton, B. W.; Moore, E. G.; Hanan, G. S.; Zysman-Colman, E.; Ogden, M. I.; Massi, M. Probing the Effect of β-Triketonates in Visible and NIR Emitting Lanthanoid Complexes. *Dalton Trans.* **2018**, *47*, 7956–7964.
28. Hasegawa, Y.; Kitagawa, Y. Thermo-sensitive Luminescence of Lanthanide Complexes, Clusters, Coordination Polymers and Metal-organic Frameworks with Organic Photosensitizers. *J. Mater. Chem. C* **2019**, *7*, 7494–7511 and the references herein.
29. Kuznetsov, K. M.; Kozlov, M. I.; Aslandukov,A. N.; Vashchenko, A. A.; Medved'ko, A. V.; Latipov, E. V.; Goloveshkin, A. S.; Tsymbarenko, D. M.; Utochnikova, V. V. $Eu(tta)_3$DPPZ-based Organic Light-emitting Diodes: Spin-coating vs. Vacuum-deposition. *Dalton Trans.* **2021**, *50*, 9685–9689.
30. Gallardo, H.; Conte, G.; Tuzimoto, P.; Bortoluzzi, A.; Peralta, R. A.; Neves, A. Synthesis, Crystal Structure and Luminescent Properties of New Tris-β-Diketonate Eu(III) Complex with Thiadiazolo Phenanthroline Derivative Ligand. *Inorg. Chem. Commun.* **2008**, *11*, 1292–1296.
31. Cabral, F. M.; Gálico, D. A.; Mazali, I. O.; Sigoli, F. A. Crystal Structure and Temperature Dependence of the Photophysical Properties of the $[Eu(tta)_3(pyphen)]$ Complex. *Inorg. Chem. Commun.* **2018**, 98, 29–33.
32. Rajamouli, B.; Devi, R.; Mohanty, A.; Krishnan, V.; Vaidyanathan, S. Effects of Electron-Withdrawing Groups in Imidazole-Phenanthroline Ligands and Their Influence on the Photophysical Properties of Eu^{III} Complexes for White Light-Emitting Diodes. *New J. Chem.* **2017**, *41*, 9826–9839.
33. Rajamouli, B.; Sood, P.; Giri, S.; Krishnan, V.; Sivakumar, V. A Dual-Characteristic Bidentate Ligand for A Ternary Mononuclear Europium(III) Complex: Synthesis, Photophysical, Electrochemical, and Theoretical Study. *Eur. J. Inorg. Chem.* **2016**, *2016*, 3900–3911.
34. Shavaleev, N. M.; Pope, S. J. A.; Bell, Z. R.; Faulkner, S.; Ward, M. D. Visible-light Sensitisation of Near-Infrared Luminescence from Yb(III), Nd(III) And Er(III) Complexes of 3,6-bis(2-pyridyl)tetrazine. *Dalton Trans.* **2003**, *5*, 808–814.
35. Hasan, N.; Iftikhar, K. Syntheses, Crystal Structure and Photophysical Properties of $[Sm(dbm)_3(impy)]$ And $[Tb(dbm)_3(impy)]$ And Their Hybrid Films. *New J. Chem.* **2019**, *43*, 4391–4405.

36. Hasegawa, Y.; Tsuruoka, S.; Yoshida, T.; Kawai, H.; Kawai, T. Enhanced deep-red Luminescence of Tris(hexafluoroacetylacetonato)samarium(III) Complex with Phenanthroline in Solution by Control of Ligand Coordination. *J. Phys. Chem. A* **2008**, *112*, 803–807.
37. Cooper, M. E.; Sammes, P. G. Synthesis and Spectral Properties of a New Luminescent Europium (III) Terpyridyl Chelate. *J. Chem. Soc., Perkin Trans. 2* **2000**, *8*, 1695−1700.
38. Andreiadis, E. S.; Gauthier, N.; Imbert, D.; Demadrille, R.; Pécaut, J.; Mazzanti, M. Lanthanide Complexes Based on β-Diketonates and A Tetradentate Chromophore Highly Luminescent as Powders and in Polymers. *Inorg. Chem.* **2013**, *52*, 14382−14390.
39. Cheng, H.-B.; Zhang, H.-Y.; Liu, Y. Dual-Stimulus Luminescent Lanthanide Molecular Switch Based on an Unsymmetrical Diaryl Perfluorocyclopentene. *J. Am. Chem. Soc.* **2013**, *135*, 10190−10193.
40. Li, Z.; Hou, Z.; Fan, H.; Li, H. Organic–inorganic Hierarchical Self-Assembly into Robust Luminescent Supramolecular Hydrogel. *Adv. Funct. Mater.* **2017**, *27*, 1604379.
41. Moore, E. G.; Benaglia, M.; Bergamini, G.; Ceroni, P. Synthesis, Stability and Sensitised Lanthanide Luminescence of Heterobimetallic d/f Terpyridine Complexes. *Eur. J. Inorg. Chem.* **2015**, *2015*, 414–420.
42. Bhaumik, C.; Das, S.; Maity, D.; Baitalik, S. A Terpyridyl-Imidazole (Tpy-Himzph$_3$) Based Bifunctional Receptor for Multichannel Detection of Fe^{2+} And F^- Ions. *Dalton Trans.* **2011**, *40*, 11795–11808.
43. Bhaumik, C.; Saha, D.; Das, S.; Baitalik, S. Synthesis, Structural Characterization, Photophysical, Electrochemical, And Anion-Sensing Studies of Luminescent Homo and Heteroleptic Ruthenium(II) And Osmium(II) Complexes Based on Terpyridyl-Imidazole Ligand. *Inorg. Chem.* **2011**, *50*, 12586−12600.
44. Bhaumik, C.; Maity, D.; Das, S.; Baitalik, S. Synthesis, Structural Characterization, Solvatochromism, And Ion-Binding Studies of A Ditopic Receptor Based on 2-(4-[2,29: 69,299]Terpyridin-49-Ylphenyl)-1H-Phenanthro[9,10-D] Imidazole (Tpy-Himzphen) Unit. *RSC Adv.* **2012**, *2*, 2581–2594.
45. Maity, D.; Das, S.; Mardanya, S.; Baitalik, S. Synthesis, Structural Characterization, and Photophysical, Spectroelectrochemical, and Anion-Sensing Studies of

Heteroleptic Ruthenium(II) Complexes Derived from 4′-Polyaromatic-Substituted Terpyridine Derivatives and 2,6-Bis(Benzimidazol-2-Yl)Pyridine. *Inorg. Chem.* **2013**, *52*, 6820–6838.

46. Karmakar, S.; Maity, D.; Mardanya, S.; Baitalik, S. Demonstration of Multiple Logic Operations in A Heteroditopic Pyrene-Phenylimidazole-Terpyridine Conjugate Based on Optical Responses by Selective Anions and Cations: An Experimental and Theoretical Investigation. *J. Phys. Chem. A* **2014**, *118*, 9397−9410.
47. Karmakar, S.; Maity, D.; Mardanya, S.; Baitalik, S. Multichromophoric Bimetallic Ru(II) Terpyridine Complexes Based on Pyrenyl-Bis-Phenylimidazole Spacer: Synthesis, Photophysics, Spectroelectrochemistry, And TD-DFT Calculations. *Inorg. Chem.* **2014**, *53*, 12036–12049.
48. Paul, A.; Bar, M.; Ahmed, T.; Baitalik, S. Anion-sensitive Photophysics of Luminescent Trimetallic Complexes of Fe (II), Ru (II), And Os (II) With Polarized NH Motifs. *Polyhedron* **2020**, *190*, 114772.
49. Deb, S.; Sahoo, A.; Ahmed, T.; Baitalik, S. Stimuli-Responsive Molecular Switches and Logic Devices Based on Ru(II)−Terpyridyl−Imidazole Coordination Motif. *J. Phys. Chem. B* **2021**, *125*, 8919−8931.
50. Abbas, Z.; Dasari, S.; Patra, A. K. Ternary Eu(III) and Tb(III) β-diketonate Complexes containing Chalcones: Photophysical Studies and Biological Outlook. *RSC Adv.* **2017**, *7*, 44272–44281.
51. Constable, E. C.; Ward, M. D.; Corr, S. A Convenient, High Yield Synthesis Of 2, 2′: 6′, 2 ″-Terpyridine and Its Iron (II) Complex. *Inorg. Chim. Acta*, **1988**, *141*, 201–203.
52. Furniss, B. S.; Hannaford, A. J.; Smith, P. W. G.; Tatchell, A. R. *Vogel's Text Book of Practical Organic Chemistry*; ELBS, Longman, London, 1989.
53. Melby, L. R.; Rose N. J.; Abramson, E.; Caris, J. C. Synthesis and fluorescence of some trivalent lanthanide complexes. *J. Am. Chem. Soc*. **1964**, *86*, 5117–25.
54. Shi, M.; Li, F.; Yi, T.; Zhang, D.; Hu, H.; Huang, C. Tuning the Triplet Energy Levels of Pyrazolone Ligands to Match the $^5D_0$ Level of Europium(III). *Inorg. Chem.* **2005**, *44*, 8929–8936.
55. (a) *SHELXTL* Reference, M. Bruker Analytical X-Ray Systems. *Inc.: W. I* **2000**. (b) G. M. Sheldrick. A short history of SHELX. *Acta Crystallogr., Sect. A: Found. Crystallogr*. 2008, **64**, 112. (c) Dolomanov, O. V.; Bourhis, L. J.; Gildea, R. J.; Howard, J. A. K.; Puschmann, H. *OLEX2*: A Complete Structure Solution,

Refinement and Analysis Program. *J. Appl. Crystallogr.* **2009**, *42*, 339–341. (d) K. Bradenburg. *Diamond*, version 3.1 e; Crystal Impact GbR: Bonn, Germany, 2005.

56. Sénéchal-David, K.; Hemeryck, A.; Tancrez, N.; Toupet, L.; Williams, J. A. G.; Ledoux, I.; Zyss, J.; Boucekkine, A.; Guégan, J.-P.; Le Bozec, H.; Maury, O. Synthesis, Structural Studies, Theoretical Calculations, and Linear and Nonlinear Optical Properties of Terpyridyl Lanthanide Complexes: New Evidence for the Contribution of f Electrons to the NLO Activity. *J. Am. Chem. Soc.* **2006**, *128*, 12243–12255.
57. Dar, W. A.; Iftikhar, K. Phase Controlled Colour Tuning of Samarium and Europium Complexes and Excellent Photostability of Their PVA Encapsulated Materials. Structural Elucidation, Photophysical Parameters, and the Energy Transfer Mechanism in the Eu^{3+} Complex by Sparkle/PM3 Calculations. *Dalton Trans.* **2016**, *45*, 8956–8971.
58. Kleinerman, M. Energy Migration in Lanthanide Chelates. *Chem. Phys.* **1969**, *51*, 2370–2381.
59. Rajendran, M.; Devi, R.; Mund, S.; Singh, K.; Vaidyanathan, S. Energy Transfer Cooperation Between Ligands and Eu^{III} Ions in Molecular Europium Complexes for Vapoluminescence Sensing (Reversible On/Off Emission Switching) and Hybrid White LED/Plant-Growth Applications. *J. Mater. Chem. C.* **2021**, 9, 15034–15046.
60. Binnemans, K. Handbook on the Physics and Chemistry of Rare Earths, ed. J.-C. G. B. Karl, A. Gschneidner and K. P. Vitalij, Elsevier, **2005**, 35, 107–272.
61. Teotonio, E. E. S.; Fett, G. M.; Brito, H. F.; Faustino, W. M.; de Sá, G. F.; Felintoe, M. C. F.C.; Santos, R. H. A. Evaluation of Intramolecular Energy Transfer Process in the Lanthanide(III) Bis- And Tris-(TTA) Complexes: Photoluminescent and Triboluminescent Behavior. *J. Lumin.* **2008**, *128*, 190–198.
62. Sivakumar, S.; Reddy, M. L. P. Bright Green Luminescent Molecular Terbium Plastic Materials Derived from 3,5-Bis(Perfluorobenzyloxy)Benzoate. *J. Mater. Chem.* **2012**, *22*, 10852–10859.
63. Bassett, A. P.; Magennis, S. W.; Glover, P. B.; Lewis, D. J.; Spencer, N.; Parsons, S.; Williams, R. M.; Cola, L. D.; Pikramenou, Z. Highly Luminescent, Triple- And Quadruple-Stranded, Dinuclear Eu, Nd, And Sm(III) Lanthanide Complexes Based on Bis-Diketonate Ligands. *J. Am. Chem. Soc.* **2004**, *126*, 9413–9424.

64. Shi, J.; Hou, Y.; Chu, W.; Shi, X.; Gu, H.; Wang, B.; Sun, Z. Crystal Structure and Highly Luminescent Properties Studies of Bis-β-Diketonate Lanthanide Complexes. *Inorg. Chem.* **2013**, *52*, 5013–5022.
65. Campiglia, A. D.; Jucov, E. V.; Timofeeva, T. V.; Belfield, K. D. Two-photon Sensitized Visible and Near-IR Luminescence of Lanthanide Complexes Using A Fluorene-Based Donor–Π-Acceptor Diketonate. *Dalton Trans.* **2014**, *43*, 16626–16639.
66. Netoa, A. N. C.; Teotonio, E. E. S.; de Sá, G. F.; Brito, H. F.; Legendziewicz, J.; Carlos, L. D.; Felinto, M. C. F. C.; Gawryszewska, P.; Moura Jr., R. T.; Longo, R. L. Faustino, W. M.; Malta, O. L. Modeling Intramolecular Energy Transfer In Lanthanide Chelates: A Critical Review And Recent Advances Handbook on the Physics and Chemistry of Rare Earths. Elsevier, **2019**, *56*, 55–162.
67. Berry, M. T.; May, P. S.; Xu, H. Temperature Dependence of the Eu^{III} $^5D_0$ Lifetime in Europium Tris(2,2,6,6-Tetramethyl-3,5-Heptanedionato). *J. Phys. Chem.* **1996**, *100*, 9216–9222.
68. Miranda, Y. C.; Pereira, L. L. A. L.; Barbosa, J. H. P.; Brito, H. F.; Felinto, M. C. F. C.; Malta, O. L.; Faustino, W. M.; Teotonio, E. E. S. The Role of the Ligand-To-Metal Charge-Transfer State in the Dipivaloylmethanate-Lanthanide Intramolecular Energy Transfer Process. *Eur. J. Inorg. Chem.* **2015**, *2015*, 3019–3027.
69. An, B. L.; Gong, M. L.; Li, M. X.; Zhang, J. M. Synthesis, Structure and Luminescence Properties of Samarium (III) And Dysprosium (III) Complexes with A New Tridentate Organic Ligand. *J. Mol. Struct.* **2004**, *687*, 1–6.
70. Latva, M.; Takalo, H.; Mukkala, V. M.; Matachescu, C.; Rodríguez-Ubis, J. C.; Kankare, J. Correlation Between the Lowest Triplet State Energy Level of the Ligand and Lanthanide(III) Luminescence Quantum Yield. *J. Lumin.* **1997**, *75*, 149–169.
71. Bettencourt-Dias, A. D. Small Molecule Luminescent Lanthanide Ion Complexes – Photophysical Characterization and Recent Developments. *Curr. Org. Chem.* **2007**, *11*, 1460–1480.
72. Samuel, A. P.; Xu, J.; Raymond, K. N. Predicting Efficient Antenna Ligands for Tb(III) Emission. *Inorg. Chem.*, **2009**, *48*, 687–698.

****

Chapter 3

A Terpyridyl-Imidazole Based Europium Tris-(β-diketonate) Complex as an Efficient Molecular Luminescent Thermometer and Single-Component White Light Emitter via Synergy in Energy Transfer Between Ligand and Eu^{3+}

3.1. Introduction

Temperature plays a crucial role in diverse aspects of scientific and industrial domains.[1] Hence, its precise measurement with utmost accuracy is essential in the related fields.[1-4] Molecular luminescent thermometers are the next-generation tool in this regard because of their several favorable advantages over the traditional thermosensors such as very fast response, high accuracy, non-invasive or non-contact functioning, nanoscale high resolution, and effectiveness in strong electromagnetic fields. These attributes count them as one of the promising candidates for various applications such as intracellular thermal imaging and early tumour detection in biological and medical fields.[1,5-6] Diverse systems, including organic dyes,[7-9] metal complexes,[10-15] ratiometric metal-organic frameworks (MOFs),[16-18] coordination polymers,[19-21] and organic-inorganic hybrid materials [22-25] have shown their credibility as molecular luminescent thermometers across a wide range of temperature, spanning from cryogenic (T<100 K) to physiological domain (298-323 K). In this regard, lanthanide complexes play important role due to their high thermal and optical stability.[26] While going through the literature, it is noticed that the majority of these optical thermosensitive systems are either lanthanide-coordination polymers or single lanthanide-doped or mixed lanthanide-doped MOFs. By contrast, lanthanide-containing discrete or small molecules are scarcely reported to address the issue.[23-30] In addition, temperature-sensitive materials are also important in the fabrication of temperature-responsive paints, wherein the material's color changes in response to temperature variation.[6]

Lanthanide complexes also demonstrate their utility in the fabrication of white light-emitting materials, which are being considered as the next-generation light sources due to their potential role in cost-effective illumination, liquid crystal display backlights, and full-color smart displays. Consequently, they hold the promise of replacing conventional incandescent bulbs and fluorescent lamps.[31-33] As per our literature knowledge, the white light emission is primarily achieved via conventional trichromatic (Red-Green-Blue, R-G-B) approach upon mixing multiple components in lanthanide-based coordination polymers (CPs) and/or MOFs.[17,34] By contrast, examples upon utilizing a single-component approach are relatively sparse, despite of their ease of preparation and stable CIE coordinates.[35-37] Of course, a few instances exist wherein this has been demonstrated, either through electroluminescence,[38,39] or by altering the excitation wavelength,[40,41] or by solvatochromism.[42] Hence, the implication of single-component white light-emitting small molecules is a sector that deserves to be explored explicitly.

Lanthanide coordination complexes have emerged as prospective candidates for designing a diverse array of molecular devices, thanks to their exceptional optical[43-46] and magnetic properties.[47-48] Due to the presence of 4f electrons, lanthanide ions exhibit some unique luminescence characteristics, such as distinct narrow emission bands that remain almost unaltered under the coordinating influence of ligands, together with long-lived excited states, which in turn make the lanthanide compounds irreplaceable fluorescent probes.[43-46] Despite these fascinating and well-resolved emission features, one of the major deterrents for achieving a bright luminescence is the Laporte forbidden nature of f-f transitions in the trivalent lanthanide ions, which leads to weak emission upon direct excitation. In this regard, organic chromophore plays an important role, exhibiting light-induced intramolecular energy transfer (IET) to the emissive excited states of the Ln^{III} ion (antenna effect).[49-50] β-dikeonates play a pivotal role as the sensitizers, and with time various substitutions and replacements have been brought into play to facilitate better energy transfer by judicious choice of the energy donor states.[51] To this end, a great variety of lanthanide-β-dikeonates were studied to design such potential luminescent probes, and among them, europium (III)-containing complexes have manifested to be a significant candidate because of their efficient red emissive properties.[37] It is important to mention that the conventional synthesis of lanthanide-β-dikeonates often leads to the formation of bis-hydrated tris(β-dikeonates) which usually exhibit weaker emission not only due to non-radiative vibrational deactivation induced by O-H bonds but also undergo solvent-induced quenching of luminescence.[52] To cut down this detrimental effect, appropriate ancillary ligands,[52] very often bipyridine- and terpyridine-type coordinating motifs,[53-54] have been incorporated to the lanthanide core.[55-56] Our group has been working with various polyheterocyclic ligands during last one decade[57-59] and among them, a terpyridyl-imidazole based tridentate ligand, tpy-Himzphen has demonstrated its efficacy for the synthesis of various useful platinum metal complexes.[60-61] Recently, we have reported a series of four different lanthanide complexes of the type, $Ln(tta)_3$(tpy-HImzphen) [Ln= La, Eu, Sm, Tb] derived from the said tpy-Himzphen ligand.[62] Among others, one of our major observations with regard to $Eu(tta)_3$(tpy-HImzphen) complex was that the extent of energy transfer from tpy-HImzphen to Eu^{III} is not as high as could be expected from their favorable energy difference. The molecular structure of the said Eu(III) complex is provided in Scheme 3.1. Besides, we also observed that the relative intensity, as well as the excited state lifetime at 614 nm of the said Eu-complex, was amplified upon lowering the temperature to 77K as compared to room temperature. These two phenomena motivate us to

explore whether this complex manifests thermosensitivity at the expense of Eu-centered luminescence alteration.

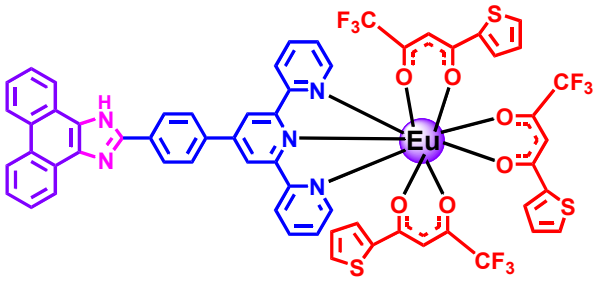

Scheme 3.1. Molecular structure of the Eu(III) complex in the present study

Herein, we have thoroughly investigated the thermosensitive behavior of $Eu(tta)_3$(tpy-HImzphen) complex through steady-state and time-resolved emission spectroscopy. We found that its relative temperature sensitivity (S_r) is the highest among the earlier reported cases of ternary lanthanide tris-(β-dikeonate) complexes.[63-67] The unique thermosensing behavior offered by the Eu-complex also leads to thermochromism, and we hardly found any example from this genre to show such exceptional thermochromism in the temperature domain of 263-343 K, among the very few reported thermochromic systems.[68,69] Additionally, the complex also displays the emitting color variation quite efficiently upon variation of solvents in which Eu^{III}-complex is no longer compelled to emit its anticipated or characteristic red color only. Finally, by amalgamating the thermochromic and solvatochromic responses, we have achieved the white light emission from a single component, which is also a major accomplishment of this work. In the end, we made an effort to elucidate the observed thermosensing phenomenon, counting the role of the ligand to metal charge transfer (LMCT) state.

3.2. Experimental Section

3.2.1. Materials. 2-theonyltrifluoroacetone (Htta) and europium chloride or nitrate salts were purchased from Merck as their hexa- or pentahydrated forms and used as received. Solvents were dried and distilled following the standard procedure. 4′-(*p*-formylphenyl)-2,2′:6′,2″-terpyridine (tpy-PhCHO) and 9,10-phenanthrenedione were synthesized by following reported literature method.[70-73]

3.2.2. Instruments and Physical Methods. The Diffuse Reflectance Spectroscopic (DRS) measurements of the samples were collected from a Shimadzu-3600 UV–Vis-NIR

spectrophotometer. Barium sulfate powder was used as the reflectance standard during the DRS measurements. The rest of the details have already been presented in Chapter 2.

3.3. Results and Discussions

3.3.1. Synthesis and Characterization. Synthesis and thorough characterization of the complex, [Eu(tta)$_3$(tpy-HImzphen)], has already been described in chapter 2.[62]

3.3.2. Thermosensing and Thermochromic Behavior of the Complex. Intercomponent energy transfer in the lanthanide complexes usually takes place through two distinct pathways. In the first pathway, there is a transfer of energy from the ligand to the metal via the ligand's lowest triplet state to the emissive resonance energy level of the lanthanide ion in accordance with Dexter's electron exchange interaction theory. In the second mechanism, energy transfer occurs from the metal to the ligand through a low-lying ligand-to-metal charge transfer state (LMCT). While there isn't direct proof of this yet, diffuse reflectance spectroscopy (DRS) serves as a valuable tool for investigating this phenomenon. Consequently, the second mechanism exhibits a substantial temperature dependency, leading to thermal quenching of the emission from the lanthanide center as the temperature rises. In our investigation of the temperature sensitivity of the Eu^{III} complex, we first examined its thermal stability, which has been documented in our previous report, which reveals that the complex maintains its structural integrity up to 290 °C. Following this, we have performed temperature-dependent emission spectral measurements of the complex. We collected both steady-state emission spectra (λ_{ex}=340 nm) and the excited-state decay profiles (λ_{ex}=370 nm spectraLED source) for Eu(tta)$_3$(tpy-HImzphen) in acetonitrile upon varying the temperature between 268K and 343K (Figures 3.1a and 3.1b). It is evident that as the temperature increases the intensity of the europium-centered emission peak at 614 nm gradually diminishes, and at its expense, the peak at ~465 nm associated with the ligand-centered emission progressively intensifies. The influence of temperature on the emission spectral profile of the Eu^{III} complex is also depicted in the corresponding chromaticity diagram as shown in Figure 3.1c. A noticeable change in color from red (at 268 K) to violet (at 313 K) and finally to blue (at 343 K) is observed upon gradual increase in temperature. In line with the steady-state spectra, the excited state lifetime of the complex at the monitoring

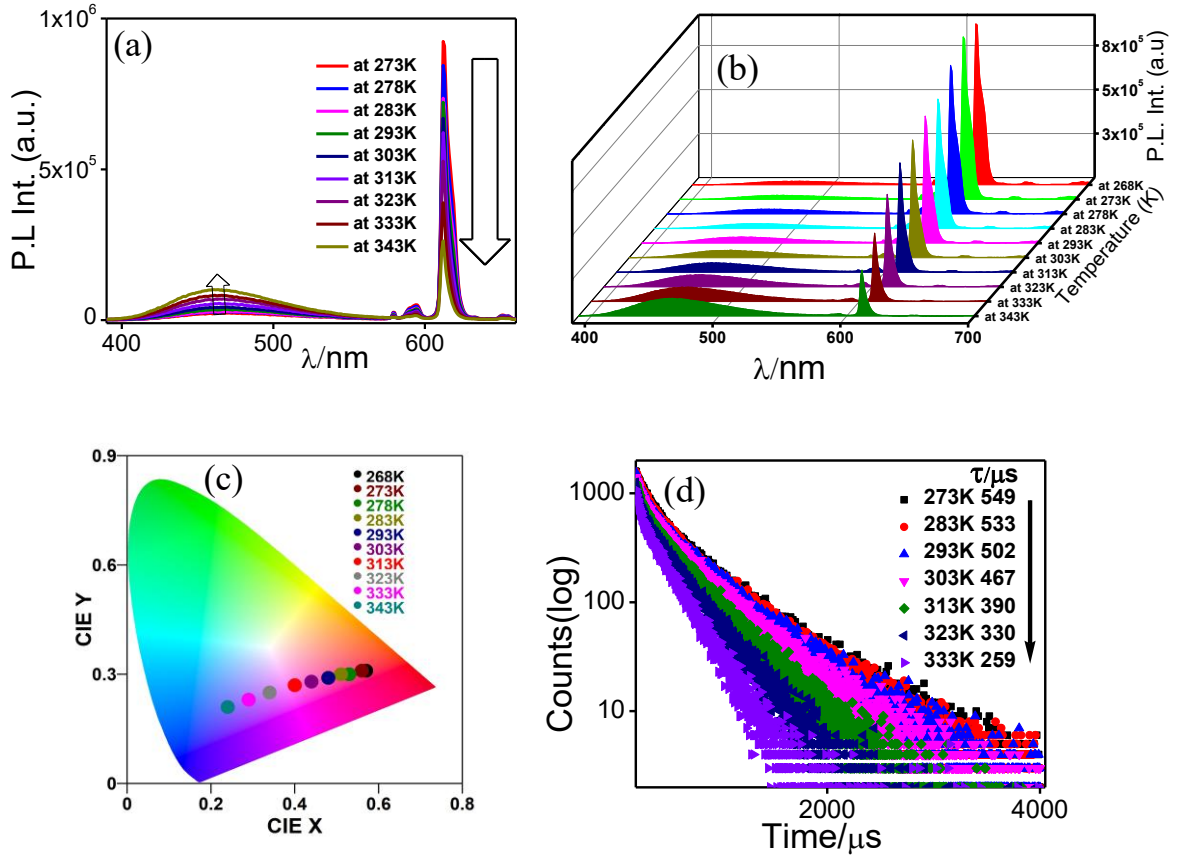

Figure 3.1. Temperature-dependent steady-state emission spectra portrayed in both 2D (a) and 3D (b) mode. (c) Corresponding chromaticity diagram and (d) excited-state lifetime decay plot for $Eu(tta)_3(tpy\text{-}HImzphen)$ in MeCN.

wavelength of 614 nm (λ_{ex}=370 nm), is found to decrease systematically from 549 μs at 268K to 259 μs at 343K (Figure 3.1d). Now, the temperature sensing aspect of the Eu(III) complex has been assessed in two different ways, viz., decay time method and intensity ratio algorithm. The decay time method relies on the temperature-dependent variation in the lifetime of an emitting excited level, while the intensity ratio algorithm directly utilizes the intensity of one or more transition(s) to gauge the temperature. When temperature sensing measurements are carried out based on a single transition band, it could be influenced by factors like the nature of the excitation source and the detector. To circumvent these limitations, we assess the thermo-sensitivity of the complex based on the intensity ratio of two transitions. The intensity of each transition is directly proportional to the total number of atoms (population) in a specific excited state at temperature T. This relationship can be expressed by equation (3.1) as follows:

$$I = \frac{I_0}{1 + A\,exp\left(\frac{-E_a}{kT}\right)} \quad \text{.. (3.1)}$$

where A is connected to the ratio of non-radiative (at T = 0 K) and radiative process rates, k represents the Boltzmann constant, and E_a stands for the activation energy of the de-excitation pathway relative to the energy of the $^5D_0$ level. A thermometric parameter Δ at temperature T is used to quantify the temperature dependence of the complex, which can be denoted by equation (3.2).

$$\Delta = \frac{I_1}{I_2} \quad \text{.. (3.2)}$$

where I_1 and I_2 are the intensities of two different transitions. It is worth noting that many thermosensitive materials have been designed by combining two distinct lanthanide ions within metal-organic frameworks or other polymeric structures. For such systems, equation (2) represents two separate transitions involving the respective lanthanide centers. As far as our literature knowledge goes, there are very few reports on discrete coordination environments, and these reports suggest that one can use either I_{MD}/I_{ED} or I_M/I_{Lig} as the intensity ratio for such discrete systems.[26,63-67] Here, I_{MD} and I_{ED} represent the emission intensity of magnetic dipole and electric dipole transitions, while I_M and I_{Lig} correspond to the emission intensity of the lanthanide center and the intensity of the ligand center, respectively. It's worth noting that the emission from the ligand center is also influenced by temperature, allowing us to employ the I_M/I_{Lig} ratio. The relationship between the intensity ratio Δ (Here, I_M/I_{Lig}) and temperature can be best fitted with an empirical polynomial equation as narrated below (equation 3.3).

$$\Delta = 0.0034T^2 - 2.5023T + 461.22 \qquad (R^2 = 0.99) \quad \text{.. (3.3)}$$

where T is the temperature and R^2 is the correlation coefficient of the best-fitted curve.

In line with intensity-based detection, the temperature-dependent variation of lifetime at the monitoring wavelength of 614 nm can also be fitted through the following empirical formula (equation 3.4):

$$\Delta = -0.06T^2 + 31.403T - 3549.7 \qquad (R^2 = 0.996) \quad \text{.. (3.4)}$$

The corresponding Δ vs T plots have been depicted in Figures 3.2 and 3.3.

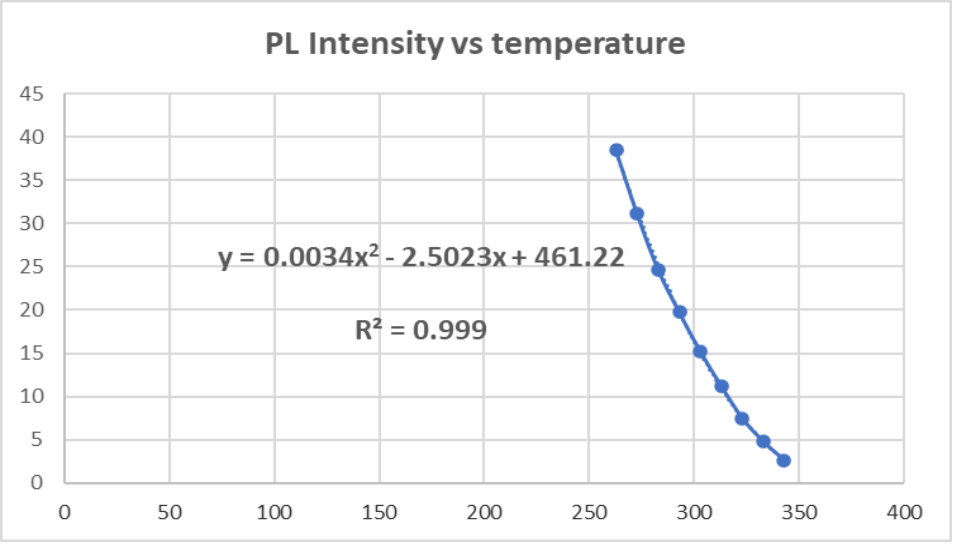

Figure 3.2. Change in photoluminescence intensity ratio with varying temperature from 273-343 K. The dotted line indicates the best-fitted curve.

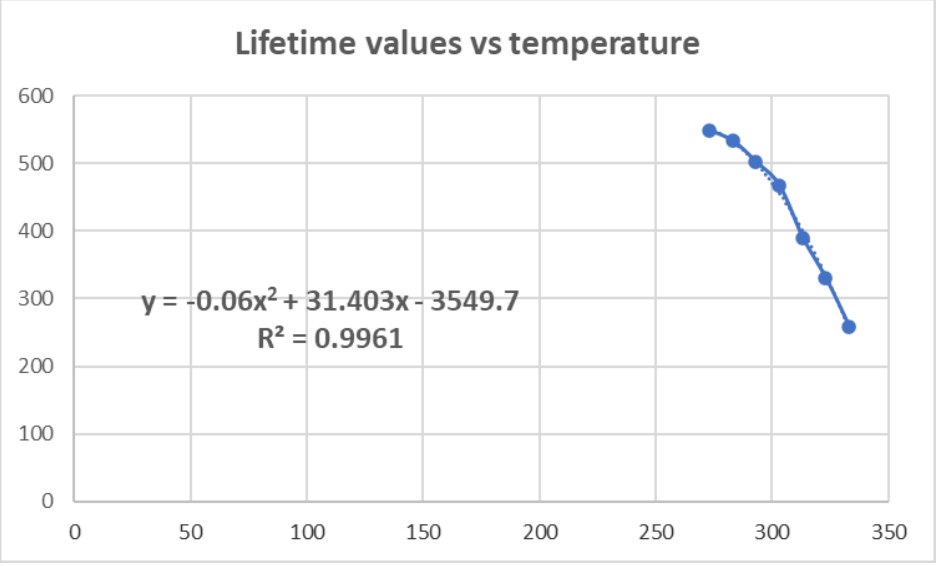

Figure 3.3. Change in lifetime values with varying temperature from 273- 343 K. The dotted line indicates the best-fitted curve.

From these two equations, the thermo-sensing efficiency of our synthesized complex can be quantified. The temperature-dependent performance could be assessed via different parameters. Herein, we employed the relative thermal sensitivity (S_r) parameter that signifies

the proportional change in a thermometric parameter Δ (as defined in equation 5) with per degree of temperature alteration (% K^{-1}; denoted as S_r, i.e., relative thermal sensitivity)

$$S_r = \frac{1}{\Delta}\left(\frac{\partial \Delta}{\partial T}\right) \quad .. (5)$$

The maximum S_r value that is observed is referred to as S_m and the corresponding temperature is designated as T_m. The thermal sensitivity (S_r) for the present Eu^{3+}-complex ranges from 1.86 to 5.78 % K^{-1} (S_m=5.78 % K^{-1} at T_m=343 K), indicating that our system undoubtedly serves as one of the best lanthanide-based temperature sensors launched till date as compared to others reported in the literature (Table 3.1). We have also assessed the

Table 3.1. Comparative Study of Some Earlier Reported Lanthanide (β-diketonate) Complexes

Complex	S_r (%K^{-1})	Temp. range	Ref.
$[Eu(tta)_3(pyphen)]$; tta= thenoyltrifluoroacetone and pyphen= pyrazino[2,3-f][1,10]phenanthroline	1.68	283–323 K	63
$Eu(CPDK3\text{-}5)_3phen$; CPDK3-5=1-(4-(4-propylcyclohexyl)phenyl)octane-1,3-dione and phen=1,10-phenanthroline	2.2-1.5	298-348 K	64
$Eu(L)_3$; L= 1,3-di(thienyl)propane-1,3-diones	0.65	100K< T < 400K	65
Eu-DT; DT= Dinaphthoylmethane (DNM) and trioctylphosphine oxide	2.2	298-318 K	66
[CHOL][Eu(FOD)4]; CHOL=choline and FOD= tetrakis-1,1,1,2,2,3,3-heptafluoro-7,7-dimethyloctane-4,6-dionate	0.45-7.0	298-368 K	67

thermal sensitivity (S_r) in terms of lifetime values, and the result ranges from 0.25-3.36 % K^{-1} (S_m=3.36 % K^{-1} at T_m=333 K), which seems much better than those of the earlier reported systems. Another critical parameter is the temperature uncertainty (δT), also referred to as temperature resolution, which can be determined by using equation 6 as described below:

$$\delta T = \frac{1}{S_r}\left(\frac{\delta \Delta}{\Delta}\right) \quad .. (6)$$

This parameter defines the smallest resolvable change in temperature (δT) that the thermometer can detect. Our synthesized complex exhibits δT value of 0.012 K in terms of intensity ratio and 0.009 K with regard to lifetimes, both of which are well-below the acceptable limit of δT<1 K. Thus, the complex can be recommended as an excellent

temperature sensor in a wide temperature domain of 273-343 K covering the physiological region (298-323 K) in terms of emission intensity ratio, lifetime alteration as well as variation of its emitting color.

3.3.3. Solvatochromic Behaviors of Eu(tta)$_3$(tpy-HImzphen). We are also interested in investigating the influence of different solvents on the emission characteristics of the present complex. Taking advantage of fairly good solubility, we acquired the emission spectrum (λ_{ex}=340 nm) as well as the lifetime (λ_{ex}=370 nm SpectraLED) of the complex in a wide variety of solvents, viz. PhCH$_3$, CHCl$_3$, DCM, Me$_2$CO, EtOAc, DMSO, MeCN, EtOH, MeOH, and the results are summarized in Figure 3.4 and Table 3.2. Although the intensities

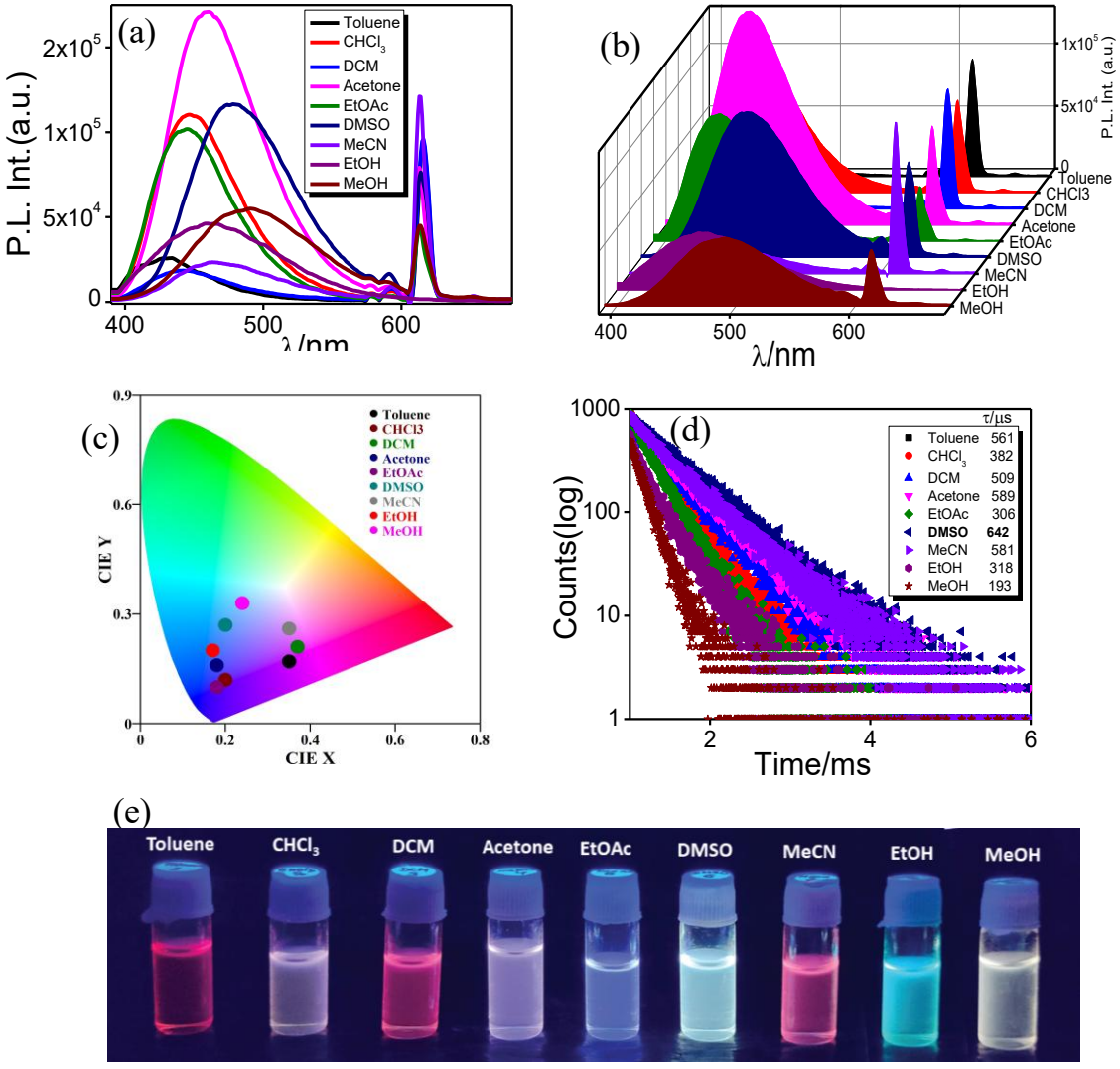

Figure 3.4. Photoluminescence spectrum of the complex in different solvents (a and b). Corresponding chromaticity diagram (c), lifetime decay profiles (d), and photograph in different solvents under UV light irradiation (e).

Table 3.2. Solvatochromic Emission Spectral Parameters of Eu(tta)$_3$(tpy-HImdzphen) at RT

Solvents	λ_{em}, nm (Ligand-centered)	λ_{em}, nm (Eu^{3+}-centered)	τ, µs (λ_{em}=614 nm)	CIE colour coordinates	
				x	***y***
Toluene	433	579, 593, 614, 652	561	0.35	0.17
Chloroform	447	do	381	0.20	0.12
Dichloromethane	443	do	507	0.37	0.21
Acetone	460	do	588	0.18	0.16
Ethyl acetate	444	do	306	0.18	0.10
Dimethylsulfoxide	478	do	641	0.20	0.27
Acetonitrile	465	do	581	0.35	0.26
Ethanol	460	do	318	0.17	0.20
Methanol	490	do	193	0.24	0.33

of both metal- and ligand-centered emission peaks get altered upon solvent variation, the peak position of only the ligand-centered emission gets affected. Among all the solvents, the ligand-centered peak is most intense in Me_2CO while least in DCM. By contrast, the characteristic f-f transition peaks are prominent in almost all the solvents (except EtOH), which indicates substantial but incomplete ligand→Eu^{III} energy transfer (Figure 3.4a). The hypersensitive peak is most intense in MeCN with respect to its corresponding ligand-centered peak, while the least intense in EtOH (Figure 3.4b). The latter process may be attributed to the coordination of solvent molecule and non-radiative quenching associated with the first vibrational overtone of O-H bond. The other probable reason is the quenching of the triplet state energy of the ligand by dipole-dipole coupling of ligands with the solvent molecules.[74] On monitoring the lifetime at λ_{em}=614 nm upon irradiation with a 370 nm SpectraLED source, we observed that the lifetime decay profiles of the complex in all the solvents are well-fitted with a mono-exponential function as shown in equation (3.7), indicating the presence of a single emissive species in all cases:

$$I(t) = I_0 + A_1 \exp\left(\frac{-t}{\tau}\right) \quad \text{.. (3.7)}$$

where A_1 is the scalar quantity obtained upon curve fitting, t is the time in ms, $I_0 = 0$ is the offset value, and τ is the decay time for the exponential component. The highest lifetime value is achieved in DMSO (τ_1 =641 µs), whereas the lowest in MeOH (τ= 193 µs) (Figure 3.4d) and Table 3.2. This lower lifetime value in methanol can be attributed to the

coordinating solvent quenching, resulting in non-radiative deactivation via high-energy oscillators like O-H. The emission spectral response in various solvents is utilized to construct respective CIE diagrams. It is interesting to note that the tuning of the emission color of the present Eu^{III}-complex is made possible across the entire visible region (blue→green→red) upon varying the nature of the solvents (Figure 3.4c). This variation in emitting color is because of its dual-emission characteristics. The photograph of different emission colors that are evolved under UV illumination of the complex in different solvents is also displayed in Figure 3.4e.

3.3.4. Modulation of the Photophysics by Solvent-Mixing. Solvent-dependent CIE diagram motivates us to investigate the white-light emission characteristics of the present Eu(III)-complex. The luminescence response of the complex in methanol and hexane is of particular interest in this regard. Upon illuminating the complex at 340 nm, the hypersensitive $^5D_0 \rightarrow {}^7F_2$ transition is found to be relatively more intense in hexane with respect to the ligand-centered emission, leading to its characteristic red color emission with the CIE color coordinates of x=0.54 and y=0.28 as depicted in Figure 3.5. By contrast, the intensity of the peak due to the same transition is dramatically less, in fact even less than that of the ligand-

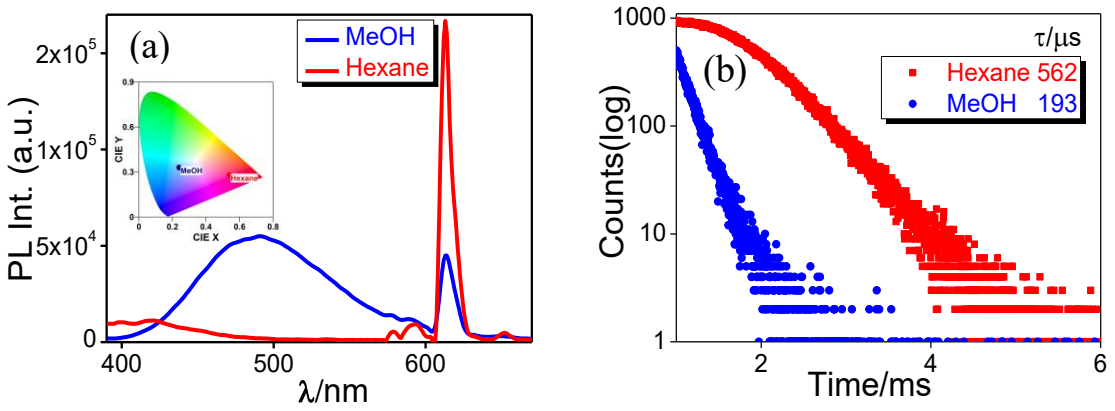

Figure 3.5. Photoluminescence spectra (a) and lifetime decay profiles (b) of the complex in hexane and methanol at RT. inset to Figure (a) shows the corresponding CIE diagram.

centered one, in methanol. This may be ascribed to solvent-induced quenching induced by high-energy oscillator like O-H. However, this dual emission in methanol provides a cyan colored-emission with CIE color coordinates of x=0.24 and y=0.33 (inset, Figure 3.5a). The higher excited state lifetime value (λ_{ex}=370 nm spectraLED) in hexane (τ=562 μs) as compared to that in methanol (τ=193 μs) is also in line with the solvent quenching aspect.

The relative positions of two points in the CIE plot further guide us to acquire the emission spectrum of the complex by varying the ratio of the said solvents to achieve white light emission. We noticed an overall decrease in emission intensity upon a systematic increase in the ratio of the methanol fraction. Interestingly, our complex exhibits near-white light emission in a 9:1 (v/v) methanol:hexane mixture (λ_{ex}=340 nm) at room temperature (Figure 3.6a and 3.6c). We also acquired the lifetime of the complex (λ_{ex}=370 nm spectraLED) upon systematic increase in the methanol fraction in methanol:hexane mixture at RT (Figure 3.6b). A gradual decrease in lifetime from 435μs to 298 μs takes place upon increasing the ratio of methanol, which is also in good agreement with the acquired lifetime value in both pure methanol and pure hexane.

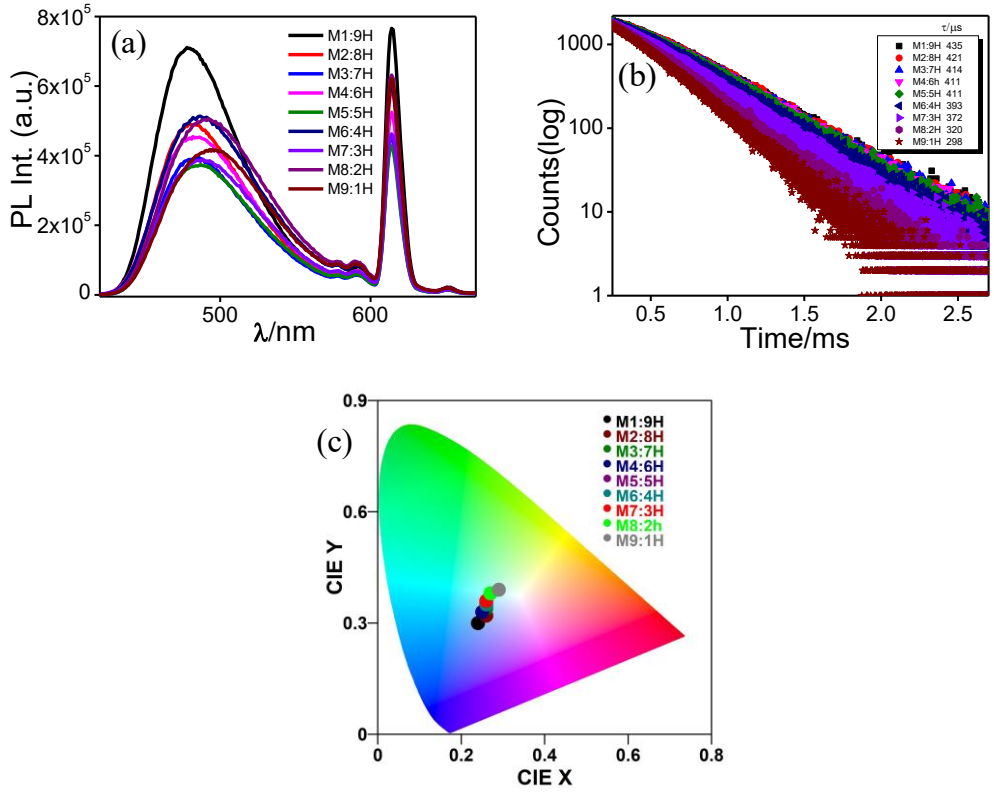

Figure 3.6. Changes in photoluminescence spectra (a) and lifetime decay profiles (b) of the complex upon varying the relative amount of methanol and hexane at RT.

In the temperature-dependent experiment of $Eu(tta)_3$(tpy-HImzphen) in pure MeCN, we observed a horizontal variation of the emission position in CIE plot upon changing the temperature as depicted in Figure 3.1c. Here also, we adopted the same strategy in case of 9:1 (v/v) methanol-hexane mixture and carried out the emission spectral measurement (λ_{ex}=340 nm) by varying the temperature. Interestingly, we are successful in achieving our desired

white light emission at 283 K as reflected in the chromaticity diagram of the complex (Figure 3.7).

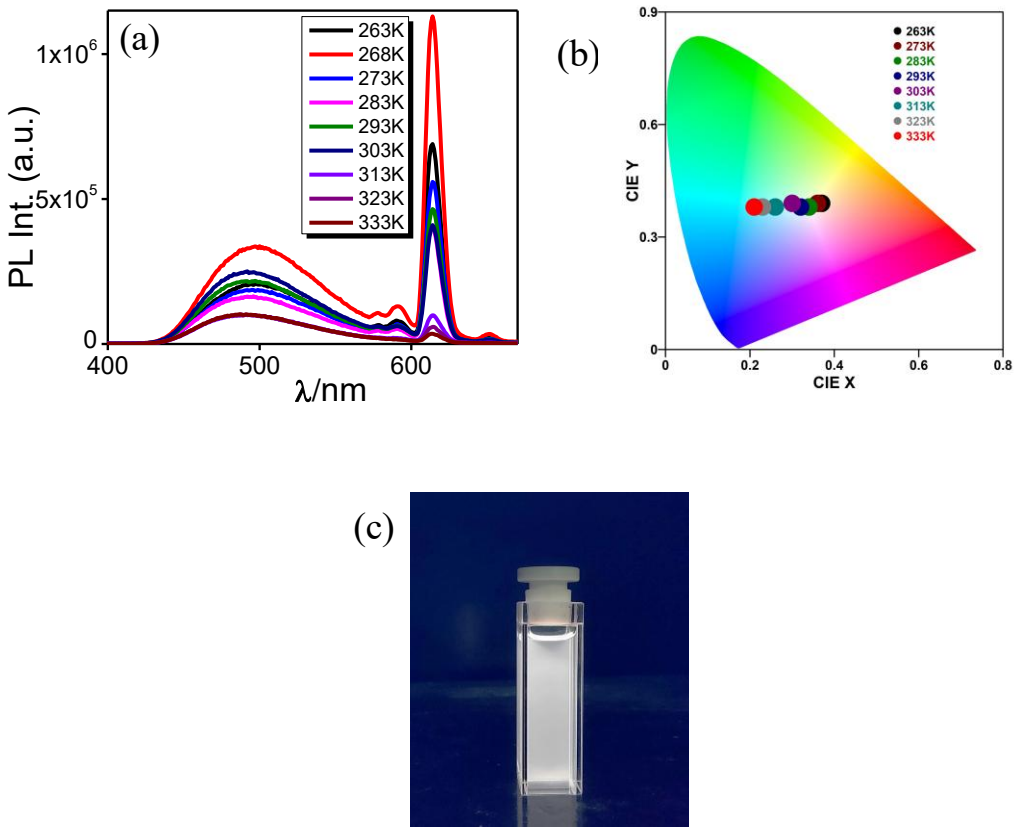

Figure 3.7. (a) Changes in photoluminescence spectra of the complex in methanol-hexane mixture (9:1, v/v) upon varying temperature. (b) Corresponding CIE diagram is presented in figure b, while white light emission under UV light illumination (λ_{ex}=366 nm) is displayed in figure c.

3.3.5. Elucidation for the Temperature-Sensitive Behavior of Eu(tta)$_3$(tpy-HImzphen). It is well-known that to achieve effective sensitization of the lanthanide metal, one should abide by an empirical rule with regard to the energy gap between the T_1 level of ligand and the lowest emitting state of the lanthanide ion (Ln*) which should preferably be within the domain of 2500-4000 cm^{-1}. In spite of fulfilling the required condition, the extent of tpy-HImzphen→Eu^{III} energy transfer in our recently reported [Eu(tta)$_3$(tpy-HImzphen)] complex is not as high as could be expected from the favourable energy difference {$\Delta E(T_1$-Ln*)} (η_{sens}=37%, Table 3.3). The intrinsic quantum yield (Φ_{ff}), the energy transfer efficiency of the ligand tpy-HImzphen (η_{sens}), radiative (k_r) and non-radiative (k_{nr}) rate constants were calculated using the following equations[75]:

$$k_r = A_{MD,0} n^3 \left(\frac{I_{tot}}{I_{MD}}\right) \quad .. (3.8)$$

$$\tau_{rad} = \frac{1}{k_r} \quad .. (3.9)$$

$$k_{nr} = \frac{1}{\tau_{obs}} - \frac{1}{\tau_{rad}} \quad .. (3.10)$$

$$\tau_{obs} = \frac{1}{k_r + k_{nr}} \quad .. (3.11)$$

$$\Phi_{ff} = \frac{k_r}{k_r + k_{nr}} = \frac{\tau_{obs}}{\tau_{rad}} \quad .. (3.12)$$

Table 3.3. Relative Quantum Yield (Φ_{rel}), Intrinsic Quantum Yield (Φ_{ff}), Observed Lifetime (τ_{obs}), Radiative (k_r) and Non-Radiative Rate Constants (k_{nr}), and the Energy Transfer Efficiency of the Ligand tpy-HImzphen (η_{sens})

Φ_{rel} (%)	Φ_{ff} (%)	τ_{obs} (µs)	k_r (s^{-1})	k_{nr} (s^{-1})	η_{sens} (%)
10	27	507	532	1440	37

Besides, we also observed that on lowering the temperature up to 77K, the relative intensity of the electric dipole transition ($^5D_0 \rightarrow {}^7F_2$) as well as the excited state lifetime at 614 nm of the said Eu-complex gets substantially enhanced relative to RT. These two phenomena further motivate us to explore the observed thermosensitivity at the expense of Eu-centered luminescence quenching. Upon going through the literature, it appears that there could be two distinct possibilities for quenching of the Eu-centred luminescence, viz. (i) $Eu^{3+} \rightarrow$tpy-HImzphen back-energy-transfer and (ii) involvement of low-lying ligand-to-metal charge transfer (LMCT) state. In order to investigate the possibility of back-energy-transfer from $^5D_0$ state of Eu^{III} to T_1 state of tpy-HImzphen, we recorded the lifetime of [$Gd(tta)_3$(tpy-HImzphen)] complex (since the energy transfer from T_1 state of tpy-HImzphen to the lowest excited level of Gd^{III} is not possible) at 77K which is found to be 6.24 ms. The sufficiently large $T_1 \rightarrow$Ln* energy gap along with a substantially long lifetime of T_1 prevents us from believing that this mechanism is responsible for the observed thermosensitive behavior.[71] Hence, we surmise that the involvement of closely associated low-lying LMCT state could be

a distinct possibility. The formation of the LMCT state could also be feasible because of the lower reduction potential for Eu^{III}/Eu^{II} couple (-0.35 V).[76,77] In order to acquire direct support, we recorded the Diffuse Reflectance UV-vis Spectra of $Eu(tta)_3$(tpy-HImzphen) along with its Gd^{3+}-analogue. From the overlayed spectra, we observed a peak at ~580 nm (~17240 cm^{-1}) in case of the Eu-complex and extracted the peak to get the range of the LMCT state by following earlier literature (Figure 3.8).[72,77] We observed that the LMCT state

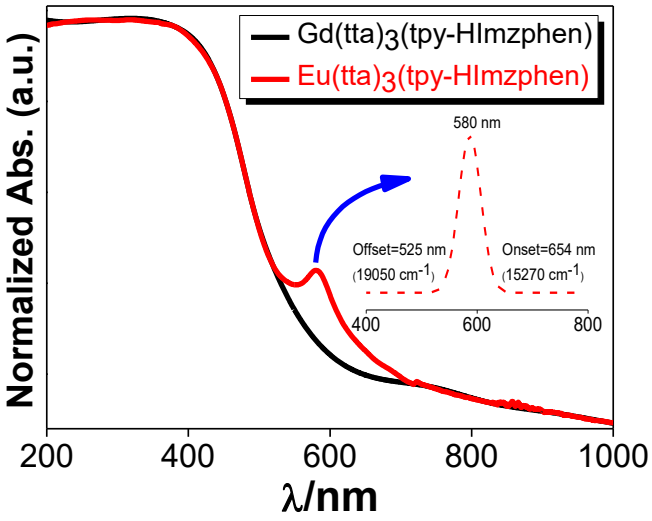

Figure 3.8. UV-diffuse reflectance spectra (DRS) for the LMCT state.

lies between ~15270 cm^{-1} and ~19050 cm^{-1}. It is also noteworthy to mention that the position of the LMCT state can play both in constructive[77,78] as well as in destructive[77,79] ways in terms of effective sensitization. But in the present case, the non-radiative LMCT state is lying below the T_1 energy level of the tpy-HImzphen ligand, and the emissive $^5D_0$ state of Eu^{III} is also lying within the range of LMCT. So, the energy can be transferred from either the ligand T_1 level or the $^5D_0$ state of Eu^{III}. In either case, since the population of the $^5D_0$ state of Eu^{III} gets decreased, we are observing a fall in both the emission intensity and lifetime associated to the $^5D_0 \rightarrow {}^7F_2$ transition at 614 nm. Hence, crossover to this LMCT state is probably responsible for the quenching of the transferred energy in our case. The energy transfer pathway is also undergoing slight modification, resulting in this sort of thermosensitive behaviour. A tentative energy transfer scheme that is operating in the $Eu(tta)_3$(tpy-HImzphen) complex is presented below in Scheme 3.2.

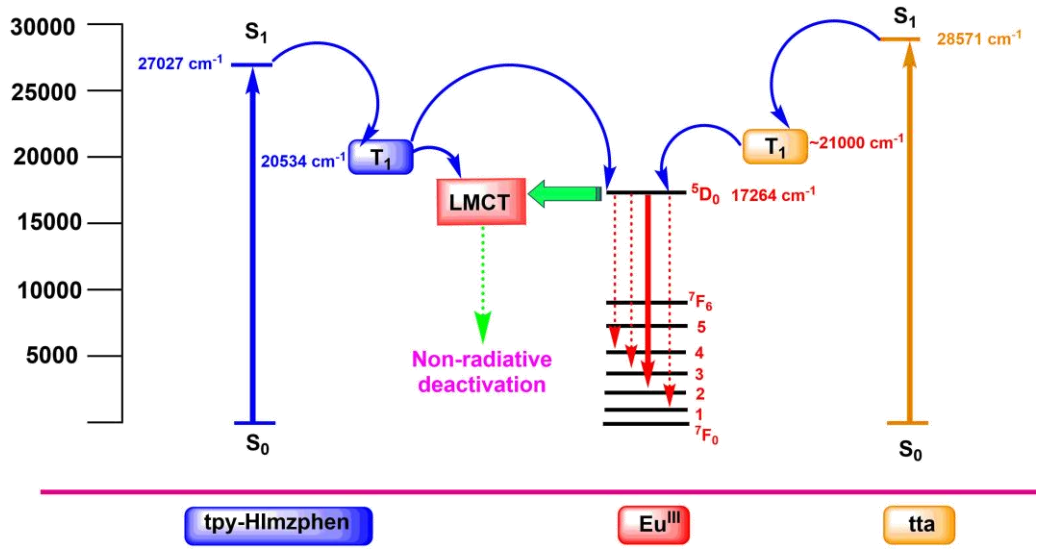

Scheme 3.2. Tentative Energy Transfer Mechanism for Eu(tta)$_3$(tpy-HImzphen) Complex

3.4. Conclusion

Detailed investigation on thermochromic as well as solvatochromic behaviour of a terpyridyl-imidazole based ternary europium tris-(β-diketonate) complex has been thoroughly investigated in this work. Notably, our investigations revealed that the complex possesses remarkable thermosensing as well as thermochromic properties. This complex could be considered a highly promising molecular luminescent thermometer, capable of operating effectively over a broad temperature range spanning from 273 K to 343 K. In fact, the complex manifests multichannel thermosensing through emission intensity ratio, lifetimes and even via change in its emitting colour. Furthermore, via the modulation of its dual emissive characteristics in response to different solvents, the complex exhibits its merit by emitting a bunch of colors, along with characteristic red emission. Essentially, the complex behaves as a chameleon luminophore upon administering suitable stimuli like temperature or solvent. Finally, by combining its unique thermochromic and solvatochromic features, we have successfully developed a small molecule based single-component white light emitter. We have also proposed a plausible energy transfer mechanism where the LMCT state is supposed to be responsible for the thermal quenching of emission. Hence, this work holds significant future prospects with regard to modulation of photoluminescence response under the influence of multiple and appropriate stimuli like temperature and solvent. Besides, if the

LMCT state is closing a window by its thermal quenching, it also opens up a broader door towards molecular luminescent thermometers.

3.5. References

1. Bussche, F. V.; Kaczmarek, A. M.; Speybroeck, V. V.; Voort, P. V. D.; Stevens, C. V. Overview of N-Rich Antennae Investigated in Lanthanide-Based Temperature Sensing. *Chem. Eur. J.* **2021**, *27*, 7214 – 7230.
2. Wang, X. D.; Wolfbeis, O. S.; Meier, R. J. Luminescent Probes and Sensors for Temperature. *Chem. Soc. Rev.* **2013**, *42*, 7834-7869, and references cited therein.
3. Benedict, R. P. Fundamentals of Temperature, Pressure and Flow Measurements. Wiley, New York, **1977**.
4. Brites, C. D. S.; Millán, A.; Carlos, L. D. Lanthanides in Luminescent Thermometry. Handbook on the Physics and Chemistry of Rare Earths, *Vol. 49* (Eds.: B. Jean-Claude, K. P. Vitalij), Elsevier, **2016**, pp. 339–427.
5. Arai, S.; Suzuki, M.; Park, S. J.; Yoo, J. S.; Wang, L.; Kang, N. Y.; Ha H. H.; Chang, Y. T. Mitochondria-targeted Fluorescent Thermometer Monitors Intracellular Temperature Gradient. *Chem. Commun.* **2015**, *51*, 8044-8047.
6. Okabe, K.; Inada, N.; Gota, C.; Harada, Y.; Funatsu T.; Uchiyama, S. Intracellular Temperature Mapping with A Fluorescent Polymeric Thermometer and Fluorescence Lifetime Imaging Microscopy. *Nat. Commun*. **2012**, *3*, 705-713.
7. Feng, J.; Tian, K.; Hu, D.; Wang, S.; Li, S.; Zeng, Y.; Li, Y.; Yang, G. A Triarylboron-Based Fluorescent Thermometer: Sensitive Over a Wide Temperature Range. *Angew. Chem. Int. Ed.* **2011**, *50*, 8072 –8076.
8. Kim, J. H.; Jung, Y.; Lee, D.; Jang, W. D. Thermoresponsive Polymer and Fluorescent Dye Hybrids for Tunable Multicolor Emission. *Adv. Mater.* **2016**, *28*, 3499–3503.
9. Ye, F.; Wu, C.; Jin, Y.; Chan, Y.-H.; Zhang, X.; Chiu, D. T. Ratiometric Temperature Sensing with Semiconducting Polymer Dots. *J. Am. Chem. Soc.* **2011**, *133*, 8146–8149.
10. Hofbeck, T.; Lam, Y. C.; Kalbáč, M.; Záliš, S.; Vlček, Jr., A.; Yersin, H. Thermally Tunable Dual Emission of the d^8–d^8 Dimer $[Pt_2(\mu\text{-}P_2O_5(BF_2)_2)_4]^{4-}$. *Inorg. Chem.* **2016**, *55*, 2441−2449.

11. Surbella, R. G.; Ducati, L. C.; Autschbach, J.; Deifel, N. P.; Cahill, C. L. Thermochromic Uranyl Isothiocyanates: Influencing Charge Transfer Bands with Supramolecular Structure. *Inorg. Chem.* **2018**, *57*, 2455−2471.
12. Borisov, S. M.; Vasylevska, A. S.; Krause, C.; Wolfbeis, O. S. Composite Luminescent Material for Dual Sensing of Oxygen and Temperature. *Adv. Funct. Mater.* **2006**, *16*, 1536–1542.
13. Deshmukh, M. S.; Yadav, A.; Pant, R.; Boomishankar, R. Thermochromic and Mechanochromic Luminescence Umpolung in Isostructural Metal−Organic Frameworks Based on Cu6I6 Clusters. *Inorg. Chem.* **2015**, *54*, 1337−1345.
14. Lochenie, C.; Schötz, K.; Panzer, F.; Kurz, H.; Maier, B.; Puchtler, F.; Agarwal, S.; Köhler, A.; Weber, B. Spin-Crossover Iron(II) Coordination Polymer with Fluorescent Properties: Correlation between Emission Properties and Spin State. *J. Am. Chem. Soc.* **2018**, *140*, 700−709.
15. Tang, J.-H.; Sun, Y.; Gong, Z.-L.; Li, Z.-Y.; Zhou, Z.; Wang, H.; Li, X.; Saha, M. L.; Zhong, Y.-W.; Stang, P. J. Temperature-Responsive Fluorescent Organoplatinum(II) Metallacycles. *J. Am. Chem. Soc.* **2018**, *140*, 7723−7729.
16. Cadiau, A.; Brites, C. D. S.; Costa, P. M. F. J.; Ferreira, R. A. S.; Rocha, J.; Carlos, L. D. Ratiometric Nanothermometer Based on an Emissive Ln^{3+}-Organic Framework. *ACS Nano* **2013**, *7*, 7213–7218.
17. Zhao, S.-N.; Li, L.-J.; Song, X.-Z.; Zhu, M.; Hao, Z.-M.; Meng, X.; Wu, L.-L.; Feng, J.; Song, S.-Y.; Wang, C.; Zhang, H.-J. Lanthanide Ion Codoped Emitters for Tailoring Emission Trajectory and Temperature Sensing. *Adv. Funct. Mater.* **2015**, *25*, 1463–1469.
18. Feng, T.; Ye, Y.; Liu, X.; Cui, H.; Li, Z.; Zhang, Y.; Liang, B.; Li, H.; Chen, B. A Robust Mixed Lanthanide PolyMOF Membrane for Ratiometric Temperature Sensing. *Angew. Chem. Int. Ed.* **2020**, *59*, 21752-21757.
19. Miyata, K.; Konno, Y.; Nakanishi, T.; Kobayashi, A.; Kato, M.; Fushimi, K.; Hasegawa, Y. Chameleon Luminophore for Sensing Temperatures: Control of Metal-to-Metal and Energy Back Transfer in Lanthanide Coordination Polymers. *Angew. Chem. Int. Ed.* **2013**, *52*, 6413 –6416.
20. Cui, Y.; Zou, W.; Song, R.; Yu, J.; Zhang, W.; Yang, Y.; Qian, G. A Ratiometric and Colorimetric Luminescent Thermometer over A Wide Temperature Range Based on Lanthanide Coordination Polymer. *Chem. Commun.* **2014**, *50*, 719-721.

21. Hatanaka, M.; Hirai, Y.; Kitagawa, Y.; Nakanishi, T.; Hasegawa, Y.; Morokuma, K. Organic Linkers Control the Thermosensitivity of the Emission Intensities from Tb(III) and Eu(III) in A Chameleon Polymer. *Chem. Sci.* **2017**, *8*, 423–429.
22. de Souza, K. M. N.; Silva, R. N.; J. Silva, A. B.; Brites, C. D. S.; Francis, B.; Ferreira, R. A. S.; Carlos, L. D.; Longo, R. L. Novel and High-Sensitive Primary and Self-Referencing Thermometers Based on the Excitation Spectra of Lanthanide Ions. *Adv. Opt. Mater.* **2022**, *10*, 2200770-81.
23. Shahi, P. K.; Singh, A. K.; Singh, S. K.; Rai, S. B.; Ullrich, B. Revelation of the Technological Versatility of the Eu(tta)$_3$phen Complex by Demonstrating Energy Harvesting, Ultraviolet Light Detection, Temperature Sensing, and Laser Applications, *ACS Appl. Mater. Interfaces* **2015**, *7*, 18231−18239.
24. Shahi, P. K.; Singh, A. K.; Raia, S. B.; Ullrich, B. Lanthanide Complexes for Temperature Sensing, UV Light Detection, And Laser Applications. *Sens. Actuator A* **2015**, *222*, 255–261.
25. Devi, R.; Singh, K.; Vaidyanathan, S. Synergy in The Energy Transfer Between Ligands and Eu^{III} Ions in Molecular Europium Complexes: Single-Component White Light-Emitting Luminogens. *J. Mater. Chem. C* **2020**, *8*, 8643–8653.
26. Kovalenko, A.; Rublev, P. O.; Tcelykh, L. O.; Goloveshkin, A. S.; Lepnev, L. S.; Burlov, A. S. A.; Vashchenko, A.; Marciniak, L.; Magerramov, A. M.; Shikhaliyev, N. G.; Vatsadze, S. Z. V.; Utochnikova, V. Lanthanide Complexes With 2-(Tosylamino)-Benzylidene- N-(Aryloyl)Hydrazones - Universal Luminescent Materials. *Chem. Mater.* **2019**, *31*, 759–773.
27. Gálico, D. A.; Mazali, I. O.; Sigoli, F. A. Nanothermometer Based on Intensity Variation and Emission Lifetime of Europium(III) Benzoylacetonate Complex. *J. Lumin.* **2017**, *192*, 224–230.
28. Lapaev, D. V.; Nikiforov, V. G.; Lobkov, V. S.; Knyazev, A. A.; Galyametdinov, Y. G. Reusable Temperature-Sensitive Luminescent Material Based on Vitrified Film of Europium(III) β-diketonate Complex. *Opt. Mater.* **2018**, *75*, 787–795.
29. Cabral, F. M.; Gálico, D. A.; Mazali, I. O.; Sigoli, F. A. Crystal Structure and Temperature Dependence of the Photophysical Properties of the [Eu(tta)$_3$(pyphen)] Complex. *Inorg. Chem. Commun.* **2018**, *98*, 29–33.
30. Lyubov, D. M.; Neto, A. N. C.; Fayoumi, A.; Lyssenko, K. A.; Korshunov, V. M.; Taydakov, I. V.; Salles, F.; Guari, Y.; Larionova, J.; Carlos, L. D.; Long, J.; Trifonov,

A. A. Employing Three-Blade Propeller Lanthanide Complexes as Molecular Luminescent Thermometers: Study of Temperature Sensing Through a Concerted Experimental/Theory Approach. *J. Mater. Chem. C* **2022**, *10*, 7176–7188.

31. Zhang, H.; Shan, X.; Zhou, L.; Lin, P.; Li, R.; Ma, E.; Guo, X.; Du, S. Full-Colour Fluorescent Materials Based on Mixed-Lanthanide(III) Metal–Organic Complexes With High-Efficiency White Light Emission. *J. Mater. Chem. C* **2013**, *1*, 888–891.
32. Ramya, A. R.; Varughese, S.; Reddy, M. L. P. Tunable White-Light Emission from Mixed Lanthanide (Eu^{3+}, Gd^{3+}, Tb^{3+}) Coordination Polymers Derived from 4-(Dipyridin-2-Yl)- Aminobenzoate. *Dalton Trans.* **2014**, *43*, 10940–10946.
33. Li, X. Y.; Shi, W. J.; Wang, X. Q.; Ma, L. N.; Hou, L.; Wang, Y. Y. Luminescence Modulation, White Light Emission, and Energy Transfer in a Family of Lanthanide Metal−Organic Frameworks Based on a Planar π-Conjugated Ligand. *Cryst. Growth Des.* **2017**, *17*, 4217−4224.
34. Mahapatra, T. S.; Singh, H.; Maity, A.; Dey, A.; Pramanik, S. K.; Suresha, E.; Das, A. White-Light-Emitting Lanthanide and Lanthanide-Iridium Doped Supramolecular Gels: Modular Luminescence and Stimuli Responsive Behaviour. *J. Mater. Chem. C* **2018**, *6*, 9756–9766.
35. Zhang, Y.-H.; Li, X.; Song, S. White Light Emission Based on A Single Component Sm(III) Framework and A Two Component Eu(III)-Doped Gd(III) Framework Constructed From 2,2'-Diphenyl Dicarboxylate And 1H-Imidazo[4,5-F][1,10]-Phenanthroline. *Chem. Commun.* **2013**, *49*, 10397—10399.
36. Zhang, J.; Li, H.; Chen, P.; Sun, W.; Gao, T.; Yan, P.; A New Strategy for Achieving White-Light Emission of Lanthanide Complexes: Effective Control of Energy Transfer from Blue-Emissive Fluorophore to Eu(III) Centres. *J. Mater. Chem. C* **2015**, *3*, 1799–1806.
37. Singh, K.; Boddula, R.; Vaidyanathan, S. Versatile Luminescent Europium (III)− β-Diketonate-Imidazo-Bipyridyl Complexes Intended for White Leds: A Detailed Photophysical and Theoretical Study. *Inorg. Chem.* **2017**, *56*, 9376–9390.
38. Law, G.-L.; Wong, K.-L.; Tam, H.-L.; Cheah, K.-W.; Wong, W.-T. White OLED with a Single-Component Europium Complex. *Inorg. Chem.* **2009**, *48*, 10492–10494.
39. Ilmi, R.; Khan, M. S.; Sun, W.; Zhou, L.; Wong, W.-Y.; Raithby, P. R. A Single Component White Electroluminescent Device Fabricated from A Metallo-Organic Terbium Complex. *J. Mater. Chem. C* **2019**, *7*, 13966—13975.

40. O'Neil, A. T.; Chalard, A.; Malmström, J.; Kitchen, J. A. White Light And Colour-Tunable Emission from A Single Component Europium-1,8-Naphthalimide Thin Film. *Dalton Trans.* **2023**, *52*, 2255–2261.
41. He, G.; Guo, D.; He, C.; Zhang, X.; Zhao, X.; Duan, C. A Color-Tunable Europium Complex Emitting Three Primary Colors and White Light. *Angew. Chem. Int. Ed.* **2009**, *121*, 6248 –6251.
42. Shelton, A. H.; Sazanovich, I. V.; Weinstein, J. A.; Ward, M. D. Controllable Three-Component Luminescence from A 1,8-Naphthalimide/ Eu(III) Complex: White Light Emission From A Single Molecule. *Chem. Commun.* **2012**, *48*, 2749–2751.
43. Bünzli, J. C.; Piguet, C. Taking Advantage of Luminescent Lanthanide Ions. *Chem. Soc. Rev.* **2005**, *34*, 1048–1077.
44. Parker, D.; Fradgley J. D.; Wong, K.-L. The Design of Responsive Luminescent Lanthanide Probes and Sensors. *Chem. Soc. Rev.* **2021**, *50*, 8193–8213.
45. Bünzli, J. C. G. Lanthanide Luminescence for Biomedical Analyses and Imaging. *Chem. Rev.* **2010**, *110*, 2729–2755.
46. Fradgley, J. D.; Starck, M.; Laget, M.; Bourrier, E.; Dupuis, E.; Lamarque, L.; Trinquet, E.; Zwierb, J. M.; Parker, D. Targeted pH Switched Europium Complexes Monitoring Receptor Internalisation in Living Cells. *Chem. Commun.* **2021**, *57*, 5814–5817.
47. Chakraborty, A.; Acharya, J.; Chandrasekhar, V. Ferrocene-Supported Compartmental Ligands for the Assembly of 3d/4f Complexes. *ACS Omega* **2020**, *5*, 9046−9054.
48. Chakraborty, A.; Ahmed, N.; Ali, J.; Moorthy, S.; Goura, J.; Singh, S. K.; Rogez, G.; Chandrasekhar, V. Exchange-Driven Slow Relaxation of Magnetization in $Ni^{II}_2Ln^{III}_2$ (Ln^{III} = Y, Gd, Tb and Dy) Butterfly Complexes: Experimental and Theoretical studies. *Dalton Trans.* **2022**, *51*, 14721–14733.
49. Moore, E. G.; Samuel, A. P. S.; Raymond, K. N. From Antenna to Assay: Lessons Learned in Lanthanide Luminescence. *Acc. Chem. Res.* **2009**, *42*, 542–552.
50. Ward, M. D. Mechanisms of Sensitization of Lanthanide(III)-Based Luminescence in Transition Metal/Lanthanide and Anthracene/Lanthanide Dyads. *Coord. Chem. Rev.* **2010**, *254*, 2634–2642.

51. Nehra, K.; Dalal, A.; Hooda, A.; Bhagwan, S.; Saini, R. K.; Mari, B.; Kumar, S.; Singh, D. Lanthanides β-diketonate Complexes as Energy-Efficient Emissive Materials: A Review. *J. Mol. Struct.* **2022**, *1249*, 131531.
52. Eliseeva, S. V.; Pleshkov, D. N.; Lyssenko, K. A.; Lepnev, L. S.; Bünzli, J.-C. G.; Kuzmina, N. P.; Deciphering Three Beneficial Effects of 2,2'-Bipyridine-N,N'-Dioxide on the Luminescence Sensitization of Lanthanide(III) Hexafluoroacetylacetonate Ternary Complexes. *Inorg. Chem.* **2011**, *50*, 5137–5144.
53. Hasegawa, Y.; Kitagawa, Y. Thermo-Sensitive Luminescence of Lanthanide Complexes, Clusters, Coordination Polymers and Metal–Organic Frameworks with Organic Photosensitizers. *J. Mater. Chem. C* **2019**, *7*, 7494–7511 and the references therein.
54. Shavaleev, N. M.; Pope, S. J. A.; Bell, Z. R.; Faulkner, S.; Ward, M. D. Visible-light Sensitisation of Near-Infrared Luminescence From Yb(III), Nd(III) and Er(III) Complexes of 3,6-Bis(2-Pyridyl)Tetrazine. *Dalton Trans.* **2003**, *5*, 808–814.
55. Moore, E. G.; Benaglia, M.; Bergamini, G.; Ceroni, P. Synthesis, Stability and Sensitised Lanthanide Luminescence of Heterobimetallic d/f Terpyridine Complexes. *Eur. J. Inorg. Chem.* **2015**, *2015*, 414–420.
56. Mahapatra, T. S.; Dey, A.; Singh, H.; Hossain, S. S.; Mandal, A. K.; Das, A. Two-Dimensional Lanthanide Coordination Polymer Nanosheets for Detection of FOX-7. *Chem. Sci.* **2020**, *11*, 1032–1042.
57. Maity, D.; Das, S.; Mardanya, S.; Baitalik, S. Synthesis, Structural Characterization, And Photophysical, Spectroelectrochemical, and Anion-Sensing Studies of Heteroleptic Ruthenium(II) Complexes Derived From 4′-Polyaromatic-Substituted Terpyridine Derivatives and 2,6-Bis(Benzimidazol-2-yl)Pyridine. *Inorg. Chem.* **2013**, *52*, 6820–6838.
58. Bhaumik, C.; Das, S.; Maity, D.; Baitalik, S. A Terpyridyl-Imidazole (tpy-HImzPh_3) Based Bifunctional Receptor for Multichannel Detection of Fe^{2+} and F^- Ions. *Dalton Trans*. **2011**, *40*, 11795–11808.
59. Paul, A.; Bar, M.; Ahmed, T.; Baitalik, S. Anion-Sensitive Photophysics of Luminescent Trimetallic Complexes of Fe (II), Ru (II), and Os (II) with Polarized NH Motifs. *Polyhedron* **2020**, *190*, 114772.
60. Bhaumik, C.; Saha, D.; Das, S.; Baitalik, S. Synthesis, Structural Characterization, Photophysical, Electrochemical, and Anion-Sensing Studies of Luminescent Homo

and Heteroleptic Ruthenium(II) and Osmium(II) Complexes based on Terpyridyl-Imidazole Ligand. *Inorg. Chem.* **2011**, *50*, 12586−12600.

61. Deb, S.; Sahoo, A.; Ahmed, T.; Baitalik, S. Stimuli-Responsive Molecular Switches and Logic Devices Based on Ru(II)–Terpyridyl-Imidazole Coordination Motif. *J. Phys. Chem. B*, **2021**, *125*, 8919–8931.
62. Ahmed, T.; Chakraborty, A.; Paul, A.; Baitalik, S. Synthesis, Characterization, Luminescence Properties and Deciphering the Role of A Terpyridylimidazole Based Ligand in the Dissimilar Luminescence Sensitization of Ternary Lanthanide(III) tris-(β-diketonate) Complexes. *Dalton Trans.* **2023**, *52*, 14027–14038.
63. Cabral, F. M.; Gálico, D. A.; Mazali I. O.; Sigoli, F. A. Crystal Structure and Temperature Dependence of the Photophysical Properties of the $[Eu(tta)_3(pyphen)]$ Complex. *Inorg. Chem. Commun.* **2018**, *98*, 29–33.
64. Lapaev, D. V.; Nikiforov, V. G.; Lobkov, V. S.; Knyazev, A. A.; Galyametdinov, Y. G. Reusable Temperature-Sensitive Luminescent Material Based on Vitrified Film of Europium(III) β-diketonate complex. *Opt. Mater.* **2018**, *75*, 787–795.
65. Ondrus, V.; Meier, R. J.; Kleinc, C.; Hennec, U.; Schäferling, M.; Beifuss, U. Europium 1,3-di(thienyl)propane-1,3-diones with Outstanding Properties for Temperature Sensing. *Sens. Actuator A Phys.* **2015**, *233*, 434–441.
66. Peng, H.; Stich, M. I. J.; Yu, J.; Sun, L.; Fischer, L. H.; Wolfbeis, O. S. Luminescent Europium(III) Nanoparticles for Sensing and Imaging of Temperature in the Physiological Range. *Adv. Mater.* **2010**, *22*, 716–719.
67. Outis, M.; Laia, C. A. T.; Oliveira, M. C.; Monteiro, B.; Pereira, C. C. L. A Europium(III) Complex with an Unusual Anion–Cation Interaction: A Luminescent Molecular Thermometer for Ratiometric Temperature Sensing. *ChemPlusChem*, **2020**, *85*, 580–586.
68. Stewart, Jr., O. C.; Marwitz, A. C.; Swanson, J.; Bertke, J. A.; Hartman, T.; Monteiro, J. H. S. K.; de Bettencourt-Dias, A.; Knope, K. E.; Stoll, S. L. Lanthanide Luminescence and Thermochromic Emission from Soft- Atom Donor Dichalcogenoimidodiphosphinate Ligands. *Inorg. Chem.* **2022**, *61*, 15547−15557.
69. Turchetti, D. A.; Domingues, R. A.; Zanlorenzi, C.; Nowacki, B.; Atvars T. D. Z.; Akcelrud, L. C. A Photophysical Interpretation of the Thermochromism of a Polyfluorene Derivative–Europium Complex. *J. Phys. Chem. C* **2014**, *118*, 30079-300786.

70. Potts, K. T.; Usifer, D. A.; Guadalupe, A.; Abruna, H. D. 4-Vinyl-, 6-Vinyl-, and 4'-Vinyl-2,2':6',2"-Terpyridinyl Ligands: Their Synthesis and the Electrochemistry of Their Transition-Metal Coordination Complexes. *J. Am. Chem. Soc.* **1987**, *109*, 3961–3967.
71. Case, F. H.; Kasper, T. J. The Preparation of Some Substituted 2,6-Bis-(2-Pyridyl)-Pyridines. *J. Am. Chem. Soc.* **1956**, *78*, 5842–5844.
72. Spahni, W.; Calzaferri, G. Synthese von *Para*-substituierten Phenyl-terpyridin Liganden. *Helv. Chim. Acta* **1984**, *67*, 450–454.
73. Constable, E. C.; Ward, M. D.; Corr, S. A Convenient, High Yield Synthesis of 2,2′:6′,2″-Terpyridine and Its Iron(II) Complex. *Inorg. Chim. Acta* **1988**, *141*, 201–203.
74. Dar, W. A.; Iftikhar, K. Phase Controlled Colour Tuning of Samarium And Europium Complexes and Excellent Photostability of Their PVA Encapsulated Materials. Structural Elucidation, Photophysical Parameters and The Energy Transfer Mechanism in the Eu^{3+} Complex by Sparkle/PM3 Calculations. *Dalton Trans.* **2016**, *45*, 8956–8971.
75. Kitagawa, Y.; Kumagai, M.; Nakanishi, T.; Fushimi K. Hasegawa, Y. The Role of π–f Orbital Interactions in Eu(III) Complexes for an Effective Molecular Luminescent Thermometer. *Inorg. Chem.* **2020**, *59*, 5865–5871.
76. Fu, L. M.; Ai, X. C.; Li, M. Y.; Wen, X. F.; Hao, R.; Wu, Y. S.; Wang Y.; Zhang, J. P. Role of Ligand-to-Metal Charge Transfer State in Nontriplet Photosensitization of Luminescent Europium Complex. *J. Phys. Chem. A* **2010,** *114,* 4494–4500.
77. Miranda, Y. C.; Pereira, L. L. A. L.; Barbosa, J. H. P.; Brito, H. F.; Felinto, M. C. F. C.; Malta, O. L.; Faustino, W. M.; Teotonio, E. E. S. The Role of the Ligand-to-Metal Charge-Transfer State in the Dipivaloylmethanate-Lanthanide Intramolecular Energy Transfer Process. *Eur. J. Inorg. Chem.* **2015**, *2015*, 3019–3027.
78. Pasatoiu, T. D.; Madalan, A. M.; Kumke, M. U.; Tiseanu C.; Andruh, M. Temperature Switch of LMCT Role: From Quenching to Sensitization of Europium Emission in a Zn^{II}–Eu^{III} Binuclear Complex. *Inorg. Chem.* **2010**, *49*, 2310–2315.
79. Berry, M. T.; May, P. S.; Xu, H. Temperature Dependence of the Eu^{3+} $^5D_0$ Lifetime in Europium Tris(2,2,6,6-tetramethyl-3,5-heptanedionato). *J. Phys. Chem.* **1996**, *100*, 9216–9222.

****

Chapter 4

Terpyridyl-Imidazole based Ligand Coordinated to Ln(Hexafluoroacetyl acetonate)$_3$ Core: Synthesis, Structural Characterization, Luminescence Properties and Thermosensing Behaviors in Solution and PMMA Film

4.1. Introduction

Lanthanide coordination complexes are now attracting increasing interest to the concerned community for their appealing features in molecular magnetism as well as in photoluminescence.[1-6] Special attention is being paid to trivalent lanthanide-based luminescent materials owing to their sharp emission with high color purity, large ligand-induced pseudo-Stokes shift, and longer excited state lifetimes.[7-10] Despite their attractive and well-resolved photophysics, lanthanide complexes often face an unwelcome disadvantage of their weak absorption and emission properties, arising out of spin as well as symmetry forbidden f-f transitions in Ln^{III} ions. To bypass this pitfall, organic chromophoric ligands possessing high absorptivity ($\varepsilon > 10000$ L M^{-1} cm^{-1}), are often brought into play, which could efficiently absorb light and transfer its energy to the coordinated Ln^{III} core, resulting in an indirect sensitization (antenna ligand).[7-10] The structures and excited state energy levels of the antenna ligands play a decisive role in such sensitization process for generating fertile lanthanide luminescence. Among the variety, β-diketonates are notable building blocks for the formation of Ln^{III}-complexes due to their ease of synthesis, uni-negative charge, and efficient coordinating abilities.[11] However, the presence of high-energy oscillators like C-H and O-H bonds within the β-diketonates often lead to non-radiative quenching of the sensitized Ln^{III} luminescence, resulting in reduced luminescence intensities and shorter excited-state lifetimes. To overcome the lacuna, several strategies have been adopted, viz. substitution of CH_3 moiety with CF_3[12], phenyl,[13] thiophene[14] group or other aromatic and heteroaromatic moieties.[11,15,16] The maximum desired luminescence is still to be achieved as lanthanide ions often coordinated with water or solvent molecules to satisfy their higher coordination, which in turn induces non-radiative luminescence-quenching.[17-18] Another useful strategy is to introduce appropriate chelating ancillary ligands, mostly consisting of O- or N- donors to protect the lanthanide core from the environment.[12-16,18-26] The extent and direction of energy transfer in the resulting metal-ligand assembly critically depend on the excited state energy level of the incoming ancillary ligands.[27-29] Among the polypyridyl luminophores, terpyridine and its derivatives exhibit substantial light absorption coefficients, favorable σ electron-donating as well as π electron-accepting abilities, and high affinity for coordination.[30-32] To our surprise, reported systems comprising terpyridine-appended Ln^{III}-complexes are very few, leaving room for extensive exploration.[13,14,24-26,33-36]

Luminescent lanthanide complexes are now emerging as the next-generation tools for precise measurement of temperature over the traditional thermometers in medical and

industrial applications, mostly owing to their non-invasive nature and nanoscale miniaturization.[37-46] Lanthanide luminescent thermometers possess all the necessary criteria to be suitable for luminescence thermometry viz., intense luminescence with high-temperature sensitivity as well as photostability, a longer decay time, and thermostability.[40,41] Most of the earlier reported luminescent lanthanide thermometers are either lanthanide-based coordination polymers[43,44] or mix-doped MOFs.[38,45,46] As per our literature survey, Ln^{III}-based discrete molecule luminescent thermometers are relatively less explored,[37,39,47-54] while reports on terpyridyl-ligand-based lanthanide luminescent thermometers are even more sparse.[55]

In our recent report, we have designed a series of lanthanide(III) complexes comprising of 2-theonyltrifluoroacetonate (tta) and the same terpyridyl-imidazole ligand (tpy-HImzphen) and investigated their dissimilar luminescence characteristics.[29] We noticed that only Eu^{III} among the four lanthanides (La^{III}, Eu^{III}, Sm^{III} and Tb^{III}) gets substantially sensitized. However, the cumulative energy transfer from tta as well as from tpy-HImzphen to Eu^{III} is quite low (η_{sens}=~37%),[55] despite maintaining the required energy gap between lowest triplet state (T_1) of the ligands and lowest emissive state of Eu^{III} ($^5D_0$). Herein, we considered replacing the tta moiety with another fluorinated β-diketonate moiety having a higher T_1 level (~22000 cm^{-1}) than that of tta (~21000 cm^{-1}) so that intercomponent energy transfer from ligand-to-metal becomes more facile.

In this work, our major aim is to investigate the sensitization effect of a fluorinated diketonate (hfa) antenna together with a terpyridyl-imidazole motif (tpy-HImzphen), especially how they can alter the customary photophysics of four Ln^{III} ions. To explore this, we have prepared four lanthanide(III) tris-(β-diketonate) complexes of the form, [$Ln(hfa)_3$(tpy-HImzphen)] where Ln= La^{III} (**1**), Eu^{III} (**2**), Sm^{III} (**3**), and Tb^{III} (**4**) and thoroughly characterized via standard analytical tools and spectroscopic techniques. To get insight into the binding nature of the complexes, we have acquired single-crystal X-ray structures of two *in situ*-generated complexes, which will be presented later. The photophysical behaviors of the complexes have been thoroughly investigated through absorption and both steady-state and time-resolved emission spectroscopy. Interestingly, the absorption spectral window of the resulting complexes shifted towards the visible region (with the onset at ~450 nm) in contrast to most of the reported Ln^{III}-based complexes that display their absorption window within the UV region (<390 nm). Steady-state and time-resolved emission spectral measurements indicate four distinct behaviors in the complexes. Additionally, by virtue of their suitable

positioning of triplet energy levels, very efficient inter-component energy transfer (~95%) takes place from the triplet levels of both hfa and tpy-HImzphen to the Eu^{III} center which is much higher relative to our previously reported analogous Eu(III) complex with tta ligand, wherein the energy transfer efficiency was found to be only ~37%.

We further delved into the scope of thermosensing characteristics of the Eu^{III}-complex in solution as well as in a hybrid thin film of poly(methyl methacrylate) (PMMA) for its probable practical utility. On going through the literature, it is revealed that thermo-sensing behavior of Ln^{III}-based discrete molecules are very few, while terpyridyl-appended Ln-complexes are even more sparse, leaving room for its extensive exploration. Additionally, in most of the earlier reported cases, only the Ln-centered emission responses have been employed for this purpose. In the present case, simultaneous alteration of ligand (tpy-HImzphen) as well as Ln-centered emission takes place upon changing the temperature. In fact, the Ln-centered emission decreases with concomitant enhancement of the ligand-centered emission upon increase in temperature. Interestingly, by virtue of its dual emissive nature, the Eu^{III}-complex becomes a blue-emitter at 273K, while cyan-emitter at 353K. It is also noteworthy to mention that we propose herein a new thermometric parameter (Δ), defined by the ratio of emission intensity and lifetime at a particular wavelength for a given temperature. Subsequently, we estimated the values of relative thermal sensitivity (S_r) and temperature resolution (δT), to evaluate the thermosensing efficacy of Eu(III) complex. It is postulated that to be a good thermosensor, the S_r value must be greater than 1% K^{-1}, and the δT value must be well-below than 1 K. The present terpyridyl-appended Eu^{III}-based thermosensor not only satisfies the above criteria but also offers far better values than those of the earlier reported Ln^{III}-based discrete thermosensors that operate in the physiological temperature domain. The thermosensitive luminescence response in solution has been further deployed to emulate Set-Reset Flip-flop logic operation, suitable for fabricating molecular logic devices which is indeed a growing sector in fields of molecular devices and machines.[56,57] In the end, we have suggested a feasible intercomponent energy transfer mechanism operating within the complexes, wherein we surmise that the triplet-state energy levels of both hfa and tpy-HImzphen are responsible for the four distinctive luminescence behaviors among the analogous complexes. Additionally, the role of the ligand-to-metal-charge-transfer (LMCT) state is counted for complex **2** for its efficient thermosensitivity.

4.2. Experimental Section

4.2.1. Materials. Hexafluoroacetylacetone (Hhfa), poly(methyl methacrylate) (PMMA), and the nitrate or chloride salts of lanthanides were procured from Merck. Solvents and other regular reagents were dried by adopting standard methods.

4.2.2. Synthesis of the Ligand (tpy-HImdzphen). The detailed synthetic procedure of the ligand has already been described in chapter 2.[58,59]

4.2.3. Synthesis of $Ln(hfa)_3(H_2O)_2$. All the four lanthanide precursors of the type, $Ln(hfa)_3(H_2O)_2$, Ln^{III}= La^{III}, Eu^{III}, $Sm^{III,}$ and Tb^{III} are synthesized by a slight modification of some reported literature procedures (Scheme 4.1).[60-62] Hexafluoroacetylacetone (Hhfaa) is solidified by dissolving it in water (1:9, v/v) and kept for stirring in an ice bath for 2h to make $Hhfa.2H_2O$. The solid $Hhfa.2H_2O$ is then dissolved in 50 mL diethyl ether, and a requisite amount of 25% ammonia solution is added to it. Then it was extracted in a separating funnel with a 2 mL aqueous solution of $LnCl_3 \cdot xH_2O$ (x=6 or 7) or $Ln(NO_3)_3.xH_2O$ (x=5 or 6) and the resulting light yellowish oily product was air dried for 1d. Then, it was recrystallized in hexane and the product was collected after keeping it to air-dry for 1d.

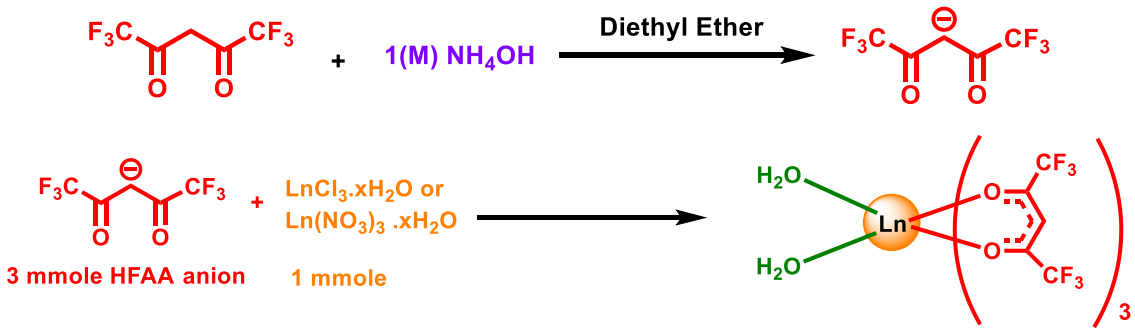

Scheme 4.1. Synthesis of the Ln^{III} Precursors and $Ln(hfa)_3(H_2O)_2$ [Ln=La, Eu, Sm, and Tb]

$La(hfa)_3(H_2O)_2$: $LaCl_3 \cdot 7H_2O$ (186 mg, 0.5 mmol). Yield 239 mg (~60 %). FT-IR: υ (in cm^{-1}) =1647, 3490. Anal. Calcd for $C_{15}H_7F_{18}O_8La$: C, 22.63; H, 0.89; Found: C, 22.46; H, 0.81. ^1H NMR (DMSO-d_6, 400 MHz, δ/ppm): 4.32 (s, 3H, H_1 methine).

$Eu(hfa)_3(H_2O)_2$: $EuCl_3 \cdot 6H_2O$ (183 mg, 0.5 mmol). Yield 252 mg (62.2 %). FT-IR: υ (in cm^{-1}) =1646, 3457. Anal. Calcd for $C_{15}H_7F_{18}O_8Eu$: C, 22.27; H, 0.87; Found: C, 22.08; H, 0.79. ^1H NMR (DMSO-d_6, 400 MHz, δ/ppm): 5.80 (s, 3H, H_1 methine).

$Sm(hfa)_3(H_2O)_2$: $Sm(NO_3)_3 \cdot 6H_2O$ (182 mg, 0.5 mmol). Yield 216 mg (53.5 %). FT-IR: υ (in cm^{-1}) =1649, 3430. Anal. Calcd for $C_{15}H_7F_{18}O_8Sm$: C, 22.31; H, 0.87; Found: C, 22.16; H, 0.76. ^1H NMR (DMSO-d_6, 400 MHz, δ/ppm): 5.65 (s, 3H, H_1 methine).

Tb(hfa)$_3$(H$_2$O)$_2$: $TbCl_3 \cdot 6H_2O$ (187 mg, 0.5 mmol). Yield 265 mg (65 %). FT-IR: υ (in cm^{-1}) =1648, 3450. Anal. Calcd for $C_{15}H_7F_{18}O_8Tb$: C, 22.08; H, 0.86; Found: C, 21.95; H, 0.81. ^{1}H NMR (DMSO-d_6, 400 MHz, δ/ppm): 7.20 (s, 3H, H_1 methine).

4.2.4. Synthesis of the Lanthanide Complexes. All the four lanthanide complexes of the type [Ln(hfa)$_3$(tpy-HImzphen)] where Ln^{III}=La^{III} (**1**), Eu^{III} (**2**), Sm^{III} (**3**), and Tb^{III} (**4**) were prepared by adopting a general synthetic procedure (Scheme 4.2). Respective lanthanide precursor, Ln(hfa)$_3$(H$_2$O)$_2$ was added to a stirred suspension of tpy-HImzphen in a 1:1 molar ratio in chloroform-methanol (1:1 v/v) mixture, followed by refluxing overnight at 60 ºC. The resulting solution was then evaporated to dryness in a rotary evaporator and poured down into dichloromethane-hexane (1:1 v/v) mixture. On keeping, a yellow color product deposited which was filtered off in sintered crucible and kept in vacuum desiccators for 1d. All the complexes have been thoroughly characterized by standard analytical tools and spectroscopic techniques.

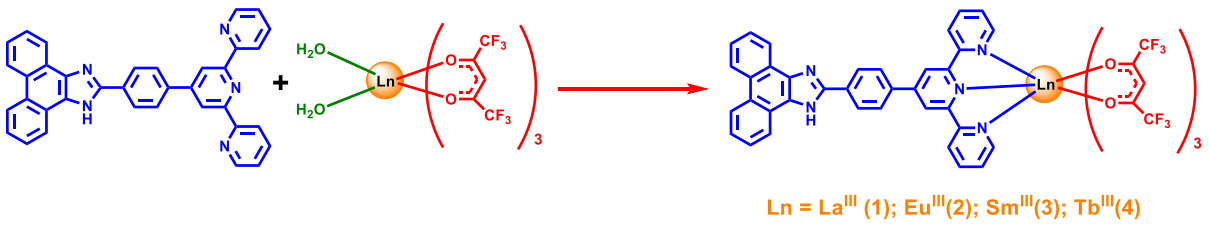

Scheme 4.2. Terpyridyl-Imidazole Ligand, (tpy-HImzphen), Ln^{III} Precursors, [Ln(hfa)$_3$(H$_2$O)$_2$] and Ternary Ln^{III} Complexes of the Type, Ln(hfa)$_3$(tpy-HImzphen)] (1-4)

[La(hfa)$_3$(tpy-HImzphen)] (1). La(hfa)$_3$(H$_2$O)$_2$ (38 mg, 0.048 mmol); Yield: 38 mg (62%). Anal. Calcd. for $C_{51}H_{26}F_{18}N_5O_6La$: C, 47.65; H, 2.04; N, 5.45. Found: C, 47.52; H, 1.96; N, 5.36. FT-IR: υ (in cm^{-1}) = 1525, 1651, 3190. MALDI-TOF (DCTB, positive mode): *m/z* = 1077.927 (100 %) $[M\text{-hfa}]^+$. ^{1}H NMR (DMSO-d_6, 400 MHz, δ/ppm): 8.88 (d, 2H, *J* = 5.48 Hz, H_9), 8.85 (s, 2H, H_6), 8.81 (d, 2H, *J* = 5.3 Hz, H_5), 8.72 (d, 2H, *J* = 8.3 Hz, H_2), 8.63 (t, 2H, *J* = 8.0 Hz, H_{12}), 8.55 (d, 2H, *J* = 8.3 Hz, H_8), 8.22 (d, 2H, *J* = 7.4 Hz, H_7), 8.07 (d, 2H, *J* = 5.9 Hz, H_3), 7.77 (t, 2H, *J* = 5.9 Hz, H_{11}), 7.67 (d, 2H, *J* = 8.0 Hz, H_{10}), 7.56 (d, 2H, *J* = 8.0 Hz, H_4), 5.55 (s, 3H, H_1 methine).

[Eu(hfa)$_3$(tpy-HImzphen)] (2). Eu(hfa)$_3$(H$_2$O)$_2$ (38 mg, 0.047 mmol); Yield: 37 mg (61%). Anal. Calcd for $C_{51}H_{26}F_{18}N_5O_6Eu$: C, 47.17; H, 2.02; N, 5.39. Found: C, 46.94; H, 1.88; N, 5.19. FT-IR: υ (in cm^{-1}) = 1528, 1651, 3015. MALDI-TOF (DCTB, positive mode): *m/z* = 1091.739 (100%) $[M\text{-hfa}]^+$ ^{1}H NMR (DMSO-d_6, 400 MHz, δ/ppm): 8.89 (s, 2H, H_9),

8.86 (s, 2H, H_6), 8.81 (d, 2H, J = 8.0 Hz, H_5), 8.72 (d, 2H, J = 8.0, H_2), 8.63 (d, 2H, J = 8.0 Hz, H_{12}), 8.56 (d, 2H, J = 8.0 Hz, H_8), 8.23 (d, 2H, J = 8.0 Hz, H_7), 8.07 (d, 2H, J = 8.0 Hz, H_3), 7.77 (t, 2H, J = 8.0 Hz, H_{11}), 7.67 (t, 2H, J = 8.0 Hz, H_{10}), 7.56 (d, 2H, J = 8.0 Hz, H_4), 5.58 (s, 3H, H_1 methine).

[Sm(hfa)$_3$(tpy-HImzphen)] (3). Sm(hfa)$_3$(H_2O)$_2$ (38 mg, 0.047 mmol); Yield: 35 mg (58%). Anal. Calcd for $C_{51}H_{26}F_{18}N_5O_6Sm$: C, 47.22; H, 2.02; N, 5.40. Found: C, 47.13; H, 1.94; N, 5.29. FT-IR: υ (in cm^{-1}) = 1527, 1652, 3450. MALDI-TOF (DCTB, positive mode): *m/z*= 1090.943 (100%) $[M\text{-hfa}]^+$ ^{1}H NMR (DMSO-d_6, 400 MHz, δ/ppm): 8.88 (d, 2H, J = 8.0 Hz, H_9), 8.85 (s, 2H, H_6), 8.80 (d, 2H, J = 4.8 Hz, H_5), 8.72 (d, 2H, J = 8.0, H_2), 8.62 (d, 2H, J = 8.0 Hz, H_{12}), 8.55 (d, 2H, J = 8.0 Hz, H_8), 8.22 (d, 2H, J = 8.0 Hz, H_7), 8.07 (t, 2H, J = 8.0 Hz, H_3), 7.77 (t, 2H, J = 8.0 Hz, H_{11}), 7.67 (t, 2H, J = 8.0 Hz, H_{10}), 7.57 (d, 2H, J = 8.0 Hz, H_4), 5.72 (s, 3H, H_1 methine).

[Tb(hfa)$_3$(tpy-HImzphen)] (4). Tb(hfa)$_3$(H_2O)$_2$ (38 mg, 0.047 mmol); Yield: 42 mg (68%). Anal. Calcd for $C_{51}H_{26}F_{18}N_5O_6Tb$: C, 46.91; H, 2.01; N, 5.36. Found: C, 46.77; H, 1.89; N, 5.13. FT-IR: υ (in cm^{-1}) = 1526, 1654, 3030. MALDI-TOF (DCTB, positive mode): *m/z*= 1097.967 (100%) $[M\text{-hfa}]^+$. ^{1}H NMR (DMSO-d_6, 400 MHz, δ/ppm): 10.14 (s, 3H, H_1 methine), 8.87 (s, 2H, H_9), 8.80 (s, 2H, H_6), 8.75 (t, 2H, J = 4.0 Hz, H_5), 8.72 (t, 2H, J = 4.0, H_2), 8.65 (t, 2H, J = 4.0 Hz, H_{12}), 8.58 (d, 2H, J = 8.0 Hz, H_8), 8.24 (d, 2H, J = 8.0 Hz, H_7), 8.07 (q, 2H, H_3), 7.74 (t, 2H, J = 4.0 Hz, H_{11}), 7.67 (d, 2H, J = 8.0 Hz, H_{10}), 7.55 (q, 2H, H_4).

4.2.5. Preparation of Hybrid Thin Film of PMMA Embedded with Eu(hfa)$_3$(tpy-HImzphen) (2@PMMA). A general procedure is followed for preparation of all four composites viz., 2% (2% **2@PMMA**), 4% (4% **2@PMMA**), 6% (6% **2@PMMA**), and 8% (8% **2@PMMA**) from complex **2.** The as-purchased PMMA is taken in 50 mL DCM and requisite amount of complex **2** is then added, resulting in a straw-yellow coloured solution. The mixture is stirred for 45 min and resulting solution is then drop-casted onto quartz slides and left overnight to get the films ready after complete evaporation of excess DCM.

4.2.6. Instruments and Physical Methods. The details of this section have already been discussed in Chapter 2.

4.3. Results and Discussions

4.3.1. Synthesis and Characterization. The reaction of the stoichiometric amount of respective lanthanide precursor, Ln(hfa)$_3$(H_2O)$_2$, with the terpyridyl-imidazole ligand (tpy-HImzphen) in a 1:1 (v/v) chloroform-methanol mixture afforded the desired mononuclear

complexes in reasonably good yield. All four synthesized complexes were thoroughly characterized via standard analytical tools and spectroscopic techniques viz. elemental (C, H, N) analysis, Fourier Transform infrared (FT-IR) spectroscopy, ^{1}H Nuclear magnetic resonance (NMR) spectroscopy, matrix-assisted laser desorption ionization-time of flight (MALDI-TOF) mass spectrometry as well as by powdered X-ray diffraction (PXRD) analysis. The outcomes of the above measurements also conclude that all four complexes are isostructural. Besides, to get insight into the binding mode among the lanthanide(III) ion and the ligands, we have grown single crystals of two representative complexes upon slow evaporation of a stoichiometric mixture of tpy-HImzphen, respective lanthanide salts, hexafluoroacetylacetone, and triethylamine in a 1:1 (v/v) chloroform-methanol mixture. The structure of the two *in situ*-generated complexes was elucidated via X-ray diffraction.

4.3.2. FT-IR Spectra. The IR spectra of the resulting complexes, along with their respective lanthanide precursor and tpy-HImzphen ligand, were acquired within the 400-4000 cm^{-1} region, and related representative spectra for complex **3** as well as selected stretching frequencies of the complexes are presented in Figure 4.1 and Table 4.1. The ligand exhibited a peak at ~1583 cm^{-1} due to C=N stretching of the pyridine moieties, whereas a characteristic peak at ~3180 cm^{-1} for the imidazole N-H stretch. Due to the presence of the hexafluoroacetylacetonate unit, all the lanthanide precursors, $Ln(hfa)_3(H_2O)_2$ show a characteristic C=O stretching within 1645-1649 cm^{-1} region and a broad hump spanning within 3430-3490 cm^{-1} for the water molecules. The complexes also revealed a sharp peak within the range of 1651-1654 cm^{-1} associated with C=O stretching frequency. It is to be noted that the broad peak for coordinated water molecules disappeared. Simultaneously, two new peaks emerged within 1525-1528 cm^{-1} and 3015-3450 cm^{-1} domain for C=N and N-H stretching, respectively in the complexes.

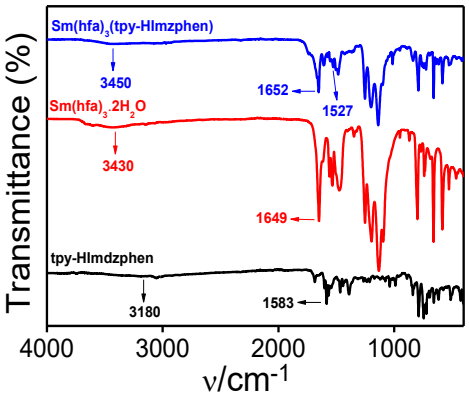

Figure 4.1. FT-IR spectra of tpy-HImzphen, $Sm(hfa)_3(H_2O)_2$ and $Sm(hfa)_3$tpy-HImzphen **(3)**.

Table 4.1. Stretching Frequencies of Selected Groups in Their FT-IR Spectra

Complex	$\nu_{C=O}$	$\nu_{C=N}$	ν_{N-H}	ν_{OH}
Tpy-HImdzphen	-	1583	3180	-
$La(hfa)_3(H_2O)_2$	1647	-	-	3490
Complex **1**	1651	1525	3190	-
$Eu(hfa)_3(H_2O)_2$	1646	-	-	3457
Complex **2**	1651	1528	3015	-
$Sm(hfa)_3(H_2O)_2$	1649	-	-	3430
Complex **3**	1652	1527	3450	-
$Tb(hfa)_3(H_2O)_2$	1648	-	-	3450
Complex **4**	1654	1526	3030	-

4.3.3. ^{1}H NMR Spectra. Thorough characterization of the complexes (**1**-**4** and their corresponding metal precursors) has been carried out via ^{1}H NMR spectroscopy in DMSO-d_6. Representative ^{1}H NMR spectra for **1**, along with tentative assignments of the protons, are presented in Figure 4.2. The chemical shift values for all the proton resonances are also tabulated in Table 4.2. It is observed that the only the proton associated with the hfa moiety experienced remarkable chemical shifts without alteration of multiplicity. By contrast, the peaks associated with the protons of tpy-HImzphen ligand experienced alteration in both multiplicity and chemical shifts, albeit to a small extent. The methine protons in the free Hhfa show a singlet at 4.32 ppm, which gets downfield-shifted to 5.50 ppm upon incorporation of diamagnetic La^{III} ion in $La(hfa)_3(H_2O)_2$ precursor. The very same proton gets further downfield-shifted to 5.55 ppm in the diamagnetic $La(hfa)_3$(tpy-HImzphen) complex (Figure 4.2). Among the other three complexes, this methine proton experiences an up-field shift from 5.80 to 5.58 ppm in case of Eu^{III}, while it gets downfield-shifted from 5.65 to 5.72 ppm for Sm^{III} and from 7.20 to 10.14 ppm in case of Tb^{III}, as compared to their respective $Ln(hfa)_3(H_2O)_2$ precursors, respectively (Table 4.2). The signals due to protons on the ancillary ligand, on the other hand, experience only a minor shift (either up- or downfield) together with an alteration in multiplicities.

4.3.4. Mass Spectra. MALDI-TOF mass spectra of the complexes are also acquired in DCM. A similar spectral pattern is found for all four complexes, with a strong and prominent peak for the respective $[Ln(hfa)_2$(tpy-HImzphen)$]^+$ fragment. A representative spectrum of **2**, along with experimental and simulated isotopic patterns, is presented in Figure

4.3. The correspondence between the experimental and simulated isotopic patterns is also found to be good in all cases.

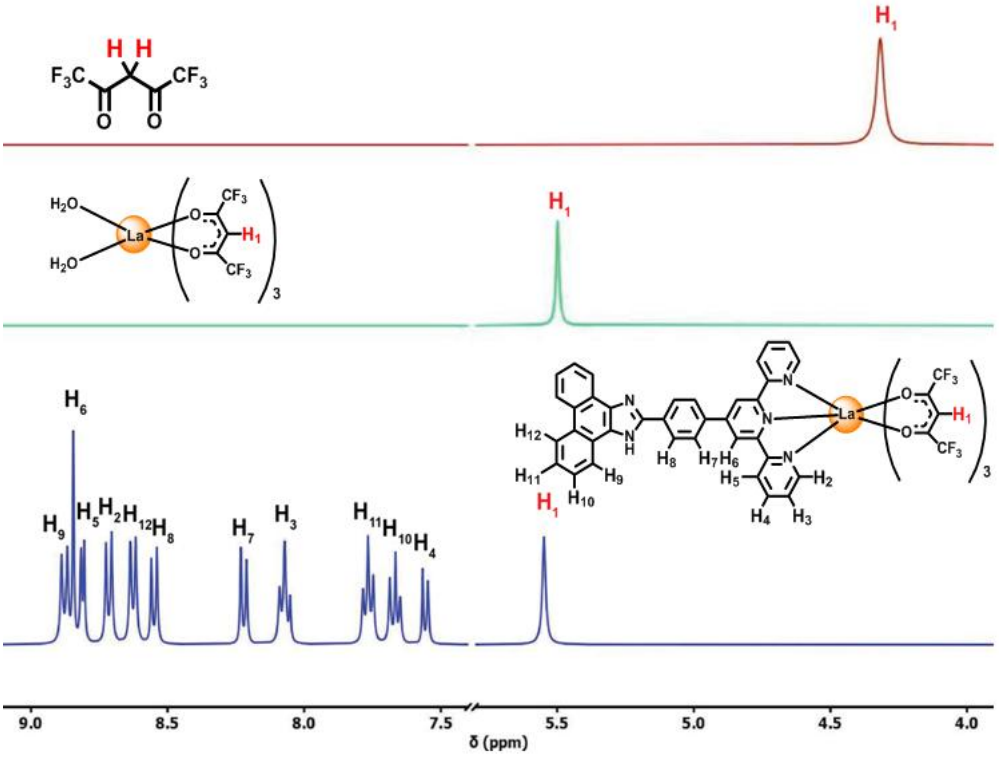

Figure 4.2. 400 MHz ^{1}H NMR spectra of free Hhfa (top), La(hfa)$_3$(H$_2$O)$_2$ (middle) and La(hfa)$_3$(tpy-HImzphen) (**1**) (bottom) in DMSO-d_6.

Table 4.2. Chemical Shifts of the Protons of All Four Complexes in DMSO-d_6

Proton	Chemical shift (ppm) of Lanthanide complexes (1-4) {J= Hz}			
	1 (La^{III})	**2** (Eu^{III})	**3** (Sm^{III})	**4** (Tb^{III})
H_1 (methine)	5.55 (s, 3H)	5.58 (s, 3H)	5.72 (s, 3H)	10.14 (s, 3H)
H_2	8.72 (d, 2H, J = 8.3)	8.72 (d, 2H, J = 8.0)	8.72 (d, 2H, J = 8.0)	8.72 (t, 2H, J = 4.0)
H_3	8.07 (t, 2H, J = 5.9)	8.07 (d, 2H, J = 8.0)	8.07 (t, 2H, J = 8.0)	8.07 (q, 2H)
H_4	7.56 (d, 2H, J = 8.0)	7.56 (d, 2H, J = 8.0)	7.57 (d, 2H, J = 8.0)	7.55 (q, 2H)
H_5	8.81 (d, 2H, J = 5.3)	8.81 (d, 2H, J = 8.0)	8.80 (d, 2H, J = 4.8)	8.75 (t, 2H, J = 4.0)
H_6	8.85 (s, 2H)	8.86 (s, 2H)	8.85 (s, 2H)	8.80 (s, 2H)
H_7	8.22 (d, 2H, J = 7.4)	8.23 (d, 2H, J = 8.0)	8.22 (d, 2H, J = 8.0)	8.24 (d, 2H, J = 8.0)
H_8	8.55 (d, 2H, J = 8.3)	8.56 (d, 2H, J = 8.0)	8.55 (d, 2H, J = 8.0)	8.58 (d, 2H, J = 8.0)
H_9	8.88 (d, 2H, J = 5.48)	8.89 (d, 2H, J = 8.0)	8.88 (d, 2H, J = 8.0)	8.87 (s, 2H)
H_{10}	7.67 (t, 2H, J = 8.0)	7.67 (t, 2H, J = 8.0)	7.67 (t, 2H, J = 8.0)	7.67 (d, 2H, J = 8.0)
H_{11}	7.77 (t, 2H, J = 6.0)	7.77 (t, 2H, J = 8.0)	7.77 (t, 2H, J = 8.0)	7.74 (t, 2H, J = 4.0)
H_{12}	8.63 (d, 2H, J = 8.0)	8.63 (d, 2H, J = 8.0)	8.62 (d, 2H, J = 8.0)	8.65 (t, 2H, J = 4.0)

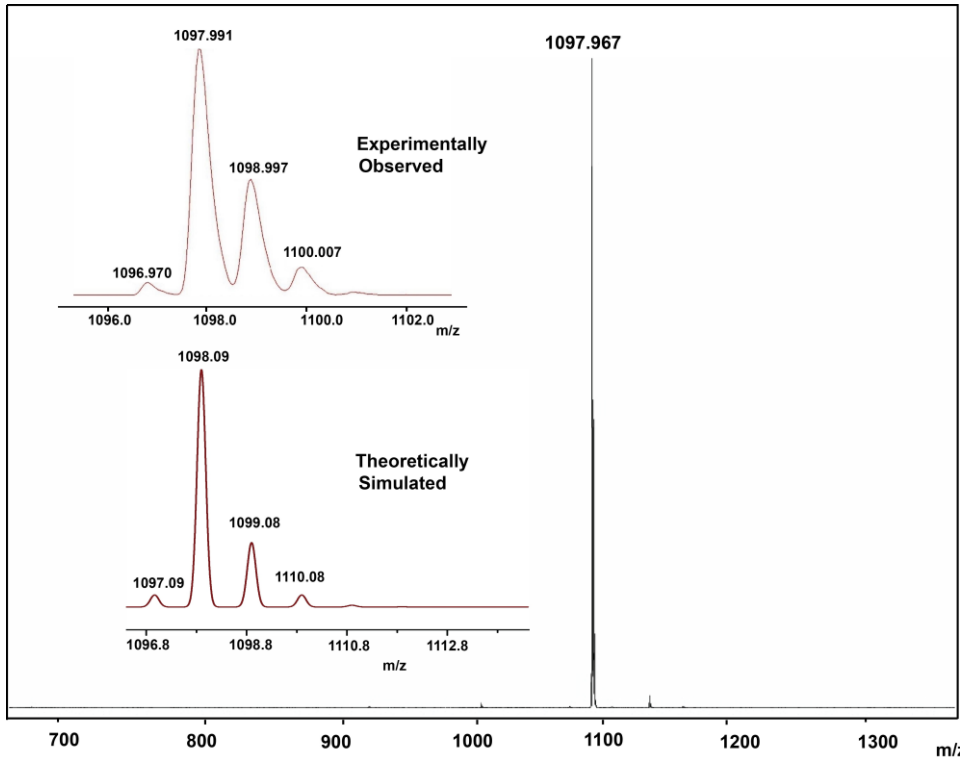

Figure 4.3. MALDI-TOF-MS of $Tb(hfa)_3$(tpy-HImzphen) (**4**) in dichloromethane solution (positive mode). The upper left portion shows the experimentally observed isotopic distribution pattern (b) and the lower left portion shows the simulated isotopic distribution pattern (c).

4.3.5. X-ray Crystallography. Single-crystal X-ray structural analysis is carried out for two in-situ synthesized Tb(III) complexes (**5** and **6**). Despite our several attempts, we are unable to grow suitable single crystals with as-synthesized complexes. Alternatively, upon treatment of tpy-HImzphen with terbium chloride ($TbCl_3 \cdot 6H_2O$) and terbium nitrate {$Tb(NO_3)_3 \cdot 6H_2O$} in $CHCl_3$-MeOH mixture (1:1, v/v) followed by sequential addition of hexafluoroacetylacetone and triethylamine and allowing the solutions for slow evaporation, we obtained yellowish needle-shaped tiny crystals suitable for X-ray diffraction.

Both **5** and **6** are crystallized in the C2/c space group with monoclinic system. The asymmetric unit reveals the entire structural motif. The solid-state molecular structure of the **5** and **6** is shown in Figure 4.4, and the crystallographic parameters are given in Table 4.3. Both the compounds are neutral and the solvents of crystallization are different. The structural inspection depicts the incorporation of only two diketonate ligands in both cases, providing a similar type of core structure of the form, Tb(tpy-HImzphen)$(hfa)_2$-X, where X is

either CF_3COO^- or NO_3^- for balancing the charge. It is observed that CF_3COO^- motif gets coordinated to Tb^{III} in complex **5**, although we do not use any trifluoroacetate salt of Tb. The exact reason is not clear to us, although in-situ decomposition of hexafluoroacetyl-acetonate is a finite possibility, which is also precedented in the literature.[63] The structure of complex **5** reveals that the terpyridine moiety gets coordinated to the Tb^{III}-center in tridentate fashion, whereas two diketonates chelate in bidentate mode and one trifluoroacetate unit coordinated in a monodentate fashion to the central metal ion. Thus, the Tb^{III} ion has eight coordination number with a square antiprism geometry. The coordination mode for complex **6** is almost similar to that of complex **5,** with the exception that nitrate ion (NO_3^-) gets coordinated to Tb(III) in a bidentate chelated mode. Consequently, Tb^{III} possesses nine-coordination number

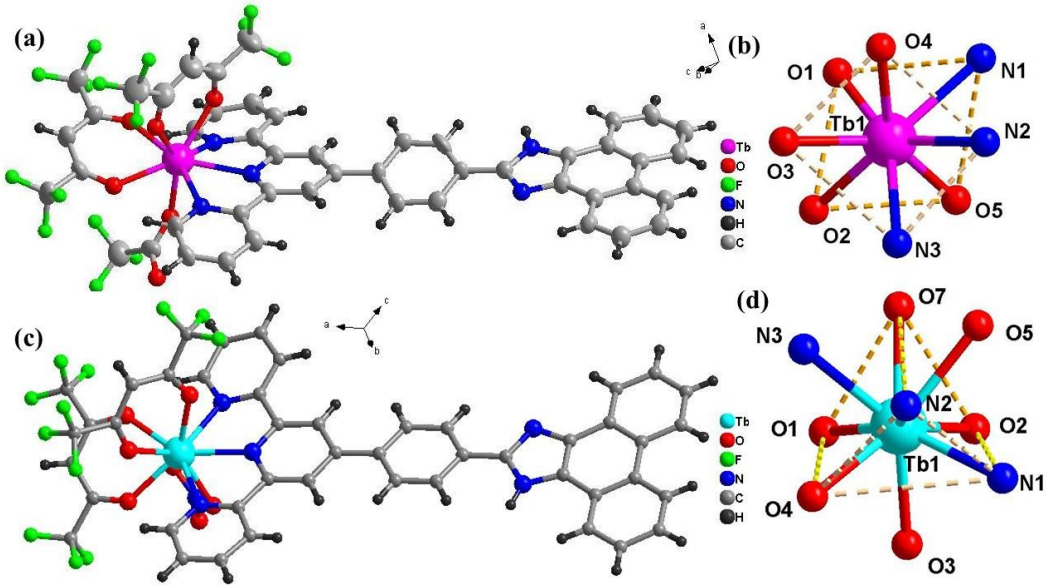

Figure 4.4. X-ray crystallographic structure of **5**, displaying distorted square anti-prism geometry around Tb^{III} ion (a and b) and **6,** wherein Tb^{III} ion possessed distorted tricapped trigonal prism geometry (c and d).

with tri-capped trigonal prism geometry in complex **6**. The Tb-N bond length varies within 2.491(6)-2.499(7) Å for **5** while between 2.484(5) and 2.514(4) Å for **6.** The Tb-O bond distance varies between 2.296(7)-2.401(6) Å and 2.334(4)-2.559(5) Å for **5** and **6**, respectively. Thus, we can predict that due to the presence of more electron-withdrawing groups in **5**, the average Tb-N and Tb-O distances are shorter than complex **6**, suggesting better overlap with the metal center. The bite angles around Tb^{III} centre ranges from 64.9(2) to 147.1(2)° and from 70.12(15) to 149.11(17) for **5** and **6**, respectively.

Table 4.3. Crystallographic Parameters for 5 and 6

Compound	**5**	**6**
CCDC Number	2340054	2340055
Empirical formula	$C_{48}H_{25}F_{15}N_5O_6Tb$	$C_{46}H_{25}F_{12}N_6O_7Tb$
Formula weight ($gmol^{-1}$)	1211.66	1160.65
Temperature (K)	105.0	145.03
Crystal system	Monoclinic	Monoclinic
Space group	C2/c	C2/c
Unit cell lengths (Å)	a= 43.279(3)	36.109(4)
	b = 9.4755(7)	15.2718(15)
	c = 23.0492(14)	19.444(2)
Unit cell angles (°)	α= 90	α= 90
	β = 98.895(4)	β = 106.848(5)
	γ = 90	γ = 90
Volume ($Å^3$)	9338.5(11)	10262.2(19)
Z	8	8
Density (calculated)	1.725	1.503
μ(mm^{-1})	8.497	1.474
F(000)	4776.0	4576.0
Crystal size (mm)	0.1 × 0.02 × 0.01	0.28 × 0.26 × 0.24
2θ range for data collection (°)	4.132 to 137.07	4.428 to 55.078
Reflections collected	166866	57384
Index ranges	-12 ≤ h ≤ 12, -29 ≤ k ≤ 30, -48 ≤ l ≤ 47	-46 ≤ h ≤ 46, -15 ≤ k ≤ 19, -25 ≤ l ≤ 25
Independent reflections	8524 [Rint = 0.1895, Rsigma = 0.0683]	11811 [R_{int} = 0.0958, R_{sigma} = 0.0852]
Data/Restraints/Parameter	8524/0/676	11811/0/649
Goodness-of-fit on F^2	1.108	0.994
Final R indices [I>2sigma(I)]	R1 = 0.0950, wR2 = 0.2353	R_1 = 0.0517, wR_2 = 0.1084

The ligand structure in both cases is almost unaltered, with the exception that the phenanthrene moiety in **5** gets out of the polypyridyl plane {dihedral angle between the two planes is 12.18 (5)º} (Figure 4.5), unlike complex **6**, where all the polyaromatic ring persists almost in the same plane. The intermolecular hydrogen bond plays an important role in forming zig-zag-like architecture for **5** [O6-H4, 1.987 (7) Å; O6-H4-N4, 171.0 (5)°] as shown in Figure 4.6.

4.3.6. Thermogravimetric Analysis of the Complexes. The thermal stability of the complexes was checked via thermogravimetry in N_2 atmosphere within the temperature domain of 30-800 °C. The rate of heating was maintained at 10 °C/m. Similarity in

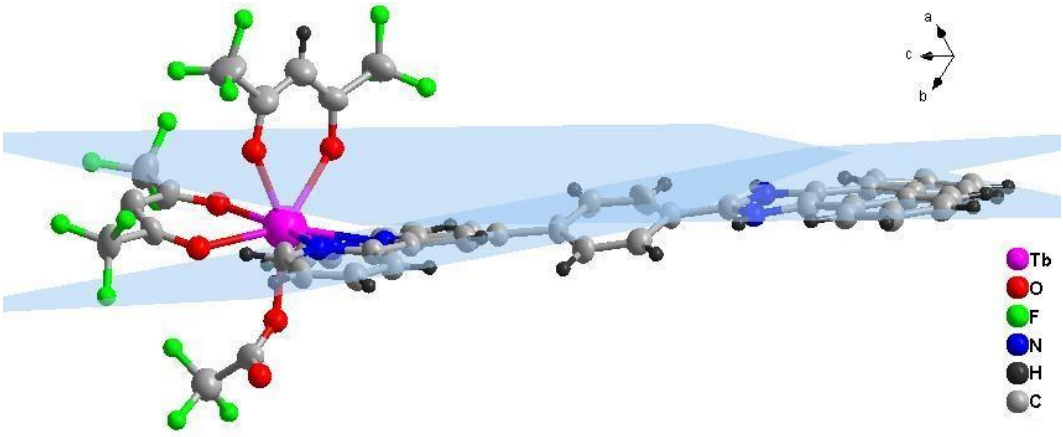

Figure 4.5. Diamond diagram of two planes for complex **5** containing the terpyridyl and phenanthrene moiety of the ligand tpy-HImzphen, respectively.

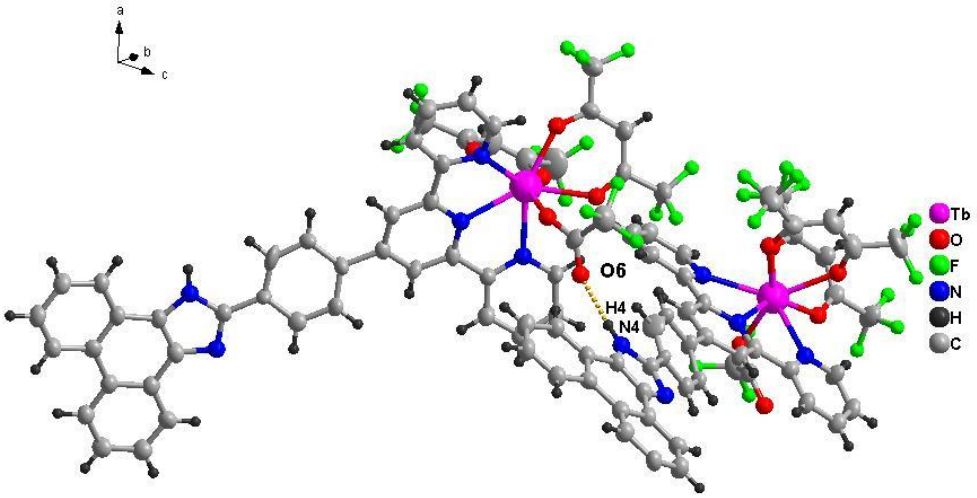

Figure 4.6. Diamond diagram of complex **5** exhibiting the inter-molecular hydrogen bonding between O6 and H4.

decomposition pattern and weight loss is noticed in all cases (Figure 4.7). Very small weight loss takes place at ~190 °C, probably because of moisture loss from the samples. Upon reaching at ~250 °C, decay starts and continues up to ~330 °C (up to ~40% weight loss) which is probably due to dissociation of tpy-HImzphen. The next major weight-loss begins at ~530 °C and continues thereafter possibly due to generation of the respective metal oxides. It is to be noted that the synthesized complexes are thermally more stable (onset temperature ~250 °C) than that of their respective lanthanide precursors (onset temperature ~180 °C). Thus, it seems that the complexes possess adequate thermal stability up to ~250 °C.

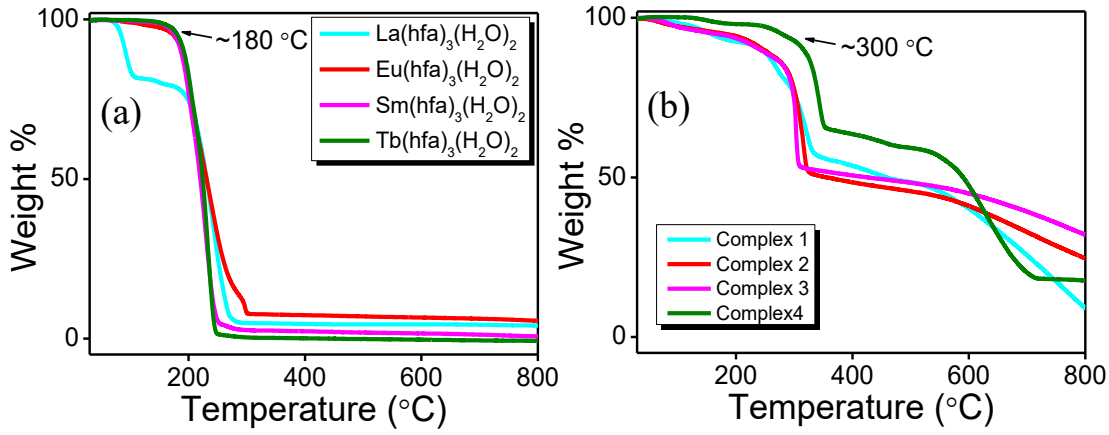

Figure 4.7. Thermogravimetric analysis of all four metal precursors $Ln(hfa)_3(H_2O)_2$ (a) and their corresponding complexes **1-4** (b).

4.3.7. Powdered X-ray Diffraction (PXRD). We also conducted PXRD analysis for all the four complexes as shown in Figure 4.8. The PXRD show broad peaks which probably indicates their amorphous nature. As already mentioned, despite our sincere efforts, we were unable to obtain single crystal X-ray structure of the complexes probably because of amorphous nature (Scheme 4.2). This observation is also aligned with earlier literature findings.[64] The similar PXRD pattern observed for complexes **1-4** suggests that they are all isostructural.

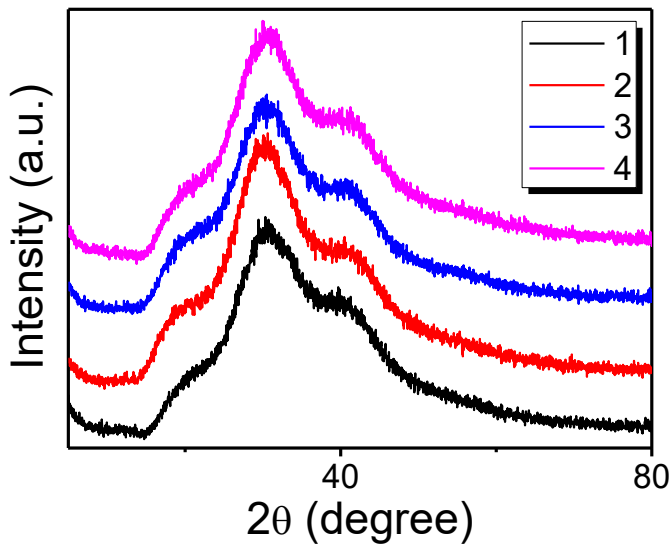

Figure 4.8. PXRD patterns of complexes **1-4**

4.3.8. Photophysical Properties. The photophysical measurements of all four lanthanide complexes are carried out in dried dichloromethane, and the relevant spectral data are presented in Table 4.4. Associated spectra are shown in Figures 4.9-4.11. For free tpy-

Table 4.4. Photophysical Parameters of Complexes 1-4 along with tpy-HImzphen Ligand at RT and 77K

	Compounds	Absorption, λ_{max}/nm (ε/$M^{-1}cm^{-1}$)($\times10^4$)	λ_{max}		Lifetime (τ)	Relative Quantum Yield (Φ_{rel}/%)
			Ligand centered	Metal centered		
RT	**tpy-HImzphen**[59]	254(6.50), 343(2.52), 370 (2.60)	446	-	2.3 ns	-
	1	260(4.45), 289(5.30), 304 (5.10), 380(1.76)	532	-	3.3 ns	57.3
	2	260(4.70), 290(5.40), 304 (5.00), 377(2.33)	445	579, 593, 614, 652	473.1 µs	30.4
	3	260(6.75), 288(5.70), 307 (4.65), 381(3.05)	444	561, 597, 645	41.3 µs	4.4
	4	260(2.79), 288(2.30), 307 (1.83), 378(1.14)	448	545, 615	1.7 ns	35.2
77K	**1**	-	523	-	2.0 ns	-
	2	-	444	579, 590, 593, 614, 650	674.2 µs	-
	3	-	470	562, 596, 643	47.7 µs	-
	4	-	442	489, 544, 583, 620	720.4 µs	-

HImzphen ligand, the lowest energy absorption band at 370 nm (ε= 26000 M^{-1} cm^{-1}) is ascribed to intra-ligand charge transfer (ILCT) transitions whereas the band at 254 nm (ε= 65000 M^{-1} cm^{-1}) is because of π-π* transitions associated with aromatic and heteroaromatic motifs within the framework (Figure 4.9a).[59] Besides, the λ_{max} for all four $Ln(hfa)_3(H_2O)_2$ precursors appear at ~300 nm (Figure 4.9a). Upon complexation with Ln-hfa moiety, the lowest energy absorption band underwent a bathochromic shift to ~380 nm (ε=11400-30500 M^{-1} cm^{-1}) together with generation of a new band at ~300 nm region (ε= 18250-51000 M^{-1} cm^{-1}), indicating the incorporation of $Ln(hfa)_3$ moiety [λ_{max}=301-303 nm] in the complex backbone (Figure 4.9b). One intriguing aspect here is that the Ln^{III} complexes often face criticism because of having their absorption window confined within the UV region (<390 nm). Herein, upon coordination of the Ln-hfa moiety with the tpy-HImzphen ligand, the absorption window gets expanded into the visible region with the onset at ~450 nm.

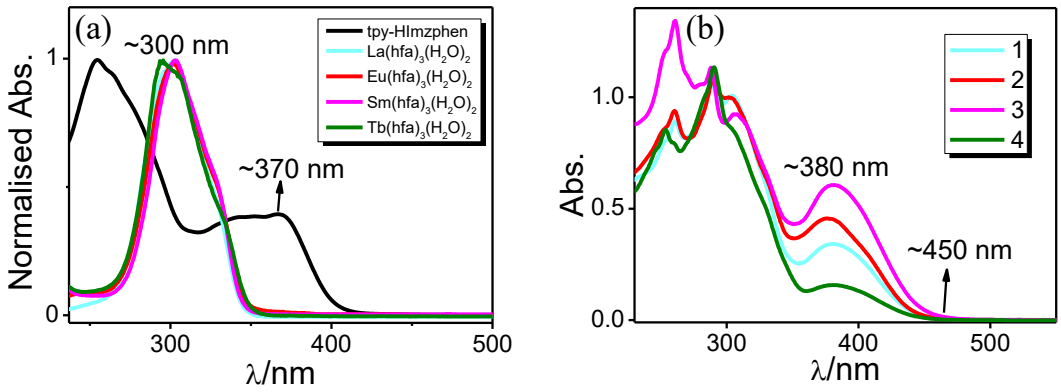

Figure 4.9. UV-visible absorption spectra of the tpy-HImzphen and four $Ln(hfa)_3(H_2O)_2$ precursors (a) along with complexes **1**-**4** (b) in dichloromethane at RT.

The emission spectra of the complexes, recorded in dry DCM solvent at room temperature upon excitation at ~330 nm, are shown in Figure 4.10 (a and b). Free tpy-HImzphen exhibits a broad emission signal centered at 446 nm.[59] For the La^{III} complex (**1**), a red-shifted ligand-centered emission is observed at 532 nm, making it a green emitter from the non-emissive La^{III} ion. In case of Eu^{III} complex (**2**), the lanthanide-centered emission signals at 579, 592, 614 and 652 nm associated to intra-configurational $^5D_0 \rightarrow {}^7F_0$, $^5D_0 \rightarrow {}^7F_1$, $^5D_0 \rightarrow {}^7F_2$, and $^5D_0 \rightarrow {}^7F_3$ transitions, are clearly observed. The peak at ~614 nm due to hypersensitive $^5D_0 \rightarrow {}^7F_2$ electric dipole transition is the most intense among the four peaks which indicate high asymmetry around the central Eu^{III} ion. Besides, the intensity of the ligand-centered peak at ~445 nm is almost negligible as compared to the Eu^{III}-centered peaks which manifest an efficient (almost complete) intramolecular ligand-to-metal energy transfer. For the Sm^{III} complex (**3**), the characteristic Sm^{III}-centered peaks at 561 ($^5G_{5/2} \rightarrow {}^5H_{5/2}$), 597 ($^5G_{5/2} \rightarrow {}^5H_{7/2}$), and 645 nm ($^5G_{5/2} \rightarrow {}^5H_{9/2}$) are also observed but the intensities of the peaks are substantially lower as compared to that of the ligand-associated signal at ~444 nm, suggesting the occurrence of either very weak ligand-to-metal energy transfer or strong quenching via some sort of non-radiative deactivation. The Tb^{III}-complex (**4**) displays the ligand-centered broad signal at ~448 nm as the paramount peak with a slight signature of the characteristic Tb^{III}-centered f-f intra-configurational peaks at ~545 nm and 615 nm, corresponding to $^5D_4 \rightarrow {}^7F_5$ and $^5D_4 \rightarrow {}^7F_3$ transition, respectively. This phenomenon indicates reverse or back energy transfer from the Tb^{III}-center to the ligand moiety. Thus, the observed emission phenomena reveal that the ancillary tpy-HImzphen ligand drives the Ln^{III} ions to respond in four distinct ways. We have estimated the relative quantum yield (Φ_{rel}) of the complexes with reference to quinine sulphate in 0.1 M H_2SO_4 (λ_{ex}=344 nm and Φ=0.546) and the values are

found to be 57.3%, 30.4%, 4.4%, and 35.2%, for **1**, **2**, **3**, and **4**, respectively, which resemble well with those of the earlier reported values.[19,65-72] We also determined the radiative- (k_r) and non-radiative rate constant (k_{nr}), lifetime (τ_{rad}), and intrinsic quantum yield (Φ_{ff}) for the Eu^{III}-complex (**2**) and the values presented in Table 4.5. Appropriate analysis of the observed parameters substantiates that the tpy-HImzphen→Eu^{3+} energy transfer process is very efficient (η_{sens}=~95%).

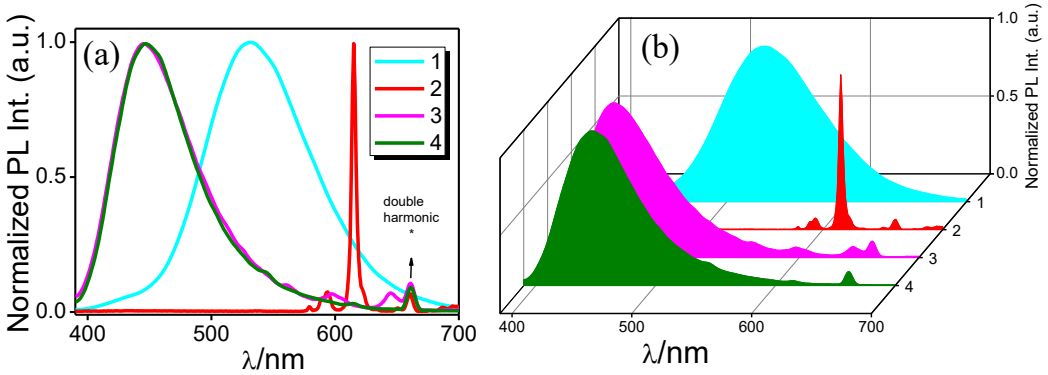

Figure 4.10. Normalized photoluminescence spectra of the complexes **1-4** in dichloromethane at RT in both 2D (a) and 3D representation (b).

Table 4.5. Lifetime (τ_{obs}), Radiative (k_r) and Non-radiative Rate Constants (k_{nr}), Intrinsic Quantum Yield (Φ_{ff}), Relative Quantum Yield (Φ_{rel}) and Energy Transfer Efficiency (η_{sens}) of the Eu^{III}-complex (2)

τ_{obs} (μs)	k_r (s^{-1})	k_{nr} (s^{-1})	Φ_{ff} (%)	Φ_{rel} (%)	η_{sens} (%)
473.1	662.6	1440	32	30.4	95

The emission lifetimes for all the complexes are also acquired in dichloromethane by time-correlated single photon counting (TCSPC) as well as by multi-channel scaling (MCS) methods, depending upon the range of lifetime of the complexes, and the associated decay profiles are presented in Figure 4.11. The complexes are excited either with a 370 nm delta diode or a spectra LED source. The excited state decay profiles for all four complexes are best fitted with a mono-exponential function. The lifetimes of **1** and **4** lie within the domain of 1.7-3.3 ns (Figures 4.11a and 4.11d), while complexes **2** and **3** display substantially longer lifetimes, viz. 473.1 μs and 41.3 μs, respectively (Figure 4.11b and 4.11c, Table 4.4). Thus, the observed lifetime values indicate that the radiative deactivation primarily occurs through the ligand center for complexes **1** and **4**. By contrast, due to parity-forbidden f-f transitions in Ln^{III} ions, complexes **2** and **3** have much longer excited state lifetimes, which range from tens to hundreds of microseconds.

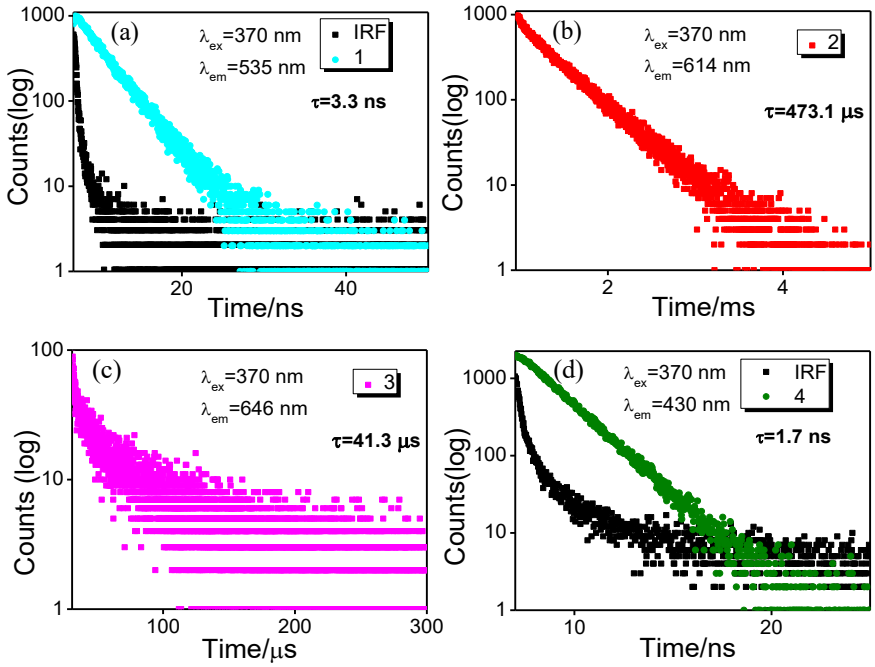

Figure 4.11. Luminescence decay profiles of the complexes **1**-**4** (a-d) in dichloromethane at RT.

We have also recorded the steady state luminescence spectra and lifetimes of all four complexes at 77K to elucidate the temperature-assisted non-radiative deactivation as well as to comprehend the deactivation dynamics of the complexes (Figure 4.12). No significant change is observed in case of La^{III}-complex (**1**), except a small blue shift in the ligand-centered broad peak from 532 nm to 522 nm, upon cooling down to 77K (Figure 4.12a). In line with the steady state spectrum, almost no such change in the lifetime value (2 ns) is noticed (Figure 4.12b). In case of Eu^{III}-complex (**2**), a huge enhancement of the Eu^{III}-centered peaks is observed at 77K. To our surprise, concomitant enhancement accompanied with small blue-shift of the ligand-centered emission, also takes place on cooling down to 77K (Figure 4.12c). The lifetime of **2** also gets considerably increased from 473.1 μs to 674.2 μs, upon going down to 77K (Figure 4.12d). The Sm^{III}-complex (**3**), on the contrary, displays a red-shifted ligand-centered peak at ~470 nm along with an increase in the peak intensities for Sm^{III}-center, on passing from RT to 77K. The lifetime of **3** also increases from 41.3 μs to 47.7 μs as depicted in Figures 4.12e and 4.12f. The effect of cooling down the temperature is found to be most dramatic in case of Tb^{III}-complex (**4**). On cooling down to 77K, the Tb^{III}-centered peaks associated with $^5D_4 \rightarrow {}^7F_{J\ (J\ =\ 6\text{-}3)}$ transitions get immensely intensified with small blue-shift (448→442 nm) together with diminution of the ligand-centered peak (Figure 4.12g). In addition, the lifetime is found to be as high as 720.4 μs at the monitoring

wavelength of 545 nm, as compared to its ligand-centered lifetime of 1.7 ns at RT (Figure 4.12h). The corresponding values for all four complexes at RT and 77K are summarized in Table 4.4.

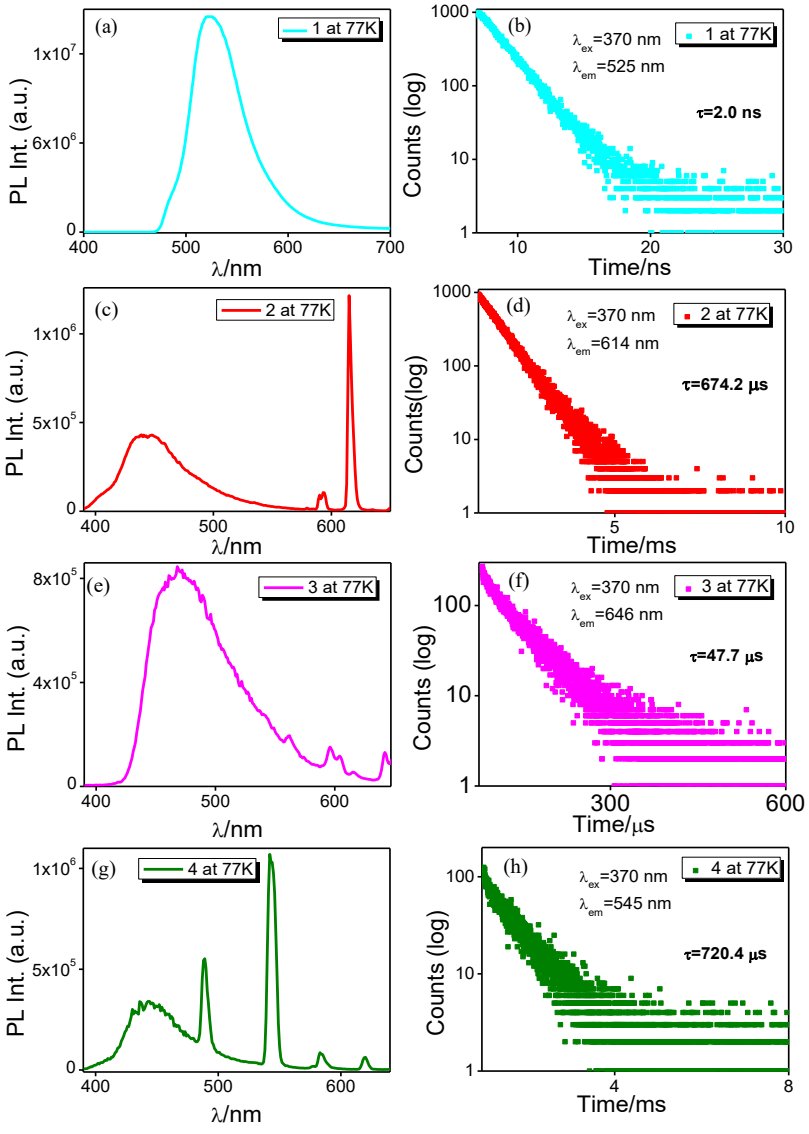

Figure 4.12. Photoluminescence spectra and lifetime decay plots of **1-4** in ethanol-methanol (4:1, v/v) glass at 77K.

4.3.9. In-situ Generation of the Ternary Ln^{III} Complexes. In-situ generation of all the four complexes is feasible upon gradual addition of respective $Ln(hfa)_3(H_2O)_2$ precursor to the dichloromethane solution of tpy-HImzphen and the progress of the reactions has been monitored via absorption and emission spectroscopy. Relevant titration profiles are presented

in Figures 4.13-4.16. The lowest energy absorption maximum undergoes a downfield shift, stretching up to 450 nm region (Figures 4.13a, 4.14a, 4.15a, and 4.16a). It is noticed that consecutive spectral lines pass through two sharp isosbestic points (at ~340 nm and ~375 nm). Spectral saturation takes place upon addition of 1 equiv. of the lanthanide precursors in all cases. The spectrum at saturation resemble closely to that of the isolated complexes.

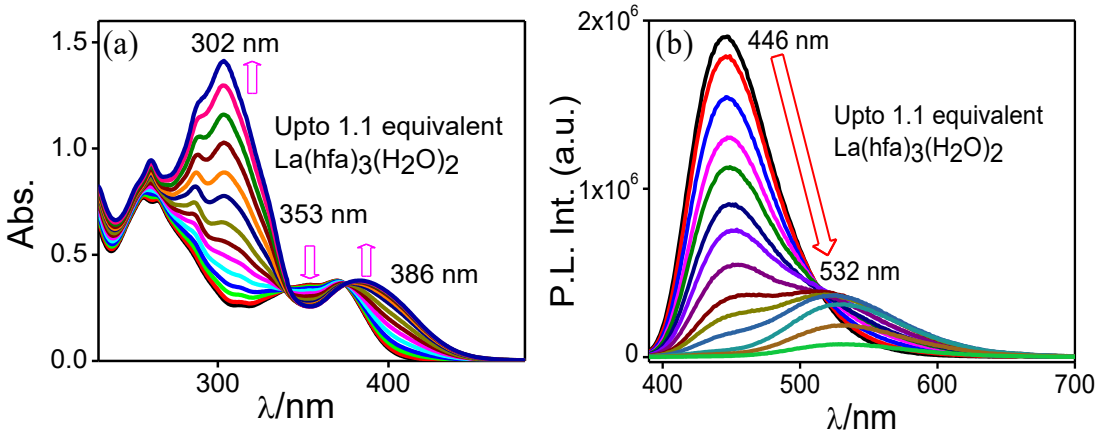

Figure 4.13. Changes in UV-vis absorption (a) and photoluminescence spectra (λ_{ex}=370nm) (b) of tpy-HImzphen ligand upon gradual addition of $La(hfa)_3(H_2O)_2$ in dichloromethane at RT.

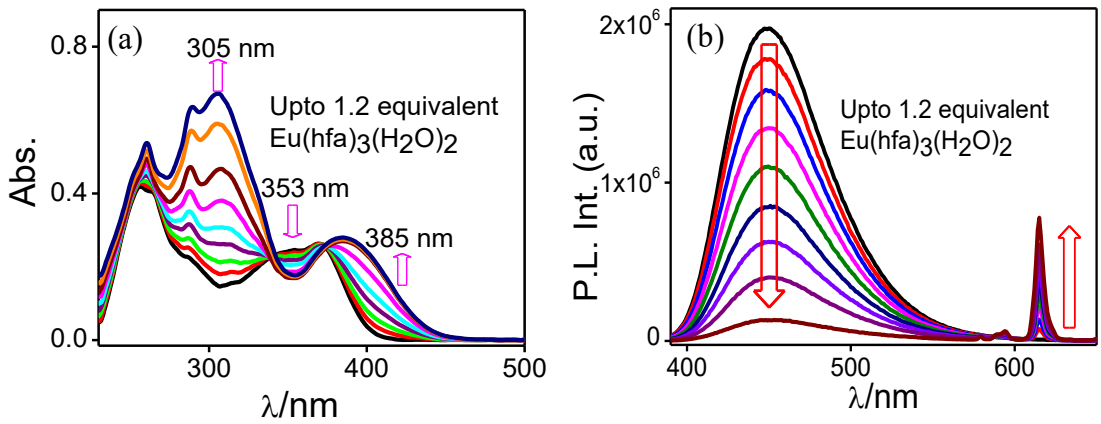

Figure 4.14. Changes in UV-vis absorption (a) and photoluminescence spectra (λ_{ex}=370nm) (b) of tpy-HImzphen ligand upon gradual addition of $Eu(hfa)_3(H_2O)_2$ in dichloromethane at RT.

In the emission side, upon gradual addition of $La(hfa)_3(H_2O)_2$, the ligand-centered peak at ~446 nm gets systematically quenched, accompanied by a red-shift of the maximum to 532 nm, and saturation takes place on adding ~1 equiv of the La^{3+} precursor (Figure 4.13b). In case of Eu^{3+}, systematic quenching in the ligand-centered emission at 448 nm

occurs and at its expense evolution and gradual intensification in peak intensities at 579, 592, and 614 nm, due to f-f intraconfigurational $^5D_0 \rightarrow {}^7F_{J(J=0\text{-}2)}$ transitions, also takes place (Figure 4.14b). The spectral pattern in Sm^{III} is someway comparable to that of Eu^{III}, albeit the intensities of the signals at ~597 ($^5G_{5/2} \rightarrow {}^5H_{7/2}$) and 645 nm ($^5G_{5/2} \rightarrow {}^5H_{9/2}$) are much less (Figure 4.15b). In contrast to Eu^{III} and Sm^{III}, systematic quenching of only the ligand-centered emission at 446 nm takes place without any signature of typical Tb^{III}-centered signals due to $^5D_4 \rightarrow {}^7F_{J(J=6\text{-}3)}$ transitions (Figure 4.16b).

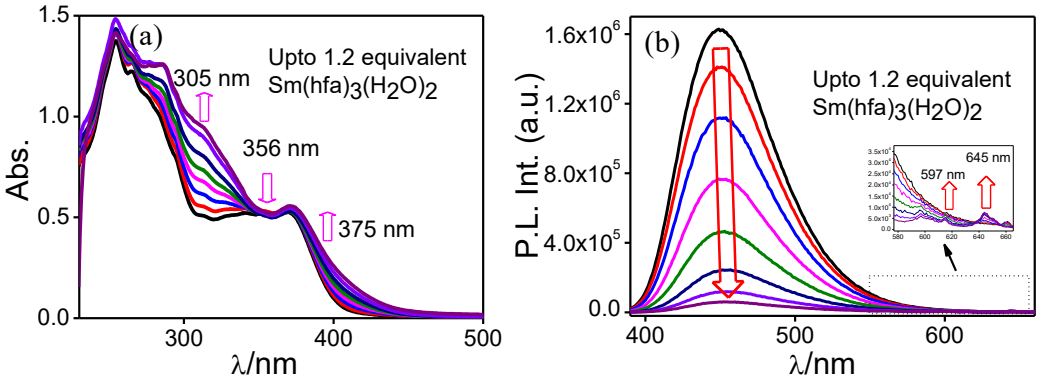

Figure 4.15. Changes in UV-vis absorption (a) and photoluminescence spectra (λ_{ex}=370nm) (b) of tpy-HImzphen ligand upon incremental addition of $Sm(hfa)_3(H_2O)_2$ in dried dichloromethane at RT.

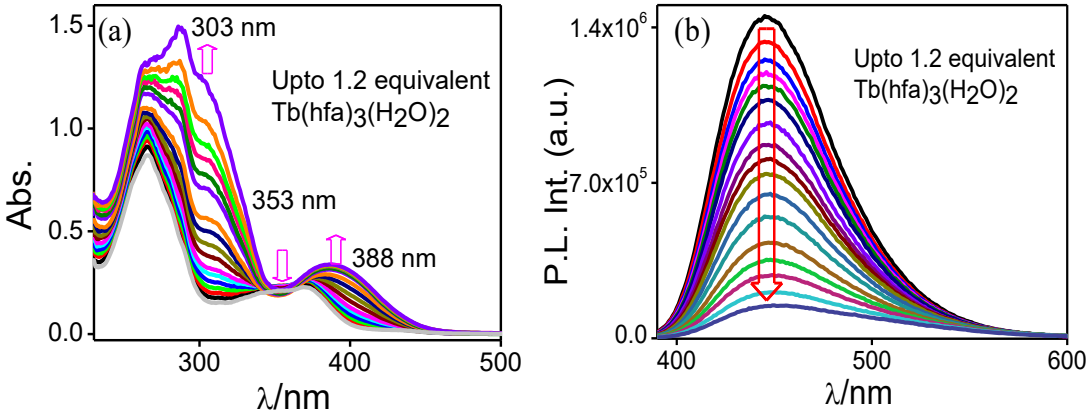

Figure 4.16. Changes in UV-vis absorption (a) and photoluminescence spectra (λ_{ex}=370nm) (b) of tpy-HImzphen ligand upon incremental addition of $Tb(hfa)_3(H_2O)_2$ in dried dichloromethane at RT.

4.3.10. Thermosensing and Thermochromic Behaviors of $Eu(hfa)_3$(tpy-HImzphen). The emission spectral analysis clearly indicates that only the Eu^{III}, among the four studied lanthanides, gets effectively sensitized upon incorporation of tpy-HImzphen ancillary ligand. In addition to the hypersensitive peak at 614 nm due to the $^5D_0 \rightarrow {}^7F_2$

transition, the Eu(III) complex displays a weak but finite band at 445 nm due to ligand-centered emission. The TGA profile suggests that the Eu-complex remains structurally intact up to ~250 °C (~523 K). Taking advantage of thermal stability as well as dual emission characteristics, temperature-dependent emission spectral measurements of the complex are carried out upon varying the temperature between 273 K and 353 K. Both steady-state and time-resolved emission spectra are acquired in MeCN in the said temperature domain. It is noticed that with an increase in temperature, the intensity of the Eu^{III}-centered signal at 614 nm diminishes systematically while the ligand-centered emission at ~470 nm progressively intensifies accompanied by a small blue shift (Figures 4.17a and 4.17b). Accordingly, the emitting color changes from blue (at 273 K) to cyan at 353 K, as depicted in the corresponding Commission Internationale de l'Éclairage (CIE) plot (Figure 4.17c). In line with the steady-state emission phenomena, the lifetime of the complex monitored at 614 nm is found to decrease systematically from 759.2 µs at 273K to 475.6 µs at 353K (Figure 4.17d). It is to be noted that in most of the earlier reported cases, only the Ln-centered emission response have been employed for thermosensing. In the present study, emission responses of both ligand (tpy-HImzphen) and Ln-centre have been utilized simultaneously to access the thermosensing efficacy of the Eu(III) complex.

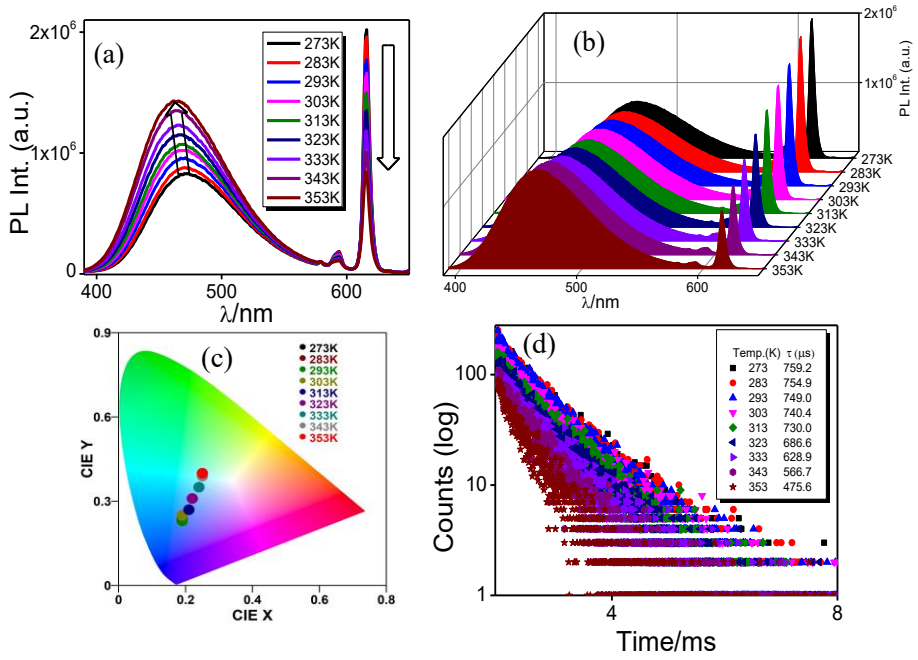

Figure 4.17. Changes in photoluminescence spectrum of **2** in MeCN upon varying temperature in 2D (a) and 3D (b) representation; corresponding chromaticity diagram (c) and changes in lifetime at the monitoring wavelength of 614 nm upon varying temperature (d).

The efficacy of the thermosensing aspect of the lanthanide complexes could be assessed by monitoring various temperature-dependent parameters (Δ), viz., widely used 'intensity ratio'[39,43,73,77] or 'lifetime'[40,50-52,75-78] and comparatively less used 'bandwidth'[49] or 'quantum yield'[80]. Herein, we have proposed a new thermometric parameter Δ (at temperature T) which can be denoted by equation (4.1).

$$\Delta = \frac{I_{ED}(T)}{\tau(T)} \qquad \text{.. (4.1)}$$

where I_{ED}(T) is the intensity of $^5D_0 \rightarrow {}^7F_2$ transition (at 614 nm) at temperature T, while τ(T) is the excited state lifetime (expressed in seconds) monitored at the same wavelength at temperature T. The relationship between this ratio, Δ $\{I_{ED}(T)/\tau(T)\}$ and T was found to be best fitted by an empirical polynomial equation as follows (equation 4.2).

$$\Delta = 34085\times T^2 - 4\times10^7\times T + 10^{10} \qquad (R^2=0.9932) \qquad \text{..(4.2)}$$

where T is the temperature and R^2 is the correlation coefficient of the best-fitted curve. The Δ *vs.* T plots have been depicted in Figure 4.18.

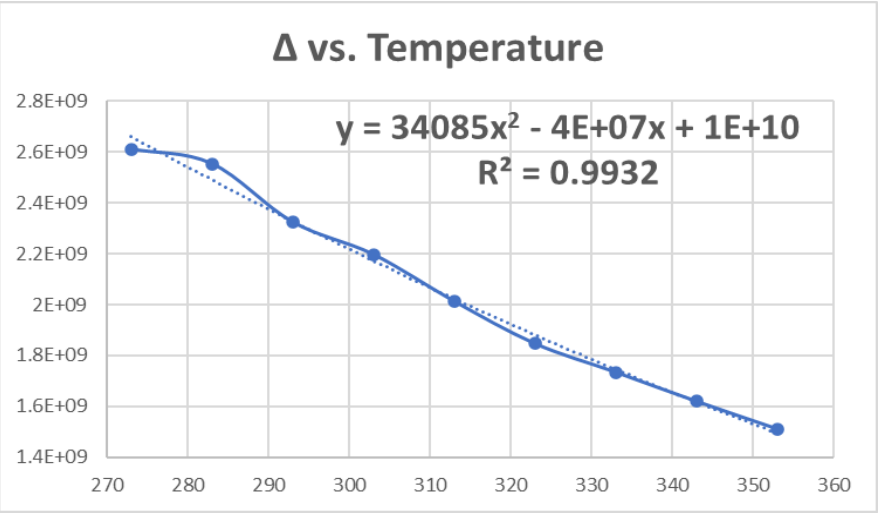

Figure 4.18. Change in the ratio Δ $\{I_{ED}(T)/\tau(T)\}$ of complex **2** in acetonitrile upon variation of temperature. The dotted line represents the best-fitted curve.

Now, the thermosensing efficiency of a system can be quantified by some well-known parameters, viz., relative thermal sensitivity (S_r) or temperature resolution (δT). The relative thermal sensitivity (S_r) (expressed in % K^{-1}) indicates the systematic change in a thermometric parameter per degree of temperature alteration as defined equation 4.3.

$$S_r = \frac{1}{\Delta}\left(\frac{\partial \Delta}{\partial T}\right) \quad .. (4.3)$$

The maximum obtained S_r value is designated as S_m, and the respective temperature value is termed as T_m. Here, the thermal sensitivity (S_r) for the complex $Eu(hfa)_3$(tpy-HImzphen) ranges from 1.32 to 12.52 % K^{-1} (S_m=12.52 % K^{-1} at T_m=353 K) which, to the best of our knowledge, is the highest value reported till date among the single Ln^{III}-based small-molecule temperature sensors operative in physiological temperature domain (Table 4.6).[40,43,49-52,73,74,79] Another reliable parameter is the temperature uncertainty (δT), also referred to as temperature resolution, which can be determined by using equation 4.4 as described below:

$$\delta T = \frac{1}{S_r}\left(\frac{\delta \Delta}{\Delta}\right) \quad .. (4.4)$$

This parameter defines the smallest resolvable change in temperature (δT) that the thermometer can detect, and its value should be as low as possible than 1 K. In our case, we found that the δT value is 0.0098 K. Thus, the Eu^{III}-complex can be considered an efficient luminescent thermo-sensor in a broad temperature range of 273-343 K, in terms of the standard and widely-used thermosensing efficacy-scaling parameters like S_r and δT.

Table 4.6. Comparative Table of Some Earlier Reported Ln^{III}-Based Thermosensors

Complex	S_m (%K^{-1})	ΔT (K)	T_m(K)	Optical parameter	Ref.
[Eu(DK12–14)$_3$phen]	1.0	270–370	270	Lifetime	40
$Tb(hfa)_3(H2O)_2$ [Tb(hfa)$_3$(dpbp)]n [Eu(hfa)$_3$(dpbp)]n	0.70 0.64 <0.05	200–450 K	400	Intensity ratio	43
Eu(keto)$_3$(H_2O) Keto= ketoprofen	7.0×10^{-2}	12–300	50	Bandwidth	49
Eu(bzac)$_3$(H_2O)$_2$	1.4	188–303	293	Lifetime	50
Eu(CPDK$_{3\text{-}5}$)$_3$phen	2.2	298-348 K	298	Lifetime	51
Eu(tta)$_3$(pyphen)	1.7	*283–323*	323	Lifetime	52
(Eu(HL)$_2$X, X = Cl, NO_3) H_2L= 2-(tosylamino)-benzylidene-N-benzoylhydrazone	7.7	77-298	*85*	Intensity ratio	73
Ln(btfa)$_3$(H_2O)$_2$ (Ln = Eu, Tb)	5.8	295–315	296	Intensity ratio	79

Interestingly, the photoluminescence response of the Eu^{III}-complex upon variation of temperature allows us to configure a “Set-Reset” (SR) flip-flop logic gate consisting of two

inputs, labelled as Set and Reset ('S' and 'R'). The SET input 'S' sets the device or produces the output 1, and the RESET input 'R' resets the device or produces the output 0. Here, 273K and 353K are considered Input 1 and Input 2, respectively. The emission peak at 465 nm and 614 nm corresponds to the Outputs (Out 1 and Out 2, respectively) (Figure 4.19a). The 'write-read-erase-read' cycle can be established via the appropriate use of these inputs and outputs.[56,57] In each cycle, certain temperatures are applied to demonstrate both the Write ('S', 273 K) as well as the Erase ('R', 353 K) course. When the temperature is 353 K, the input combination is 0 1, and high output 1 signal (1) and low output 2 signal (0) are obtained, creating the 'Write' process. Similarly, when the temperature is 273 K, the input combination is 1 0, and low output 1 signal (0) and high output 2 signal (1) are obtained, generating the 'Erase' process (Figure 4.19b). The corresponding truth table is also depicted in Figure 4.19c. Thus, the thermosensitive emission behaviour of the complex $Eu(hfa)_3$(tpy-HImzphen) can mimic the function of set-reset flip-flop logic and thus creates room for the fabrication of molecular logic devices.

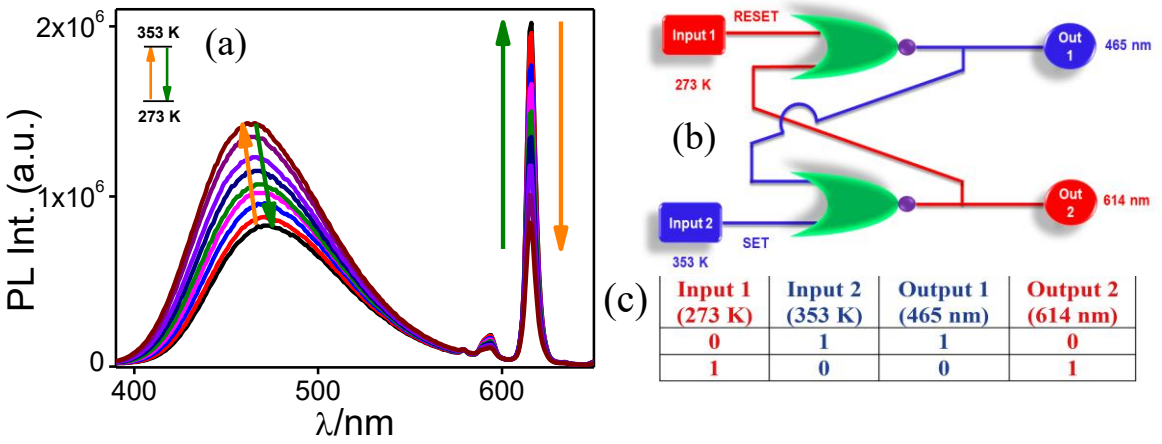

Figure 4.19. Thermosensitive photoluminescence response of complex **2** in MeCN (a); schematic representation of the responses in Set-Reset Flip-flop logic operation (b); corresponding truth table (c).

In order to exploit its favorable luminescence characteristics for practical application, we fabricated a hybrid thin film of the Eu(III) complex in poly(methyl methacrylate) (PMMA) polymer and thoroughly studied its emission characteristics. Keeping in mind about plausible appearance of turbidity at very high concentrations, we prepared 2%, 4%, 6%, and 8% (w/w) composite of $Eu(hfa)_3$(tpy-HImzphen) in the PMMA matrix. The embedding of complex **2** onto the PMMA matrix is verified via appropriate analyses of X-ray photoelectron

spectra (XPS), Fourier-transformed infrared spectra (FT-IR), and Scanning Electron Microscope (SEM) results.

4.3.11. XPS. To characterize the hybrid material based on Eu^{III}-embedded PMMA, XPS measurements are conducted on both the free PMMA as well as **2@PMMA** composite. The XPS spectrum of the free PMMA polymer exhibits distinct peaks at 283.8 and 531.7, corresponding to C 1s and O 1s, respectively (Figure 4.20a). Furthermore, the high-resolution C 1s spectrum is deconvoluted into three subpeaks at 283.5, 284.9 and 287.4 eV, corresponding to C-C and C-O, and C=O bonds, respectively (Figure 4.20b), whereas, O 1s spectrum reveals two sub-peaks for C=O and O-C=O bonds at 530.7 and 532.1, respectively (Figure 4.20c). In contrast, the full range spectrum for **2@PMMA** displays peaks in the C 1s, O 1s, and Eu 3d regions, with a relatively weaker N 1s peak (Figure 4.20d). The Eu^{III} analogue displays peaks of C 1s (283.24 eV) and O 1s (530.87 eV), in the similar region as free PMMA (Figure 4.20e and 4.20f) along with weak N 1s peak at 397.62 eV (Figure 4.20g) which is assigned for the terpyridyl ligand. It is noteworthy to mention that two distinct peaks at 1134.7 and 1164.5 eV are also observed for Eu, corresponding to $3d_{5/2}$ and $3d_{3/2}$, respectively, featuring a stable +3 oxidation state of europium (Figure 4.20d). Notably, these two peaks are absent in the XPS spectrum of free PMMA. These outcomes via XPS analysis align with the previously reported Eu^{III}-loaded PMMA hybrid materials, confirming the successful incorporation of Eu^{III}-complex into the PMMA matrix.

4.3.12. FT-IR. We conducted FT-IR characterization on pure PMMA as well as on **2@PMMA** composite in their solid states, keeping air as the background. In the previous section, we scrutinized the FT-IR spectra of all four ternary Ln^{III} complexes. Those spectra revealed characteristic peaks in the ranges of 1651 and 1528 cm^{-1}, corresponding to C=O and C=N bonds, respectively. Here, the distinctive peaks of PMMA emerged within 2700-3000 cm^{-1} assignable as the C–H stretching band and at 1716 cm^{-1}, attributed to the vibration of the C=O group. Notably, in the **2@PMMA** composite, two additional peaks at 1698 and 1539 cm^{-1} are evolved corresponding to the C=O and C=N bonds present in the free complex (Figure 4.21). Therefore, the FT-IR analysis also indicates the embedding of complex **2** into the PMMA matrix.

4.3.13. SEM. We also conducted SEM analysis on the **2@PMMA** composite and compared with the free PMMA polymer. To achieve this, both the free PMMA and **2@PMMA** composite are drop-casted using DCM onto the silicon wafers (0.5X0.5 cm) using the spin-coating method. The SEM images reveal a hollow-sphere architecture for the

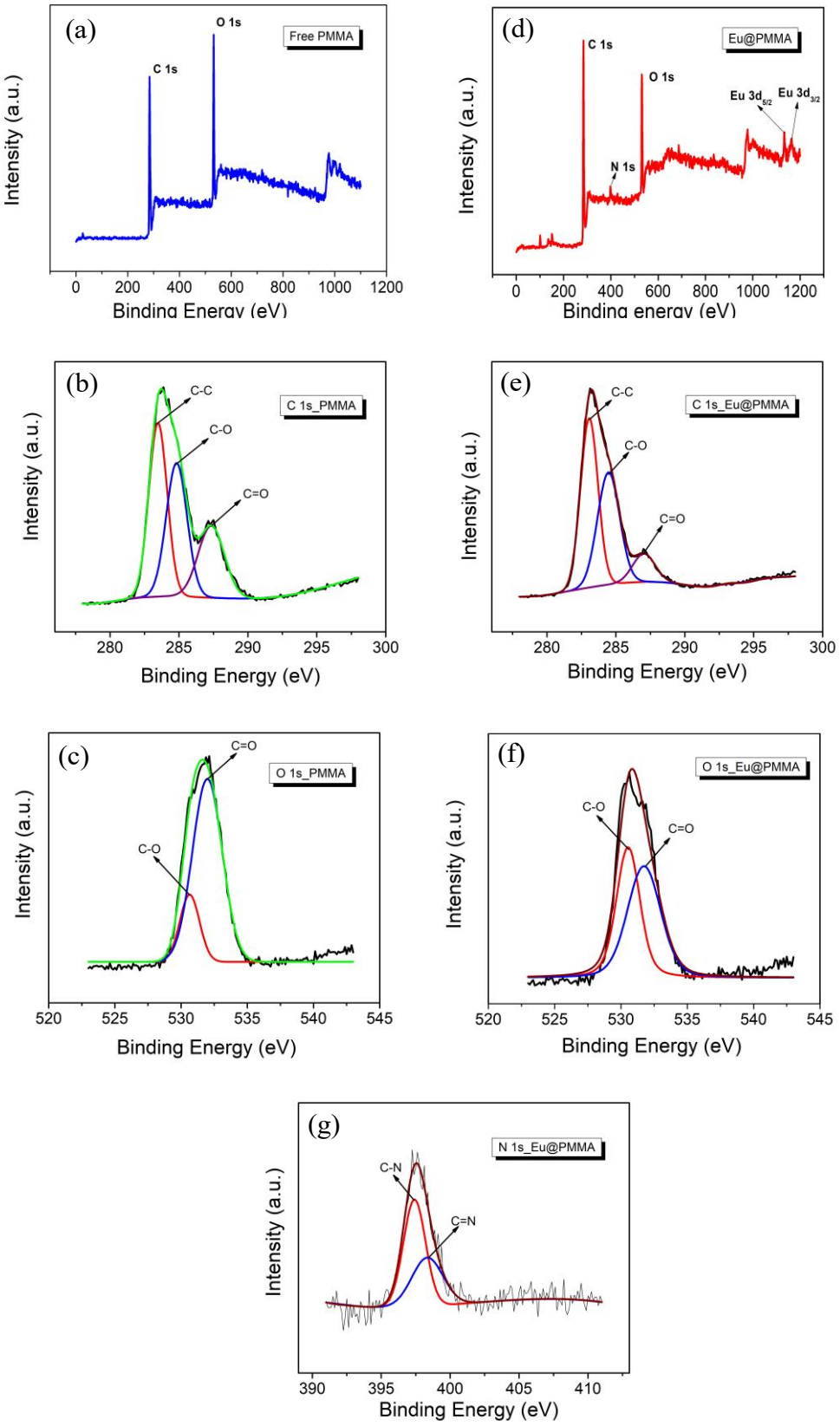

Figure 4.20. XPS analysis for 4% **2**@PMMA.

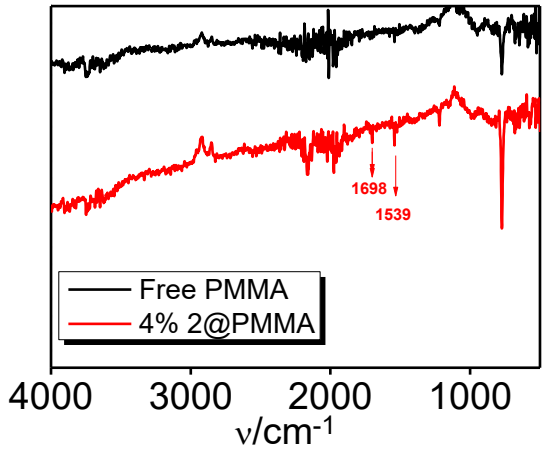

Figure 4.21. Comparative IR spectra of free PMMA and 4% **2**@PMMA.

free PMMA, while the Eu^{3+}-embedded material exhibits well-distributed particles on the hollow spheres, indicating the incorporation of complex **2** into the PMMA matrix (Figure 4.22). Thus, the SEM analysis also supports the embedding of complex **2** into the PMMA matrix. A schematic representation for the fabrication of the hybrid thin film of 4% **2@PMMA** along with its exhibition in daylight and under UV light is presented in Figure 4.22.

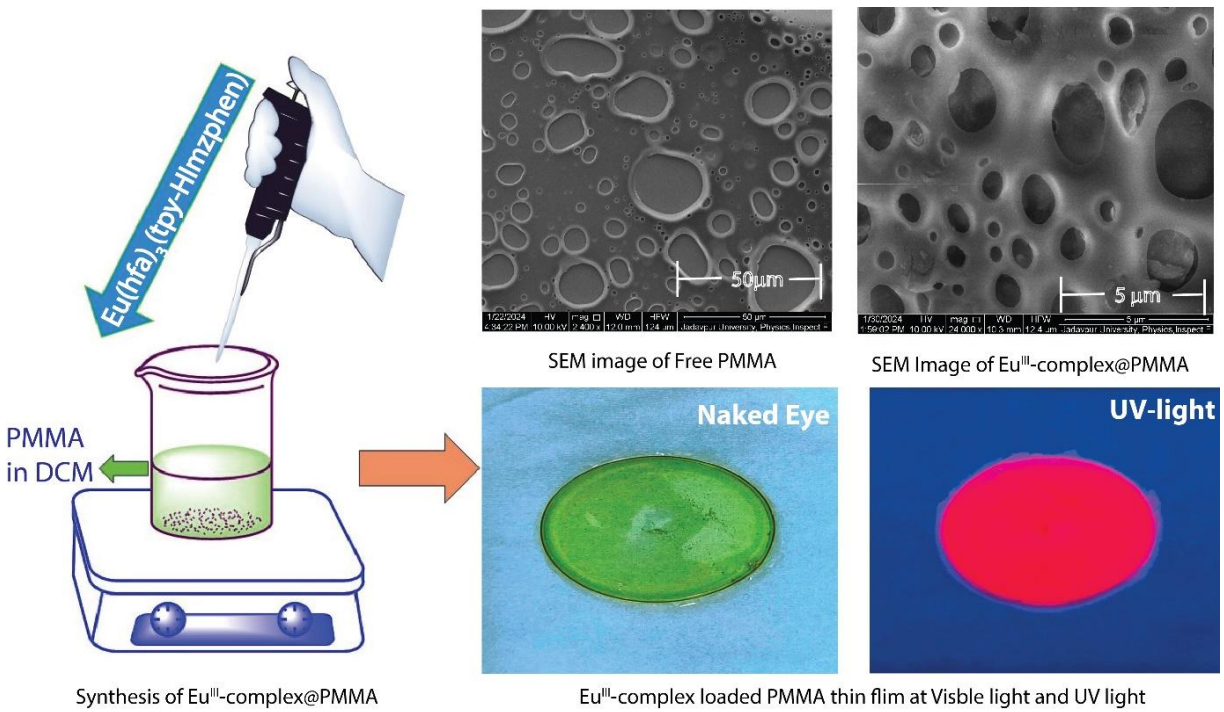

Figure 4.22. Schematic representation for fabrication of the thin hybrid film of PMMA composed of $Eu(hfa)_3$(tpy-HImzphen) (**2**) (**2@PMMA**). The upper right portion reveals the SEM images for the free PMMA as well as **2@PMMA**. The lower right portion shows the film under daylight (straw yellow) and UV light (deep red).

Upon successful incorporation of the Eu(III) complex in PMMA, we first acquired both steady-state and time-resolved emission spectra of the said four polymer films and presented them in Figure 4.23. It is of interest to note that the ligand-centered emission peak

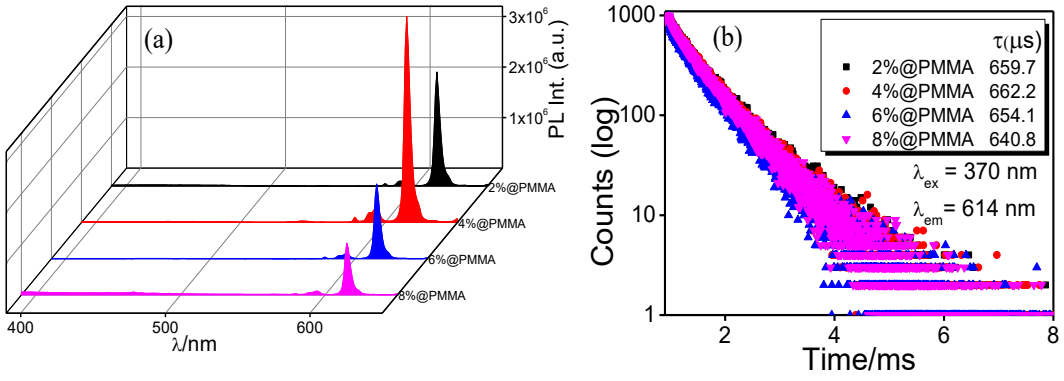

Figure 4.23. Photoluminescence spectra upon excitation at λ_{ex}=330 nm (a) and lifetime decay plot monitored at λ_{em}=614 nm (b) of $Eu(hfa)_3$(tpy-HImzphen) (**2**) embedded as 2%, 4%, 6%, and 8% (w/w) in PMMA at RT.

at ~445 nm completely disappeared from all four composites. We surmise that a rigid atmosphere around the Eu^{III} ion efficiently restricts the non-radiative deactivation channels. The emission intensity as well as the lifetime monitored at 614 nm is found to be maximum for 4% embedded film which is denoted as 4% **2@PMMA** as shown in Figures 4.23a and 4.23b. We further checked the photostability of 4% film by monitoring the emission intensity for up to 6h. No significant fall in the intensity is observed during the said time span (Figure 4.24).

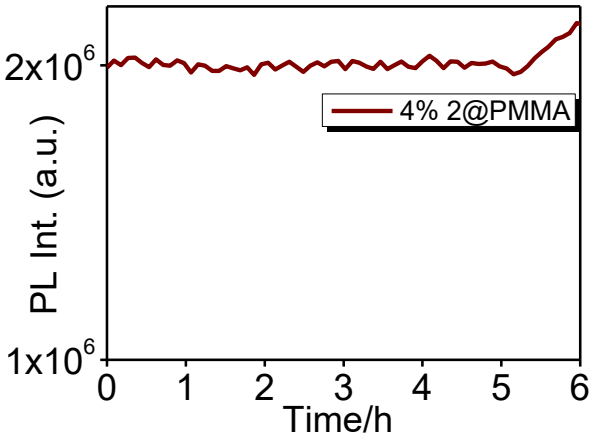

Figure 4.24. Changes in photoluminescence intensity of 4% **2**@PMMA with time at rt.

Interestingly, upon embedding the complex onto the PMMA matrix, the intrinsic quantum yield improved dramatically from 32% to 52%, which in turn indicates that the non-radiative deactivation channels get restricted upon rigidification. The relevant values are tabulated in Table 4.7.

Table 4.7. Lifetime (τ_{obs}), Radiative (k_r) and Non-radiative Rate Constants (k_{nr}), Intrinsic Quantum Yield (Φ_{ff}), Relative Quantum Yield (Φ_{rel}) and Energy Transfer Efficiency (η_{sens}) of the Eu^{III}-complex (2) in PMMA Film

τ_{obs} (μs)	τ_r (μs)	k_r (s^{-1})	k_{nr} (s^{-1})	Φ_{ff} (%)
662.2	1300	759.6	680	52

4.3.14. Thermosensing Behavior of Eu(III) Complex in PMMA Film. After verifying the existence of luminescence properties of the complex on PMMA matrix, we further tend to investigate whether this thin film can sustain its thermosensing ability. So, we recorded the photoluminescence behaviour of 4% **2@PMMA** film upon varying temperature from 273 K to 343 K. Just like the responses in solution state, here also we observed a systematic diminution in the Eu^{III}-centered emission intensities, especially of the peak at 614 nm associated to $^5D_0 \rightarrow {}^7F_2$ transition as well as lifetimes (722.14 μs at 273 K to 633.41 μs at 333 K) monitored at that wavelength (Figure 4.25).

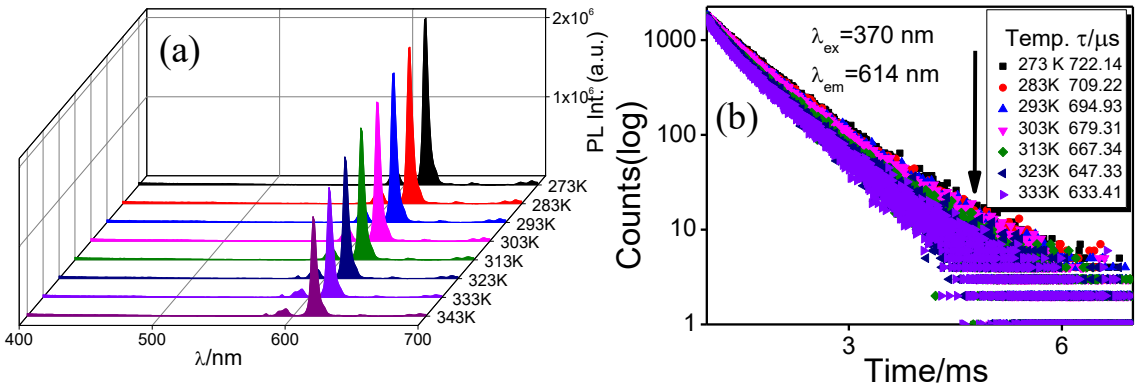

Figure 4.25. Change in photoluminescence spectrum (a) and lifetime decay plot (b) of 4% **2@PMMA** upon varying temperature.

We have also determined the thermosensing efficiency through the use of equations 4.1, 4.3, and 4.4. The relationship between the thermometric ratio Δ $\{I_{ED}(T)/\tau(T)\}$ and T is found to be well-fitted by the following polynomial equation (equation 4.5).

$$\Delta = -6597.8\times T^2 + 3\times 10^6 \times T - 7\times 10^6 \qquad (R^2 = 0.9941) \qquad ..(4.5)$$

The change in the thermometric parameter Δ as a function of temperature is depicted in Figure 4.26.

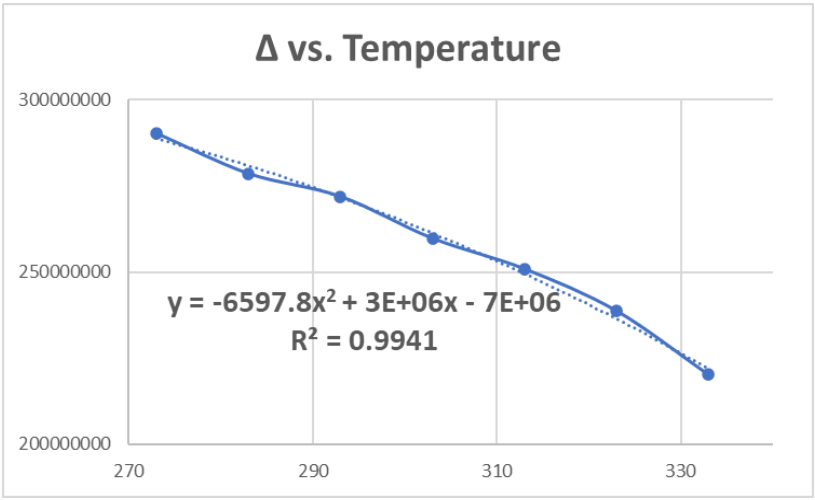

Figure 4.26. Change in Δ $\{I_{ED}(T)/\tau(T)\}$ of 4% **2**@PMMA upon variation of temperature. The dotted line represents the best-fitted curve.

We found that the relative temperature sensitivity (S_r) ranges from 2.06 to 2.84 % K^{-1} (S_m= 2.84 % K^{-1} at T_m=333 K) and the temperature resolution (δT) is 0.0014 K, which is well below the benchmark value of 1 K. Again, as per our literature survey, we hardly found any better value of those thermometric parameters in earlier reported cases regarding hybrid thin film doped with Ln^{III} containing discrete molecules effective in physiological temperature domain (Table 4.8).[39,74-78,80] Hence, the present Eu(III) complex (**2**), by virtue of its desirable photoluminescence and thermosensing characteristics, could be a suitable candidate for practical applications.

Table 4.8. Comparison of the Thermosensing Efficiency of Some Previously Reported Lanthanide Complexes Embedded in a Polymer Matrix

Complex	Sr (%K^{-1})	Polymer Matrix	Parameter	Temperature range	Ref.
$Eu(DBM)_3Phen$	1.75	PMMA	Intensity ratio	50-318	39
$Eu(tta)_3(DEADIT)$	1.3	PMAN	Lifetime	274–323	75
$Eu(tta)_3$	0.7	PS-A	Lifetime	273–363	76
$Eu(DTP)_3$	1.2	3C-PU	Lifetime	283–323	77
Eu-tris(dinaphthoylmethane)-bis-(trioctylphosphine oxide)	2.2	NPs	Lifetime	298-318	78
$Eu(tta)_3(dpbt)$	0.94	PVMK	Quantum Yield	274–339	80

4.3.15. Interpretation of Dissimilar Luminescence Characteristics in the Complexes. In order to induce the antenna effect appropriately operative in Ln^{III}-based complexes via the 'Dexter exchange' pathway[81], it is postulated that the triplet energy level (T_1) of the ligand should be ~2500-4000 cm^{-1} higher than that of the lowest emissive state of Ln^{III} (Ln*).[82] On the other hand, if the energy gap between the T_1 and Ln* happens to be <1800 cm^{-1}, reverse or back energy transfer to the ligand occurs instead of lanthanide sensitization.[27] Now, the lowest-lying emitting excited level of Eu^{III} ($^5D_0$), Sm^{III} ($^4G_{5/2}$), and Tb^{III} ($^5D_4$) in the present study is located at ~17300[83], ~17900[84], and ~20500[85] cm^{-1}, respectively, while the T_1 state of the ancillary ligand tpy-HImzphen is at ~20534 cm^{-1}, as determined from 77K emission spectrum of its Gd^{III}-analogue[29].

Herein, only the ligand-centered emission as well as lifetime is detected for La(III) complex (**1**) as expected. The observation related to Eu(III) complex (**2**) is interesting. In our previously reported tta analogues,[29] we found that cumulative energy transfer (both from tta and tpy-HImzphen) to Eu^{III} was not up to the mark as anticipated on the basis of the suitable $T_1 \rightarrow Ln^*$ energy gap where the T_1 level of tta is situated at ~21000 cm^{-1}. In the present study, the T_1 level of hfa resides at ~22000 cm^{-1},[86] and consequently, the extent of energy transfer (η_{sens}) to Eu^{III} is found to be substantially improved, in fact, almost complete (~95%). Hence, just by replacing the antenna ligand from tta to hfa, a huge modulation of intercomponent energy transfer is achieved in the respective Eu^{III} complex, which is also mirrored in its photoluminescence spectral behavior. Additionally, diminution of Eu^{III}-centered emission intensity and lifetime upon temperature rise can be attributed to the involvement of the low-lying LMCT state which is not very unusual in such Eu^{III}-complexes as the reduction potential for Eu^{III}/Eu^{II} couple is very low (-0.35 V).[20,55,82,87-90] On the other hand, a systematic increase in the ligand-centered emission peak at ~465 nm upon the rise in temperature may be ascribed to LMCT-state mediated back-energy transfer to S_1 state of tpy-HImzphen.[89] Complex **3** exhibits very low relative emission intensity and lifetime associated with the Sm^{III}-centered electric dipole peak at ~646 nm. This very poor extent of energy transfer is probably because of the low-lying LMCT state as well as multi-phonon deactivation as mentioned in some previous literature.[82,91] Lastly, in case of complex **4**, since the T_1-Tb* energy gap is only ~34 cm^{-1}, reverse or back energy transfer to tpy-HImzphen is the predominant path which is also reflected in its lifetime. Thus, the energetic positions of T_1 states for both hfa and tpy-HImzphen are responsible for the distinctive luminescence responses from four Ln^{III} complexes. A tentative energy level diagram is also proposed below

(Scheme 4.3) to decipher the divergence in luminescence characteristics among the four lanthanide(III) tris-hfa complexes.

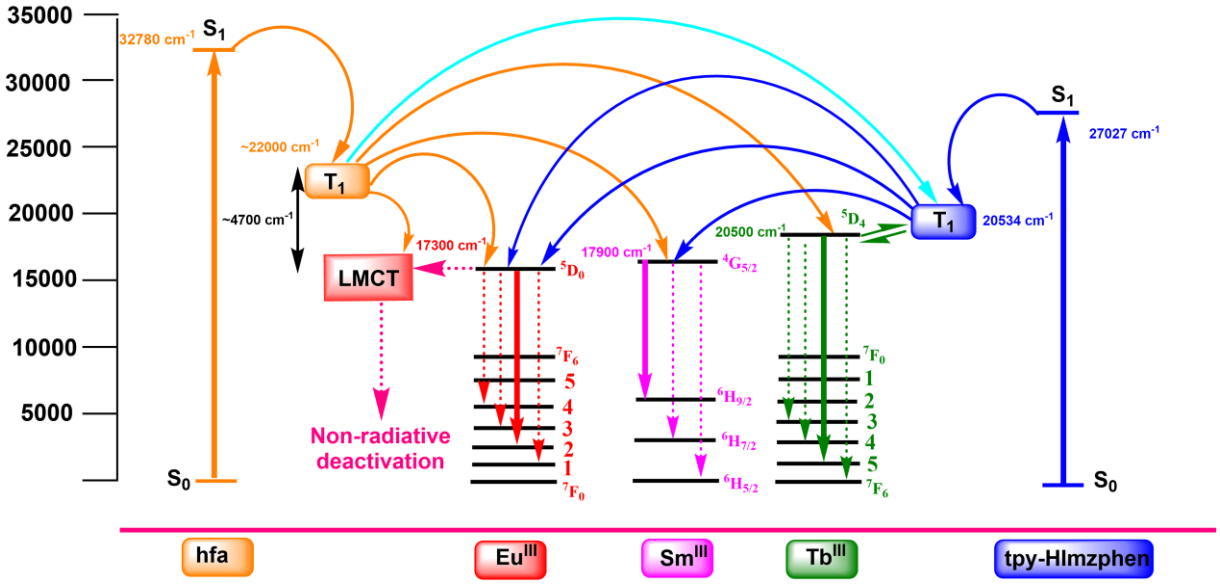

Scheme 4.3. Tentative energy transfer mechanism operating in the Ln^{III}-complexes. The other excited states for Eu^{III} ($^5D_1$~19000 cm^{-1}) and Sm^{III} ($^4G_{7/2}$ ~20000 cm^{-1} and $^4F_{3/2}$ ~18700 cm^{-1}) are omitted for simplification.

4.4. Conclusion

Synthesis, thorough characterization and detailed investigations on the photophysical and in particular the luminescence behaviors of a new array of four ternary lanthanide (III) tris-hexafluoroacetylacetonate complexes have been undertaken in this work. The comprehensive photophysical behaviors of all four complexes are investigated by means of absorption and both steady-state and time-resolved emission spectroscopic techniques. Interestingly, the incorporation of terpyridyl-imidazole-based ligand leads to bathochromic shift of the absorption window in the complexes into the visible domain, which is in contrary to most of the reported Ln^{III}-based complexes that display their absorption window within the UV region. Detailed luminescence measurements conducted at both RT and 77 K, elucidate the deactivation dynamics in the complexes as well as their dissimilar luminescence responses, viz., almost complete ligand-to-metal energy transfer in Eu^{III}, very little energy transfer for Sm^{III}, while back energy transfer in case of Tb^{III}.

Additionally, Eu(III) complex exhibits excellent thermosensing capability in both solution state as well as in a hybrid thin film of PMMA, which highlights its probable

practical utility. Interestingly, upon increase in temperature, the Eu(III)-centered emission is found to decrease gradually and at its expense the ligand-centered emission increases systematically and this sort of dual-monitoring of thermosensing efficacy of the lanthanide complexes is unprecedented in the literature. Furthermore, by virtue of its dual emissive nature, the Eu^{III}-complex becomes a blue-emitter at 273K, while cyan-emitter at 353K. The thermosensitive luminescence response of the Eu^{III}-complex has also been utilized to mimic Set-Reset Flip-flop logic operation. We evaluated thermosensing efficacy of Eu(III) complex by proposing a new thermometric parameter (Δ), defined by the ratio of emission intensity and lifetime at a particular wavelength and the estimated values of relative thermal sensitivity (S_r) and temperature resolution (δT) are found to be superior over the earlier reported Ln^{III}-based discrete thermosensors that operate in physiological temperature domain.

4.5. References

1. Binnemans, K. Lanthanide-based Luminescent Hybrid Materials. *Chem. Rev.* **2009**, *109*, 4283–4374.
2. Armelao, L.; Quici, S.; Barigelletti, F.; Accorsi, G.; Bottaro, G.; Cavazzini, M.; Tondello, E. Design of Luminescent Lanthanide Complexes: From Molecules to Highly Efficient Photo-Emitting Materials. *Coord. Chem. Rev.* **2010**, *254*, 487–505.
3. Feng, J.; Zhang, H. Hybrid Materials Based on Lanthanide Organic Complexes: A Review. *Chem. Soc. Rev.* **2013**, *42*, 387–410.
4. Wei, C.; Ma, L.; Wei, H.; Liu, Z.; Bian, Z.; Huang, C. Advances in Luminescent Lanthanide Complexes and Applications. *Sci. China Technol. Sci.* **2018**, *61*, 1265–1285.
5. Li, P.; Li, H. Recent Progress in the Lanthanide-Complexes Based Luminescent Hybrid Materials. *Coord. Chem. Rev.* **2021**, *441*, 213988–214004.
6. Chakraborty, A.; Ahmed, N.; Ali, J.; Moorthy, S.; Goura, J.; Singh, S. K.; Rogez, G.; Chandrasekhar, V. Exchange-Driven Slow Relaxation of Magnetization in $Ni^{II}_2Ln^{III}_2$ (Ln^{III} = Y, Gd, Tb and Dy) Butterfly Complexes: Experimental and Theoretical Studies. *Dalton Trans.* **2022**, *51*, 14721–14733.
7. Hasegawa, Y.; Wada, Y.; Yanagida, S. Strategies for the Design of Luminescent Lanthanide(III) Complexes and Their Photonic Applications. *J. Photochem. Photobiol., C* **2004**, *5*, 183–202.

8. Bünzli, J.-C. G. On the Design of Highly Luminescent Lanthanide Complexes. *Coord. Chem. Rev.* **2015**, *293*, 19–47.
9. Parker, D.; Fradgley, J. D.; Wong, K.-L. The Design of Responsive Luminescent Lanthanide Probes and Sensors. *Chem. Soc. Rev.* **2021**, *50*, 8193–8213.
10. Montgomery, C. P.; Murray, B. S.; New, E. J.; Pal, R.; Parker, D. Cell-Penetrating Metal Complex Optical Probes: Targeted and Responsive Systems Based on Lanthanide Luminescence. *Acc. Chem. Res.* **2009**, *42*, 925–937.
11. Nehra, K.; Dalal, A.; Hooda, A.; Bhagwan, S.; Saini, R. K.; Mari, B.; Kumar, S.; Singh, D. Lanthanides β-Diketonate Complexes as Energy-Efficient Emissive Materials: A Review. *J. Mol. Struct.* **2022**, *1249*, 131531–131555.
12. Fratini, A.; Richards, G.; Larder, E.; Swavey, S. Neodymium, Gadolinium, and Terbium Complexes Containing Hexafluoroacetylacetonate and 2, 2'-Bipyrimidine: Structural and Spectroscopic Characterization. *Inorg. Chem.* **2008**, *47*, 1030–1036.
13. De Silva, C. R., Maeyer, J. R., Dawson, A.; Zheng, Z. Adducts of Lanthanide β-Diketonates with 2,4,6-Tri(2-pyridyl)-1,3,5-Triazine: Synthesis, Structural Characterization, and Photoluminescence Studies. *Polyhedron*, **2007**, *26*, 1229–1238.
14. Fu, L.-M.; Wen, X.-F.; Ai, X.-C.; Sun, Y.; Wu, Y.-S.; Zhang, J.-P.; Wang, Y. Efficient Two-Photon-Sensitized Luminescence of A Europium(III) Complex. *Angew. Chem. Int. Ed.* **2005**, *44*, 747–750.
15. Gangan, T. U.; Sreenadh, S.; Reddy, M. L. P. Visible-Light Excitable Highly Luminescent Molecular Plastic Materials Derived from Eu^{3+}-Biphenyl Based β-Diketonate Ternary Complex and Poly(Methylmethacrylate). *J. Photochem. Photobiol., A* **2016**, *328*, 171–181.
16. Shi, J.; Hou, Y.; Chu, W.; Shi, X.; Gu, H.; Wang, B.; Sun, Z. Crystal Structure and Highly Luminescent Properties Studies of Bis-β-Diketonate Lanthanide Complexes. *Inorg. Chem.* **2013**, *52*, 5013–5022.
17. Bag, P.; Chakraborty, A.; Rouzières, M.; Clérac, R.; Butcher, R. J.; Chandrasekhar, V. Oxalato–Bridged Neutral Octanuclear Heterometallic Complexes $[Ln_4K_4(L)_4(\mu\text{-}H_2O)_4(NO_3)_2(\mu\text{-Ox})]$(Ln=Dy(III), Gd(III), Tb(III), Ho(III); LH_3=N[CH_2CH_2N=CH-C_6H_3-2–OH–3–OMe]$_3$; Ox=$(C_2O_4)^{2-}$): Synthesis, Structure, Magnetic and Luminescent Properties. *Cryst. Growth Des*. **2014**, *14*, 4583−4592.
18. Eliseeva, S. V.; Pleshkov, D. N.; Lyssenko, K. A.; Lepnev, L. S.; Bünzli, J.-C. G.; Kuzmina, N. P.; Deciphering Three Beneficial Effects of 2,2'-Bipyridine-N,N'-

Dioxide on the Luminescence Sensitization of Lanthanide(III) Hexafluoroacetylacetonate Ternary Complexes. *Inorg. Chem.* **2011**, *50*, 5137–5144.

19. Ahmed, Z.; Iftikhar, K. Efficient Layers of Emitting Ternary Lanthanide Complexes for Fabricating Red, Green, and Yellow OLEDs. *Inorg. Chem.* **2015**, *54*, 11209–11225.
20. Kitagawa, Y.; Kumagai, M.; Nakanishi, T.; Fushimi, K.; Hasegawa, Y. The Role of π–f Orbital Interactions in Eu(III) Complexes for an Effective Molecular Luminescent Thermometer. *Inorg. Chem.* **2020**, *59*, 5865–5871.
21. Moudam, O.; Rowan, B. C.; Alamiry, M.; Richardson, P.; Richards, B. S.; Jones, A. C.; Robertson, N. Europium Complexes with High Total Photoluminescence Quantum Yields in Solution and in PMMA. *Chem. Commun.* **2009**, *43*, 6649–6651.
22. Khistiaeva, V. V.; Melnikov, A. S.; Slavova, S. O.; Sizov, V. V.; Starova, G. L.; Koshevoy, I. O.; Grachova, E. V. Heteroleptic β-diketonate Ln(III) Complexes Decorated with Pyridyl Substituted Pyridazine Ligands: Synthesis, Structure and Luminescence Properties. *Inorg. Chem. Front.* **2018**, *5*, 3015–3027.
23. Al Sabea, H.; Hamon, N.; Galangau, O.; Norel, L.; Maury, O.; Riobé, F.; Tripier, R.; Rigaut, S. Efficient Luminescence Control in Dithienylethene Functionalized Cyclen Macrocyclic Lanthanide Complexes. *Inorg. Chem. Front.* **2020**, *7*, 2979–2989.
24. Armelao, L.; Dell'Amico, D. B.; Bellucci, L.; Bottaro, G.; Di Bari, L.; Labella, L.; Marchetti, F.; Samaritani, S.; Zinna, F. Circularly Polarized Luminescence of Silica-Grafted Europium Chiral Derivatives Prepared through a Sequential Functionalization. *Inorg. Chem.* **2017**, *56*, 7010–7018.
25. Andreiadis, E. S.; Gauthier, N.; Imbert, D.; Demadrille, R.; Pecaut, J.; Mazzanti, M. Lanthanide Complexes Based on β-Diketonates and A Tetradentate Chromophore Highly Luminescent as Powders and in Polymers. *Inorg. Chem.* **2013**, *52*, 14382–14390.
26. Stanley, J. M.; Zhu, X.; Yang, X.; Holliday, B. J. Europium Complexes of A Novel Ethylenedioxythiophene-Derivatized Bis(pyrazolyl)pyridine Ligand Exhibiting Efficient Lanthanide Sensitization. *Inorg. Chem.* **2010**, *49*, 2035–2037.
27. Latva, M.; Takalo, H.; Mukkala, V. M.; Matachescu, C.; Rodríguez-Ubis, J. C.; Kankare, J. Correlation Between the Lowest Triplet State Energy Level of the Ligand and Lanthanide(III) Luminescence Quantum Yield. *J. Lumin.* **1997**, *75*, 149–169.

28. Samuel, A. P.; Xu, J.; Raymond, K. N. Predicting Efficient Antenna Ligands for Tb(III) Emission. *Inorg. Chem.* **2009**, *48*, 687–698.
29. Ahmed, T.; Chakraborty, A.; Paul, A.; Baitalik, S. Synthesis, Characterization, Luminescence Properties and Deciphering the Role of Terpyridyl-Imidazole Based Ligand on Dissimilar Luminescence Sensitization of Ternary Lanthanide(III) Tris-(β-Diketonate) Complexes. *Dalton Trans*. **2023**, *52*, 14027–14038.
30. Maity, D.; Das, S.; Mardanya, S.; Baitalik, S. Synthesis, Structural Characterization, and Photophysical, Spectroelectrochemical, and Anion-Sensing Studies of Heteroleptic Ruthenium(II) Complexes Derived from 4′-Polyaromatic-Substituted Terpyridine Derivatives and 2,6-Bis(benzimidazole-2-yl)pyridine. *Inorg. Chem.* **2013**, *52*, 6820–6838.
31. Paul, A.; Bar, M.; Ahmed, T.; Baitalik, S. Anion-Sensitive Photophysics of Luminescent Trimetallic Complexes of Fe(II), Ru(II), and Os(II) with Polarized NH Motifs. *Polyhedron*, **2020**, *190*, 114772.
32. Deb, S.; Sahoo, A.; Ahmed, T.; Baitalik, S. Stimuli–Responsive Molecular Switches and Logic Devices Based on Ru(II)-Terpyridyl-Imidazole Coordination Motif. *J. Phys. Chem. B* **2021**, *125*, 8919–8931.
33. Zaïm, A.; Nozary, H.; Guénée, L.; Besnard, C.; Lemonnier, J. F.; Petoud, S.; Piguet, C. N-Heterocyclic Tridentate Aromatic Ligands Bound to [Ln(hexafluoroacetylacetonate)$_3$] Units: Thermodynamic, Structural, and Luminescent Properties. *Chem. Eur. J.* **2012**, *18*, 7155–7168.
34. Zaïm, A.; Favera, D. N.; Guénée, L. Nozary, H.; Hoang, T. N. Y.; Eliseeva, S. V.; Petoud, S.; Piguet, C. Lanthanide Hexafluoroacetylacetonates vs. Nitrates for the Controlled Loading of Luminescent Polynuclear Single-Stranded Oligomers. *Chem. Sci*. **2013**, *4*, 1125–1136.
35. Fioravanti, L.; Bellucci, L.; Armelao, L.; Bottaro, G.; Marchetti, F.; Pineider, F.; Poneti, G.; Samaritani, S.; Labella, L. Stoichiometrically Controlled Assembly of Lanthanide Molecular Complexes of the Heteroditopic Divergent Ligand 4′-(4-Pyridyl)-2, 2′: 6′, 2 ″-terpyridine N-Oxide in Hypodentate or Bridging Coordination Modes. Structural, Magnetic, and Photoluminescence Studies. *Inorg. Chem.* **2021**, *61*, 265–278.

36. Zhang, Z.; He, L.; Feng, J.; Liu, X.; Zhou, L.; Zhang, H. Unveiling the Relationship Between Energy Transfer and the Triplet Energy Level by Tuning Diarylethene within Europium(III) Complexes. *Inorg. Chem.* **2019**, *59*, 661–668.
37. Kovalenko, A.; Rublev, P. O.; Tcelykh, L. O.; Goloveshkin, A. S.; Lepnev, L. S.; Burlov, A. S. A.; Vashchenko, A.; Marciniak, L.; Magerramov, A. M.; Shikhaliyev, N. G.; Vatsadze, S. Z. V.; Utochnikova, V. Lanthanide Complexes With 2-(Tosylamino)-Benzylidene- N-(Aryloyl)Hydrazones - Universal Luminescent Materials. *Chem. Mater.* **2019**, *31*, 759–773.
38. Feng, T.; Ye, Y.; Liu, X.; Cui, H.; Li, Z.; Zhang, Y.; Liang, B.; Li, H.; Chen, B. A Robust Mixed Lanthanide PolyMOF Membrane for Ratiometric Temperature Sensing. *Angew. Chem. Int. Ed.* **2020**, *59*, 21752–21757.
39. Shahi, P. K.; Singh, A. K.; Rai, S. B.; Ullrich, B. Lanthanide Complexes for Temperature Sensing, UV Light Detection, and Laser Applications. *Sens. Actuators, A* **2015**, *222*, 255–261.
40. Lapaev, D. V.; Nikiforov, V. G.; Lobkov, V. S.; Knyazev, A. A.; Ziyatdinova, R. M.; Galyametdinov, Y. G. A Vitrified Film of an Anisometric Europium(III) β–Diketonate Complex with a Low Melting Point as a Reusable Luminescent Temperature Probe with Excellent Sensitivity in the Range of 270-370 K. *J. Mater. Chem. C* **2020**, *8*, 6273–6280.
41. Bussche, V. F.; Kaczmarek, A. M., Speybroeck, V. V.; Voort, V. D. P.; Stevens, C. V. Overview of N-Rich Antennae Investigated in Lanthanide-Based Temperature Sensing. *Chem. Eur. J.* **2021**, *27*, 7214–7230.
42. Brites, C. D. S.; Balabhadra, S.; Carlos, L. D. Lanthanide-Based Thermometers: At the Cutting-Edge of Luminescence Thermometry. *Adv. Opt. Mater*. **2019**, *7*, 1801239–69.
43. Miyata, K.; Konno, Y.; Nakanishi, T.; Kobayashi, A.; Kato, M.; Fushimi, K.; Hasegawa, Y. Chameleon Luminophore for Sensing Temperatures: Control of Metal-to-Metal and Energy Back Transfer in Lanthanide Coordination Polymers. *Angew. Chem. Int. Ed*. **2013**, *52*, 6413–6416.
44. Cui, Y.; Zou, W.; Song, R.; Yu, J.; Zhang, W.; Yang, Y.; Qian, G. A Ratiometric and Colorimetric Luminescent Thermometer Over a Wide Temperature Range Based on a Lanthanide Coordination Polymer. *Chem. Commun.* **2014**, *50*, 719–721.

45. Cadiau, A.; Brites, C. D. S.; Costa, P. M.; Ferreira, R. A.; Rocha, J.; Carlos, L. D. Ratiometric Nanothermometer Based on an Emissive Ln^{3+}-Organic Framework. *ACS nano*, **2013**, *7*, 7213–7218.
46. Zhao, S. N.; Li, L. J.; Song, X. Z.; Zhu, M.; Hao, Z. M.; Meng, X.; Wu, L. L.; Feng, J.; Song, S. Y.; Wang, C.; Zhang, H. J. Lanthanide Ion Codoped Emitters for Tailoring Emission Trajectory and Temperature Sensing. *Adv. Funct. Mater.* **2015**, *25*, 1463–1469.
47. Shahi, P. K.; Singh, A. K.; Singh, S. K.; Rai, S. B.; Ullrich, B. Revelation of the Technological Versatility of the $Eu(tta)_3phen$ Complex by Demonstrating Energy Harvesting, Ultraviolet Light Detection, Temperature Sensing, and Laser Applications, *ACS Appl. Mater. Interfaces* **2015**, *7*, 18231−18239.
48. Devi, R.; Singh, K.; Vaidyanathan, S. Synergy in the Energy Transfer Between Ligands and Eu^{III} Ions in Molecular Europium Complexes: Single-Component White Light-Emitting Luminogens. *J. Mater. Chem. C* **2020**, *8*, 8643–8653.
49. Lahoud, M. G.; Frem, R. C. G.; Gálico, D. A.; Bannach, G.; Nolasco, M. M.; Ferreira, R. A. S.; Carlos, L. D. Intriguing Light-Emission Features of a Ketoprofen-Based Eu(III) Adduct due to Strong Electron–Phonon Coupling. *J. Lumin*. **2016**, *170*, 357–363.
50. Gálico, D. A.; Mazali, I. O.; Sigoli, F. A. Nanothermometer Based on Intensity Variation and Emission Lifetime of Europium(III) Benzoylacetonate Complex. *J. Lumin.* **2017**, *192*, 224–230.
51. Lapaev, D. V.; Nikiforov, V. G.; Lobkov, V. S.; Knyazev, A. A.; Galyametdinov, Y. G. Reusable Temperature-Sensitive Luminescent Material Based on Vitrified Film of Europium(III) β-Diketonate Complex. *Opt. Mater.* **2018**, *75*, 787–795.
52. Cabral, F. M.; Gálico, D. A.; Mazali, I. O.; Sigoli, F. A. Crystal Structure and Temperature Dependence of the Photophysical Properties of the $[Eu(tta)_3(pyphen)]$ Complex. *Inorg. Chem. Commun.* **2018**, *98*, 29–33.
53. Lyubov, D. M.; Neto, A. N. C.; Fayoumi, A.; Lyssenko, K. A.; Korshunov, V. M.; Taydakov, I. V.; Salles, F.; Guari, Y.; Larionova, J.; Carlos, L. D.; Long, J.; Trifonov, A. A. Employing Three–Blade Propeller Lanthanide Complexes as Molecular Luminescent Thermometers: Study of Temperature Sensing Through a Concerted Experimental/Theory Approach. *J. Mater. Chem. C* **2022**, *10*, 7176–7188.

54. Bellucci, L.; Bottaro, G.; Labella, L.; Causin, V.; Marchetti, F.; Samaritani, S.; Dell'Amico, D. B.; Armelao, L. Composition–Thermometric Properties Correlations in Homodinuclear Eu^{3+} Luminescent Complexes. *Inorg. Chem.* **2020**, *59*, 18156–18167.
55. Ahmed, T.; Chakraborty, A.; Maity, S.; Baitalik, S. A Terpyridyl–Imidazole Based Europium Tris-(β-Diketonate) Complex as Efficient Molecular Luminescent Thermometer and Single Component White Light Emitter via Synergy in Energy Transfer between Ligand and Eu^{3+}. *Dalton Trans*. **2024**, 53, 3065–3074.
56. Sahoo, A.; Bhattacharya, S.; Jana, S.; Baitalik, S. Neural Network and Decision Tree-Based Machine Learning Tools to Analyse the Anion-Responsive Behaviours of Emissive Ru(II)-Terpyridine Complexes. *Dalton Trans*. **2023**, *52*, 97–108.
57. Sahoo, A.; Ahmed, T.; Deb, S.; Baitalik, S. Neuro-Fuzzification Architecture for Modelling of Electrochemical Ion-Sensing Data of Imidazole-Dicarboxylate-Based Ru(II)-Bipyridine Complex. *Inorg Chem*. **2022**, *61*, 10242–10254.
58. Constable, E. C.; Ward, M. D.; Corr, S. A Convenient, High Yield Synthesis of 2, 2′: 6′, 2 ″-Terpyridine and Its Iron(II) Complex. *Inorg. Chim. Acta*, **1988**, *141*, 201–203.
59. Bhaumik, C.; Maity, D.; Das, S.; Baitalik, S. Synthesis, Structural Characterization, Solvatochromism, and Ion-Binding Studies of a Ditopic Receptor Based on 2-(4-[2,2′:6′,2″]terpyridin-4′-yl-phenyl)-1H-phenanthro[9,10-d]Imidazole (tpy-HImzphen) Unit. *RSC Adv.* **2012**, *2*, 2581–2594.
60. Halverson, F.; Brinen, J. S.; Leto, J. R. Luminescence of Europium Hexafluoroacetylacetonate. *J. Chem. Phys.* **1964**, *40*, 2790–2792.
61. Richardson, M. F.; Wagner, W. F.; Sands, D. E. Rare-earth Trishexafluoroacetylacetonates and Related Compounds. *J. Inorg. Nucl. Chem.* **1968**, *30*, 1275–1289.
62. Lannes, A.; Intissar, M.; Suffren, Y.; Reber, C.; Luneau, D. Terbium(III) and Yttrium(III) Complexes with Pyridine-Substituted Nitronyl Nitroxide Radical and Different β-Diketonate Ligands. Crystal Structures and Magnetic and Luminescence Properties. *Inorg. Chem.* **2014**, *53*, 9548–9560.
63. De Silva, C. R.; Wang, R.; Zheng, Z. Highly Luminescent Eu(III) Complexes with 2,4,6-Tri(2-pyridyl)-1,3,5-triazine Ligand: Synthesis, Structural Characterization, and Photoluminescence Studies. *Polyhedron* **2006**, *25*, 3449–3455.

64. Rajamouli, B.; Viswanath, C. S. D; Giri, S.; Jayasankar, C. K.; Sivakumar, V. Carbazole Functionalized New Bipolar Ligand for Monochromatic Red Light Emitting Europium(III) Complex: Combined Experimental and Theoretical Study. *New J. Chem.* **2017**, 41, 3112–3123.
65. Andres, J.; Chauvin, A. S. 6-Phosphoryl Picolinic Acids as Europium and Terbium Sensitizers. *Inorg. Chem.* **2011**, *50*, 10082–10090.
66. Ilmi, R.; Khan, M. S.; Li, Z.; Zhou, L.; Wong, W. Y.; Marken, F.; Raithby, P. R. Utilization of Ternary Europium Complex for Organic Electroluminescent Devices and as a Sensitizer to Improve Electroluminescence of Red-Emitting Iridium Complex. *Inorg. Chem.* **2019**, *58*, 8316–8331.
67. Raj, D. A.; Francis, B.; Reddy, M. L. P.; Butorac, R. R.; Lynch, V. M.; Cowley, A. H. Highly Luminescent Poly(Methyl Methacrylate)-Incorporated Europium Complex Supported by a Carbazole-Based Fluorinated β-Diketonate Ligand and A 4,5-Bis(Diphenylphosphino)-9,9-Dimethylxanthene Oxide Co-Ligand. *Inorg. Chem.* **2010**, *49*, 9055–9063.
68. Freund, C.; Porzio, W.; Giovanella, U.; Vignali, F.; Pasini, M.; Destri, S.; Mech, A.; Di Pietro, S.; Di Bari, L.; Mineo, P. Thiophene Based Europium β-Diketonate Complexes: Effect of the Ligand Structure on the Emission Quantum Yield. *Inorg. Chem.* **2011**, *50*, 5417–5429.
69. Liu, D.; Zhou, Y. N.; Zhao, J.; Xu, Y.; Shen, J.; Wu, M. An Intensive Green Emitting Terbium Complex Using a Newly Designed Aromatic Hyperbranched Polyester as an Efficient Antenna Ligand. *J. Mater. Chem. C* **2017**, *5*, 11620–11630.
70. Lo, W. S.; Zhang, J.; Wong, W. T.; Law, G. L. Highly Luminescent Sm^{III} Complexes with Intraligand Charge-Transfer Sensitization and the Effect of Solvent Polarity on Their Luminescent Properties. *Inorg. Chem.* **2015**, *54*, 3725–3727.
71. Ahmed, Z.; Iftikhar, K. Red, Orange-Red and Near-Infrared Light Emitting Ternary Lanthanide Tris β-Diketonate Complexes with Distorted C_{4v} Geometrical Structures. *Dalton Trans.* **2019**, *48*, 4973–4986.
72. Chauhan, A.; Langyan, R. Photosensitization in Highly Luminescent Nonmacrocyclic Samarium(III) Complexes for Application in Light-Emitting Systems. *J. Photochem. Photobiol., A* **2022**, *424*, 113627.
73. Kovalenko, A. D.; Bushmarinov, I. S.; Burlov, A. S.; Lepnev, L. S.; Ilina, E. G.; Utochnikova, V. V. The Peculiarities of Complex Formation and Energy Transfer

Processes in Lanthanide Complexes With 2-(Tosylamino)-Benzylidene-N-Benzoylhydrazone. *Dalton Trans.* **2018**, *47*, 4524–4533.

74. Hasegawa, Y.; Kitagawa, Y. Thermo-Sensitive Luminescence of Lanthanide Complexes, Clusters, Coordination Polymers and Metal-Organic Frameworks with Organic Photosensitizers. *J. Mater. Chem. C* **2019**, *7*, 7494–7511.
75. Borisov, S. M.; Klimant, I. Blue LED Excitable Temperature Sensors Based on a New Europium(III) Chelate. *J. Fluoresc.* **2008**, *18*, 581–589.
76. Borisov, S. M.; Klimant, I. New Luminescent Oxygen-Sensing and Temperature-Sensing Materials Based on Gadolinium(III) and Europium(III) Complexes Embedded in an Acridone-Polystyrene Conjugate. *Anal. Bioanal. Chem.* **2012**, *404*, 2797–2806.
77. Ondrus, V.; Meier, R. J.; Klein, C.; Henne, U.; Schäferling, M.; Beifuss, U. Europium 1, 3-Di(thienyl)Propane-1,3-Diones with Outstanding Properties for Temperature Sensing. *Sens. Actuators, A* **2015**, *233*, 434–441.
78. Peng, H.; Stich, M. I.; Yu, J.; Sun, L. N.; Fischer, L. H.; Wolfbeis, O. S. Luminescent Europium(III) Nanoparticles for Sensing and Imaging of Temperature in the Physiological Range. *Adv. Mater.* **2010**, *22*, 716–719.
79. Ananias, D.; Firmino, A. D.; Mendes, R. F.; Paz, F. A. A.; Nolasco, M.; Carlos, L. D.; Rocha, J. Excimer Formation in a Terbium Metal-Organic Framework Assists Luminescence Thermometry. *Chem. Mater.* **2017**, *29*, 9547–9554.
80. Borisov, S. M.; Wolfbeis, O. S. Temperature–Sensitive Europium(III) Probes and Their Use for Simultaneous Luminescent Sensing of Temperature and Oxygen. *Anal. Chem.* **2006**, *78*, 5094–5101.
81. Mara, M. W.; Tatum, D. S.; March, A. M.; Doumy, G.; Moore, E. G.; Raymond, K. N. Energy Transfer from Antenna Ligand to Europium(III) Followed Using Ultrafast Optical and X-Ray Spectroscopy. *J. Am. Chem. Soc.* **2019**, *141*, 11071–11081.
82. Bünzli, J.-C. G.; Eliseeva, S. V. Basics of Lanthanide Photophysics. In Lanthanide Luminescence; Hänninen, P., Härmä, H., Eds.; Springer Series on Fluorescence, Vol. 7; Springer: Berlin, Heidelberg, 2010.
83. De Shazer, L. G.; Dieke, G. H. Spectra and Energy Levels of Eu^{3+} In $LaCl_3$. *J. Chem. Phys.* **1963**, *38*, 2190–2199.

84. Yan, B.; Song, Y. S. Spectroscopic Study on the Photophysical Properties of Lanthanide Complexes with 2,2′-Bipyridine-N,N′-Dioxide. *J. Fluoresc.* **2004**, *14*, 289–294.
85. Horrocks, W. D., Jr.; Albin, M. Lanthanide Ion Luminescence in Coordination Chemistry and Biochemistry. In Progress in Inorganic Chemistry; Lippard, S. J., Ed.; 1984.
86. Dawson, W. R.; Kropp, J. L.; Windsor, M. W. Internal-Energy-Transfer Efficiencies in Eu^{3+} And Tb^{3+} Chelates Using Excitation to Selected Ion Levels. *J. Chem. Phys.* **1966**, *45*, 2410–2418.
87. Berry, M. T.; May, P. S.; Xu, H. Temperature Dependence of the Eu^{3+} $^5D_0$ Lifetime in Europium Tris(2,2,6,6-tetramethyl-3,5-heptanedionato). *J. Phys. Chem.* **1996**, *100*, 9216–9222.
88. Pasatoiu, T. D.; Madalan, A. M.; Kumke, M. U.; Tiseanu C.; Andruh, M. Temperature Switch of LMCT Role: From Quenching to Sensitization of Europium Emission in a Zn^{II}-Eu^{III} Binuclear Complex. *Inorg. Chem.* **2010**, *49*, 2310–2315.
89. Fu, L. M.; Ai, X. C.; Li, M. Y.; Wen, X. F.; Hao, R.; Wu, Y. S.; Wang, Y.; Zhang, J. P. Role of Ligand-To-Metal Charge Transfer State in Nontriplet Photosensitization of Luminescent Europium Complex. *J. Phys. Chem. A* **2010**, *114*, 4494–4500.
90. Vicinelli, V.; Ceroni, P.; Maestri, M.; Balzani, V.; Gorka, M.; Vögtle, F. Luminescent Lanthanide Ions Hosted in a Fluorescent Polylysin Dendrimer. Antenna-Like Sensitization of Visible and Near-Infrared Emission. *J. Am. Chem. Soc.* **2002**, *124*, 6461–6468.
91. Bassett, A. P.; Magennis, S. W.; Glover, P. B.; Lewis, D. J.; Spencer, N.; Parsons, S.; Williams, R. M.; De Cola, L.; Pikramenou, Z. Highly Luminescent, Triple- and Quadruple-Stranded, Dinuclear Eu, Nd, and Sm(III) Lanthanide Complexes Based on Bis–Diketonate Ligands. *J. Am. Chem. Soc.* **2004**, *126*, 9413–9424.

****

Chapter 5

Thermally Activated Delayed Fluorescence-Assisted Thermosensing and Thermochromic Behaviors of Bimetallic Lanthanide(III) Complexes Based on Heteroditopic Phenanthroline-Terpyridine Ancillary Ligand

5.1. Introduction

The design of luminescent trivalent lanthanide coordination complexes has always been attracting researchers of the concerned community. The motivation behind this is to leverage their unique and well-defined luminescence spectral features (atom-like sharp emission and long excited state lifetimes) arising out of the Ln^{III} ions.[1-9] During the course of time, they have shown their supremacy over the traditional luminescent probes in varied applications, viz., fabrication of light-harvesting materials; sensing of temperature, pressure, acid, base, or specific analytes, as well as in medical diagnostics.[8-13] Despite their multipurpose utility, direct excitation of the Ln^{III} ions cannot yield a fruitful emission because of their spin and parity forbidden intra-configurational f-f transitions. To overcome this pitfall, anchoring suitable sensitizers is often needed, which can indirectly sensitize the coordinated Ln^{III} ion by transferring its absorbed energy (antenna effect). Since its inception, numerous efforts have been devoted to design suitable sensitizers for achieving enhanced Ln^{III}-based luminescence. After several years of this quest, fluorinated β-diketonates have been recognized as one of the most popular candidates for lanthanide sensitizers, which in turn pushes the momentum for the design and synthesis of diverse Ln^{III} tris-β-diketonate-based molecular assemblies. Eventually, several modifications have been made to the structures of β-diketonates that can put an impact on the excited energy levels as well as sensitization efficacies in the resulting β-diketonate-based Ln(III)-complexes.[14-16] Despite sincere efforts, the utmost desired luminescence is still to be achieved from Ln^{III} tris-(β-diketonate) moieties as the Ln^{III} ions often coordinate with water or neighboring solvent molecules to fulfill their higher coordination, which in turn invites a detrimental impact on the anticipated enhanced sensitized luminescence.[17] To evade this, Lewis's bases, usually comprised of N- or O-donors and connected to polyaromatic organic chromophores, are brought into play (ancillary ligands).[17-29] These ligands are usually capable of coordinating with Ln^{III} ions by replacing the coordinated water or solvent molecules, resulting in the formation of a new genre of luminescent ternary Ln^{III}-complexes. Now, the structures and the excited state energy levels of both β-diketonate and incoming ancillary ligand govern the sensitization outcomes in terms of both the extent as well as direction of energy transfer. In essence, the cumulative influences of the two types of ligands can induce an additive or a subtractive impact on the overall Ln^{III} sensitization process, which is ultimately governed by the energetic position of their lowest triplet states (T_1).[30-33] Hence, judicious selection of both the antenna and ancillary ligands is the most important factor for designing such luminescent Ln^{III}-based

complexes. Literature survey reveals that majority of the ancillary ligands are composed of a bidentate (bipyridine and/or phenanthroline)-type coordinating motif covalently coupled with polyaromatic and heteroaromatic moieties.[5,20,26-29] On the other hand, reports based on tridentate motifs,[22-24,34-38] especially on terpyridyl-appended ligands,[32,39-41] have been found to be surprisingly very few in spite of their certain favourable structural attributes, leaving room for further exploration. Also, to the best of our knowledge, there is no report wherein a heteroditopic bipyridine-terpyridine type ancillary ligand has been employed for effective lanthanide sensitization.

Luminescent Ln^{III}-based coordination complexes have proven their credibility as molecular luminescent thermometers, which are now being considered superior to traditional thermometers, mostly due to their non-invasive nature and efficacy in the nanoscale domain.[42-48] Accordingly, enormous efforts have now been devoted to the design of efficient Ln^{III}-based luminescent thermosensors.[45-48] While going through the literature, it is noticed that either Ln^{III}-based MOFs[45,47] or coordination polymers[45,48] are mostly employed for this purpose. By contrast, Ln^{III}-based discrete molecules have been far less explored.[45,49-57] Besides, in dealing with luminescence thermometry, alteration of only the Ln^{III}-based luminescence is usually considered, leaving aside the residual ancillary ligand-centered emission. But close scrutiny of the relative intensity of Ln^{III}-based emission and ligand-centered emission, if observed, offers some indications for the occurrence of temperature-assisted metal-to-ligand back energy transfer[31,58] (usually applicable for Tb^{III}-complexes) or low-lying ligand-to-metal-charge-transfer (LMCT)-state mediated back energy transfer to ligand[33,59,60] (often occurs in case of Eu^{III}-complexes). These two phenomena are mostly responsible for the hitherto reported thermosensitive luminescence behaviors of Ln^{III}-complexes.

Thermally-activated delayed fluorescence (TADF) is also a temperature-induced phenomenon. One can also think of achieving the luminescence thermometric prospect by exploiting this TADF event, if possible. Several groups across the globe are now actively engaged in the design of novel TADF-active molecules.[61-63] However, amalgamating the TADF and luminescence thermometry, especially in the domain of Ln^{III}-based discrete molecules, is yet to be explored. TADF usually occurs in two ways, viz. (i) triplet-triplet annihilation (TTA) and (ii) reverse intersystem crossing (RISC). For TTA to happen, the energy value of the lowest singlet state (S_1) of a molecule should be almost double that of its lowest triplet (T_1) state. On the other hand, to have the RISC process operating in a ligand,

several criteria should be fulfilled. Firstly, the energy gap between the S_1 and T_1 states (ΔE_{ST}) of the ligand is expected to be <0.25 eV.[64] To this end, a donor-acceptor (D-A) type molecular architecture should be maintained while designing such a ligand, which further generates a charge transfer (CT) character. This CT character, in turn, reduces the HOMO-LUMO overlap as well as the ΔE_{ST} value in the ligand framework. More specifically, a mixing between CT and local excitation (LE) character is often desired as pure CT character could lead to weak fluorescence. Besides, a potential TADF-active molecule is expected to be highly fluorescent so that sufficient singlet excitons are available after the RISC process. Hence, molecular rigidity is also supposed to be maintained in the ligand, which could lead to the suppression of the non-radiative decay pathways. Appropriately designed polypyridyl ligands could possess all of these prescribed criteria necessary for a molecule to display TADF activity via the RISC pathway.

Hence, our primary objective is to judiciously choose a polypyridyl ligand that holds the prospect of displaying TADF by taking advantage of its high-energy lowest triplet (T_1) state. To this end, we have employed a heteroditopic bridging ligand, phen-Hbzim-tpy=2-[4-(2,6-dipyridin-2-ylpyridin-4-yl)phenyl]-1H-imidazole[4,5-f][1,10]phenanthroline, incorporating both phenanthroline- as well as terpyridine-type coordinating motifs covalently connected via phenyl-imidazole spacer. The said bridging ligand has been utilized here to synthesize a new array of four ternary homobimetallic Ln^{III}-complexes of type, $\{(Ln_2(tta)_6(phen\text{-}Hbzim\text{-}tpy)\}$ where Ln=La^{III} (**1**), Eu^{III} (**2**), Sm^{III} (**3**), and Tb^{III} (**4**), and tta is 2-thenoyltrifluoroacetonate as the antenna ligand.

Following synthesis, thorough characterization of the complexes has been made by standard analytical tools and spectroscopic techniques. It is to be mentioned here that the phen-Hbzim-tpy bridging ligand has previously been employed to design luminescent and redox-active monometallic as well as homo- and hetero-multimetallic complexes of Ru(II) and Os(II) by our group.[65-68] However, its credibility as an Ln^{III}-sensitizer as well as TADF characteristics are being reported for the first time. Herein, the room temperature photophysical behaviors and temperature-dependent luminescence spectral characteristics of the synthesized Ln(III) complexes, including the free phen-Hbzim-tpy ligand, have been thoroughly investigated. Finally, the role of the higher energy T_1 state of the phen-Hbzim-tpy and the lower-lying T_1 state of the β-diketonate antenna ligand on the RT luminescence spectral characteristics, as well as TADF-assisted thermo-sensing and thermochromic behaviors of the complexes, have also been elucidated via plausible energy transfer pathways.

5.2. Experimental Section

5.2.1. Materials. 2-Theonyltrifluoroacetone (Htta), solvents, and all the lanthanide(III) salts in their hydrated forms, containing either nitrate or chloride as counter anions, were procured from Merck. All the solvents were dried well via distillation before use.

5.2.2. Synthesis of the Ancillary Ligand and Lanthanide(III) Precursors. The bridging phen-Hbzim-tpy ligand has been synthesized upon condensation of phenanthroline-5,6-dione and 4′-(*p*-formyl phenyl)-2,2′:6′,2″-terpyridine (tpy-PhCHO) in presence of ammonium acetate and acetic acid, following our previously reported procedure (Scheme 1).[65] The procedure to synthesize the lanthanide(III) tris-(β-diketonate) precursors of type $[Ln(tta)_3(H_2O)_2]$, wherein Ln=La, Eu, Sm, Tb, are already described in Chapter 2.

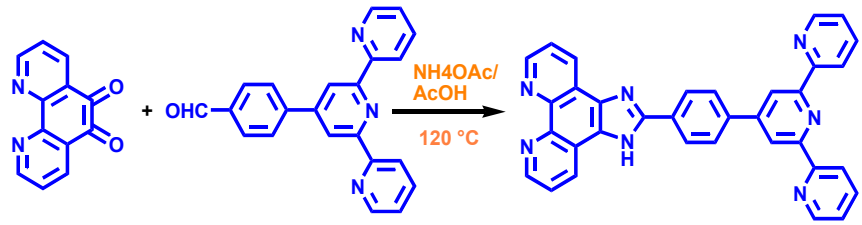

Scheme 1. Synthesis of the ancillary ligand (phen-Hbzim-tpy)

5.2.3. Synthesis of the Lanthanide Complexes. A general synthetic strategy has been adopted to synthesize all the four lanthanide complexes, $[Ln_2(tta)_6$(phen-Hbzim-tpy)], where Ln=La^{III} (**1**), Eu^{III} (**2**), Sm^{III} (**3**), and Tb^{III} (**4**) (Scheme 2). To a stirred suspension of phen-Hbzim-tpy (20 mg, 0.038 mmol) in a chloroform-methanol (1:1 v/v) mixture, an

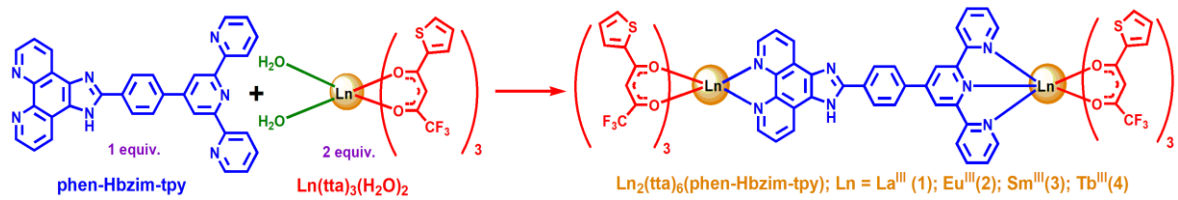

Scheme 2. Molecular structures of terpyridine-phenanthroline type ancillary ligand (phen-Hbzim-tpy), Ln^{III} precursors, $Ln(tta)_3(H_2O)_2$, and homobimetallic complexes, $\{Ln_2(tta)_6$(phen-Hbzim-tpy)} (1-4**).**

appropriate amount of respective lanthanide precursors $Ln(tta)_3(H_2O)_2$ (~67 mg, ~0.078 mmol) is added in a 1:2 ratio and kept under reflux for 6h at ~60 ºC. The resulting straw

yellow solution was then evaporated to dryness in a rotavapor, and the solid residue was dissolved in an acetonitrile-hexane (1:5 v/v) mixture to get a pale yellow colored product. The product was filtered, washed several times with hexane, and kept in a vacuum desiccator for 1d.

[$La_2(tta)_6$((phen-Hbzim-tpy)] (1). $La(tta)_3(H_2O)_2$ (66 mg, 0.078 mmol); Yield: 49 mg (61%). Anal. Calcd. for $C_{82}H_{45}F_{18}N_7O_{12}S_6La_2$: C, 46.19; H, 2.13; N, 4.60. Found: C, 46.09; H, 2.05; N, 4.47. FT-IR: υ (in cm^{-1}) = 1532, 1604, 3097. HRMS: *m/z* = 1910.8302 (100 %) $[M\text{-tta}]^+$. ^1H NMR (DMSO-d_6, 400 MHz, δ/ppm): 9.04 (d, 2H, *J* = 7.6 Hz, H_{14}), 8.84 (s, 2H, H_5), 8.80 (d, 2H, *J* = 5.0 Hz, H_9), 8.70 (d, 2H, *J* = 7.8 Hz, H_8), 8.54 (d, 2H, *J* = 8.2 Hz, H_{12}), 8.19 (d, 2H, *J* = 8.9 Hz, H_{11}), 8.06 (t, 2H, *J* = 7.7 Hz, H_{10}), 7.93 (t, 2H, *J* = 6.2 Hz, H_7), 7.84 (m, 2H, H_{13}), 7.84 (m, 6H, H_2), 7.84 (m, 6H, H_4), 7.55 (t, 2H, *J* = 6.1 Hz, H_6), 7.14 (t, 6H, *J* = 4.5 Hz, H_3), 6.25 (s, 6H, H_1 methine).

[$Eu_2(tta)_6$(phen-Hbzim-tpy)] (2). $Eu(tta)_3(H_2O)_2$ (67 mg, 0.078 mmol); Yield: 52 mg (63%). Anal. Calcd for $C_{82}H_{45}F_{18}N_7O_{12}S_6Eu_2$: C, 45.63; H, 2.10; N, 4.54. Found: C, 45.14; H, 2.01; N, 4.41. FT-IR: υ (in cm^{-1}) = 1538, 1601, 3103. HRMS: *m/z* = 1937.8662 (100 %) $[M\text{-tta}]^+$. ^1H NMR (DMSO-d_6, 400 MHz, δ/ppm): 9.05 (s, 2H, H_{14}), 8.98 (s, 2H, H_5), 8.84 (s, 2H, H_9), 8.81 (s, 2H, H_8), 8.71 (d, 2H, *J* = 8.5 Hz, H_{12}), 8.51 (s, 2H, H_{11}), 8.24 (d, 2H, *J* = 7.6 Hz, H_{10}), 8.07 (t, 2H, *J* = 7.7 Hz, H_7), 7.86 (s, 2H, H_{13}), 7.56 (t, 2H, *J* = 6.3 Hz, H_6), 7.44 (s, 6H, H_2), 6.48 (s, 6H, H_3), 6.31 (s, 6H, H_4), 2.69 (s, 6H, H_1 methine).

[$Sm_2(tta)_6$(phen-Hbzim-tpy)] (3). $Sm(tta)_3(H_2O)_2$ (67 mg, 0.078 mmol); Yield: 49 mg (60%). Anal. Calcd for $C_{82}H_{45}F_{18}N_7O_{12}S_6Sm_2$: C, 45.70; H, 2.10; N, 4.55. Found: C, 45.32; H, 1.98; N, 4.27. FT-IR: υ (in cm^{-1}) = 1537, 1601, 3096. HRMS: *m/z* = 1934.7539 (100 %) $[M\text{-tta}]^+$. ^1H NMR (DMSO-d_6, 400 MHz, δ/ppm): 9.06 (s, 2H, H_{14}), 8.99 (d, 2H, *J* = 6.6 Hz, H_5), 8.84 (s, 2H, H_9), 8.81 (d, 2H, *J* = 4.84 Hz, H_8), 8.71 (d, 2H, *J* = 8.2 Hz, H_{12}), 8.53 (d, 2H, *J* = 7.9 Hz, H_{11}), 8.24 (d, 2H, *J* = 8.2 Hz, H_{10}), 8.14 (s, 6H, H_1 methine), 8.06 (t, 2H, *J* = 7.7 Hz, H_7), 7.87 (m, 2H, H_{13}), 7.87 (m, 6H, H_2), 7.56 (t, 2H, *J* = 6.1 Hz, H_6), 7.31 (s, 6H, H_3), 7.21 (s, 6H, H_4).

[$Tb_2(tta)_6$(phen-Hbzim-tpy)] (4). $Tb(tta)_3(H_2O)_2$ (68 mg, 0.078 mmol); Yield: 55 mg (66%). Anal. Calcd for $C_{82}H_{45}F_{18}N_7O_{12}S_6Tb_2$: C, 45.34; H, 2.09; N, 4.51. Found: C, 45.03; H, 2.02; N, 4.37. FT-IR: υ (in cm^{-1}) = 1540, 1600, 3101. HRMS: *m/z* = 1950.7737 (100 %) $[M\text{-tta}]^+$. ^1H NMR (DMSO-d_6, 400 MHz, δ/ppm): 98.26 (s, 6H, H_1 methine), 29.91 (s, 6H, H_2), 12.36 (s, 6H, H_3), 9.07 (s, 2H, H_{14}), 9.02 (s, 2H, H_5), 8.88 (s, 2H, H_9), 8.80 (s, 2H, H_8),

8.68 (d, 2H, J = 8.2 Hz, H_{12}), 8.60 (s, 2H, H_{11}), 8.30 (d, 2H, J = 9.1 Hz, H_{10}), 7.99 (t, 2H, J = 5.4 Hz, H_7), 7.90 (s, 2H, H_{13}), 7.50 (s, 2H, H_6), 6.49 (s, 6H, H_4).

5.2.4. Theoretical Calculations. The geometry optimization of the phen-Hbzim-tpy ligand was performed using Gaussian 09 software upon employing a global hybrid functional PBE0 (Perdew-Burke-Ernzerhof). 6-31G* basis set was employed for C, H, and N atoms. Solvent effects of acetonitrile were included using the PCM (Polarizable Continuum Model). Time-dependent density functional (TD-DFT) calculations at the same level of theory were also executed to acquire calculated absorption and emission spectra of ligand. Orbital and fractional contribution analysis was done with Gauss View 5.0 and Gauss Sum 2.1. The orbital overlap integral value between HOMO and LUMO was calculated via Multiwfn software (version 3.8).

5.2.5. Instruments and Physical Methods. The delayed fluorescence and delayed lifetime data for all compounds were recorded in Edinburgh FLS1000 instrument using a μF-400 flash lamp and PMT-900 detector. The data were analyzed using Fluoracle software (version 2.9.3). The relative quantum yield at room temperature was measured for all the four complexes (**1-4**) in acetonitrile solvent, using quinine bisulfate in 1N H_2SO_4 (η = 1.338, Φ_{rel} = 54.6%) as reference for the system. In this regard, we have utilized a general equation (5.1) for the calculation of quantum yield:

$$\frac{\Phi_s}{\Phi r} = \frac{A_r \eta_s^2 I_s}{A_s \eta_r^2 I_r} \quad \ldots (5.1)$$

where 'r' represents the reference and 's' the sample. 'A' implies the absorbance at the excitation wavelength, whereas 'I' is the integrated luminescence intensity, and 'η' represents the refractive index of the solution. The refractive index is supposed to be equivalent to that of the pure solvent (η = 1.344 for acetonitrile). The rest of this section have already been discussed in Chapter 2.

5.3. Results and Discussions

5.3.1. Synthesis and Characterization. The reaction between phen-Hbzim-tpy and respective lanthanide precursors, $Ln(tta)_3(H_2O)_2$ (1:2 molar ratio) in chloroform-methanol (1:1 v/v) mixture yields the desired dinuclear ternary complexes with good yields. The resulting complexes are then characterized via standard analytical tools and spectroscopic techniques, viz. elemental (C, H, N) analysis, FT-IR and ^{1}H NMR spectroscopy, HRMS,

PXRD, as well as thermogravimetric analysis. Associated figures and tables are provided in Figures 5.1-5.11 and Tables 5.1-5.2. All the four complexes are found to be isostructural.

5.3.2 FT-IR Spectra. The IR spectra of the resulting complexes along with their respective lanthanide precursors and phen-Hbzim-tpy ligand were acquired within 400-4000 cm^{-1} region and related spectra as well as selected stretching frequencies of the complexes are presented in Figure 5.1 and Table 5.1. The ligand exhibited a peak at ~1586 cm^{-1} due to

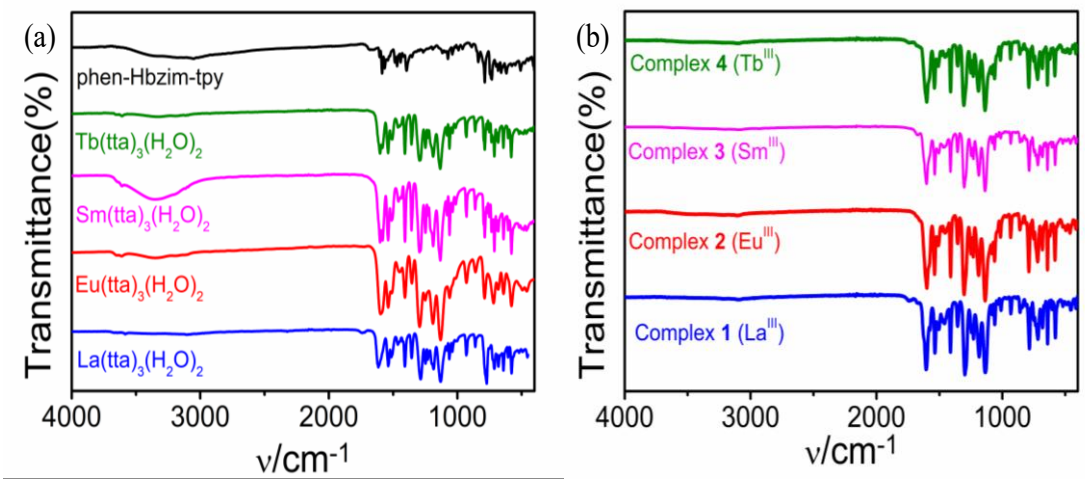

Figure 5.1. FT-IR spectra of phen-Hbzim-tpy, and all four $Ln(tta)_3(H_2O)_2$ precursors (a) and complexes **1-4** (b).

Table 5.1. Stretching Frequencies of Selected Groups in Their FT-IR spectra

Complex	$\nu_{C=O}$	$\nu_{C=N}$	ν_{N-H}	ν_{OH}
phen-Hbzim-tpy	-	1586	3154	-
$La(tta)_3(H_2O)_2$	1601	-	-	3360
Complex 1	1604	1532	3097	-
$Eu(tta)_3(H_2O)_2$	1603	-	-	3351
Complex 2	1601	1538	3103	-
$Sm(tta)_3(H_2O)_2$	1602	-	-	3353
Complex 3	1601	1537	3096	-
$Tb(tta)_3(H_2O)_2$	1601	-	-	3400
Complex 4	1600	1540	3101	-

C=N stretching of the pyridine moieties, whereas a characteristic peak at ~3154 cm^{-1} for the imidazole N-H stretch. Due to the presence of the 2-thenoyltrifluoroacetylacetonate unit, all the lanthanide precursors, $Ln(tta)_3(H_2O)_2$ show a characteristic C=O stretching within 1601-1603 cm^{-1} and a broad hump in the spectral domain of 3350-3400 cm^{-1} for the water molecules. The complexes also revealed a sharp peak within the range from 1600-1604 cm^{-1}

associated with C=O stretching frequency and interestingly the broad peak for coordinated water is disappeared. Simultaneously, two new peaks emerged within 1532-1540 cm^{-1} and 3096-3103 cm^{-1} for C=N and N-H stretching, respectively in the complexes.

5.3.3. ^{1}H NMR Spectra. Thorough characterization of the complexes **1-4** and their respective $Ln(tta)_3(H_2O)_2$ precursors is performed via ^{1}H NMR spectroscopy in DMSO-d_6. The ^{1}H NMR spectra along with the tentative assignments of protons are provided in Figures 5.2-5.5, and Table 5.2. It is observed that the protons associated with the tta moiety

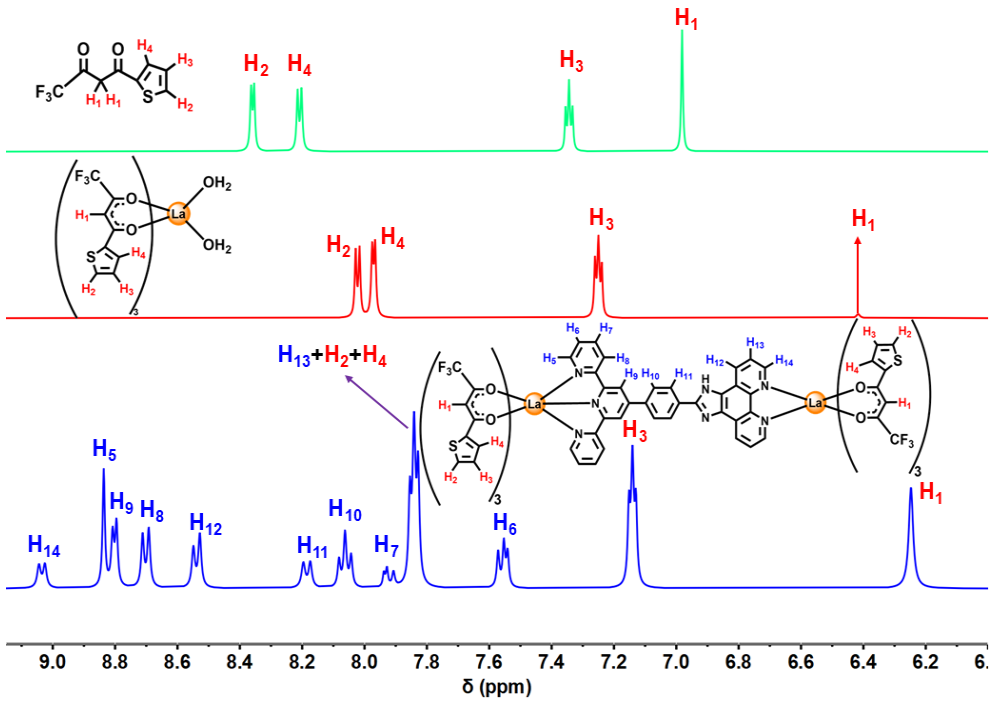

Figure 5.2. 400 MHz ^{1}H NMR spectra of Htta (top), $La(tta)_3(H_2O)_2$ (middle) and $[La_2(tta)_6$(phen-Hbzim-tpy)] (**1**) (bottom) in DMSO-d_6.

experienced huge chemical shifts with unprecedented change in multiplicity, especially in the three cases comprising of the paramagnetic ions. On the other hand, the protons attached to the phen-Hbzim-tpy ligand underwent slight alteration in the chemical shift of the signals but experienced unpredictable alteration in multiplicity. The protons in the free Htta get up-field shifted from 6.98 (s) ppm to 6.40 (s) ppm upon incorporation of diamagnetic La^{III} ion in $La(tta)_3(H_2O)_2$ precursor. The very same proton keeps the trend of up-field shifting up to 6.25 (s) ppm in the resulting La^{III}-complex (**1**) (Figure 5.2). Among the other three complexes, this methine proton experiences a down-field shift from 1.10 (s) to 2.69 (s) ppm in case of Eu^{III}

complex (**2**), and from 95.96 (s) to 98.26 (s) ppm for the Tb^{III}-complex (**4**) while it remains almost unperturbed {from 8.13 (s) to 8.14 (s) ppm} for the Sm^{III} complex (**3**) as compared to their respective $Ln(tta)_3(H_2O)_2$ precursors. The comparative changes in chemical shift values for all the proton resonances are also presented in Table 5.2.

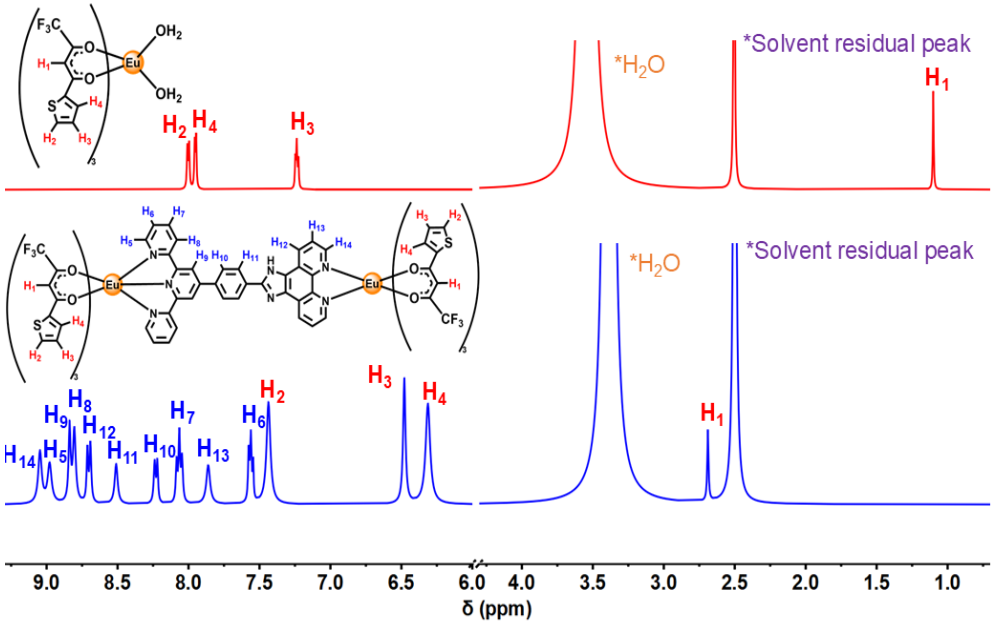

Figure 5.3. 400 MHz ^{1}H NMR spectra of $Eu(tta)_3(H_2O)_2$ (top) and $[Eu_2(tta)_6$(phen-Hbzim-tpy)] (**2**) (bottom) in DMSO-d_6.

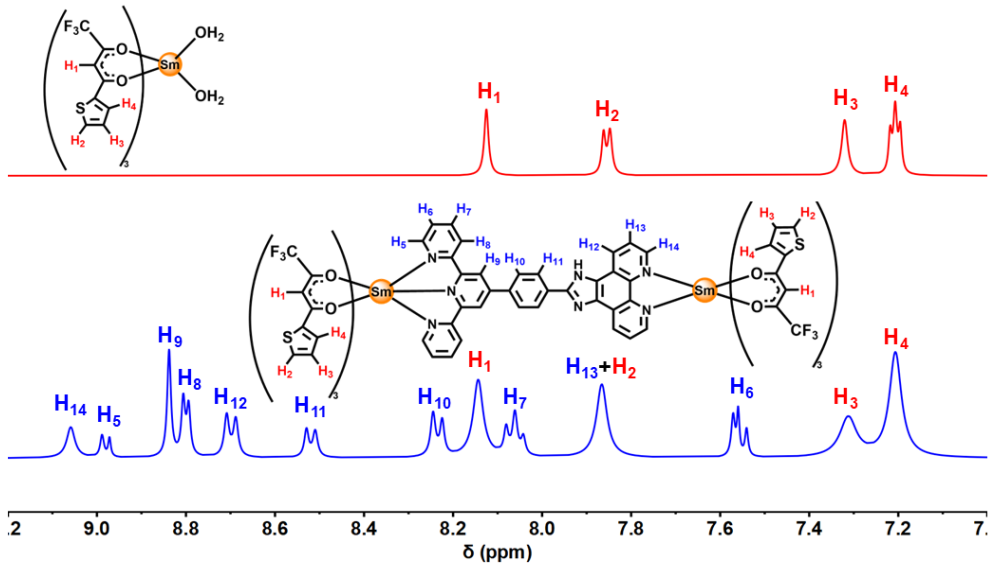

Figure 5.4. 400 MHz ^{1}H NMR spectra of $Sm(tta)_3(H_2O)_2$ (top) and $[Sm_2(tta)_6$(phen-Hbzim-tpy)] (**3**) (bottom) in DMSO-d_6.

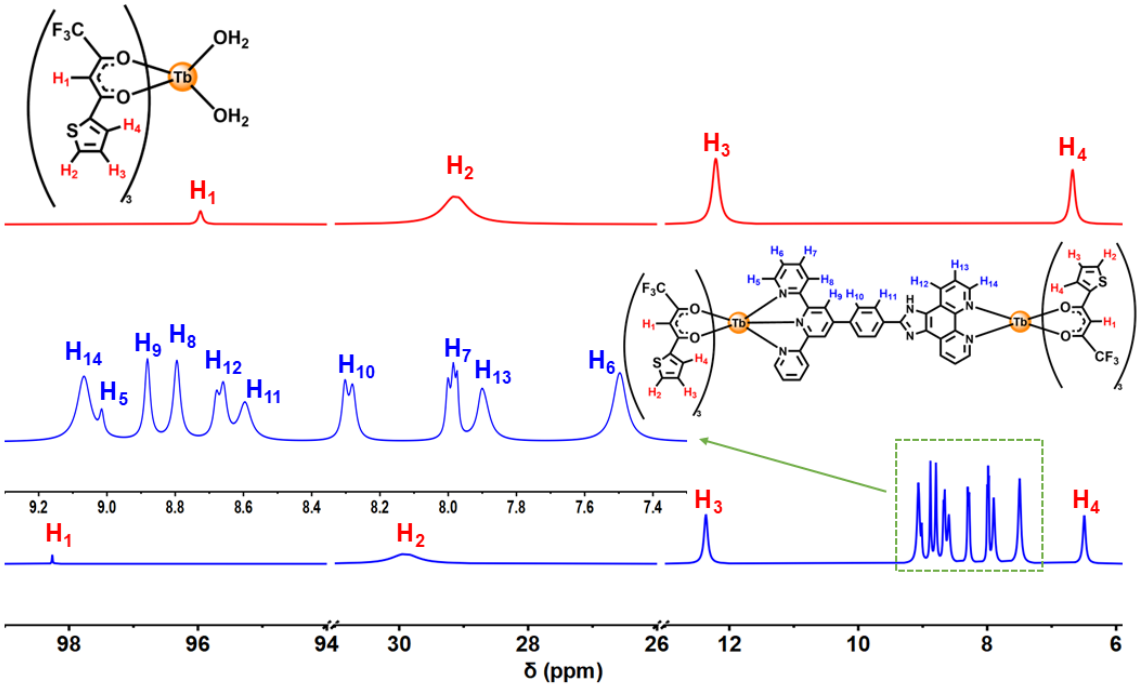

Figure 5.5. 400 MHz ^{1}H NMR spectra of $Tb(tta)_3(H_2O)_2$ (top) and $[Tb_2(tta)_6$(phen-Hbzim-tpy)] (**4**) (bottom) in DMSO-d_6.

Table 5.2. Chemical Shifts of the Protons of All the Four Complexes in DMSO-d_6

Proton	Chemical shift (ppm) of Lanthanide complexes (1-4) {J= Hz}			
	1 (La^{III})	**2** (Eu^{III})	**3** (Sm^{III})	**4** (Tb^{III})
H_1 (methine)	6.25 (s, 6H)	2.69 (s, 6H)	8.14 (s, 6H)	98.26 (s, 6H)
H_2 (tta)	7.84 (m, 6H)	7.44 (s, 6H)	7.87 (s, 6H)	29.91 (s, 6H)
H_3 (tta)	7.14 (t, 6H, J = 4.5)	6.48 (s, 6H)	7.31 (s, 6H)	12.36 (s, 6H)
H_4 (tta)	7.84 (m, 6H)	6.31 (s, 6H)	7.21 (s, 6H)	6.49 (s, 6H)
H_5	8.84 (s, 2H)	8.98 (s,2H)	8.99 (d, 2H, J = 6.6)	9.02 (s, 2H)
H_6	7.55 (t, 2H, J = 6.1)	7.56 (t, 2H, J = 6.3)	7.56 (t, 2H, J = 6.1)	7.50 (s, 2H)
H_7	7.93 (t, 2H, J = 6.2)	8.07 (t, 2H, J = 7.7)	8.06 (t, 2H, J = 7.7)	7.99 (t, 2H, J = 5.4)
H_8	8.70 (d, 2H, J = 7.8)	8.81 (s, 2H)	8.81 (d, 2H, J = 4.8)	8.80 (s, 2H)
H_9	8.80 (d, 2H, J = 5.0)	8.84 (s, 2H)	8.84 (s, 2H)	8.88 (s, 2H)
H_{10}	8.06 (d, 2H, J = 7.7)	8.24 (d, 2H, J = 7.6)	8.24 (d, 2H, J = 8.2)	8.30 (d, 2H, J = 9.1)
H_{11}	8.19 (d, 2H, J = 8.9)	8.51 (s, 2H)	8.53 (d, 2H, J = 7.9)	8.60 (s, 2H)
H_{12}	8.54 (d, 2H, J = 8.2)	8.71 (d, 2H, J = 8.5)	8.71 (d, 2H, J = 8.2)	8.68 (d, 2H, J = 8.2)
H_{13}	7.84 (m, 2H)	7.86 (s, 2H)	7.87 (s, 2H)	7.90 (s, 2H)
H_{14}	9.04 (d, 2H, J = 7.6)	9.05 (s, 2H)	9.06 (s, 2H)	9.07 (s, 2H)

5.3.4. Mass Spectra. The HRMS data for all four complexes are recorded in $CHCl_3$ to further confirm their stability in solution. Similar spectral patterns are noticed for all cases

with a prominent peak for respective $[\{Ln_2(tta)_5(phen\text{-}Hbzim\text{-}tpy)\}]^+$ or $[M\text{-}tta]^+$ fragment (Figures 5.6-5.9). The correspondence between the experimental and simulated isotopic patterns is also found to be very close in all cases.

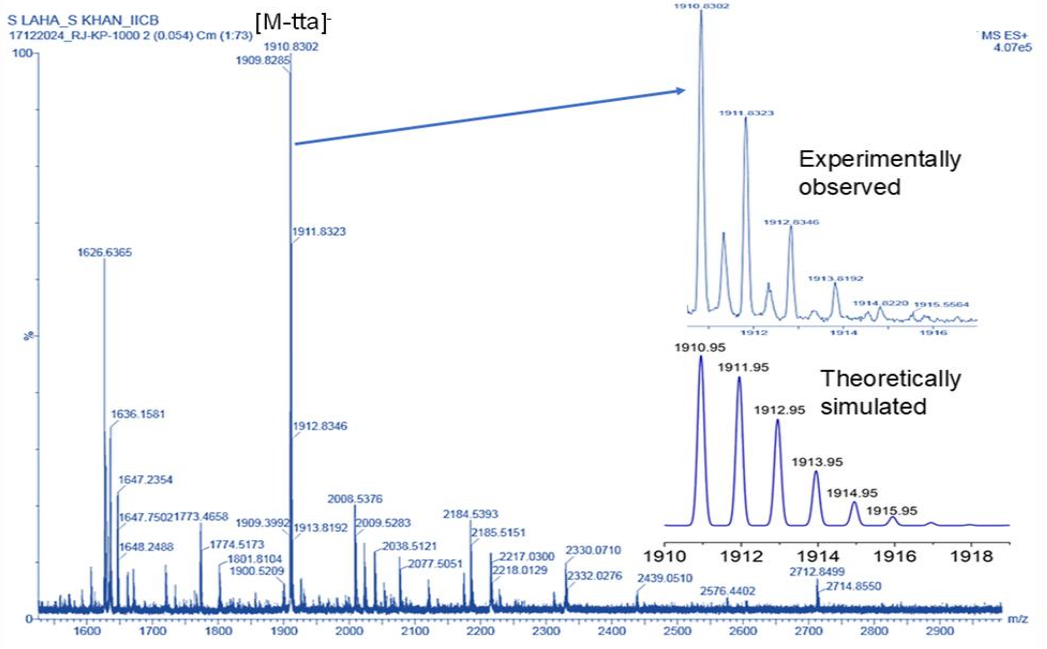

Figure 5.6. HRMS of **1** in dichloromethane. The upper right portion shows the experimentally observed isotopic distribution pattern for $[La_2(tta)_5(phen\text{-}Hbzim\text{-}tpy)]^+$ fragment and the lower right portion shows the simulated isotopic distribution pattern.

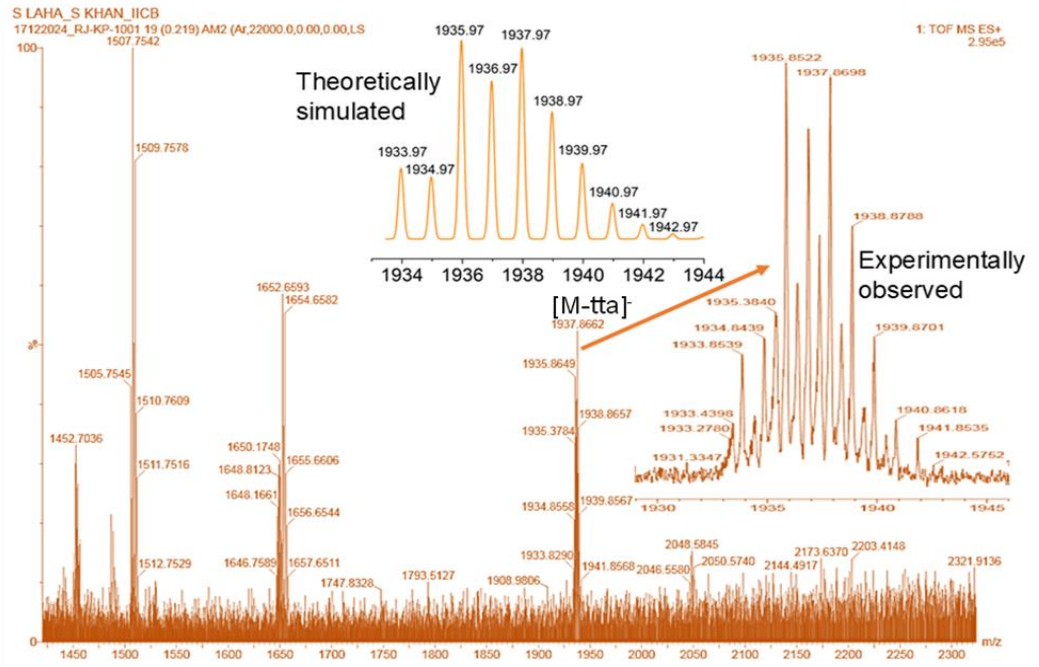

Figure 5.7. HRMS of **2** in dichloromethane with the experimentally observed and simulated isotopic distribution pattern for $[Eu_2(tta)_5(phen\text{-}Hbzim\text{-}tpy)]^+$ fragment.

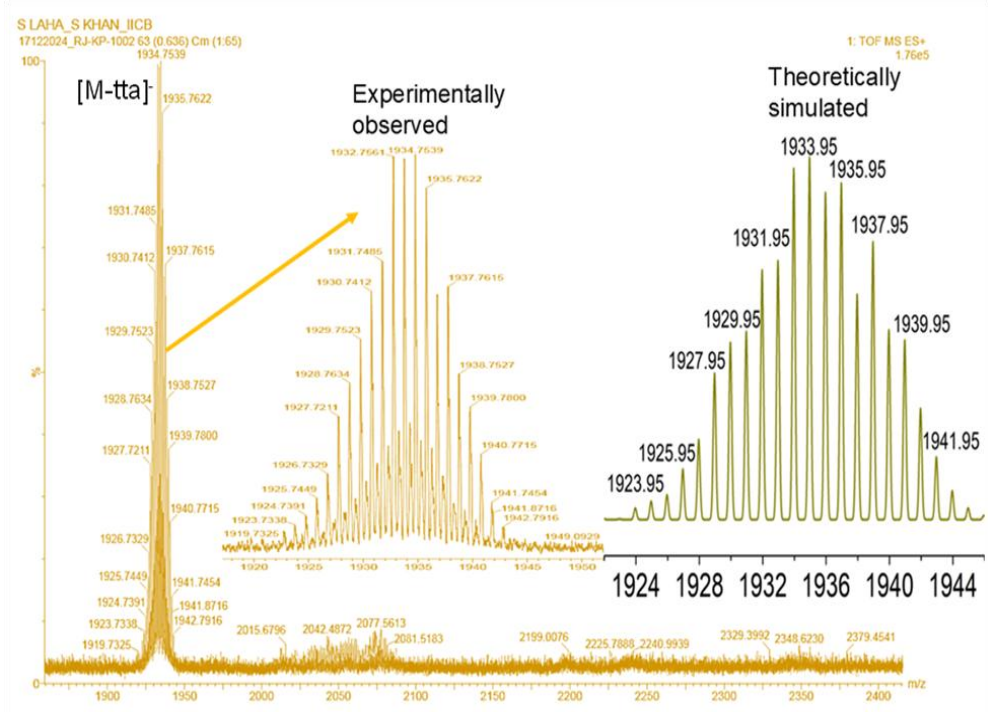

Figure 5.8. HRMS of **3** in dichloromethane with the experimentally observed and simulated isotopic distribution pattern for $[Sm_2(tta)_5(phen\text{-}Hbzim\text{-}tpy)]^+$ fragment.

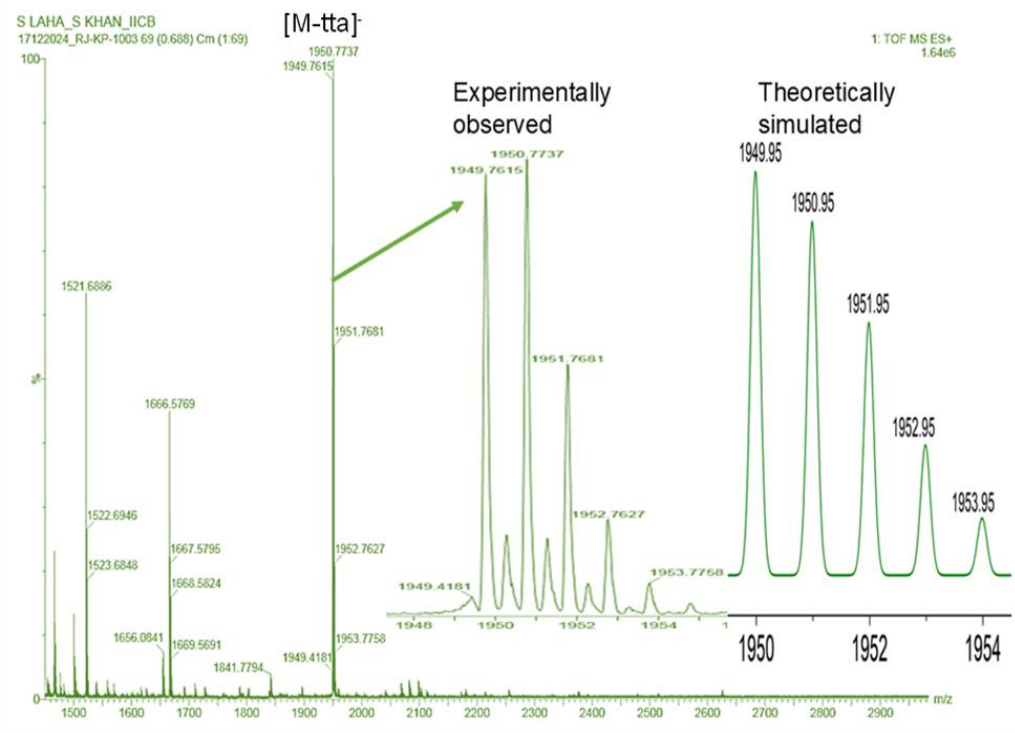

Figure 5.9. HRMS of **4** in dichloromethane with the experimentally observed and simulated isotopic distribution pattern for $[Tb_2(tta)_5(phen\text{-}Hbzim\text{-}tpy)]^+$ fragment.

5.3.5. Powdered X-ray Diffraction (PXRD). The PXRD analysis for all four complexes shows broad peaks with similar patterns, indicating their amorphous nature (Figure 5.10). The consistent pattern observed for complexes **1-4** suggests that they are all isostructural.

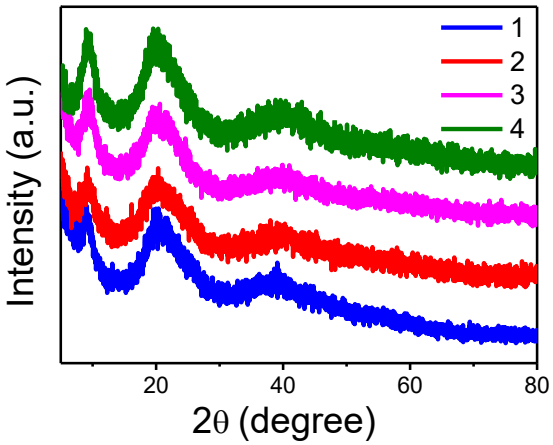

Figure 5.10. PXRD patterns of complexes **1-4**.

5.3.6. Thermogravimetric Analysis of the Complexes. The thermal stability of the complexes was inspected via thermogravimetry in N_2 atmosphere within the temperature domain of 30-700 °C with a heating rate of 10 °C/m. The similarity in decomposition pattern and weight loss is noticed in all cases (Figure 5.11). Upon reaching ~300 °C, major decay starts and continues up to ~400 °C (up to ~40% weight loss), which is probably due to dissociation of phen-Hbzim-tpy. The next major weight-loss begins at ~550 °C and continues

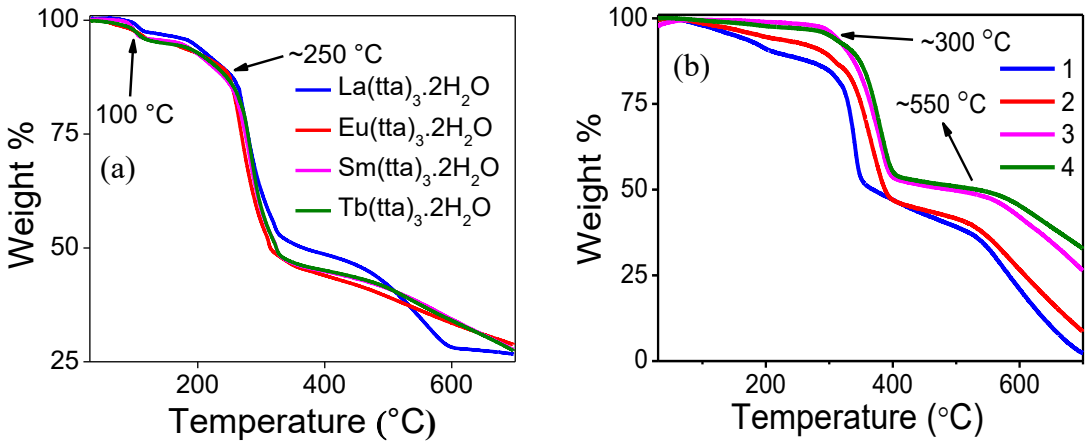

Figure 5.11. Thermogravimetric analysis of all four metal precursors $Ln(tta)_3(H_2O)_2$[32] (a) and their corresponding complexes **1-4** (b).

thereafter possibly due to the generation of the respective metal oxides. It is to be noted that the synthesized complexes are thermally more stable (onset temperature ~300 °C) than their respective lanthanide precursors (onset temperature ~250 °C). Thus, it seems that the complexes possess adequate thermal stability up to ~300 °C.

5.3.7. Absorption and Emission Spectral Characteristics. The photophysical responses of all the four lanthanide complexes together with the bridging phen-Hbzim-tpy ligand are recorded in acetonitrile. Associated spectra are shown in Figures 5.12-5.13 and relevant spectral data are presented in Table 5.3. As the ligand plays a crucial role in

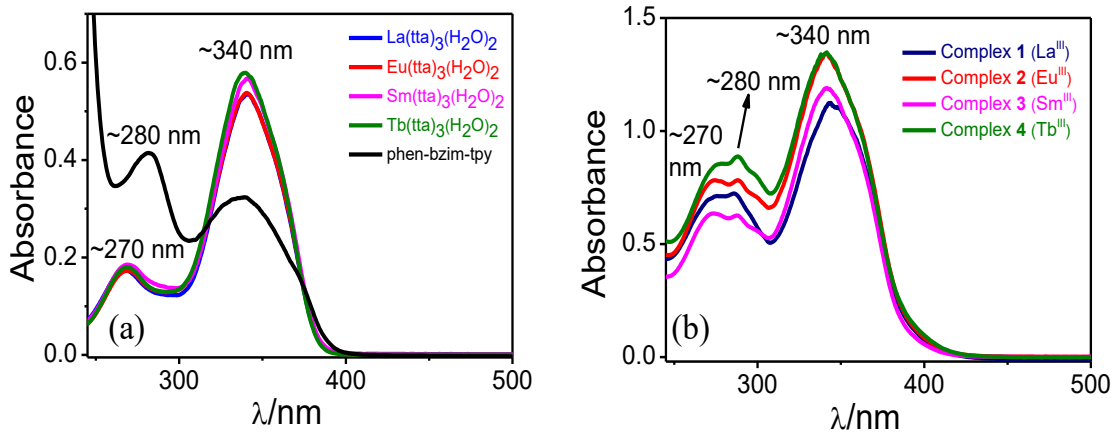

Figure 5.12. UV-visible absorption spectra of phen-Hbzim-tpy together with $Ln(tta)_3(H_2O)_2$ precursors (a) and complexes **1**-**4** (b) in dried acetonitrile at RT.

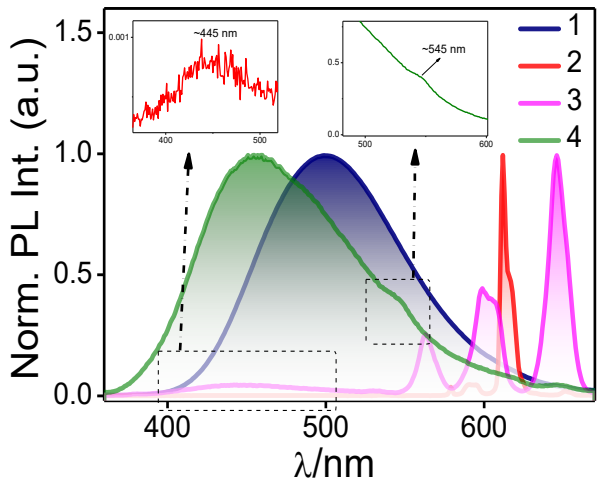

Figure 5.13. Normalised photoluminescence (λ_{ex}=340 nm) spectra of complexes **1**-**4** in dried acetonitrile at RT. Insets show the weak ligand-centered emission band of **2** and the weak Tb^{III}-centered emission peak in **4**.

Table 5.3. Photophysical Parameters of Complexes 1-4 at RT and at 77 K

	Complex	Absorption, λ_{max}/nm (ε/$M^{-1}cm^{-1}$)($\times 10^4$)	Emission, λ_{max}/nm			Relative Quantum Yield (Φ_{rel})
			Ligand centered	Metal centered	Lifetime (τ)	
RT	**1**	270 (7.04), 285 (7.32), 343 (11.32)	495	-	τ=2.6 ns	0.68
	2	274 (7.93), 287 (7.99), 340 (13.52)	445	579, 589, 612, 651	τ_1=480.7 µs τ_2=551.4 µs	0.61
	3	273 (6.46), 287 (6.35), 341 (11.98)	445	563, 599, 646	τ_1=28.6 µs τ_2=68.8 µs	0.04
	4	274 (8.58), 287 (8.96), 340 (13.48)	455	545, 620, 647	τ_1=0.4 µs τ_2=4.6 µs	0.46
77K	**4**	-	-	490, 545, 580, 620	τ_1=219.0 µs τ_2=604.8 µs	-

demonstrating the TADF event, we have thoroughly investigated its ground and excited state properties. To this end, geometry optimization of phen-Hbzim-tpy ligand has been performed using Gaussian 09 software upon employing PBE0 functional. The optimized geometry is presented in Figure 5.14. Selected HOMOs and LUMOs are presented in Figure 5.15 and Table 5.4.

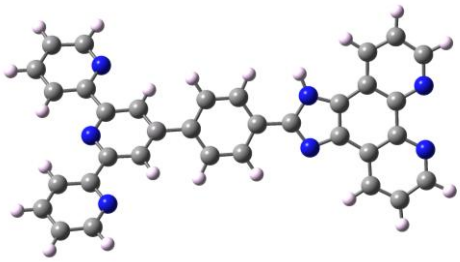

Figure 5.14. Optimized geometry of the free ligand phen-Hbzim-tpy.

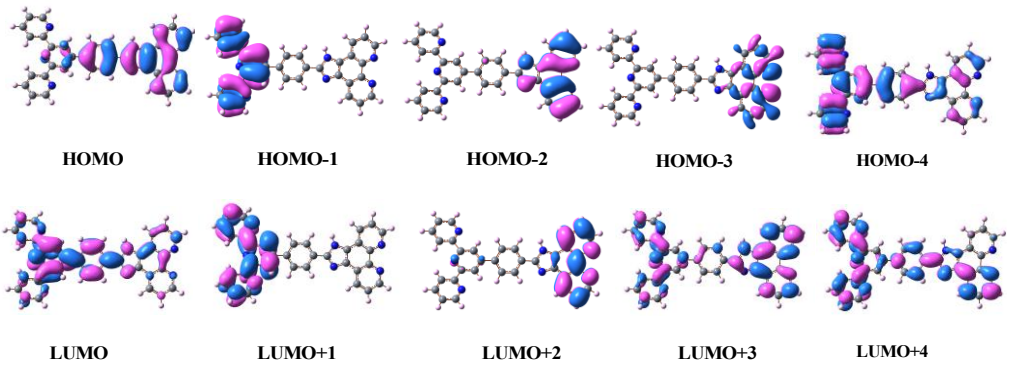

Figure 5.15. Pictorial representation of the molecular orbitals (HOMO and LUMO) in phen-Hbzim-tpy using PBE0 (PBE1PBE) functional.

Table 5.4. Selected MOs Along with Their Energies and Compositions in the Ground State of phen-Hbzim-tpy Using PBE0 (PBE1PBE)

MO	*phen-Hbzim-tpy*			
	Energy/eV	% of compositions		
		phenyl	imidazole-phen	tpy
LUMO+5	-0.56	1.13	06. 14	92.71
LUMO+4	-0.97	16.06	46.39	37.53
LUMO+3	-1.24	3.10	74. 31	22.58
LUMO+2	-1.46	0.27	96.08	3.63
LUMO+1	-1.53	0.92	0.02	99.05
LUMO	-1.87	31.28	22.33	46.38
HOMO	-5.98	20.85	75.03	4.10
HOMO-1	-6.66	0.20	0.02	99.78
HOMO-2	-6.89	1.35	98.20	0.43
HOMO-3	-7.23	0.05	99.82	0.11
HOMO-4	-7.24	18.96	16.85	64.18
HOMO-5	-7.30	4.66	0.11	95.21

TD-DFT calculations were also executed in all cases to acquire the calculated absorption spectra and overlay of the experimental and calculated spectra of ligand are provided in Figure 5.16. It is of interest to note that agreement between the experimental and calculated absorption spectrum is very well. Upon close scrutiny of the compositions of HOMOs and LUMOs, it appears that the experimentally observed absorption band at ~340 nm is due to intra-ligand charge transfer (ILCT) transitions, whereas the band at ~286 nm is attributed to π-π* transitions associated with the aromatic and heteroaromatic moieties in the molecular framework (Table 5.5). Natural transition orbital (NTO) analysis also confirms the ILCT nature of the band at ~340 nm (Figure 5.17). In line with the absorption spectra, the agreement between the experimental and calculated emission spectrum is quite good (Figure 5.18). Hence, the observed emission in ligand is due to radiative deactivation of ^{1}ILCT state.

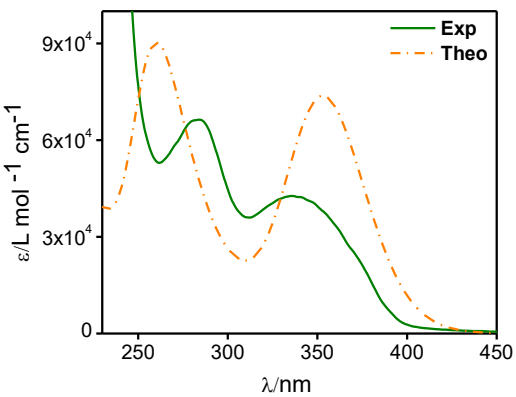

Figure 5.16. Overlay of the experimental and calculated of absorption spectra of phen-Hbzim-tpy in acetonitrile via PBE0 (PBE1PBE).

Table 5.5. Selected UV-vis Energy Transitions at the TD-DFT/ PBE0 (PBE1PBE) Level for phen-Hbzim-tpy

λ_{exp} /nm	Excited State	λ_{cal} /nm	Oscillator strength	Key transitions	Character
phen-Hbzim-tpy					
340	S1	353	1.3312	HOMO→LUMO (93%)	ILCT
286	S15	260	0.4881	H-2→ L+2 (70%), HOMO→L+3 (7%), HOMO→L+4 (6%)	π -π*
225	S56	215	0.2635	H-8→L+3 (62%), H-8→L+2 (8%)	ILCT, π -π*

Natural Transition Orbitals (NTO)		
		Key transition
HOMO	LUMO	HOMO→LUMO (93%)

Figure 5.17. NTOs illustrating the nature of the lowest energy singlet excited states in the absorption bands of phen-Hbzim-tpy via PBE0(PBE1PBE) functional.

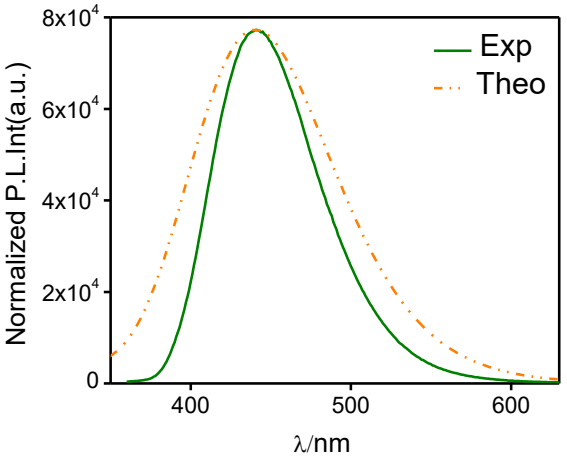

Figure 5.18. Overlay of the experimental and calculated emission spectra of phen-Hbzim-tpy in acetonitrile via PBE0 (PBE1PBE).

$Ln(tta)_3(H_2O)_2$ precursor complexes also possess two absorption bands very close to that of the ligand (Figure 5.12a). Upon complexation, the absorption window of the bimetallic $Ln_2(tta)_6$(phen-Hbzim-tpy) complexes is found to stretch towards the visible region with the onset at ~435 nm (Figure 5.12b). Additionally, the molar absorptivity (ε) of the complexes gets substantially enhanced (more than double) on going from related monometallic tris-tta precursor complexes to the bimetallic species, due to chromophore

additivity. Thus, in contrast to most of the lanthanide complexes, this new array of complexes can act as better visible light sensitizers, which is quite beneficial for diverse light-harvesting applications.

The photoluminescence spectra of the complexes are recorded in acetonitrile upon irradiating at ~340 nm at RT and depicted in Figure 5.13. The broad emission peak for free phen-Hbzim-tpy at ~440 nm undergoes a red shift to ~495 nm for the La^{III}-complex (**1**). The emission spectrum of the Eu^{III} complex (**2**) comprises strong signals at 579, 589, 612, and 651 nm, arising from intra-configurational $^5D_0 \rightarrow {}^7F_{0\rightarrow3}$ transitions, respectively, typical of the Eu^{III} ion. Besides, a very weak ligand-centered emission at ~445 nm is observed for **2** (inset of Figure 5.13), indicating a nearly complete ligand-to-metal energy transfer process. In the case of Sm^{III} complex (**3**), apart from a low-intensity ligand-centered band at ~445 nm, intense emission having the peak maxima at 563 ($^5G_{5/2} \rightarrow {}^5H_{5/2}$), 599 ($^5G_{5/2} \rightarrow {}^5H_{7/2}$), and 646 nm ($^5G_{5/2} \rightarrow {}^5H_{9/2}$) is clearly visible. This seems quite interesting as luminescence resulting from Sm^{III} ion is often very prone to quenching owing to multi-phonon relaxation,[70,71] as we have also found in our earlier reported Sm^{III} complexes.[32,33] In contrast to Eu^{III} and Sm^{III}, the Tb^{III} complex (**4**) displayed only the ligand-centered emission at ~455 nm together with a very weak peak at ~545 nm (inset of Figure 5.13). This observation is quite common for the Tb^{III} complexes, probably because of thermally-assisted back energy transfer to the ligand.[31-33,58,59] The overall relative quantum yields (Φ_{rel}) of the complexes are estimated to be 0.68, 0.61, 0.04, and 0.46 for **1**, **2**, **3**, and **4**, respectively. The observed values of Φ_{rel} are found to be much higher compared to our previously reported related mononuclear analogues,[32,33] while comparable to that of reported Ln^{III}-based discrete dinuclear complexes as narrated in Table 5.6.[5,16,39,54,72-86]

Table 5.6. Comparison of the Quantum Yield Values Among Earlier Reported Ln^{III}-Based Discrete Molecules with This Work

Complex	Absorption, λ_{max}/nm (ε/$M^{-1}cm^{-1}$)($\times10^4$)	Quantum Yield Value (%)	Method of Estimation	References
$Eu_2(BTP)_3(DME)_2$	317 (8.00)	13	Relative	*16*
$Eu_2(BTP)_3(bpy)_2(CH_2Cl_2)_2$	325 (7.20)	55		
$Eu_2(BTP)_3(phen)_2$	327 (7.26)	65		
$Eu_2(TOTPY)_2(TFA)_6$	288 (6.89)	18.7	Relative	*39*
$Tb_2(TOTPY)_2(TFA)_6$	288 (4.79)	17.8		
$Eu_2(FTPY)_2(TFA)_6$	294 (6.34)	17.3		

$Tb_2(FTTPY)_2(TFA)_6$ $Eu_2(TTPY)_2(TFA)_6$ $Tb_2(TTPY)_2(TFA)_6$	294 (7.59) 292 (6.18) 292 (6.34)	19.2 15.7 16.1		
$Eu_2(tta)_6(bipyMO)_2$ $Eu_2(dbm)_6(bipyMO)_2$ $Eu_2(bta)_6(bipyMO)_2$ $Eu_2(hfa)_6(bipyMO)_2$	-	35 38 22 10	Absolute	*54*
$Eu_2L^1{}_3$ $Sm_2L^1{}_3$ H_2L^1= 1,3-bis(3-phenyl-3-oxopropanoyl)benzene	357 (13.0)	5.0 0.16	Relative	*72*
$[Tb_2(H_2L)_2(\mu\text{-piv})_2(piv)_2]\cdot 2CHCl_3$	298 (3.52)	76.2	Relative	*73*
$Eu_2(BTPE)_3(DMSO)_4$ BTPE= 1,2-bis-(4,40-bis(4,4,4-trifluoro-1,3-dioxobutyl))phenoxyl ethane		25	Absolute	*74*
$Eu_2(hfa)_6(4\text{-NIPyNO})_2$ $Eu_2(hfa)_6(3\text{-NIPyNO})_3$	-	41.5 28.6	Absolute	*75*
$Eu_2(dbm)_6(bipyMO)_2$ $Eu_2(tta)_6(bipyMO)_2$ $Eu_2(hfa)_6(bipyMO)_3$	-	26 44 40	Absolute	*76*
$Eu_2(BTB)_3(C_2H_5OH)_2(H_2O)_2$ $Eu_2(BTB)_3(bpy)_2$ $Eu_2(BTB)_3(phen)$ $Eu_2(BTB)_3(bath)_2$	-	26 47 39 34	Absolute	*77*
$Tb_2(tmh)_6(dpbp)$	-	56	Absolute	*78*
$Eu_2(dbm)_6(dppeO2)$ $Eu_2(fod)_6(dppeO2)$	-	50 17	Absolute	*79*
$Sm_2(L\text{-}2H)_3$ L= bis{1-ethyl-2-[(6′-carboxy)pyridin-2′-yl]benzimidazol-5-yl}-methane	-	0.03	Absolute	*80*
$Eu_2(phen)_2(bza)_4(Ac)_2$ $Tb_2(phen)_2(bza)_4(Ac)_2$ $Sm_2(phen)_2(bza)_4(NO_3)_2$ $Eu_2(phen)_2(bza)_4(NO_3)_2$ $Tb_2(phen)_2(bza)_4(NO_3)_2$	-	48.51 16.17 0.35 44.50 11.76	Absolute	*81*
$Eu_2(TTA)_6$\{phen(Ph)-Ph-o-C_4H_8-o-Ph-(Ph)phen\} $Eu_2(TTA)_6$\{phen(Fl)-Ph-o-C_4H_8-o-Ph-(Fl)phen\}	-	31.8 32.4	Absolute	*82*
$Eu_2(btfa)_6(bpm)$	-	54.4	Absolute	*83*
$Eu_2(HTH)_6(bpm)$ $Sm_2(HTH)_6(bpm)$ HTH = 4,4,5,5,6,6,6-heptafluroro-1-(2-thienyl)hexane-1,3-dione	342 342	28.4 1.4	Relative	*84*
$Tb_2(HXTA)_2,Na_4$ HXTA= (N,N-(2 hydroxy-5-methyl-1,3-xylylene)bis(N-(carboxymethyl)glycine)	300	54	Relative	*85*
$Tb_2(L^{CH}{}_3)_2(NO_3)_2(DMF)_2]\cdot 2DMF$	-	3.9	Absolute	*86*

$Tb_2(L^{Cl})_2(NO_3)_2(DMF)_2]\cdot 2DMF$		10.6		
$Tb_2(L^{CH_3O})_2(NO_3)_2(DMF)_2]$		0.4		
$Tb_2(L^{COOCH_3})_2(NO_3)_2(DMF)_2]\cdot 2DMF$		13.0		
$La_2(tta)_6$(phen-Hbzim-tpy)	343 (11.32)	68.2	Relative	*This work*
$Eu_2(tta)_6$(phen-Hbzim-tpy)	340 (13.52)	61.1		
$Sm_2(tta)_6$(phen-Hbzim-tpy)	341 (11.98)	4.0		
$Tb_2(tta)_6$(phen-Hbzim-tpy)	340 (13.48)	46.2		

The excited state decay profiles of all the four complexes are also acquired in acetonitrile at RT upon exciting with a 370 nm Deltadiode/SpectralLED source and are presented in Figure 5.19. The associated lifetime values are listed in Table 5.3. The complex **1** exhibits a lifetime in the nanosecond region (τ=2.6 ns), mainly due to the ligand-centered emission. Complexes **2** and **3**, on the other hand, display substantially longer lifetimes, viz., τ_1=480.7 μs and τ_2=551.4 μs, and τ_1=28.6 μs and τ_2=68.8 μs, respectively, upon monitoring at the wavelengths associated with their respective electric dipole transitions. By contrast, the lifetime value for complex **4**, obtained upon monitoring at the Tb^{III}-centered emission, is found to be very low (τ_1=0.4 μs and τ_2=4.6 μs). This again indicates dominant back energy

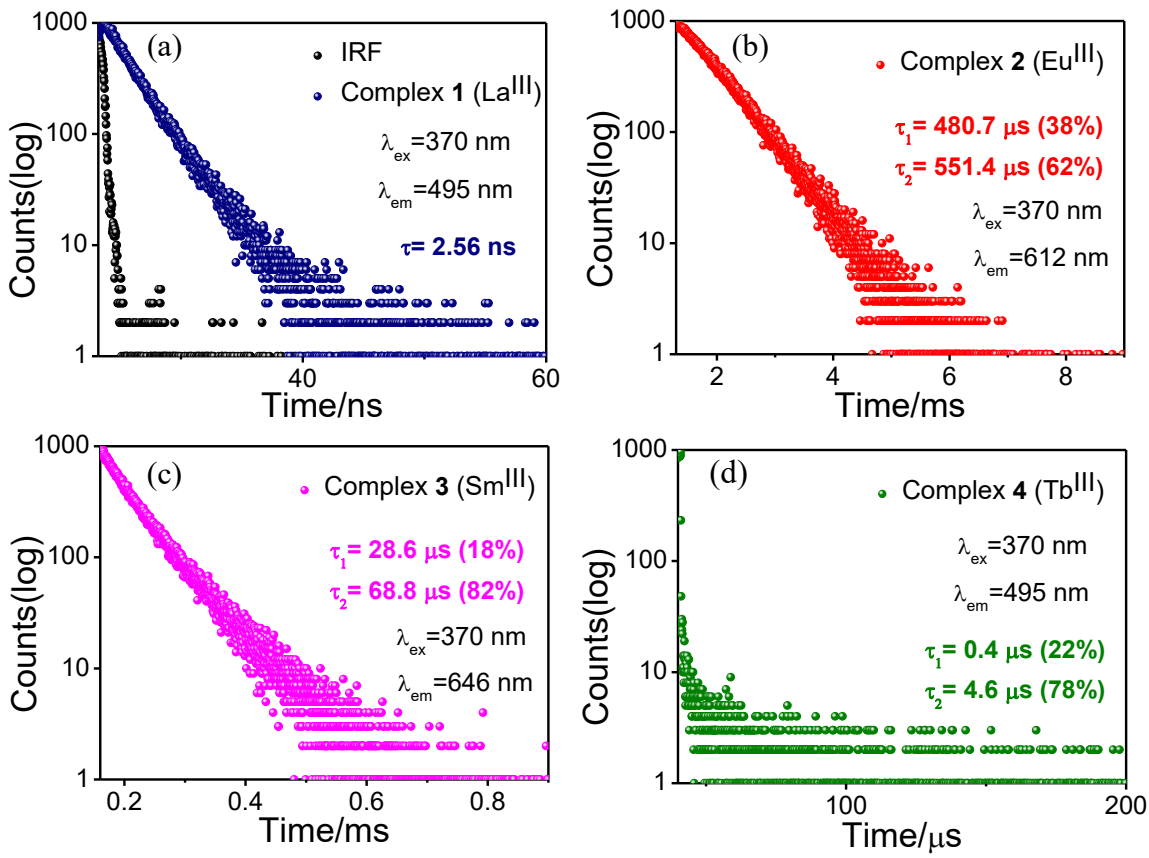

Figure 5.19. Luminescence decay profiles of complex **1-4** (a-d) in dried acetonitrile at RT.

transfer from the Tb^{III} center and deactivation via the ligand center. But upon cooling down to 77K, a huge improvement in emission characteristics is noticed with regard to radiative deactivation via the Tb^{III} center. Apart from substantial intensification of the characteristic emission peaks (corresponding to intra-configurational $^5D_4 \rightarrow {}^7F_{6\text{-}3}$ transitions for Tb^{III}) (Figure 5.20a), the lifetime also increases to a remarkably high value (τ_1=219.0 μs and τ_2=604.8 μs), upon lowering the temperature to 77K (Figure 5.20b). Noteworthy to mention here that all three Ln^{III}-centred lifetimes contain two components, indicating two asymmetrical emissive Ln^{III} centres, which is actually in line with the coordination scope of the heteroditopic bridging ancillary ligand. The longer components are arising probably from the tpy-coordinated Ln^{III} centres, as there is a better possibility of shielding the Ln^{III} centres from solvent quenching.

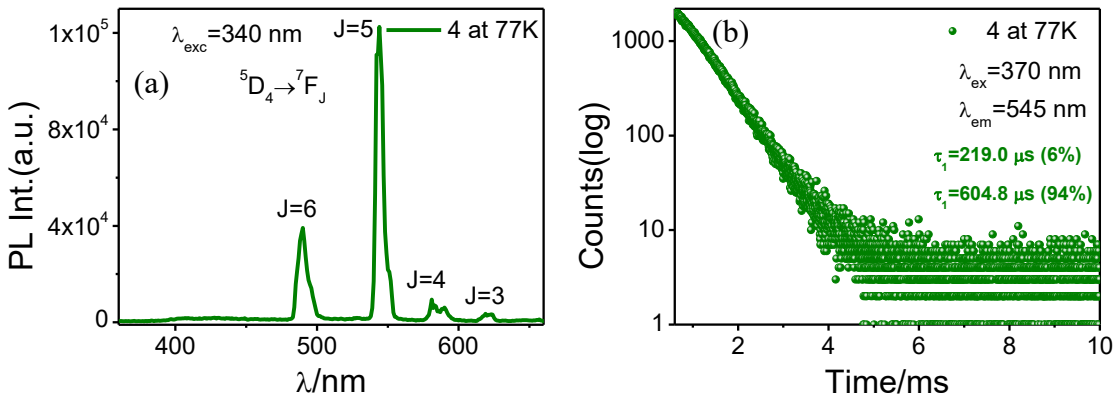

Figure 5.20. Steady-state emission spectrum and excited-state decay profile for complex **4** in glassy ethanol at 77 K.

5.3.8. Thermosensing as well as Thermochromic Behaviors of the Complexes. Taking advantage of their distinctive luminescence responses, we are interested in exploring the thermosensitive luminescence behavior of the complexes along with the phen-Hbzim-tpy ligand. To this end, both steady-state and time-resolved luminescence spectral measurements are conducted with the acetonitrile solutions of the compounds upon varying the temperature between 273 K and 353 K with an interval of 10 K.

In case of the free ligand, upon gradual increase in temperature, a systematic rise in the ligand-centered emission takes place together with a blue shift of emission maximum from 445 nm to 435 nm (Figure 5.21a). A small but finite increase in lifetime from 2.10 ns to 2.36 ns also takes place upon temperature increase (Figure 5.21b). The observed phenomena are quite contrary to expectation, wherein the emission intensity and lifetime usually decrease

upon the increase in temperature because of thermal quenching or solvent viscosity effect. The trend observed here is only possible if the population of the lowest emitting excited singlet state (S_1) of the ligand gets considerably enhanced.

We are now interested in investigating the temperature-dependent emission spectral responses of the complexes. The observed behavior of La(III) complex (**1**) is found to be just the opposite of that of the free phen-Hbzim-tpy ligand. Here, a systematic decrease in emission intensity together with a small blue shift of emission maximum from 500 nm to 490

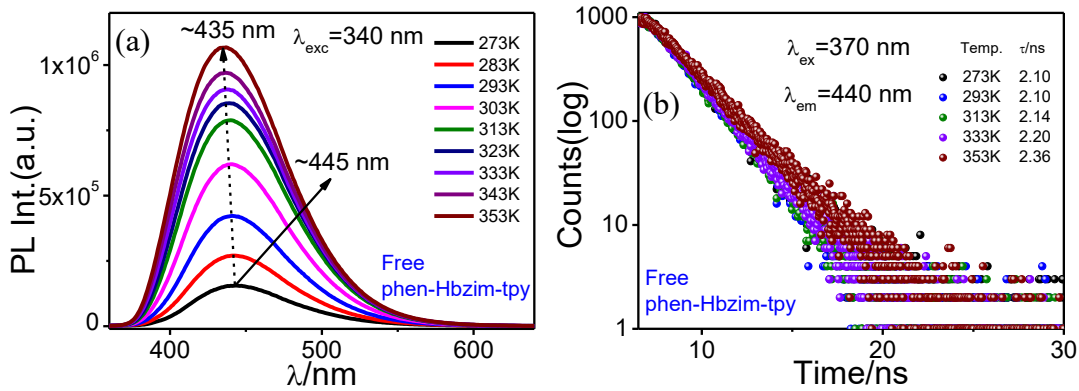

Figure 5.21. Changes in photoluminescence (a) (λ_{ex}=340 nm) and lifetime (b) at λ_{em}=440 nm of free phen-Hbzim-tpy in Acetonitrile upon varying temperature.

nm occurs upon gradual increase in temperature (Figure 5.22a). The successive emission spectrum also passes through an isoemissive point at ~442 nm. But, in case of both Eu(III) (**2**) and Sm(III) (**3**) complexes, a systematic decrease in metal-centered emission takes place upon gradual increase in temperature (Figure 5.22b and 5.22c). At the same time, the ligand-centered emission is found to increase in both cases, albeit to different extents, accompanied by a small blue shift of the emission maximum. Notably, the extent of change for the Eu(III)-centered emission at ~615 nm is found to be more marked relative to that of the Sm(III)-centered emission at ~646 nm. In case of Tb(III)-complex (**4**), again systematic increase in ligand-centered emission is noticed along with a blue shift (~465 nm to ~440 nm) but the extent of change for the Tb^{III}-centered emission at ~545 nm is almost negligible (Figure 5.22d). Hence, except for the La-complex, the observations on temperature-dependent emission spectral responses of the complexes are quite similar to that of the free ligand, as far as the ligand-centered emission is concerned.

It is quite interesting to note that both Eu(III) and Sm(III) complexes can exhibit ratiometric sensing efficacy, wherein a gradual decrease in metal-centered emission with concomitant intensification of ligand-centered emission, accompanied by a small blue shift, takes place. Among the diverse fluorescent thermometers (FTs), ratiometric FTs (RFTs) are believed to be the most dependable. Instead of monitoring the fluorescence intensity at a particular wavelength, they employ the ratio of fluorescence intensities at two different wavelengths to measure the temperature. It is also important to note that RFTs are insensitive to different factors, viz., dye concentration, excitation light intensity, and autofluorescence.

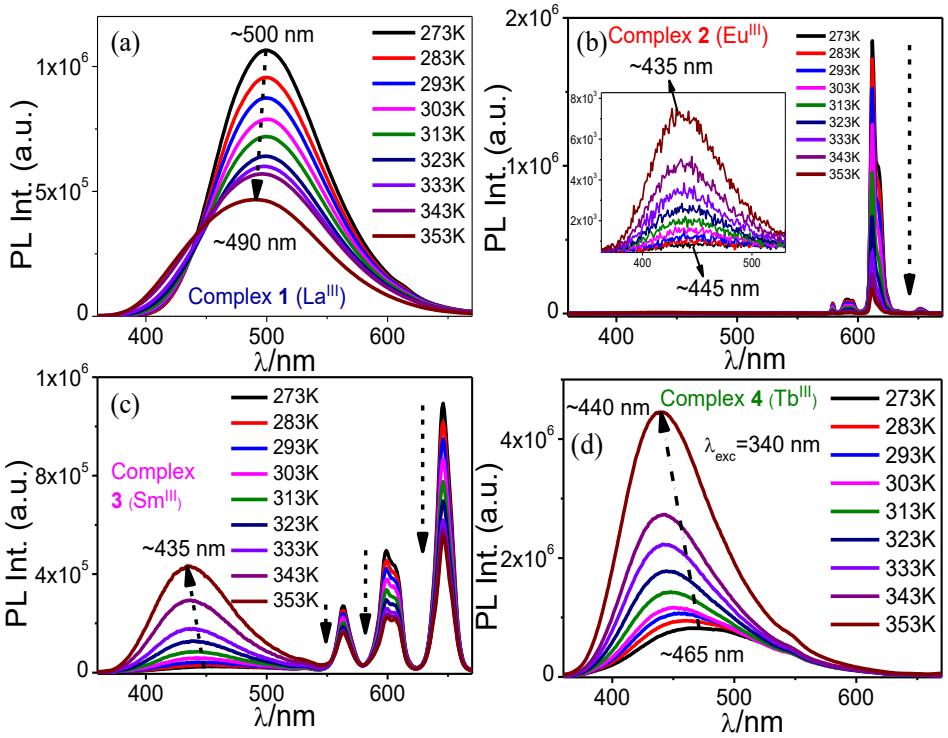

Figure 5.22. Changes in photoluminescence (λ_{ex}=340 nm) profiles of all four complexes (a-d) in Acetonitrile upon varying temperature.

However, it is interesting to note that the present lanthanide complexes not only exhibit thermo-sensitive luminescence properties but also display remarkable thermochromic behaviors (except the La-complex) within the temperature range of investigation. The emitting colors, as depicted in the corresponding Commission Internationale de l'Éclairage (CIE) plots, are found to switch from red (at 273 K) to violet (at 353 K) for the Eu^{III} (**2**) complex (Figure 5.23a); orange (273 K) to violet (323 K) to blue (353 K) for Sm^{III} complex (**3**) (Figure 5.23b), and from blue (273 K) to green (343 K) in case of Tb^{III} complex (**4**) (Figure 5.23c).

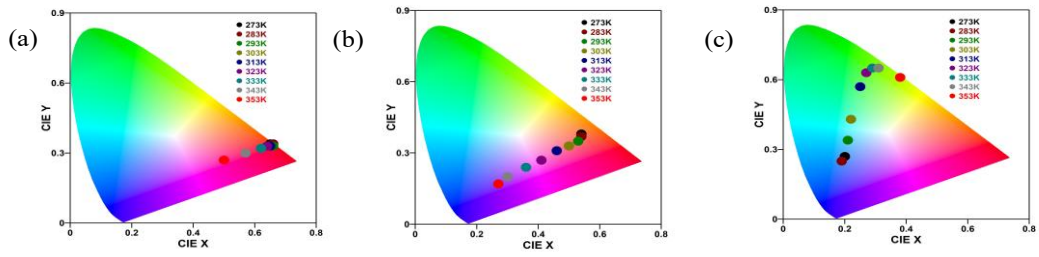

Figure 5.23. CIE chromaticity diagrams depicting the changes in emitting colors of complexes **2** (a), **3** (b), and **4** (c) (λ_{ex}=340 nm) in Acetonitrile upon varying temperature.

We also monitor the effect of temperature on the excited-state lifetimes of the complexes. In line with steady state behavior, a small but systematic drop in lifetime (2.66 ns to 2.23 ns) is noticed for the La(III) complex (**1**) (Figure 5.24a). On the other hand, in line with free phen-Hbzim-tpy, the lifetime of the ligand-centered emission (at 440 nm) for all the three remaining complexes is found to increase, albeit to a very small extent [2.12→2.33 ns for Eu(III) (**2**) (Figure 5.24b); 2.10→ 2.32 ns for Sm(III) (**3**) (Figure 5.24c) and 2.01→2.30 ns for Tb(III) (**4**) (Figure 5.24d)]. The notable observation here is that the response for complex **1** (La^{III}) is just opposite to the free ligand, as well as the other three complexes, just like the steady-state emission responses discussed in the earlier section.

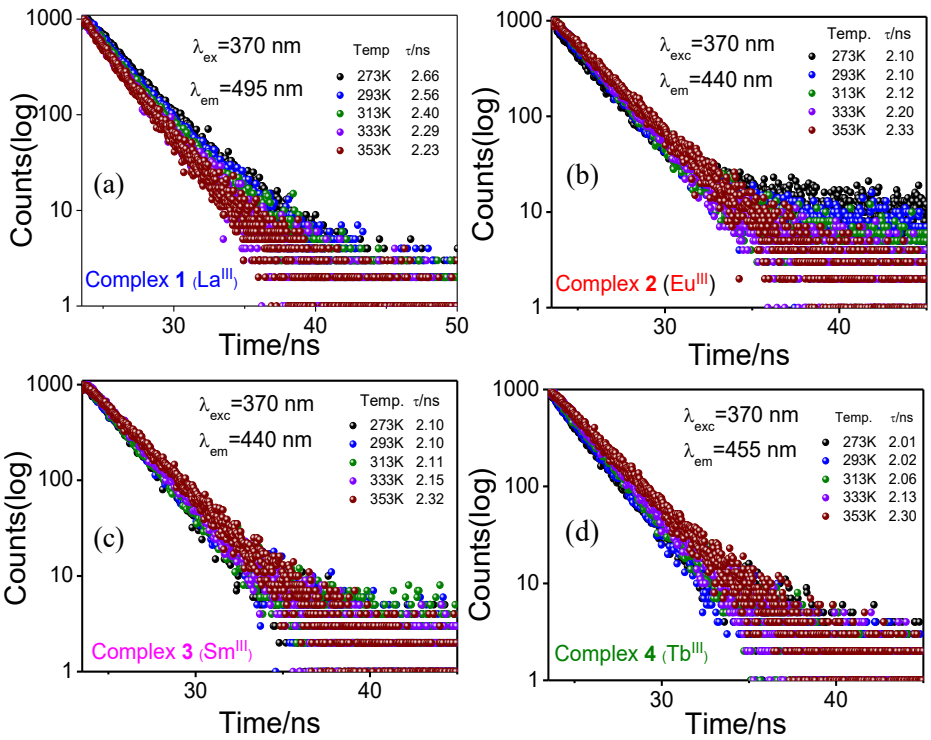

Figure 5.24. Changes in lifetime of the ligand-centered emission at λ_{em}=440 nm of all four complexes (a-d) in Acetonitrile upon varying temperature.

The observations with regard to Ln^{III}-centered decay profiles for the Eu and Sm-complexes as a function of temperature, monitored at their respective electric dipole transition wavelengths, are also worth mentioning. All the decay profiles are well-fitted with bi-exponential functions. Upon increasing the temperature up to 353 K, the lifetime values are found to fall systematically from τ_1=418.6 μs (23%), τ_2=650.2 μs (77%) to τ_1=75.0 μs (25%), τ_2=167.6 μs (75%) for Eu^{III} (**2**) (Figure 5.25a) and from τ_1=32.2 μs (12%), τ_2=73.4 μs (88%) to τ_1=17.8 μs (26%), τ_2=59.1 μs (74%) for Sm^{III} (**3**) (Figure 5.26a) , in line with their steady-state behaviors. This may be attributed to the traditional thermal quenching. But, more interestingly, it is observed that after reaching 353 K, when we cool down to 273 K, they again revert back to their initial or original decay profiles at 273 K with the lifetime values of τ_1=431.1 μs (23%), τ_2=651.0 μs (77%) for complex **2** (Figure 5.25b) and τ_1=28.8 μs (12%), τ_2=74.6 μs (88%) for complex **3** (Figure 5.26b).

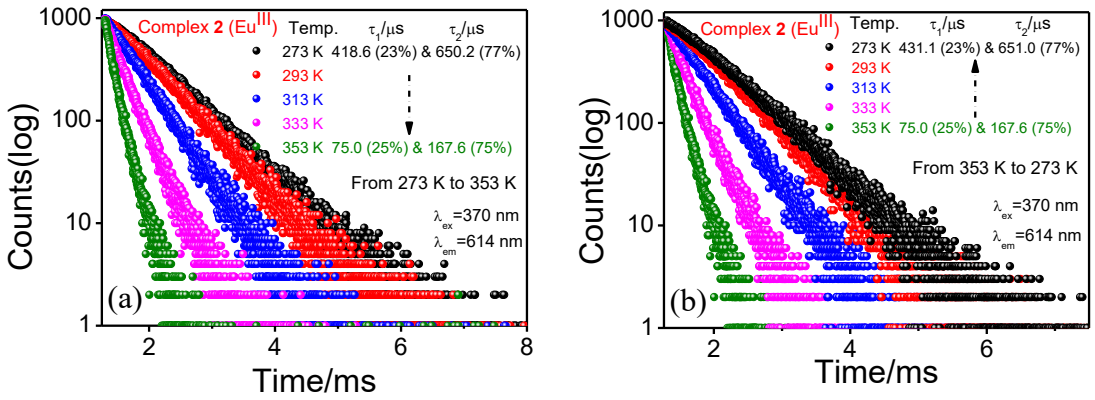

Figure 5.25. Changes in lifetime of the Eu^{III}-center (λ_{em}=614 nm) of complex **2** in acetonitrile upon varying temperature from 273 K to 353 K (a) and from 353 K to 273 K (b).

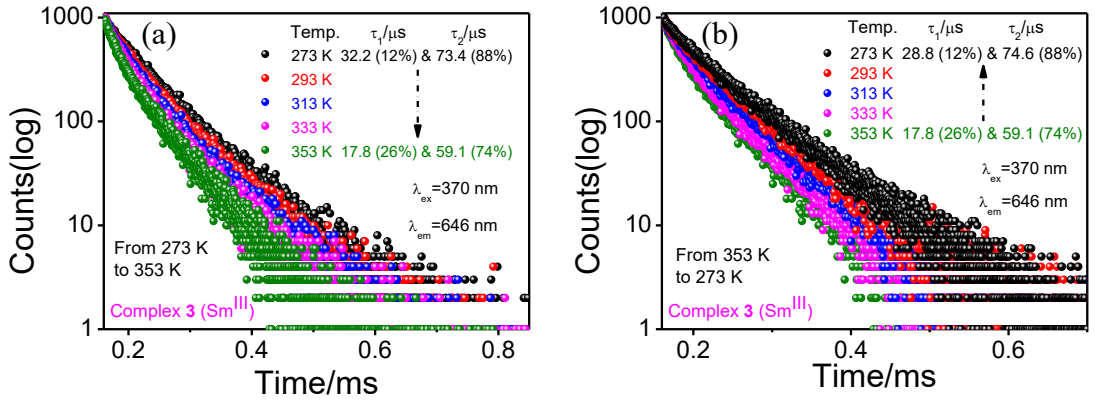

Figure 5.26. Changes in lifetime of the Sm^{III}-center (λ_{em}=646 nm) of complex **3** in acetonitrile upon varying temperature from 273 K to 353 K (a) and from 353 K to 273 K (b).

It is also noteworthy to mention that for all the four complexes, the profiles obtained in both steady-state and time-resolved emission spectroscopic measurements, after heating up to 353 K from 273 K followed by cooling down from 353 K to 273 K, resemble well with their respective original or initial profiles at 273 K. This not only makes these processes repeatable and reproducible but also suggests the retention of structural integrity of the complexes within the said temperature domain.

We are also interested in assessing the thermosensing efficacy of the complexes. To this end, we proposed a new temperature-dependent parameter (Δ) wherein two well-known thermosensing efficacy parameters, viz. relative thermosensitivity (S_r) and temperature resolution or uncertainty (δT) are taken into consideration (Equations 5.2,5.3). Herein, Δ is defined as the ratio of the ligand-centered emission intensity and its lifetime [I_{ligand}(T)/τ_{ligand}(T)], monitoring at the same wavelength and at a particular temperature.

$$\Delta_1 = \frac{I_L}{\tau_L} \quad \text{.. (5.2)}$$

We have also considered a commonly used thermometric parameter, defined as the ratio of intensity of the electric dipole (ED) transition as well as the ligand-centered band, [I_{ED}(T)/I_{ligand}(T)], at a particular wavelength and temperature.

$$\Delta_2 = \frac{I_1}{I_2} \quad \text{.. (5.3)}$$

This parameter is monitored for the cases of Eu^{III}, Sm^{III}, and Tb^{III}-complexes. The variation of both the Δ parameters as a function of temperature for all the four complexes is displayed in Figures 5.27-5.32 along with their best-fitted equations and corresponding correlation coefficients (R^2). Upon monitoring I_{ligand}(T)/τ_{ligand}(T), the S_r and δT values are found to be 1.01 and 0.09 for **1**; 3.2 and 0.06 for **2**; 7.2 and 0.03 for **3**; and 2.16 and 0.01 for **4**, respectively (Table 5.7). On the other hand, if we monitor I_{ED}(T)/I_{ligand}(T), the values for the same become 11.9 and 0.02 for **2**; and 4.6 and 0.06 for **3**, respectively. We would like to point out at this stage that among the hitherto reported Ln^{III}-based thermosensors, Eu^{III} is found to be mostly used, Tb^{III} is in distant second position, and Sm^{III} is just in the beginning stage, whereas La^{III} is hardly utilized for this purpose. Interestingly, all of the four Ln^{III} ions in the present study are found to be very efficient in demonstrating their thermosensing efficacy. A comparison of the thermosensing efficacy of earlier reported discrete Ln^{III} complexes, together with the present dinuclear complexes, is provided in Table 5.8.

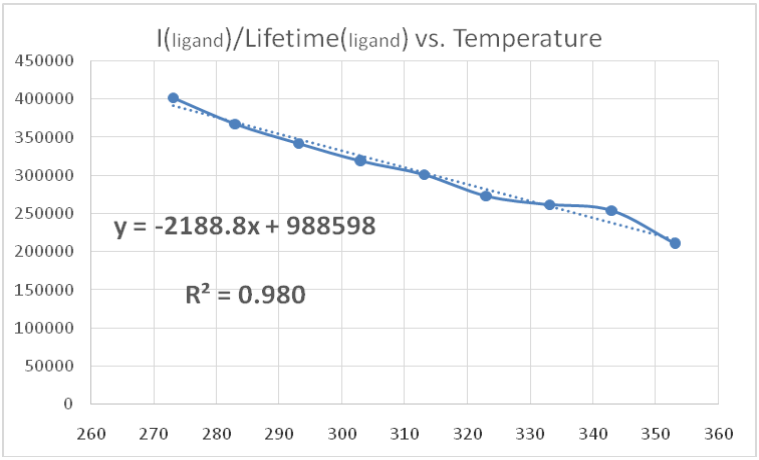

Figure 5.27. Change in the ratio Δ (I_{ligand}/τ_{ligand}) *vs* T of complex **1** in acetonitrile upon variation of temperature. The dotted line represents the best-fitted curve.

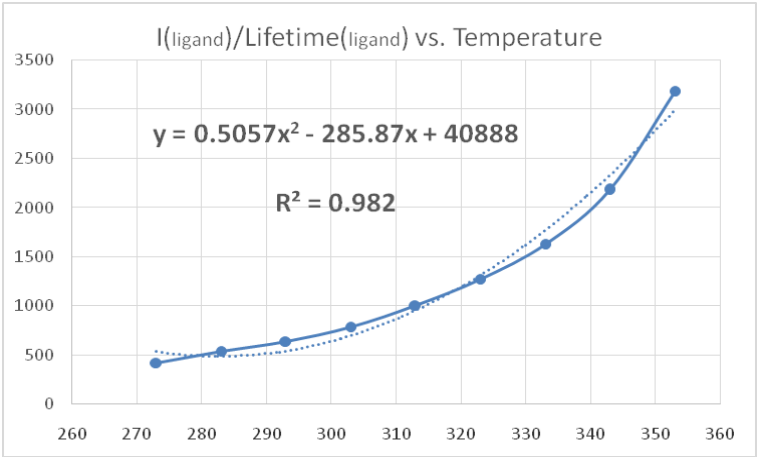

Figure 5.28. Change in the ratio Δ (I_{ligand}/τ_{ligand}) *vs* T of complex **2** in acetonitrile upon variation of temperature. The dotted line represents the best-fitted curve.

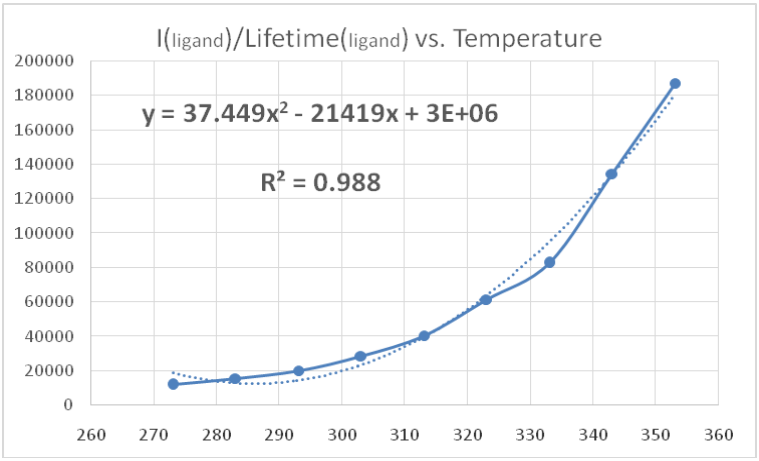

Figure 5.29. Change in the ratio Δ (I_{ligand}/τ_{ligand}) *vs* T of complex **3** in acetonitrile upon variation of temperature. The dotted line represents the best-fitted curve.

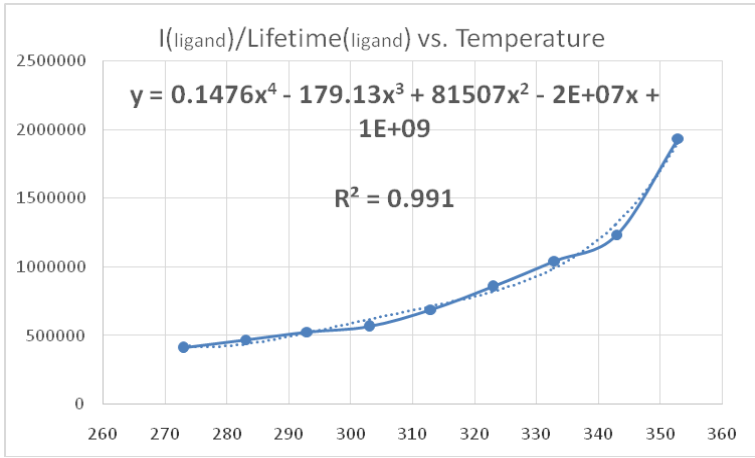

Figure 5.30. Change in the ratio Δ (I_{ligand}/τ_{ligand}) *vs.* T of complex **4** in acetonitrile upon variation of temperature. The dotted line represents the best-fitted curve.

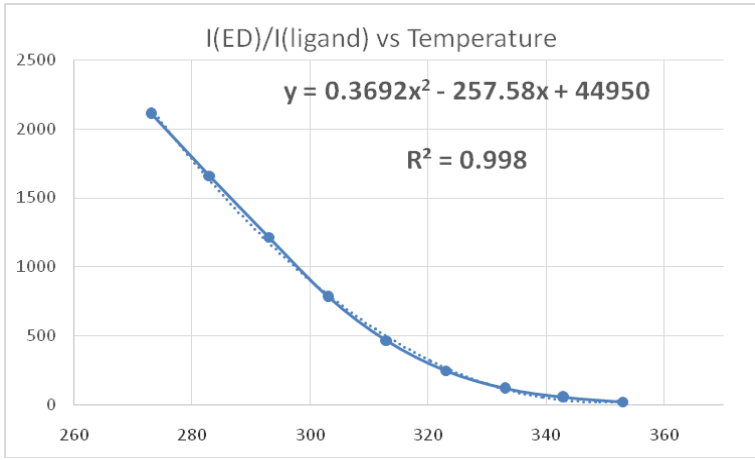

Figure 5.31. Change in the ratio Δ (I_{ED}/I_{ligand}) *vs.* T of complex **2** in acetonitrile upon variation of temperature. The dotted line represents the best-fitted curve.

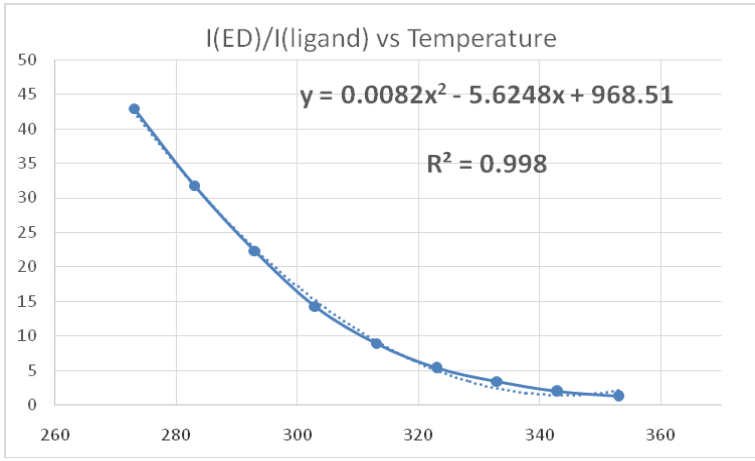

Figure 5.32. Change in the ratio Δ (I_{ED}/I_{ligand}) *vs.* T of complex **3** in acetonitrile upon variation of temperature. The dotted line represents the best-fitted curve.

Table 5.7. Thermometric and Thermosensing Efficacy Parameters for All Four Thermosensor Complexes (1-4) in the Temperature Domain of 273 K - 343 K

Comple	I_{ligand}/τ_{ligand}		I_{ED}/I_{ligand}	
	S_m ($\%K^{-1}$)	T_m	S_m ($\%K^{-1}$)	T_m
1	1.01	353 K	-	-
2	3.2	313 K	**11.9**	343 K
3	**7.2**	343 K	4.6	323 K
4	2.16	353 K	-	-

Table 5.8. Comparison of the Thermosensing Efficacy among Earlier Reported Ln^{III}-Based Discrete Molecules with this Work

Complex	S_m ($\%K^{-1}$)	ΔT (K)	T_m (K)	Optical Parameter	Ref.
Mononuclear Discrete Thermosensors					
$Eu(DBM)_3L$-mCF_3; HDBM=Dibenzoylmethane L=imidazo-bipyidyl ligand	4.9	303–460	323	Intensity ratio	49
$Eu(bzac)_3(H_2O)_2$; Hbzac= 1-phenyl-1,3-butanedione	5.25	83–303	303	Area	50
$Eu(CPDK_{3\text{-}5})_3$phen; $CPDK_{3\text{-}5}$=1-(4-(4-propylcyclohexyl)phenyl)octane-1,3-dione and phen=1,10-phenathroline)	1.2	298-348	298	Lifetime	51
$Eu(tta)_3$(pyphen); tta= 2-thenoyltrifluoroacetonate and pyphen= pyrazino[2,3-f][1,10]phenanthroline	1.98	83–303	323	Lifetime	52
$Sm(fod)_3$bath; fod=anion of 6,6,7,7,8,8,8- heptafluoro-2,2-dimethyl-3,5-octanedione bath=4,7-diphenyl-1,10-phenanthroline	1.14	50-350	60	Intensity	53
$(Eu(HL)_2Cl$ Eu(L)(HL); H_2L=2-(tosylamino)-benzylidene-N-benzoylhydrazone	5.1 7.7	77-298 80-260	185 85	Intensity ratio	55
$Eu(tta)_3$(tpy-HImzphen); Htta=2-thenoyltrifluoroacetone tpy-HImzphen= 2-(4-[2,2':6',2''] terpyridin-4'-yl-phenyl)-1H-phenanthro[9,10-d]imidazole)	5.78 3.36	273–343 273–333	343 333	Intensity ratio Lifetime	57 (this group)
$Eu(hfa)_3$(tpy-HImzphen); Hhfa=hexafluoroacetylacetone tpy-HImzphen= 2-(4-[2,2':6',2''] terpyridin-4'-yl-phenyl)-1H-phenanthro[9,10-d]imidazole)	12.52	273–353	353	I_{ED}/τ_{ED}	33 (this group)
Dinuclear Discrete Thermosensors					
$Eu_2(tta)_6(pyrzMO)_2$	7.1	223-373	353	Area	54
$Eu_2(dbm)_6(pyrzMO)_2$	4.9		373		
$Eu_2(bta)_6(pyrzMO)_2$	7.4		373		
$Eu_2(hfa)_6(pyrzMO)_2$	4.1		363		
$Eu_2(tta)_6(bipyMO)_2$	4.8		363		
$Eu_2(dbm)_6(bipyMO)_2$	4.9		343		
$Eu_2(bta)_6(bipyMO)_2$	3.4		373		
$Eu_2(hfa)_6(bipyMO)_2$	3.2		373		

PSS[Tb_2(TCA4)$_2$] PSS[Tb_2(TCA3)$_2$] TCA=thiacalix[4]arenes; 4= tetrabrominated 3=dibrominated	5.25 2.96	293–333	-	Intensity	56
$La_2(tta)_6$(phen-Hbzim-tpy) $Eu_2(tta)_6$(phen-Hbzim-tpy) $Sm_2(tta)_6$(phen-Hbzim-tpy) $Tb_2(tta)_6$(phen-Hbzim-tpy)	1.01 3.2 7.2 2.16	273-353	353 313 343 353	I_{lig}/τ_{lig}	This work
$Eu_2(tta)_6$(phen-Hbzim-tpy) $Sm_2(tta)_6$(phen-Hbzim-tpy)	11.9 4.6	273-353	343 323	I_{ED}/I_{ligand}	This work

5.3.9. Discussions on Plausible Temperature-Dependent Events. We are now interested to understand the reason behind these temperature-dependent spectral and lifetime alterations. To this end, we have considered several temperature-dependent phenomena, like the solvent viscosity effect; involvement of locally excited (LE), intramolecular charge transfer (ICT or here ILCT), twisted ICT state (TICT), and TADF. At first, we focus on the solvent viscosity effect. It is a very well-known fact that the viscosity of a solvent drops with increasing temperature. As a result, the molecules dissolved in that particular solvent get more freedom to rotate, vibrate, or twist easily, leading to facile deactivation via non-radiative pathways. Hence, the emission intensities as well as lifetimes of the corresponding compounds are expected to decrease systematically. But except the La-complex, we observe gradual intensification of emission bands as well as enhancement in lifetimes, which leads us to surmise that a simple solvent viscosity effect is not the dominant factor here. TICT could also be a common possibility here. But one would observe a red shift of the emission bands upon temperature enhancement. Here, in each case, a blue shift of ~10 nm is observed. So, TICT also does not seem applicable in the present cases. The blue shift in all the cases here can be attributed to the suppression of ICT nature, along with more LE-type emission with increasing temperatures. This is possible when a molecule possesses mixed LE-ICT character. Besides, it is also well-known for an ICT-type molecule that its polar excited state is less stabilized by a polar solvent at elevated temperatures (solvent stabilization or reorientation). This very phenomenon can also cause the blue-shifting of emission maxima for all cases. Thus, the observed sequence of events suggests the possibility of the occurrence of the TADF event in the phen-Hbzim-tpy ligand framework. Now, to have this TADF event operating, a molecule must adopt a donor-acceptor (D-A) or (D-A-D) type architecture, which in turn leads to a small energy gap between its S_1 and T_1 state. In order to have some insight, we have already executed DFT calculations. The molecular orbital analysis reveals

that the HOMO being predominantly localized on the phen-imidazole moiety (~75%) (Figure 5.15, Table 5.4), while the LUMO is primarily localized on the terpyridyl-phenyl moiety (~77%) (Figure 5.15, Table 5.4). NTO analysis also indicates a dominant HOMO→LUMO transition (ILCT, 93% contribution) (Figure 5.17). Thus, the outcomes of the computational investigations also suggest the plausibility of pronounced charge transfer between phen-imidazole donor and terpyridyl-phenyl acceptor moieties, leading to formation of a D-A type arrangement within the ligand framework. We also calculate the 'orbital overlap integral' value to quantitatively determine the spatial separation of HOMO and LUMO. It is well-known that the said value should be within 0-0.1 for a strong donor-acceptor separation, which is favourable for the occurrence of the TADF event. Herein, the observed 'orbital overlap integral' value of 0.0012 aligns well with the essential conditions for a molecule to exhibit TADF.

5.3.10. Determination of $\Delta E_{S\text{-}T}$ of phen-Hbzim-tpy Ligand. We further tend to determine the energetic positions of the lowest energy singlet and triplet states ($\Delta E_{S\text{-}T}$) of the heteroditopic ligand. The energy value of the S_1 state for phen-Hbzim-tpy is estimated to be ~3.13 eV, from the onset of the absorption spectrum.[87,88] The T_1 level of the said ligand is located at ~3.05 eV, estimated from the steady-state emission spectrum of its Gd^{III} complex at 77K (Figure 5.33).[87,88] Hence, the $\Delta E_{S\text{-}T}$ value is ~0.08 eV. The $\Delta E_{S\text{-}T}$ value (0.08 eV) for the said ligand comfortably lies within the prescribed limit (usually <0.25 eV). Hence, it is obvious that the ligand phen-Hbzim-tpy can act as a TADF-active molecule via the RISC pathway.

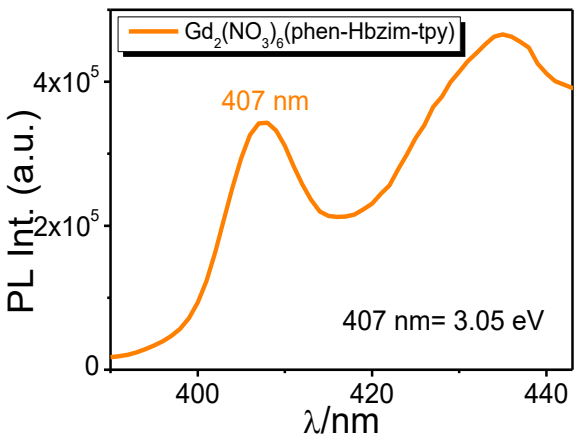

Figure 5.33. Photoluminescence spectrum of Gd^{III}-complex in glassy ethanol at 77K.

5.3.11. Measurement of Delayed Fluorescence and Lifetime. To confirm the occurrence of TADF phenomena, we further recorded the delayed fluorescence spectra (Figures 5.34a, 5.35) as well as the lifetime of all the four complexes in acetonitrile at RT (Figures 5.34b, 5.36) together with the free phen-Hbzim-tpy ligand. In our measurements, we kept the gate at 40-60 μs to exclude any prompt fluorescence. In case of the free phen-

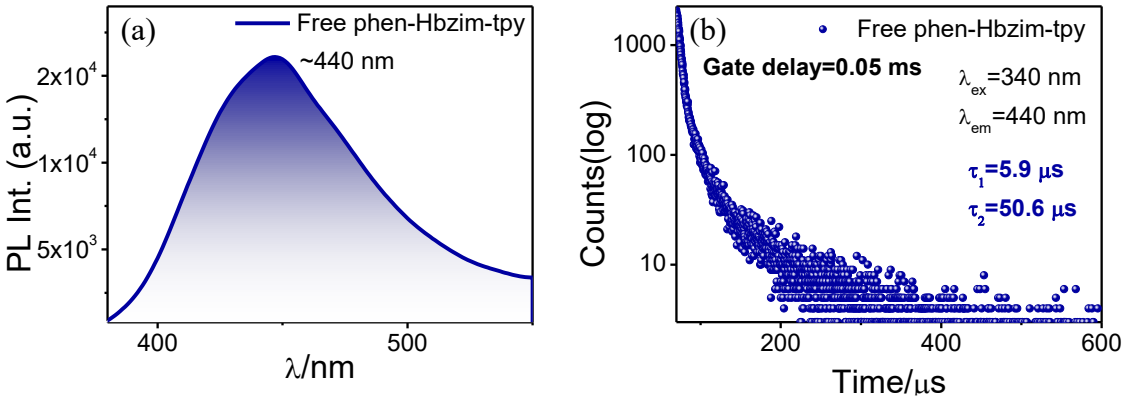

Figure 5.34. Gated emission spectrum and excited state decay profile of free phen-Hbzim-tpy (λ_{ex}=340 nm) in Acetonitrile at RT.

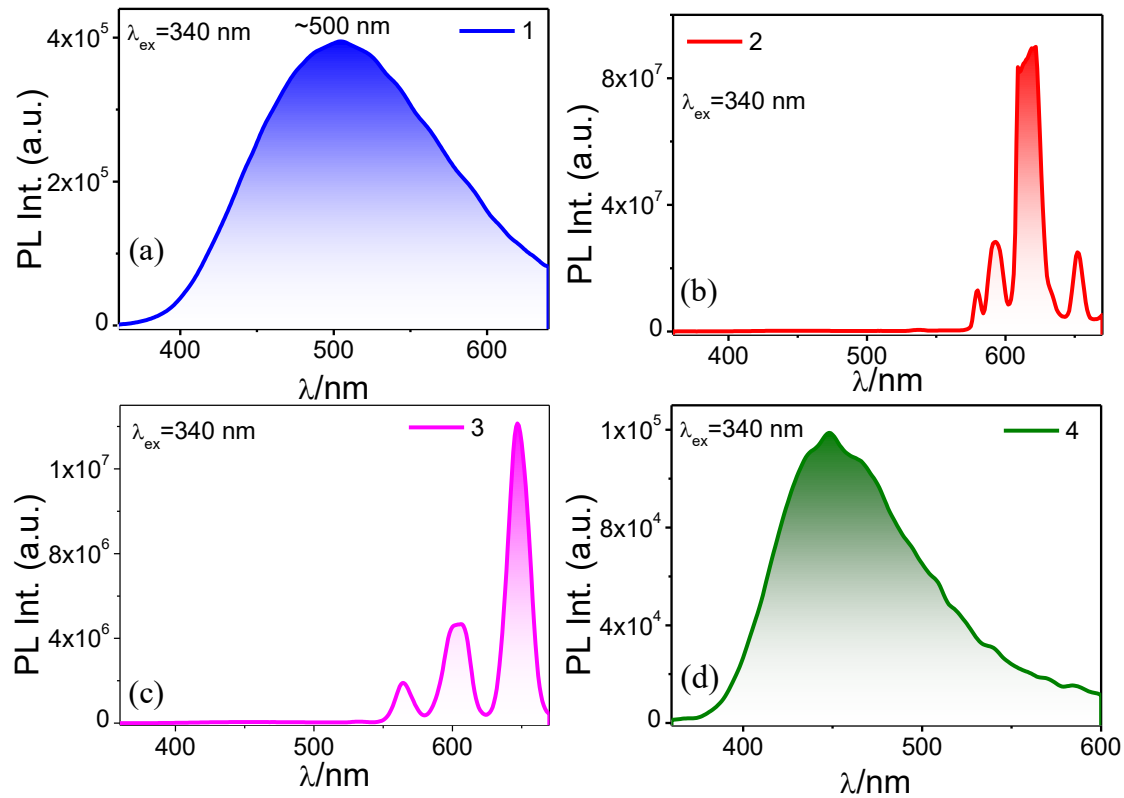

Figure 5.35. Gated emission spectra of all the four complexes (λ_{ex}=340 nm) in acetonitrile at RT.

Hbzim-tpy, we noticed a bi-exponential delayed decay upon monitoring at 440 nm. We do not know the actual reason behind this alteration from its mono-exponential nature in our usual TCSPC measurement, on maintaining the same conditions. We surmise herein that the ligand undergoes a twist at elevated temperature. The two components in the decay profile with lifetime τ_1=5.9 μs and τ_2=50.6 μs, arise probably due to the existence of phen-Hbzim-tpy in both planar and twisted conformation. The possibility of this sort of twisting, together with displaying TADF, has recently been explored in literature.[62]

Among the four studied complexes, the delayed lifetime for the La-complex is found to be much lower (τ_1=8.1 μs, τ_1=8.4 μs) (Figure 5.36a) as compared to free phen-Hbzim-tpy. This observation is in line with its steady-state and time-resolved emission response. Interestingly, the remaining three complexes (Eu^{III}, Sm^{III}, and Tb^{III}) exhibit notable delayed lifetimes in the μs domain. Upon monitoring at 440 nm, all three decay profiles are found to be bi-exponential, with lifetime values of τ_1=281.1 μs, τ_1=612.4 μs for the Eu-complex (Figure 5.36b); τ_1=30.2 μs, τ_1=80.6 μs in the case of the Sm-complex (Figure 5.36c); and τ_1=8.1 μs and τ_2=71.1 μs for the Tb-complex (Figure 5.36d).

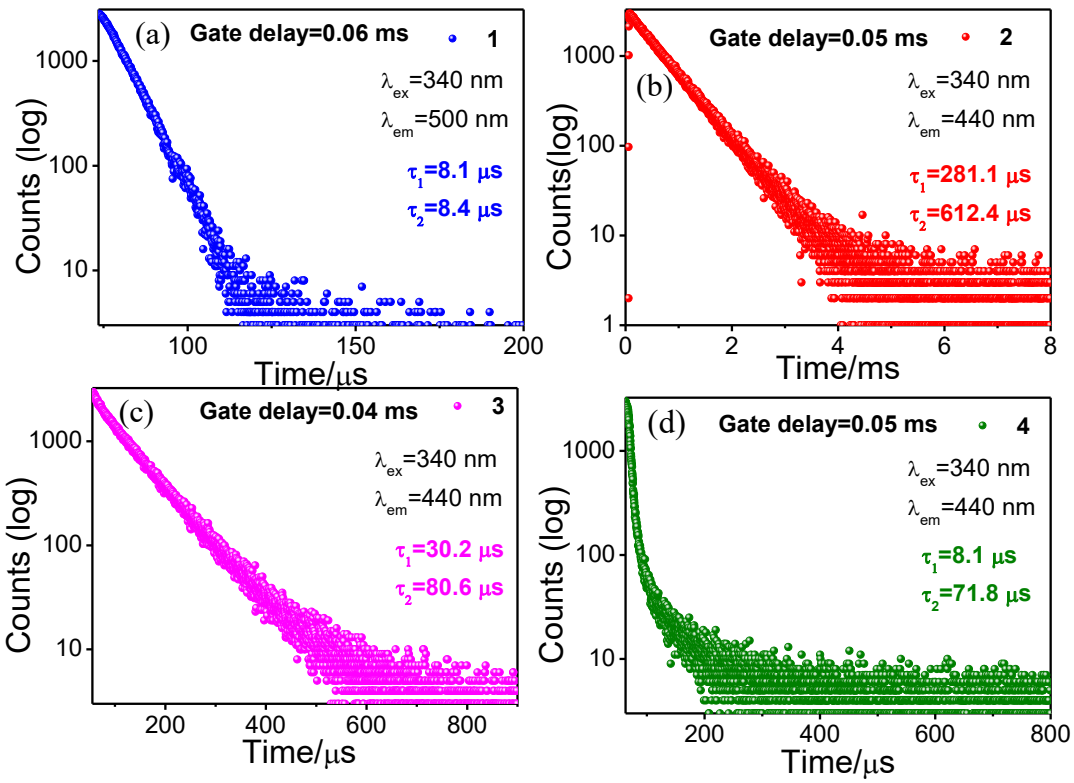

Figure 5.36. Delayed lifetime profiles for all four complexes (λ_{ex}=340 nm) in acetonitrile at RT.

5.3.12. Plausible Explanations of the Observed Luminescence as well as TADF-Assisted Thermochromic Behaviors of the Complexes. It is very well-known for the lanthanide(III) sensitization event that some empirical rules actually govern whether a sensitizer will act as an antenna or a quencher via the triplet pathway.[89,90] Firstly, the T_1 level of the sensitizer is expected to be at least ~0.31-0.50 eV higher than that of the Ln* of the coordinated Ln^{III} ion, according to Reinhoudt's empirical rule.[70] However, if by any chance, the said energy gap (between the T_1 and Ln*) happens to be <0.22 eV, back energy transfer to the sensitizer occurs instead of a fruitful lanthanide sensitization, according to Latva's empirical rule.[30] Now, the lowest-lying emitting excited level (Ln*) of Eu^{III} ($^5D_0$), Sm^{III} ($^4G_{5/2}$), and Tb^{III} ($^5D_4$) is located at ~2.14 eV, ~2.22 eV, and ~2.54 eV, respectively, whereas the position of the T_1 state of tta ligand is situated at ~2.60 eV, as reported in the literature. Hence, Eu^{III} {Δ(Eu*-T_1)=~0.47 eV} and Sm^{III} {Δ(Sm*- T_1)=~0.40 eV} possess the prescribed energy gap as mentioned above, while for Tb^{III} {Δ(Tb*-T_1)=~0.06 eV}, the observed energy barrier is favourable for thermo-assisted back energy transfer to the T_1 of tta, leading to non-radiative deactivation. The higher T_1 level position of phen-Hbzim-tpy (~3.05 eV) is too safe to induce a detrimental impact on effective sensitization. So, the extent and direction of the energy transfer process are now solely dependent on the T_1 level position of the antenna tta. Thus, we are observing the occurrence of almost complete energy transfer phenomenon in case of the Eu^{III} complex (**2**) due to fulfilling all the required conditions; substantial but incomplete energy transfer in case of Sm^{III} complex (**3**) as the energy gap here is somewhat on the marginal side, as well as due to multi-phonon relaxation; but only the ligand-centered emission for Tb^{III} complex (**4**) due to the back-energy transfer process.

We now delve into the thermosensitive luminescence responses of the complexes. In case of La^{III} complex (**1**), the T_1 state of tta (~2.54 eV) is located at a much lower position than that of phen-Hbzim-tpy (~3.05 eV). On the other hand, the $\Delta E_{S\text{-}T}$ value for phen-Hbzim-tpy (0.08 eV) is within the prescribed range of TADF. As a result, the triplet excitons of phen-Hbzim-tpy encounter two opposing forces, i.e., (i) RISC leading to TADF and (ii) Dexter-type triplet-triplet energy transfer (TET) leading to thermal quenching. It is obvious from the corresponding energetic values that the T_1 state of tta can act as a quencher state for triplet excitons of phen-Hbzim-tpy, especially in case of the La-complex, as the latter excitons do not seem to have any other way to be transferred. Thus, the Dexter quenching via TET may be responsible for the systematic drop in emission intensity and lifetime value for complex **1** upon the rise in temperature. For the rest of the complexes, the ligand-centered

emission peak gets intensified upon an increase in temperature. Had there been only Eu^{III}, this phenomenon might have been attributed to ligand-to-metal charge transfer (LMCT) state-mediated back energy transfer to S_1[59,60] of phen-Hbzim-tpy since the involvement of the low-lying LMCT state is quite common in Eu^{III}-complexes owing to its very low reduction potential for Eu^{III}/Eu^{II} couple (-0.35 V).[60,91,92] But, for Sm^{III} or Tb^{III} and even for free phen-Hbzim-tpy, the phenomenon of intensification for the ligand-centered emission peak upon temperature elevation remains similar. This drives us to surmise that thermally activated delayed fluorescence (TADF) may be a common possibility here, which is thoroughly supported by the estimated $\Delta E_{S\text{-}T}$ value of phen-Hbzim-tpy, the DFT study, the delayed luminescence, as well as the delayed decay profiles. However, in terms of the Ln^{III}-centered luminescence intensity variation, the Eu^{III}-complex exhibits the greatest extent of alteration. This may be attributed to the additional involvement of the LMCT state, which leads to a non-radiative deactivation, causing a detrimental impact on the transferred energy from the ligand to the Eu^{III} center.[59,60,93] That is why the thermosensing performance of the Eu complex appears to be the best among the four present complexes. Finally, the tuneable dual-emissive nature of Eu, Sm, and Tb complexes, along with this TADF phenomenon, result in remarkable thermochromism while exploring within the temperature range 273 K-353 K. A tentative energy level diagram is also presented below, which depicts the plausible energy transfer pathways along with the possibility for the occurrence of TADF (Scheme 2).

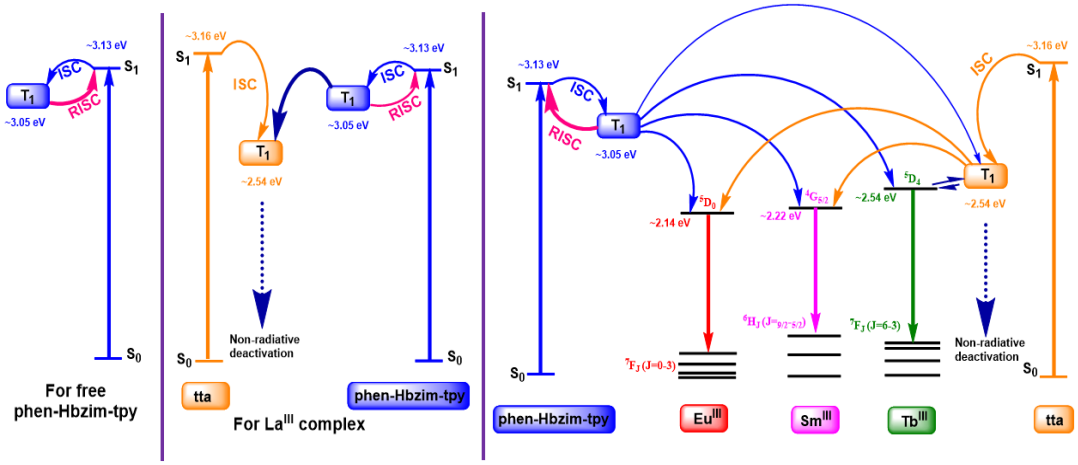

Scheme 5.2 Tentative Energy Level Diagram and Plausible Energy Transfer Pathways

5.4. Conclusion

A new array of four bimetallic lanthanide complexes comprising La^{III}, Eu^{III}, Sm^{III}, and Tb^{III}, has been designed in this work by employing a heteroditopic phenanthroline-terpyridine type

bridging ligand, and thorough investigations of their absorption and both steady-state and time-resolved emission spectroscopic behaviors have been conducted. All four complexes were found to exhibit excellent thermo-responsive luminescence attributes. Interestingly, the bridging ligand displayed thermally activated delayed fluorescence (TADF). Among the resulting four complexes, the La-complex could not sustain the TADF phenomenon, probably due to Dexter quenching. On the other hand, the remaining three complexes were found to secure the TADF event, just like the free bridging ligand phen-Hbzim-tpy. Moreover, these three complexes manifested excellent thermosensing and remarkable thermochromism properties owing to this TADF event and their respective dual-emissive nature. To the best of our knowledge, this is the first report of TADF-assisted thermosensing and thermochromism from Ln^{III}-based discrete molecules. Hence, TADF can unveil a new genre in the luminescence thermometry domain for the lanthanide(III) complexes via judicious incorporation of the bridging ancillary ligands.

5.5. References

1. Bünzli, J.-C. G. On the Design of Highly Luminescent Lanthanide Complexes. *Coord. Chem. Rev.* **2015**, *293*, 19–47.
2. Hasegawa, Y.; Wada, Y.; Yanagida, S. Strategies for the Design of Luminescent Lanthanide(III) Complexes and Their Photonic Applications. *J. Photochem. Photobiol., C* **2004**, *5*, 183–202.
3. Armelao, L.; Quici, S.; Barigelletti, F.; Accorsi, G.; Bottaro, G.; Cavazzini, M.; Tondello, E. Design of Luminescent Lanthanide Complexes: From Molecules to Highly Efficient Photo-Emitting Materials. *Coord. Chem. Rev.* **2010**, *254*, 487–505.
4. Parker, D.; Fradgley, J. D.; Wong, K.-L. The Design of Responsive Luminescent Lanthanide Probes and Sensors. *Chem. Soc. Rev.* **2021**, *50*, 8193–8213.
5. Swavey, S.; Swavey, R. Dinuclear and Polynuclear Lanthanide Coordination Complexes Containing Polyazine Ligands: Synthesis and Luminescent Properties. *Coord. Chem. Rev.* **2009**, *253*, 2627–2638.
6. Feng, J.; Zhang, H. Hybrid Materials Based on Lanthanide Organic Complexes: A Review. *Chem. Soc. Rev.* **2013**, *42*, 387–410.

7. Reddy, M. L. P.; Sivakumar, S. Lanthanide Benzoates: A Versatile Building Block for the Construction of Efficient Light Emitting Materials. *Dalton Trans.* **2013**, *42*, 2663–2678.
8. Binnemans, K. Lanthanide-based Luminescent Hybrid Materials. *Chem. Rev.* **2009**, *109*, 4283–4374.
9. de Sá, G. F.; Malta, O. L.; de Mello Donegá, C.; Simas, A. M.; Longo, R. L.; Santa-Cruz, P. A.; da Silva, E. F., Jr. Spectroscopic Properties and Design of Highly Luminescent Lanthanide Coordination Complexes. *Coord. Chem. Rev.* **2000**, *196*, 165–195.
10. Li, P.; Li, H. Recent Progress in the Lanthanide-Complexes Based Luminescent Hybrid Materials. *Coord. Chem. Rev.* **2021**, *441*, 213988–214004.
11. Wei, C.; Ma, L.; Wei, H.; Liu, Z.; Bian, Z.; Huang, C. Advances in Luminescent Lanthanide Complexes and Applications. *Sci. China Technol. Sci.* **2018**, *61*, 1265–1285.
12. Montgomery, C. P.; Murray, B. S.; New, E. J.; Pal, R.; Parker, D. Cell-Penetrating Metal Complex Optical Probes: Targeted and Responsive Systems Based on Lanthanide Luminescence. *Acc. Chem. Res.* **2009**, *42*, 925–937.
13. Aulsebrook, M. L.; Graham, B.; Grace, M. R.; Tuck, K. L. Lanthanide Complexes for Luminescence-Based Sensing of Low Molecular Weight Analytes. *Coord. Chem. Rev.* **2018**, *375*, 191–220.
14. Nehra, K.; Dalal, A.; Hooda, A.; Bhagwan, S.; Saini, R. K.; Mari, B.; Kumar, S.; Singh, D. Lanthanides β-Diketonate Complexes as Energy-Efficient Emissive Materials: A Review. *J. Mol. Struct.* **2022**, *1249*, 131531–131555.
15. Gangan, T. U.; Sreenadh, S.; Reddy, M. L. P. Visible-Light Excitable Highly Luminescent Molecular Plastic Materials Derived from Eu^{3+}-Biphenyl Based β-Diketonate Ternary Complex and Poly(Methylmethacrylate). *J. Photochem. Photobiol., A* **2016**, *328*, 171–181.
16. Shi, J.; Hou, Y.; Chu, W.; Shi, X.; Gu, H.; Wang, B.; Sun, Z. Crystal Structure and Highly Luminescent Properties Studies of Bis-β-Diketonate Lanthanide Complexes. *Inorg. Chem.* **2013**, *52*, 5013–5022.
17. Eliseeva, S. V.; Pleshkov, D. N.; Lyssenko, K. A.; Lepnev, L. S.; Bünzli, J.-C. G.; Kuzmina, N. P.; Deciphering Three Beneficial Effects Of 2,2'-Bipyridine-N,N'-

Dioxide on the Luminescence Sensitization of Lanthanide(III) Hexafluoroacetylacetonate Ternary Complexes. *Inorg. Chem.* **2011**, *50*, 5137–5144.

18. Kitagawa, Y.; Kumagai, M.; Nakanishi, T.; Fushimi, K.; Hasegawa, Y. The Role of π–f Orbital Interactions in Eu(III) Complexes for an Effective Molecular Luminescent Thermometer. *Inorg. Chem.* **2020**, *59*, 5865–5871.
19. Moudam, O.; Rowan, B. C.; Alamiry, M.; Richardson, P.; Richards, B. S.; Jones, A. C.; Robertson, N. Europium Complexes with High Total Photoluminescence Quantum Yields in Solution and in PMMA. *Chem. Commun.* **2009**, *43*, 6649–6651.
20. Khistiaeva, V. V.; Melnikov, A. S.; Slavova, S. O.; Sizov, V. V.; Starova, G. L.; Koshevoy, I. O.; Grachova, E. V. Heteroleptic β-diketonate Ln(III) Complexes Decorated with Pyridyl Substituted Pyridazine Ligands: Synthesis, Structure and Luminescence Properties. *Inorg. Chem. Front.* **2018**, *5*, 3015–3027.
21. Andreiadis, E. S.; Gauthier, N.; Imbert, D.; Demadrille, R.; Pecaut, J.; Mazzanti, M. Lanthanide Complexes Based on β-Diketonates and A Tetradentate Chromophore Highly Luminescent as Powders and in Polymers. *Inorg. Chem.* **2013**, *52*, 14382–14390.
22. He, X.; Norel, L.; Hervault, Y. M.; Métivier, R.; D'Aléo, A.; Maury, O.; Rigaut, S. Modulation of Eu (III) and Yb (III) Luminescence Using a DTE Photochromic Ligand. *Inorg. Chem.* **2016**, *55*, 12635–12643.
23. Armelao, L.; Dell'Amico, D. B.; Bellucci, L.; Bottaro, G.; Di Bari, L.; Labella, L.; Marchetti, F.; Samaritani, S.; Zinna, F. Circularly Polarized Luminescence of Silica-Grafted Europium Chiral Derivatives Prepared through a Sequential Functionalization. *Inorg. Chem.* **2017**, *56*, 7010–7018.
24. Stanley, J. M.; Zhu, X.; Yang, X.; Holliday, B. J. Europium Complexes of A Novel Ethylenedioxythiophene-Derivatized Bis(pyrazolyl)pyridine Ligand Exhibiting Efficient Lanthanide Sensitization. *Inorg. Chem.* **2010**, *49*, 2035–2037.
25. Yang, W.-Y.; Chen, L.; Wang, S. Syntheses, Structures, and Luminescence of Novel Lanthanide Complexes of Tripyridylamine, N, N, N ‘, N ‘-Tetra (2-pyridyl)-1, 4-phenylenediamine and N, N, N ‘, N ‘-Tetra (2-pyridyl) biphenyl-4, 4 ‘-diamine. *Inorg. Chem.* **2001**, *40*, 507–515.
26. Jang, H.; Shin, C. H.; Jung, B. J.; Kim, D. H.; Shim, H. K.; Do, Y. Synthesis and Characterization of Dinuclear Europium Complexes Showing Pure Red Electroluminescence. *Eur. J. Inorg. Chem.* **2006**, *2006*, 718–725.

27. Fratini, A.; Richards, G.; Larder, E.; Swavey, S. Neodymium, Gadolinium, and Terbium Complexes Containing Hexafluoroacetylacetonate and 2, 2'-Bipyrimidine: Structural and Spectroscopic Characterization. *Inorg. Chem.* **2008**, *47*, 1030–1036.
28. Zucchi, G.; Jeon, T.; Tondelier, D.; Aldakov, D.; Thuéry, P.; Ephritikhine, M.; Geffroy, B. White Electroluminescence of Lanthanide Complexes Resulting from Exciplex Formation. *J. Mater. Chem.* **2010**, *20*, 2114–2120.
29. Kalluvettukuzhy, N. K.; Maciejczyk, M. R.; Robertson, N. Thermally Activated Delayed Fluorescence Emitters for Efficient Sensitization of Europium(III). *Phys. Chem. Chem. Phys.* **2024**, *26*, 18129–18137.
30. Latva, M.; Takalo, H.; Mukkala, V. M.; Matachescu, C.; Rodríguez-Ubis, J. C.; Kankare, J. Correlation Between the Lowest Triplet State Energy Level of the Ligand and Lanthanide(III) Luminescence Quantum Yield. *J. Lumin.* **1997**, *75*, 149–169.
31. Samuel, A. P.; Xu, J.; Raymond, K. N. Predicting Efficient Antenna Ligands for Tb(III) Emission. *Inorg. Chem.* **2009**, *48*, 687–698.
32. Ahmed, T.; Chakraborty, A.; Paul, A.; Baitalik, S. Synthesis, Characterization, Luminescence Properties and Deciphering the Role of Terpyridyl-Imidazole Based Ligand on Dissimilar Luminescence Sensitization of Ternary Lanthanide(III) Tris-(β-Diketonate) Complexes. *Dalton Trans*. **2023**, *52*, 14027–14038.
33. Ahmed, T.; Chakraborty, A.; Baitalik, S. Terpyridyl-Imidazole Based Ligand Coordinated to Ln(Hexafluoroacetyl acetonate)$_3$ Core: Synthesis, Structural Characterization, Luminescence Properties, and Thermosensing Behaviors in Solution and PMMA Film. *Inorg. Chem.* **2024**, *63*, 11279–11295.
34. Zaïm, A.; Nozary, H.; Guénée, L.; Besnard, C.; Lemonnier, J. F.; Petoud, S.; Piguet, C. N-Heterocyclic Tridentate Aromatic Ligands Bound to [Ln(hexafluoroacetylacetonate)$_3$] Units: Thermodynamic, Structural, and Luminescent Properties. *Chem. Eur. J.* **2012**, *18*, 7155–7168.
35. Zhang, Z.; He, L.; Feng, J.; Liu, X.; Zhou, L.; Zhang, H. Unveiling the Relationship Between Energy Transfer and the Triplet Energy Level by Tuning Diarylethene within Europium(III) Complexes. *Inorg. Chem.* **2020**, *59*, 661–668.
36. Al-Rasbi, N. K.; Adams, H.; Suliman, F. O. Synthesis, Structure and Tunable White-Light Emission of Dinuclear Eu (III) Schiff Base Complex. *Dyes Pigm.* **2014**, *104*, 83–88.

37. Douib, H.; Gonzalez, J. F.; Speed, S.; Montigaud, V.; Lefeuvre, B.; Dorcet, V.; Riobé, F.; Maury, O.; Gouasmia, A.; Guennic, B. L.; Cador, O.; Pointillart, F. Modulation of the Magnetic and Photophysical Properties in 3d–4f and 4f–4f′ Heterobimetallic Complexes Involving a Tetrathiafulvalene-based Ligand. *Dalton Trans.* **2022**, *51*, 16486-16496.
38. Wang, Y.-J.; Wu, D.-F.; Gou, J.; Duan, Y.-Y.; Li, L.; Chen, H.-H.; Gao, H.-L.; Cui, J.-Z. Modulation of the Properties of Dinuclear Lanthanide Complexes Through Utilizing Different β-Diketonate Co-Ligands: Near-Infrared Luminescence and Magnetization Dynamics. *Dalton Trans.* **2020**, *49*, 2850–2861.
39. Fioravanti, L.; Bellucci, L.; Armelao, L.; Bottaro, G.; Marchetti, F.; Pineider, F.; Poneti, G.; Samaritani, S.; Labella, L. Stoichiometrically Controlled Assembly of Lanthanide Molecular Complexes of the Heteroditopic Divergent Ligand 4′-(4-Pyridyl)-2, 2′: 6′, 2 ″-terpyridine N-Oxide in Hypodentate or Bridging Coordination Modes. Structural, Magnetic, and Photoluminescence Studies. *Inorg. Chem.* **2022**, *61*, 265–278.
40. Dasari, S.; Maparu, A. K.; Abbas, Z.; Kumar, P.; Birla, H.; Sivakumar, S.; Patra, A. K. Bimetallic Europium and Terbium Complexes Containing Substituted Terpyridines and the NSAID Drug Tolfenamic Acid: Structural Differences, Luminescence Properties, and Theranostic Applications. *Eur. J. Inorg. Chem.* **2020**, *2020*, 2998–3009.
41. Yadav, U.; Verma, M.; Abbas, Z.; Sivakumar, S.; Patra, A. K. An Emissive Dual-Sensitized Bimetallic Eu_2^{III}-Bioprobe: Design Strategy, Biological Interactions, and Nucleolus Staining Studies. *New J. Chem.* **2022**, *46*, 16007-16018.
42. Wang, X. D.; Wolfbeis, O. S.; Meier, R. J. Luminescent Probes and Sensors for Temperature. *Chem. Soc. Rev.* **2013**, *42*, 7834–7869.
43. Brites, C. D.; Lima, P. P.; Silva, N. J.; Millán, A.; Amaral, V. S.; Palacio, F.; Carlos, L. D. Thermometry at the Nanoscale. *Nanoscale* **2012**, *4*, 4799–4829.
44. Brites, C. D.; Marin, R.; Suta, M.; Neto, A. N. C.; Ximendes, E.; Jaque, D.; Carlos, L. D. Spotlight on Luminescence Thermometry: Basics, Challenges, and Cutting-edge Applications. *Adv. Mater.* **2023**, *35*, 2302749.
45. Hasegawa, Y.; Kitagawa, Y. Thermo-sensitive Luminescence of Lanthanide Complexes, Clusters, Coordination Polymers and Metal–Organic Frameworks with Organic Photosensitizers. *J. Mater. Chem. C* **2019**, *7*, 7494–7511.

46. Bussche, F. V.; Kaczmarek, A. M.; Speybroeck, V. V.; Voort, P. V. D.; Stevens, C. V. Overview of N-Rich Antennae Investigated in Lanthanide-Based Temperature Sensing. *Chem. Eur. J.* **2021**, *27*, 7214–7230.
47. Feng, T.; Ye, Y.; Liu, X.; Cui, H.; Li, Z.; Zhang, Y.; Liang, B.; Li, H.; Chen, B. A Robust Mixed Lanthanide PolyMOF Membrane for Ratiometric Temperature Sensing. *Angew. Chem. Int. Ed.* **2020**, *59*, 21752-21757.
48. Cui, Y.; Zou, W.; Song, R.; Yu, J.; Zhang, W.; Yang, Y.; Qian, G. A Ratiometric and Colorimetric Luminescent Thermometer Over a Wide Temperature Range Based on a Lanthanide Coordination Polymer. *Chem. Commun.* **2014**, *50*, 719–721.
49. Devi, R.; Singh, K.; Vaidyanathan, S. Synergy in the Energy Transfer between Ligands and Eu^{III} Ions in Molecular Europium Complexes: Single-Component White Light-Emitting Luminogens. *J. Mater. Chem. C* **2020**, *8*, 8643–8653.
50. Gálico, D. A.; Mazali, I. O.; Sigoli, F. A. Nanothermometer Based on Intensity Variation and Emission Lifetime Of Europium(III) Benzoylacetonate Complex. *J. Lumin.* **2017**, *192*, 224–230.
51. Lapaev, D. V.; Nikiforov, V. G.; Lobkov, V. S.; Knyazev, A. A.; Galyametdinov, Y. G. Reusable Temperature-Sensitive Luminescent Material Based on Vitrified Film of Europium(III) β-Diketonate Complex. *Opt. Mater.* **2018**, *75*, 787–795.
52. Cabral, F. M.; Gálico, D. A.; Mazali, I. O.; Sigoli, F. A. Crystal Structure and Temperature Dependence of the Photophysical Properties of the $[Eu(tta)_3(pyphen)]$ Complex. *Inorg. Chem. Commun.* **2018**, *98*, 29–33.
53. Ali, A.; Ahmed, Z.; Iftikhar, K.; Uddin, R. Heteroleptic Samarium Complexes with High Quantum Yields for Temperature Sensing Applications. *Dalton Trans.* **2024**, *53*, 1105–1120.
54. Bellucci, L.; Bottaro, G.; Labella, L.; Causin, V.; Marchetti, F.; Samaritani, S.; Dell'Amico, D. B.; Armelao, L. Composition–Thermometric Properties Correlations in Homodinuclear Eu^{3+} Luminescent Complexes. *Inorg. Chem.* **2020**, *59*, 18156–18167.
55. Kovalenko, A. D.; Bushmarinov, I. S.; Burlov, A. S.; Lepnev, L. S.; Ilina, E. G.; Utochnikova, V. V. The Peculiarities of Complex Formation and Energy Transfer Processes in Lanthanide Complexes With 2-(Tosylamino)-Benzylidene-N-Benzoylhydrazone. *Dalton Trans.* **2018**, *47*, 4524–4533.

56. Zairov, R. R.; Dovzhenko, A. P.; Sapunova, A. S.; Voloshina, A. D.; Sarkanich, K. A.; Daminova, A. G.; Nizameev, I. R.; Lapaev, D. V.; Sudakova, S. N.; Podyachev, S. N.; Petrov, K. A.; Vomiero, A.; Mustafina, A. R. Terbium(III)-Thiacalix[4]Arene Nanosensor for Highly Sensitive Intracellular Monitoring of Temperature Changes within the 303–313 K Range. *Sci. Rep.* **2020**, *10*, 20541.
57. Ahmed, T.; Chakraborty, A.; Maity, S.; Baitalik, S. A Terpyridyl–Imidazole Based Europium Tris-(β-Diketonate) Complex as Efficient Molecular Luminescent Thermometer and Single Component White Light Emitter via Synergy in Energy Transfer between Ligand and Eu^{3+}. *Dalton Trans*. **2024**, *53*, 3065–3074.
58. Souza, A. S.; Nunes, L. A.; Felinto, M. C. F. C.; Brito, H. F.; Malta, O. L. On the Quenching of Trivalent Terbium Luminescence by Ligand Low Lying Triplet State Energy and the Role of the 7F5 Level: The [Tb(Tta)3 (H2O)2] Case. *J. Lumin.* **2015**, *167*, 167–171.
59. Fu, L. M.; Ai, X. C.; Li, M. Y.; Wen, X. F.; Hao, R.; Wu, Y. S.; Wang, Y.; Zhang, J. P. Role of Ligand-To-Metal Charge Transfer State in Nontriplet Photosensitization of Luminescent Europium Complex. *J. Phys. Chem. A* **2010**, *114*, 4494–4500.
60. Vicinelli, V.; Ceroni, P.; Maestri, M.; Balzani, V.; Gorka, M.; Vögtle, F. Luminescent Lanthanide Ions Hosted in a Fluorescent Polylysin Dendrimer. Antenna-Like Sensitization of Visible and Near-Infrared Emission. *J. Am. Chem. Soc.* **2002**, *124*, 6461–6468.
61. Liang, X.; Tu, Z.-L.; Zheng, Y.-X. Thermally Activated Delayed Fluorescence Materials: Towards Realization of High Efficiency through Strategic Small Molecular Design. *Chem. Eur. J.* **2019**, *25*, 5623–5642.
62. Zheng, S.-J.; Ma, J.; Su, J.; Djurovich, P. I.; Thompson, M. E.; Li, T.-Y. Simultaneous Thermally Stimulated Delayed Phosphorescence (TSDP) and Thermally Activated Delayed Fluorescence (TADF) in a Two-Coordinated Au(I) Bimetallic Complex Featuring a Tandem Carbene Structure. *J. Am. Chem. Soc.* **2024**, *146*, 19042–19049.
63. Luo, X.-F.; Xiao, X.; Zheng, Y.-X. Recent Progress in Multi-Resonance Thermally Activated Delayed Fluorescence Emitters with an Efficient Reverse Intersystem Crossing Process. *Chem. Commun.* **2024**, *60*, 1089–1099.

64. Ravinson, D. S. M.; Thompson, M. E. Thermally Assisted Delayed Fluorescence (TADF): Fluorescence Delayed Is Fluorescence Denied. *Mater. Horiz.* **2020**, *7*, 1210–1217.
65. Maity, D.; Bhaumik, C.; Karmakar, S.; Baitalik, S. Photoinduced Electron and Energy Transfer and pH-Induced Modulation of the Photophysical Properties in Homo-and Heterobimetallic Complexes of Ruthenium(II) And Rhodium(III) Based on A Heteroditopic Phenanthroline–Terpyridine Bridge. *Inorg. Chem.* **2013**, *52*, 7933–7946.
66. Maity, D.; Bhaumik, C.; Mardanya, S.; Karmakar, S.; Baitalik, S. Light Harvesting and Directional Energy Transfer in Long-Lived Homo- and Heterotrimetallic Complexes of Fe^{II}, Ru^{II}, and Os^{II}. *Chem. Eur. J.* **2014**, *20*, 13242–13252.
67. Maity, D.; Bhaumik, C.; Mondal, D.; Baitalik, S. Photoinduced Intramolecular Energy Transfer and Anion Sensing Studies of Isomeric $Ru^{II}Os^{II}$ Complexes Derived from An Asymmetric Phenanthroline–Terpyridine Bridge. *Dalton Trans.* **2014**, *43*, 1829–1845.
68. Maity, D.; Mardanya, S.; Karmakar, S.; Baitalik, S. pH-Induced Processes in Wire-like Multichromophoric Homo-and Heterotrimetallic Complexes of Fe (II), Ru (II), and Os (II). *Dalton Trans.* **2015**, *44*, 10048–10059.
69. Zheng, Z.-B.; Duan, Z.-M.; Zhang, J.-X.; Wang, K.-Z. Chromogenic and Fluorogenic Sensing Properties toward Cations and Anions by a Terpyridine/Phenylimidazo [4,5-f]Phenanthroline Hybrid. *Sens. Actuators B Chem.* **2012**, *169*, 312–319.
70. Bünzli, J.-C. G.; Eliseeva, S. V. Basics of Lanthanide Photophysics. In Lanthanide Luminescence; Hänninen, P., Härmä, H., Eds.; Springer Series on Fluorescence, Vol. 7; Springer: Berlin, Heidelberg, 2010.
71. An, B.-L.; Gong, M.-L.; Li, M.-X.; Zhang, J.-M. Synthesis, Structure and Luminescence Properties of Samarium(III) And Dysprosium(III) Complexes with A New Tridentate Organic Ligand. *J. Mol. Struct.* **2004**, *687*, 1–6.
72. Bassett, A. P.; Magennis, S. W.; Glover, P. B.; Lewis, D. J.; Spencer, N.; Parsons, S.; Williams, R. M.; De Cola, L.; Pikramenou, Z. Highly Luminescent, Triple- and Quadruple-Stranded, Dinuclear Eu, Nd, and Sm(III) Lanthanide Complexes Based on Bis–Diketonate Ligands. *J. Am. Chem. Soc.* **2004**, *126*, 9413–9424.
73. Bag, P.; Rastogi, C. K.; Biswas, S.; Sivakumar, S.; Mereacre, V.; Chandrasekhar, V. Homodinuclear Lanthanide {Ln 2}(Ln= Gd, Tb, Dy, Eu) Complexes Prepared from

an o-Vanillin Based Ligand: Luminescence and Single-Molecule Magnetism Behavior. *Dalton Trans.* **2015**, *44*, 4328–4340.

74. Zhu, T.; Chen, P.; Li, H.; Sun, W.; Gao, T.; Yan, P. Structural Effects on the Photophysical Properties of Mono-β-Diketonate and Bis-β-Diketonate Eu^{III} Complexes. *Phys. Chem. Chem. Phys.* **2015**, *17*, 16136–16144.
75. Wang, Z.; Liu, N.; Li, H.; Chen, P.; Yan, P. The Role of Blue-Emissive 1, 8-Naphthalimidopyridine N-Oxide in Sensitizing Eu^{III} Photoluminescence in Dimeric Hexafluoroacetylacetonate Complexes. *Eur. J. Inorg. Chem.* **2017**, *2017*, 2211–2219.
76. Armelao, L.; Dell'Amico, D. B.; Bellucci, L.; Bottaro, G.; Ciattini, S.; Labella, L.; Manfroni, G.; Marchetti, F.; Mattei, C. A.; Samaritani, S. Homodinuclear Lanthanide Complexes with the Divergent Heterotopic 4, 4′-Bipyridine N-Oxide (bipyMO) Ligand. *Eur. J. Inorg. Chem.* **2018**, *2018*, 4421–4428.
77. Li, H.-F.; Yan, P.-F.; Chen, P.; Wang, Y.; Xu, H.; Li, G.-M. Highly Luminescent Bis-Diketone Lanthanide Complexes with Triple-Stranded Dinuclear Structure. *Dalton Trans.* **2012**, *41*, 900–907.
78. Yanagisawa, K.; Kitagawa, Y.; Nakanishi, T.; Seki, T.; Fushimi, K.; Ito, H.; Hasegawa, Y. A Luminescent Dinuclear Eu^{III} /Tb^{III} Complex with LMCT Band as a Single-Molecular Thermosensor. *Chem. Eur. J.* **2018**, *24*, 1956–1961.
79. Santos, P. R. S.; Jesus, A. A. S. S.; Lima, W. B.; Arruda, J. G.; Faustino, W. M.; Felinto, M. C. F. C.; Sabino, J. R.; Brito, H. F.; Costa, I. F.; Moura, R. T., Jr; Carneiro Neto, A. N.; Malta, O. L.; Terraschke, H.; Teotonio, E. E. S. Shedding Light on Eu(III) β-diketonate Compounds with 1,2-bis(Diphenylphosphino)Ethane Oxide Ligand: An Optical Study. *Eur. J. Inorg. Chem.* **2024**, *27*, e202300660.
80. Gonçalves e Silva, F. R.; Malta, O. L.; Reinhard, C.; Güdel, H.-U.; Piguet, C.; Moser, J. E.; Bünzli, J.-C. G. Visible and Near-Infrared Luminescence of Lanthanide-Containing Dimetallic Triple-Stranded Helicates: Energy Transfer Mechanisms in the Sm^{III} and Yb^{III} Molecular Edifices. *J. Phys. Chem. A* **2002**, *106*, 1670–1677.
81. Meng, X.; Liu, X.; Zhang, L.; Zhou, J.; Zou, H.-H.; Zhang, J.; Xiang, D.; Zou, X. A Series of New Lanthanide Benzoates: Syntheses, Crystal Structures, and Luminescent Properties. *Dyes Pigm.* **2022**, *201*, 110182.
82. Boddula, R.; Vaidyanathan, S. Bi-Nuclear Luminescent Europium(III) Molecular Complexes for White Light Emitting Diodes: Experimental and Theoretical Study. *Inorganica Chim. Acta* **2019**, *494*, 141–153.

83. Ilmi, R.; Sun, W.; Dutra, J. D. L.; Al-Rasbi, N. K.; Zhou, L.; Qian, P.-C.; Wong, W.-Y.; Raithby, P. R.; Khan, M. S. Monochromatic Red Electroluminescence from a Homodinuclear Europium(III) Complex of a β-Diketone Tethered by 2,2′-Bipyrimidine. *J. Mater. Chem. C* **2020**, *8*, 9816–9827.
84. Li, H.-Y.; Wu, J.; Huang, W.; Zhou, Y.-H.; Li, H.-R.; Zheng, Y.-X.; Zuo, J.-L. Synthesis and Photoluminescent Properties of Five Homodinuclear Lanthanide (Ln3+=Eu3+, Sm3+, Er3+, Yb3+, Pr3+) Complexes. J. Photochem. Photobiol. A Chem. **2009**, *208*, 110–116.
85. Natrajan, L. S.; Timmins, P. L.; Lunn, M.; Heath, S. L. Luminescent Dinuclear Lanthanide Complexes of 5-Me-HXTA. *Inorg. Chem.* **2007**, *46*, 10877–10886.
86. Manzur, J.; Poblete, C.; Morales, J.; de Santana, R. C.; Queiroz Maia, L. J.; Vega, A.; Fuentealba, P.; Spodine, E. Enhancement of Terbium(III)-Centered Luminescence by Tuning the Triplet Energy Level of Substituted Pyridylamino-4-R-Phenoxo Tripodal Ligands. *Inorg. Chem.* **2020**, *59*, 5447–5455.
87. Sivakumar, S.; Reddy, M. L. P.; Bright Green Luminescent Molecular Terbium Plastic Materials Derived from 3,5-Bis(Perfluorobenzyloxy)Benzoate. *J. Mater. Chem.* **2012**, *22*, 10852–10859.
88. Teotonio, E. E.; Fett, G. M.; Brito, H. F.; Faustino, W. M.; de Sá, G. F.; Felinto, M. C. F.; Santos, R. H. Evaluation of Intramolecular Energy Transfer Process in the Lanthanide(III) Bis-and Tris-(TTA) Complexes: Photoluminescent and Triboluminescent Behavior. *J. Lumin.* **2008**, *128*, 190–198.
89. Crosby, G. A.; Whan, R. E.; Alire, R. M. Intramolecular Energy Transfer in Rare Earth Chelates. Role of the Triplet State. *J. Chem. Phys.* **1961**, *34*, 743–748.
90. Mara, M. W.; Tatum, D. S.; March, A. M.; Doumy, G.; Moore, E. G.; Raymond, K. N. Energy Transfer from Antenna Ligand to Europium(III) Followed Using Ultrafast Optical and X-Ray Spectroscopy. *J. Am. Chem. Soc.* **2019**, *141*, 11071–11081.
91. Miranda, Y. C.; Pereira, L. L. A. L.; Barbosa, J. H. P.; Brito, H. F.; Felinto, M. C. F. C.; Malta, O. L.; Faustino, W. M.; Teotonio, E. E. S. The Role of the Ligand-to-Metal Charge-Transfer State in the Dipivaloylmethanate-Lanthanide Intramolecular Energy Transfer Process. *Eur. J. Inorg. Chem.* **2015**, *2015*, 3019-3027.
92. Berry, M. T.; May, P. S.; Xu, H. Temperature Dependence of the Eu^{3+} $^5D_0$ Lifetime in Europium Tris(2,2,6,6-tetramethyl-3,5-heptanedionato). *J. Phys. Chem.* **1996**, *100*, 9216–9222.

93. Pasatoiu, T. D.; Madalan, A. M.; Kumke, M. U.; Tiseanu C.; Andruh, M. Temperature Switch of LMCT Role: From Quenching to Sensitization of Europium Emission in a Zn^{II}-Eu^{III} Binuclear Complex. *Inorg. Chem.* **2010**, *49*, 2310–2315.

****

Chapter 6

Stimuli-responsive Luminescence Behaviors of Ternary Homobimetallic Ln^{III}-tris-hfa Complexes Comprising a TADF-Active Terpyridine-Bipyridine-Based Ancillary Ligand: Display of VIBGYOR and White Light Emission

6.1. Introduction

The last decade has witnessed a substantial advancement in the design and synthesis of a wide variety of trivalent lanthanide (Ln^{III}) complexes primarily because of their unique and interesting emission spectral features.[1-9] They are often considered special owing to their atom-like sharp emission and long excited state lifetimes, which in turn make them useful in a diverse range of applications, viz. laser sources, luminescent sensors and thermometers, bio-imaging, drug delivery and medical diagnosis, to name a few.[8-13] However, direct excitation of the Ln^{III} ions cannot yield fruitful emission because of their spin and parity forbidden f-f transitions. To overcome the lacuna, suitable sensitizers are often anchored to the Ln^{III} ions for indirect sensitization (antenna effect). Fluorinated β-diketonates have emerged as one of the most popular genres for lanthanide sensitizers. Several modifications have been made to the structures of β-diketonates for appropriate positioning of the excited energy levels to achieve enhanced luminescence characteristics.[14-16] However, the desired bright luminescence is still to be achieved from Ln^{III} tris-(β-diketonate) moieties as the Ln^{III} ions often coordinate with water and/or solvent molecules to fulfil their higher coordination, which in turn invites a detrimental impact on the anticipated sensitized luminescence.[17] To circumvent this, polyaromatic organic Lewis bases, usually comprised of N- or O- O-donors, and possessing strong light absorptivities, are often brought into play.[18-24] It is to be noted that the structures of the incoming ancillary ligands and thereby their excited state energy levels govern the sensitization outcomes in the resulting metal-ligand assembly in terms of both the extent as well as direction of energy transfer. In essence, the excited state energy level positioning, particularly of the lowest triplet state (T_1), of the incoming ancillary ligand can induce either an additive or a subtractive impact on the sensitization in the resulting complexes as compared to their respective Ln^{III} tris-(β-diketonate) precursors.[25-29] While going through the literature, it appears that among the widely used polypyridyl-based ancillary ligands, terpyridine-type coordinating motifs are found to be surprisingly less explored for effective sensitization of lanthanide luminescence.[15,22-24,27-36]

Molecular luminescent thermometers are nowadays considered superior to the traditional thermometers, mostly due to their non-contact facility as well as efficacy even in the nanoscale domain. Hence, substantial efforts are now being devoted to the design of efficient molecular luminescent thermometers.[37-39] Ln^{III}-based coordination complexes have emerged as an unavoidable class for this purpose owing to their magnificent luminescence

thermometric features.[39-43] Literature survey reveals that Ln^{III}-based coordination polymers[40,42] or mixed Ln^{III}-based MOFs[40,43] are largely employed for this purpose. By contrast, Ln^{III}-based discrete molecules have been less explored,[40,44-52] while terpyridyl-ligand-appended lanthanide luminescent thermosensors are far scarcer.[28,29,52] Apart from the temperature stimulus, the luminescence behaviors of Ln^{III}-based coordination complexes are found to be responsive towards other external stimuli, viz. current,[53,54] solvent,[55] excitation wavelength,[56] etc. These stimuli could further be strategically implemented for designing several light-harvesting materials and also for achieving white light emission.

In our previous reports with monometallic Ln(tta)(tpy-HImzphen) complexes, we observed that the energy transfer was incomplete (for Eu^{III}), poor (for Sm^{III}), or in the reverse direction (for Tb^{III}).[27,52] Accordingly, we considered replacing the antenna ligand (tta) with high T_1 energy possessing hfa, keeping the ancillary ligand intact. It was noticed that although the problem regarding Eu^{III} has been managed, cases of Sm^{III} and Tb^{III} are yet to be resolved.[28] In view of that, we adopted two strategies concurrently, viz. by replacing the ancillary ligand and designing its ternary complexes comprising tta. The newly introduced sensitizing ligand, phen-Hbzim-tpy is heteroditopic in nature, and at the same time, its T_1 state resides at a higher energetic position relative to each of the tpy-HImzphen, tta, and hfa ligand moieties. In spite of adopting the said strategy, the extent of energy transfer in the Sm complex was still not up to the mark, and in case of the Tb complex, again only the ligand-centered deactivation was observed. Hence, it was realized that just doubling the Ln-tris-tta moieties and elevating the T_1 state of the ancillary ligand are not enough to have efficient sensitized luminescence responses. Besides, the luminescence behaviors of our previously reported complexes containing Eu^{III} ion are found to be well-dependent on stimuli like temperature or solvent. However, the possibility of offering these features is yet to be explored for the rest of the deployed Ln^{III} ions, viz., La^{III}, Sm^{III}, and Tb^{III}. These two factors prompted us to design a new series of ternary bimetallic Ln^{III} complexes upon replacing the tta with a higher-lying T_1-containing antenna like hfa, followed by carrying out further investigations.

Hence, we have synthesized herein a new series of homobimetallic Ln^{III} complexes of type $\{(Ln_2(hfa)_6(phen\text{-}Hbzim\text{-}tpy)\}$, where Ln=$La^{III}$ (**1**), Eu^{III} (**2**), Sm^{III} (**3**), and Tb^{III} (**4**); hfa=hexafluoroacetylacetonate, and phen-Hbzim-tpy=2-[4-(2,6-dipyridin-2-ylpyridin-4-yl) phenyl]-1H-imidazole [4,5-f][1,10]phenanthroline. The light-harvesting property of the present heteroditopic bridging ligand, phen-Hbzim-tpy, has been previously unveiled by our

group during the design of a number of Ru^{II} and Os^{II}-based mono-, bi- as well as trimetallic complexes.[57-60] But its thermally assisted delayed fluorescence (TADF) activity as well as ability to act as a sensitizer of Ln^{III} ions are yet to be explored. All the four newly synthesized complexes have been thoroughly characterized via standard analytical tools and spectroscopic techniques. Substantial improvements in their absorption and emission spectral characteristics have been noticed, as compared to their related monomeric complexes and homobimetallic analogues.[27,28] Notably, the TADF behavior of the present ancillary ligand has just been reported by our group, which was found to be inherited in the resulting complexes also (except the La^{III} complex). Here, all four complexes have manifested excellent TADF-assisted thermosensing and remarkable thermochromism, which is not at all that common for Ln^{III}-based discrete luminescent thermosensors. The luminescence properties of the complexes are also found to be responsive towards solvent and excitation wavelength. Consequently, we can fine-tune the luminescence responses of all the four complexes to achieve the seven colors of the VIBGYOR spectrum along with the white light emission upon appropriate implementation of said three stimuli. In the end, efforts have been made to elucidate the improved luminescence characteristics as well as the excellent TADF-assisted thermosensing efficacy of the complexes by considering plausible energy transfer pathways, constructing a tentative energy level diagram.

6.2. Experimental Section

6.2.1. Materials. Hexafluoroacetylacetone (Hhfa), and the chloride and nitrate salts of trivalent lanthanides in hydrated form are procured from Sigma Aldrich (Merck). The solvents are dried by adopting standard methods.

6.2.2. Synthesis of the Ligand and Lanthanide Precursors. To synthesize the terpyridyl-bipyridyl-based ligand (phen-Hbzim-tpy), we prepared 4′-(*p*-formyl phenyl)-2,2′:6′,2″-terpyridine (tpy-PhCHO), and 1,10-Phenanthroline-5,6-dione by adopting our reported literature methods (Scheme 6.1).[60,61]

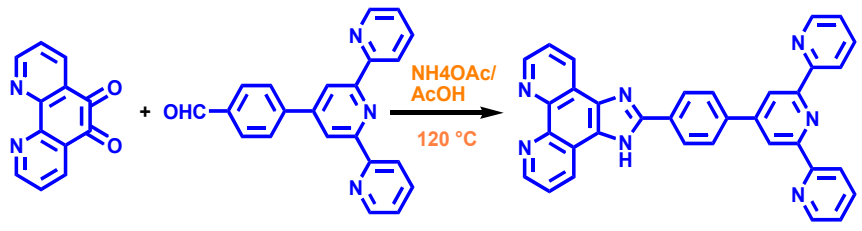

Scheme 6.1. Synthesis of the Ancillary Ligand (phen-Hbzim-tpy)

The procedure for synthesizing the lanthanide(III) tris-(β-diketonate) precursors of type [Ln(hfa)$_3$ (H_2O)$_2$], wherein Ln=La, Eu, Sm, Tb, and the details of their characterization are already presented in chapter 4.

6.2.3. Synthesis of the Lanthanide Complexes. A general synthetic scheme has been adopted to prepare all four lanthanide complexes of type [Ln_2(hfa)$_6$(phen-Hbzim-tpy)], where Ln^{III} = La^{III} (**1**), Eu^{III} (**2**), Sm^{III} (**3**), and Tb^{III} (**4**) (Scheme 6.2). To a stirred suspension of phen-Hbzim-tpy (20 mg, 0.038 mmol) in a chloroform-methanol (1:1 v/v) mixture, an appropriate amount of the lanthanide precursors Ln(hfa)$_3$(H_2O)$_2$ (~65 mg, ~0.08 mmol) is added in 1:2 molar ratio and refluxed for ~10h. The resulting straw yellow solution was then evaporated to dryness in a rotavapor, and the solid residue was dissolved in a dichloromethane-hexane (1:5 v/v) mixture to get a flesh-tinted colored product. The product was filtered and kept in a vacuum desiccator for 1d.

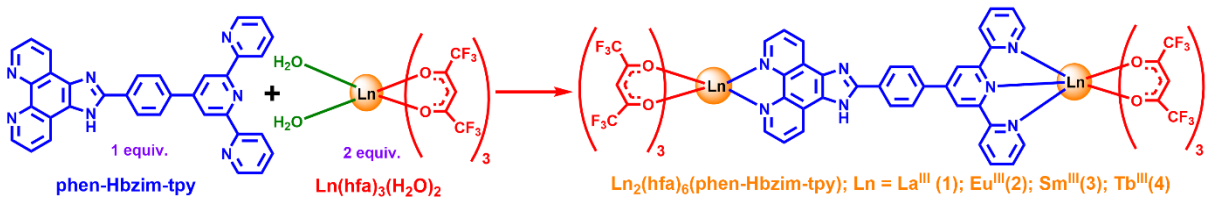

Scheme 6.2. Heteroditopic ancillary ligand (phen-Hbzim-tpy), Ln^{III} precursors, Ln(hfa)$_3$(H_2O)$_2$, and resulting homobimetallic complexes, {Ln_2(hfa)$_6$(phen-Hbzim-tpy)}

[La_2(hfa)$_6$((phen-Hbzim-tpy)] (1). La(hfa)$_3$(H_2O)$_2$ (61 mg, 0.076 mmol); Yield: 33 mg (41 %). Anal. Calcd. for $C_{64}H_{27}F_{36}N_7O_{12}La_2$: C, 37.54; H, 1.33; N, 4.79. Found: C, 37.14; H, 1.12; N, 4.15. FT-IR: υ (in cm^{-1}) = 1528, 1652, 3040. MALDI-TOF (DCTB, positive mode): *m/z* = 2046.704 (100 %) $[M-H]^+$. ^{1}H NMR (DMSO-d_6, 400 MHz, δ/ppm): 8.86 (d, 2H, *J* = 10 Hz, H_{11}), 8.83 (s, 2H, H_2), 8.79 (d, 2H, *J* = 4.4 Hz, H_6), 8.70 (d, 2H, *J* = 8.8 Hz, H_5), 8.61 (d, 2H, *J* = 8.4 Hz, H_9), 8.53 (d, 2H, *J* = 7.2 Hz, H_8), 8.20 (d, 2H, *J* = 8.4 Hz, H_7), 8.05 (t, 2H, *J* = 7.6 Hz, H_4), 7.75 (t, 2H, *J* = 8.4 Hz, H_{10}), 7.55 (t, 2H, *J* = 4.8 Hz, H_3), 5.49 (s, 6H, H_1 methine).

[Eu_2(hfa)$_6$((phen-Hbzim-tpy)]] (2). Eu(hfa)$_3$(H_2O)$_2$ (62 mg, 0.076 mmol); Yield: 36 mg (46 %). Anal. Calcd for $C_{64}H_{27}F_{36}N_7O_{12}Eu_2$: C, 37.07; H, 1.31; N, 4.73. Found: C, 36.94; H, 1.08; N, 4.14. FT-IR: υ (in cm^{-1}) = 1530, 1650, 3070. MALDI-TOF (DCTB, positive mode): *m/z* = 2072.493 (100%) $[M-H]^+$ ^{1}H NMR (DMSO-d_6, 400 MHz, δ/ppm): 8.86 (d, 2H, *J* = 8.8 Hz, H_{11}), 8.83 (s, 2H, H_2), 8.70 (d, 2H, *J* = 7.6 Hz, H_6), 8.61 (d, 2H, *J* = 8.8 Hz, H_5), 8.53 (d, 2H, *J* = 7.2 Hz, H_9), 8.20 (d, 2H, *J* = 7.6 Hz, H_8), 8.05 (t, 2H, *J* = 8.0 Hz, H_7), 7.75 (t,

2H, J = 7.6 Hz, H_4), 7.65 (t, 2H, J = 8.0 Hz, H_{10}), 7.54 (t, 2H, J = 5.6 Hz, H_3), 5.70 (s, 6H, H_1 methine).

[$Sm_2(hfa)_6$((phen-Hbzim-tpy)]] (3). $Sm(hfa)_3(H_2O)_2$ (62 mg, 0.076 mmol); Yield: 30 mg (38 %). Anal. Calcd for $C_{64}H_{27}F_{36}N_7O_{12}Sm_2$: C, 37.12; H, 1.31; N, 4.74. Found: C, 36.93; H, 1.18; N, 4.38. FT-IR: υ (in cm^{-1}) = 1528, 1650, 3000. MALDI-TOF (DCTB, positive mode): *m/z*= 2074.950 (100%) $[M-H]^+$ ^1H NMR (DMSO-d_6, 400 MHz, δ/ppm): 9.04 (s, 2H, H_{11}), 9.01 (s, 2H, H_2), 8.80 (s, 2H, H_6), 8.78 (s, 2H, H_5), 8.68 (d, 2H, J = 7.6 Hz, H_9), 8.51 (d, 2H, J = 8.4Hz, H_8), 8.21 (d, 2H, J = 8.0 Hz, H_7), 8.05 (t, 2H, J = 8.4 Hz, H_4), 7.89 (s, 2H, H_{10}), 7.54 (t, 2H, J = 5.6 Hz, H_3), 5.65 (s, 6H, H_1 methine).

[$Tb_2(hfa)_6$((phen-Hbzim-tpy)]] (4). $Tb(hfa)_3(H_2O)_2$ (62 mg, 0.076 mmol); Yield: 35 mg (44 %). Anal. Calcd for $C_{64}H_{27}F_{36}N_7O_{12}Tb_2$: C, 36.82; H, 1.30; N, 4.70. Found: C, 36.57; H, 1.16; N, 4.45. FT-IR: υ (in cm^{-1}) = 1530, 1652, 2970. MALDI-TOF (DCTB, positive mode): *m/z*= 1992.479 (100%) $[M-H]^+$. ^1H NMR (DMSO-d_6, 400 MHz, δ/ppm): 8.84 (s, 2H, H_{11}), 8.81 (s, 2H, H_2), 8.73 (s, 2H, H_6), 8.67 (d, 2H, J = 7.6 Hz, H_5), 8.60 (d, 2H, J = 6.8 Hz, H_9), 8.53 (d, 2H, J = 8.4 Hz, H_8), 8.18 (d, 2H, J = 8.4 Hz, H_7),8.00 (S, 2H, H_4), 7.69 (s, 2H, H_{10}), 7.60 (s, 2H, H_3), 7.48 (s, 6H, H_1 methine).

6.2.4. Instruments and Physical Methods. The details have already been narrated in chapter 2.

6.3. Results And Discussions

6.3.1. Synthesis and Characterization. The respective lanthanide precursor, $Ln(hfa)_3(H_2O)_2$, upon refluxing with phen-Hbzim-tpy in a 2:1 molar ratio in a chloroform-methanol 1:1 (v/v) mixture, produced the desired dinuclear complexes with fairly good yields. Following synthesis, all the four complexes are thoroughly characterized via standard analytical tools and spectroscopic techniques viz. elemental (C, H, N) analysis, Fourier Transform infrared (FT-IR) spectroscopy, ^1H nuclear magnetic resonance (NMR) spectroscopy, high resolution mass spectrometry (HRMS), powdered X-ray diffraction (PXRD) analysis as well as by thermogravimetric analysis. The above measurements also suggest that the four synthesized complexes are isostructural to each other.

6.3.2. FT-IR Spectra. The IR spectra of the resulting complexes, along with their respective lanthanide precursor and phen-Hbzim-tpy ligand were acquired within the 400-4000 cm^{-1} region. A representative spectrum is presented in Figure 6.1, and selected stretching frequencies of the complexes are presented in Table 6.1. The ligand exhibited a

peak at ~1586 cm^{-1} due to C=N stretching of the pyridine moieties, whereas a characteristic peak at ~3154 cm^{-1} was observed for the imidazole N-H stretch. Due to the presence of the hexafluoroacetylacetonate unit, all the lanthanide precursors, $Ln(hfa)_3(H_2O)_2$, show a characteristic C=O stretching with 1645-1650 cm^{-1} domain and a broad hump in the range between 3500 and 3550 cm^{-1} for the water molecules. The complexes also revealed a sharp peak within the range of 1650-1652 cm^{-1}, associated with C=O stretching frequency. It is to be noted that the broad peak for coordinated water disappeared upon complexation. Additionally, two new peaks emerged within 1528-1530 cm^{-1} and 2960-3100 cm^{-1} for C=N and N-H stretching, respectively, in the complexes.

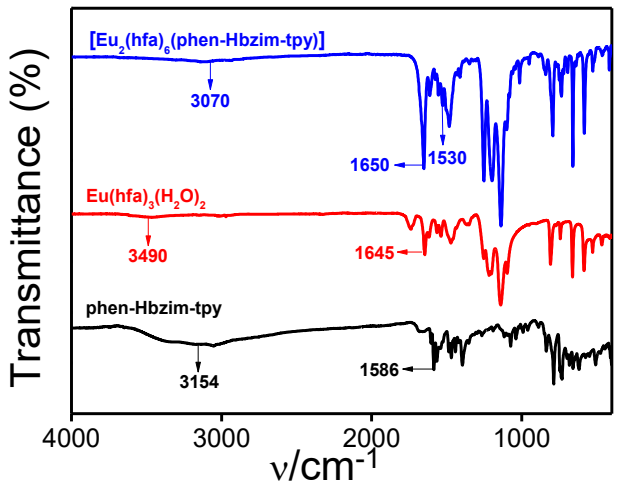

Figure 6.1. FT-IR spectra of phen-Hbzim-tpy, $Eu(hfa)_3(H_2O)_2$ and $[Eu_2(hfa)_6$ (phen-Hbzim-tpy)] (**2**).

Table 6.1. Stretching Frequencies of Selected Groups in Their FT-IR Spectra

Complex	$\nu_{C=O}$	$\nu_{C=N}$	ν_{N-H}	ν_{OH}
phen-Hbzim-tpy	-	1586	3154	-
$La(hfa)_3(H_2O)_2$	1646	-	-	3503
Complex 1	1652	1528	3040	-
$Eu(hfa)_3(H_2O)_2$	1645	-	-	3490
Complex 2	1650	1530	3070	-
$Sm(hfa)_3(H_2O)_2$	1650	-	-	3424
Complex 3	1650	1528	3000	-
$Tb(hfa)_3(H_2O)_2$	1648	-	-	3461
Complex 4	1652	1530	2970	-

6.3.3. ^{1}H NMR Spectra. ^{1}H NMR spectra of all four bimetallic lanthanide complexes (**1**-**4**), together with their respective $Ln(hfa)_3(H_2O)_2$ precursors, are acquired in DMSO-d_6. Representative ^{1}H NMR spectra for **1**, along with tentative assignments of the protons, are presented in Figure 6.2. The chemical shift values for all the proton resonances are also tabulated in Table 6.2. The methine proton in free Hhfa shows a singlet at 4.32 ppm, which gets downfield-shifted to 5.50 ppm upon incorporation of diamagnetic La^{III} ion $La(hfa)_3(H_2O)_2$ precursor. The same proton also leaves its signature in the resulting La^{III}-complex (**1**) at 5.49 ppm (Figure 6.2). Among the other three complexes, this methine proton experiences an up-field shift from 5.80 to 5.70 ppm in case of Eu^{III} (**2**), while it remains almost unaltered (from 5.65 to 5.64 ppm) for Sm^{III} (**3**). In case of Tb^{III} (**4**), it undergoes a downfield shift from 7.20 to 7.48 ppm, as compared to its $Tb(hfa)_3(H_2O)_2$ precursor. The proton signals attached to the phen-Hbzim-tpy ligand experienced unpredictable alteration in multiplicity as well as chemical shifts, dependent on the type of metal ion incorporated.

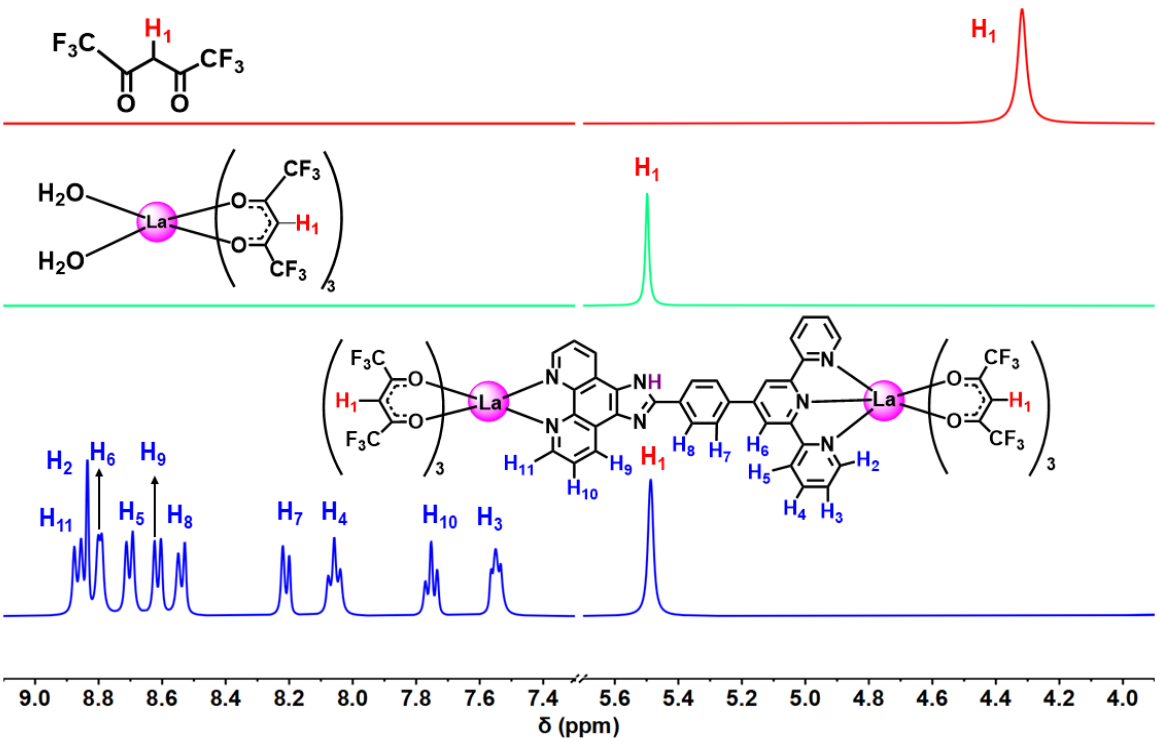

Figure 6.2. 400 MHz ^{1}H NMR spectra of Hfa (top), $La(hfa)_3(H_2O)_2$ (middle) and $[La_2(hfa)_6(phen\text{-}Hbzim\text{-}tpy)]$ (**1**) (bottom) in DMSO-d_6.

Table 6.2. Chemical Shifts of the Protons of All Four Complexes in DMSO-d_6

Proton	Chemical shift (ppm) of Lanthanide complexes (1-4) {*J*= Hz}			
	1 (La^{III})	**2** (Eu^{III})	**3** (Sm^{III})	**4** (Tb^{III})
H_1 (methine)	5.49 (s, 6H)	5.70 (s, 6H)	5.64 (s, 6H)	7.48 (s, 6H)
H_2	8.83 (s,2H)	8.83 (s,2H)	9.02 (s)	8.81 (s, 2H)
H_3	7.55 (t, 2H, *J* = 4.8)	7.54 (t, 2H, J = 5.6)	7.54 (t, 2H, *J* = 5.6)	7.59 (s, 2H)
H_4	8.06 (t, 2H, *J* = 7.6)	7.75 (t, 2H, *J* = 7.6)	8.05 (t, 2H, *J* = 8.4)	8.00 (s, 2H)
H_5	8.70 (d, 2H, *J* = 8.8)	8.61 (d, 2H, *J* = 8.8)	8.78 (s,2H)	8.67 (d, 2H, *J* = 7.6)
H_6	8.79 (d, 2H, *J*=4.4)	8.70 (d, 2H, J = 7.6)	8.81 (s, 2H)	8.73 (s, 2H)
H_7	8.20 (d, 2H, *J* = 8.4)	8.05 (d, 2H, *J* = 8.0)	8.21 (d, 2H, *J* = 8.0)	8.18 (d, 2H, *J* = 8.4)
H_8	8.54 (d, 2H, *J* = 7.2)	8.20 (d, 2H, *J* = 7.6)	8.51 (d, 2H, *J* = 8.4)	8.53 (d, 2H, *J* = 8.4)
H_9	8.61 (d, 2H, *J* = 8.4)	8.53 (d, 2H, *J* = 7.2)	8.68 (d, 2H, *J* = 7.6)	8.60 (d, 2H, *J* = 6.8)
H_{10}	7.75 (t, 2H, *J* = 8.4)	7.65 (t, 2H, *J* = 8.0)	7.90 (s, 2H)	7.69 (s, 2H)
H_{11}	8.86 (t, 2H, *J* = 10.0)	8.86 (t, 2H, *J* = 8.8)	9.04 (s, 2H)	8.84 (s, 2H)

6.3.4. Mass Spectra. The HRMS data for all four complexes are recorded in chloroform to further confirm the stability in solution. Similar spectral patterns are noticed for all cases with a prominent peak for the respective $[\{Ln_2(hfa)_5(phen\text{-}Hbzim\text{-}tpy)\}]^+$ or $[M\text{-}hfa]^+$ fragment. A representative spectrum of **2**, along with experimental and simulated isotopic patterns, is presented in Figure 6.3. The correspondence between the experimental and simulated isotopic patterns is also found to be good in all cases.

6.3.5. Powdered X-ray Diffraction (PXRD). The PXRD analysis for all four complexes depicts broad peaks having almost similar patterns, indicating that they are isostructural to each other, and at the same time, all of them are amorphous in nature (Figure 6.4).

6.3.6. Thermogravimetric Analysis of the Complexes. The thermal stability of the complexes was examined through thermogravimetric analysis in N_2 atmosphere in the temperature range between 30 and 800 °C, maintaining the heating rate at 10 °C/m. Close similarity in the dissociation pattern is observed for all the complexes (Figure 6.5). The first major dissociation starts at ~320 °C and continues up to 360 °C. During this course, up to 40% of weight loss occurs in each case, which is most probably because of the dissociation of phen-Hbzim-tpy moiety. The next major weight-loss starts at ~540 °C and continues to

decrease, probably because of the formation of their respective metal oxide. Hence, the complexes are found to be thermally more stable (onset temperature at ~320 °C) than their respective precursors (onset temperature at ~180 °C).

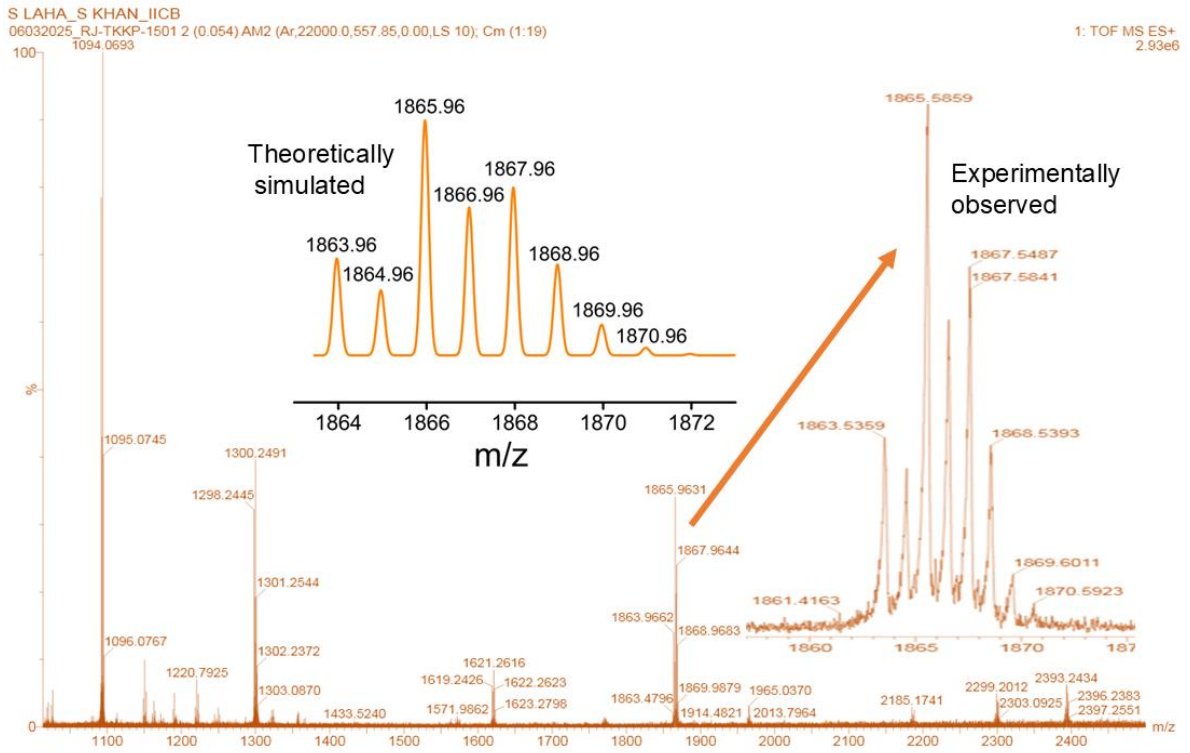

Figure 6.3. HRMS of $[Eu_2(hfa)_6(phen\text{-}Hbzim\text{-}tpy)]$ (**2**) in dichloromethane with the experimentally observed and simulated isotopic distribution pattern for $[M\text{-}tta]^-$ fragment.

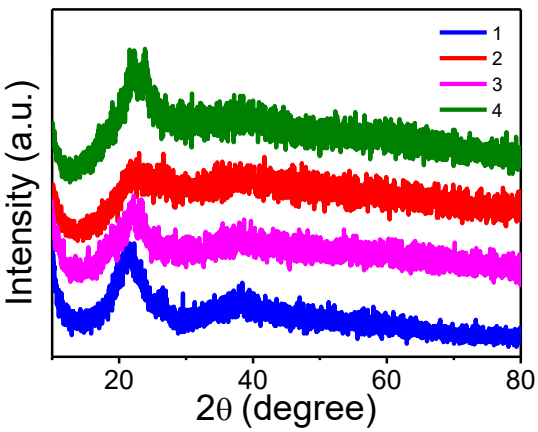

Figure 6.4. PXRD patterns of complexes **1-4**

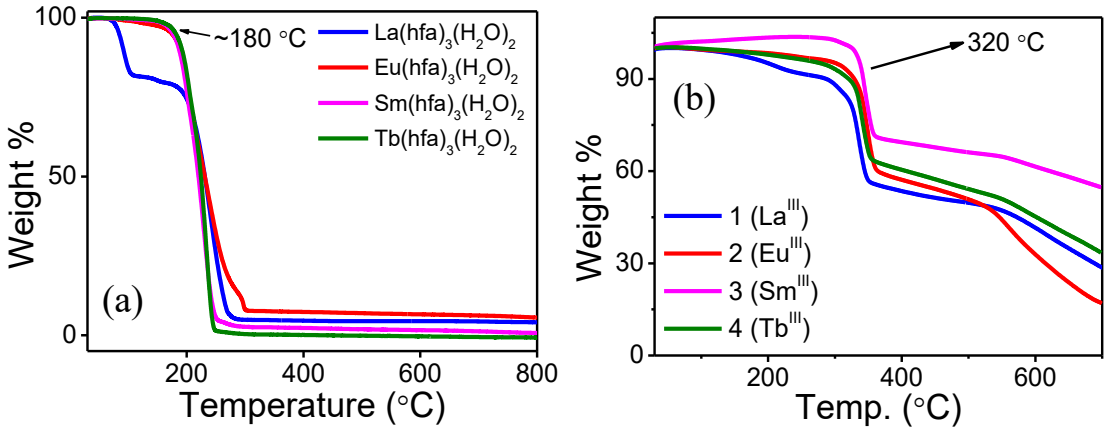

Figure 6.5. Thermogravimetric analysis of all four metal precursors $Ln(hfa)_3(H_2O)_2$[28] (a) and their corresponding complexes **1-4** (b).

6.3.7. Photophysical Properties. Absorption and emission spectral characteristics of the lanthanide complexes are recorded in dichloromethane, and relevant spectral data are presented in Table 6.3. Associated spectra are displayed in Figures 6.6-6.8. The free phen-Hbzim-tpy ligand exhibits an intense band at ~341 nm, ascribed to intra-ligand charge transfer (ILCT) as well as at ~280 nm due to π-π* transitions within the aromatic and heteroaromatic moieties (Figure 6.6a).[60] All four lanthanide precursors, $Ln(hfa)_3(H_2O)_2$, on the other hand, display an intense band with their maximum at ~300 nm (λ_{max}) (Figure 6.6a). It is of interest to note that, in contrast to most of the hitherto reported lanthanide(III) complexes, the absorption spectral window of the present $Ln_2(hfa)_3$(phen-Hbzim-tpy) complexes is found to extend towards the visible region with the onset at ~425 nm

Table 6.3. Photophysical Parameters of Complexes 1-4 at RT and 77K

	Complexes	Absorption, λ_{max}/nm (ε/$M^{-1}cm^{-1}$)($\times10^4$)	Emission, λ_{max}/nm		Lifetime (τ)	Relative Quantum Yield (Φ_{rel}/%)
			Ligand centered	Metal centered		
RT	**1**	288(4.81), 303(4.65), 328(3.61), 360(2.22)	455	-	2.0 ns	52.4
	2	288(6.69), 331(4.24)	416	579, 589, 594, 615, 650	785.4 µs	37.2
	3	288(5.91), 331(3.90)	444	561, 597, 645	56.7 µs	4.6
	4	287(7.92), 330(4.89)	455	490, 545, 584, 615	11.7 µs	45.5
77K	**1**	-	490	-	11.0 ns	-
	2	-	407	579, 589, 594, 615	830.2 µs	-
	3	-	445	562, 599, 646	59.0 µs	-
	4	-	435	488, 544, 584, 620	795.7 µs	-

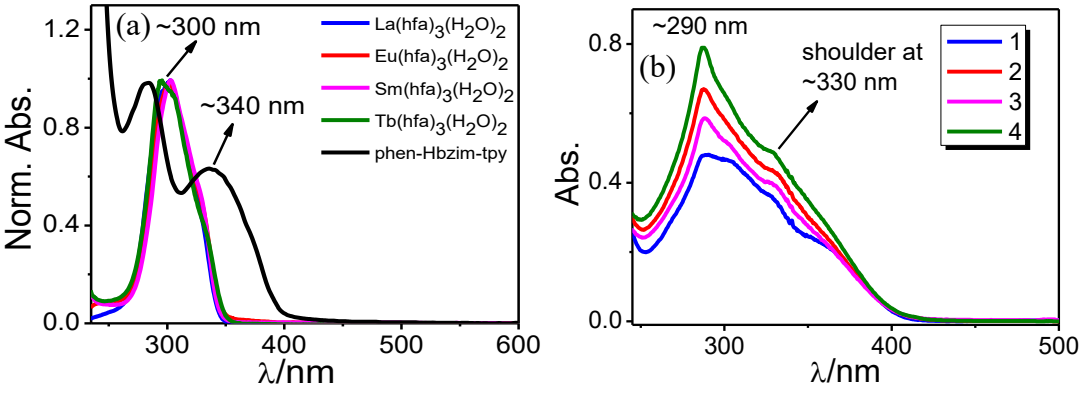

Figure 6.6. UV-visible absorption spectra of the ancillary ligand phen-Hbzim-tpy along with $Ln(hfa)_3(H_2O)_2$ precursors (a) and complexes **1**-**4** (b) in dried dichloromethane at RT.

(Figure 6.6b), which is beneficial for their probable use as visible light absorbing chromophores. Additionally, the molar absorptivity values (ε) of the resulting complexes are found to be more than double relative to their respective $Ln(hfa)_3(H_2O)_2$ precursors {2.02×10^4 for $La(hfa)_3(H_2O)_2$, 3.47×10^4 for $Eu(hfa)_3(H_2O)_2$, 2.57×10^4 for $Sm(hfa)_3(H_2O)_2$, and 3.85×10^4 for $Tb(hfa)_3(H_2O)_2$}, highlighting the utility of the complexes as efficient light absorbers.

The photoluminescence spectra of the complexes are recorded in dichloromethane at RT upon irradiating at 330 nm and depicted in Figures 6.7a and 6.7b. The broad emission band of phen-Hbzim-tpy, having its maximum at ~428 nm,[60] undergoes a red shift to 455 nm in the La^{III}-complex (**1**). The emission signals of the Eu^{III} complex (**2**) are comprised of strong signals at 579, 592, 614, and 652 nm, arising out of intra-configurational $^5D_0\rightarrow{}^7F_{0\text{-}3}$ transitions, respectively, characteristics of the Eu^{III} ion. Besides, only a very weak ligand-centered emission signal at ~420 nm is observed, indicating an almost complete ligand-to-metal energy transfer process. The observations regarding Sm^{III} (**3**) and Tb^{III} (**4**) are worth noting. In both cases, the relative intensity of the Ln^{III}-centered emission signals is much higher than that of the ligand-centered broad signal at ~450 nm. In case of Sm^{III} (**3**), apart from a weak ligand-centered signal at ~444 nm, intense Sm^{III}-centered emission is clearly visible at 561 nm ($^5G_{5/2}\rightarrow{}^5H_{9/2}$), 597 nm ($^5G_{5/2}\rightarrow{}^5H_{7/2}$), and 646 nm ($^5G_{5/2}\rightarrow{}^5H_{9/2}$). It is to be noted that the Sm^{III}-centered emissions are usually very prone to quenching owing to multi-phonon relaxation,[62] as we have also found in our earlier monometallic complexes.[27,28,63] Even after replacing the ancillary ligand with a heteroditopic ligand possessing a much higher T_1 energy level, we observed a moderate extent of energy transfer in the resulting tta-based dinuclear Sm^{III} complex.[29] But, herein, upon replacing tta with hfa, which having a higher T_1

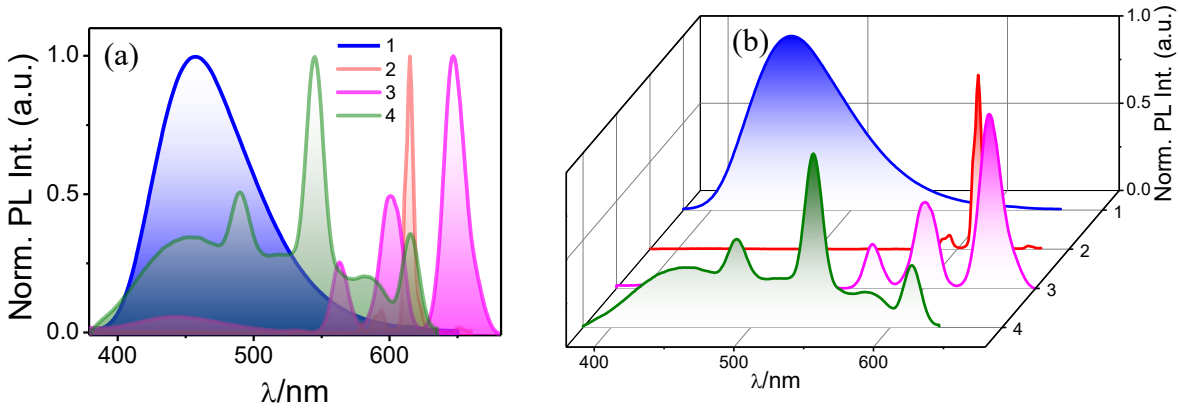

Figure 6.7. Normalized photoluminescence spectra of complex **1**-**4** in dried dichloromethane at RT in 2D (a) and 3D representation (b).

state than tta, we noticed an almost complete energy transfer to Sm^{III}. The Tb^{III}-complex (**4**) also displayed strong Tb^{III}-centered f-f intra-configurational peaks at 490, 545, 585, and 616 nm associated with $^5D_4 \rightarrow {}^7F_{6\text{-}3}$ transitions, respectively, along with a substantially reduced ligand-centered signal at ~455 nm. Of particular interest to note that in our previous works regarding the mononuclear complexes, as well as the tta-containing analogous dinuclear Tb-complex,[27-29] we observed only ligand-centered emission mainly due to back-energy transfer. By contrast, a remarkable enhancement in the emission spectral characteristics in terms of the existence of Tb^{III}-centered emission peaks has been achieved herein. Upon lowering the temperature to 77 K, this sensitized emission gets further improved via intensification of the Tb^{III}-centered emission with almost negligible existence of the ligand-centered broad peak (Figure 6.7a). Besides, the lifetime of the Tb^{III} center is enhanced up to 795.7 μs (Figure 6.8b). We also noticed a considerable enhancement in the overall (or total) quantum yields

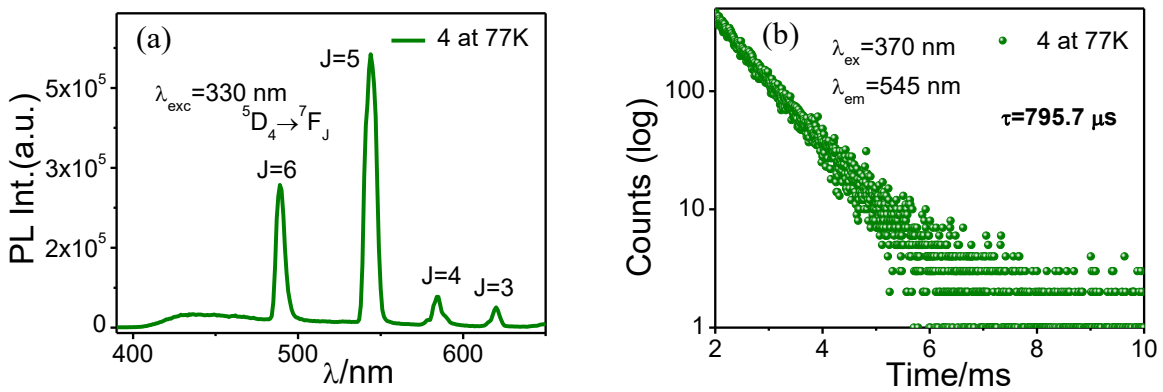

Figure 6.8. Steady-state emission spectrum and excited state decay profile for complex **4** in glassy ethanol at 77K.

(Φ_{rel}) of the present complexes, viz. 52.3%, 41.3%, 4.9%, and 47.5%, for **1**, **2**, **3**, and **4**, respectively, as compared to their nearest monomeric analogues.[28] These values are found to be comparable to the earlier reported Ln^{III}-based discrete dimeric complexes as presented in Table 6.4.[5,33-36,64-73]

Table 6.4. Comparison of Relative Quantum Yield Values Among Some Earlier Reported Dinuclear Ln^{III}-Based Discrete Molecules with This Work

Complex	Absorption, λ_{max}/nm ($\varepsilon/M^{-1}cm^{-1}$)($\times 10^4$)	Quantum Yield Value	Method of Estimation	References
$Eu_2(BTP)_3(DME)_2$ $Eu_2(BTP)_3(bpy)_2(CH_2Cl_2)_2$ $Eu_2(BTP)_3(phen)_2$	317 (8.00) 325 (7.20) 327 (7.26)	13 55 65	Relative	*16*
$Eu_2(TOTPY)_2(TFA)_6$ $Tb_2(TOTPY)_2(TFA)_6$ $Eu_2(FTPY)_2(TFA)_6$ $Tb_2(FTTPY)_2(TFA)_6$ $Eu_2(TTPY)_2(TFA)_6$ $Tb_2(TTPY)_2(TFA)_6$	288 (6.89) 288 (4.79) 294 (6.34) 294 (7.59) 292 (6.18) 292 (6.34)	18.7 17.8 17.3 19.2 15.7 16.1	Relative	*34*
$Eu_2L^1_3$ $Sm_2L^1_3$ H_2L^1= 1,3-bis(3-phenyl-3-oxopropanoyl)benzene	357 (13.0)	5.0 0.16	Relative	*80*
$[Tb_2(H_2L)_2(\mu\text{-piv})_2(piv)_2]\cdot 2CHCl_3$	298 (3.52)	76.2	Relative	65
$Eu_2(HTH)_6(bpm)$ $Sm_2(HTH)_6(bpm)$ HTH = 4,4,5,5,6,6,6-heptafluroro-1-(2-thienyl)hexane-1,3-dione	342 342	28.4 1.4	Relative	*67*
$Tb_2(HXTA)_2,Na_4$ HXTA= (N,N-(2 hydroxy-5-methyl-1,3-xylylene)bis(N-(carboxymethyl)glycine)	300	54	Relative	*70*
$La_2(tta)_6(phen\text{-}Hbzim\text{-}tpy)$ $Eu_2(tta)_6(phen\text{-}Hbzim\text{-}tpy)$ $Sm_2(tta)_6(phen\text{-}Hbzim\text{-}tpy)$ $Tb_2(tta)_6(phen\text{-}Hbzim\text{-}tpy)$	343 (6.32) 341 (6.90) 342 (6.51) 341 (7.32)	66.4 31.7 4.2 42.3	Relative	*Previous work 29*

The time-resolved emission decay profiles of all the four complexes are also acquired in dichloromethane, and associated decays as well as lifetimes are presented in Figure 6.9 and Table 6.3. All the complexes are excited with a 370 nm light source, and excited-state decay profiles are found to be well-fitted with mono-exponential function. Complex **1** exhibits a

lifetime of only 2 ns associated with the ligand-centered emission. The remaining three complexes, on the other hand, display substantially longer lifetimes, viz., 785.4 μs, 56.7 μs, and 11.7 μs, for **2**, **3**, and **4**, respectively.

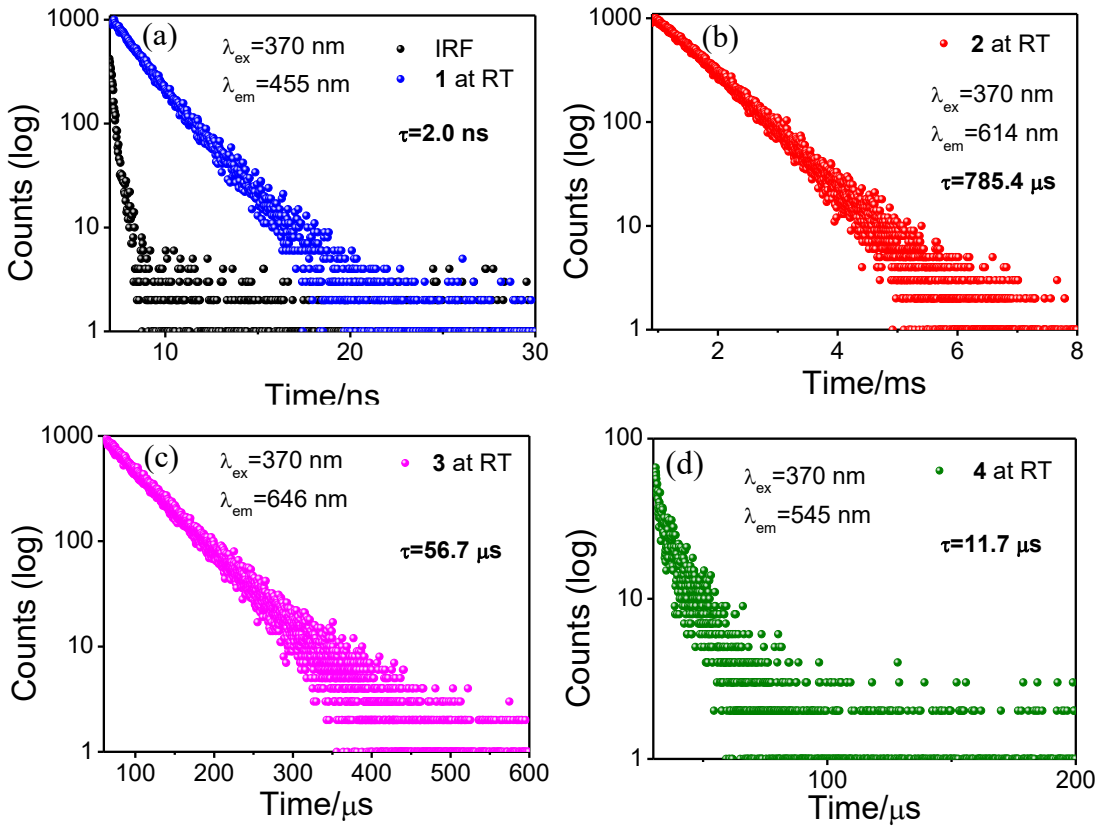

Figure 6.9. Luminescence decay profiles of complex **1-4** (a-d) in dried dichloromethane at RT.

It is noteworthy to mention again that in the Tb^{III} complexes, back-energy transfer from Tb^{III} center to the ligand usually takes place, and as a result of which lifetime of the resulting complexes remains in the nanosecond time domain. Interestingly, by employing hfa as the antenna ligand, we are able to restrict herein the back energy transfer phenomenon to a certain extent. This is also reflected in its elevated lifetime value in the microsecond time region at RT as compared to earlier reported analogues possessing their lifetime in the nanosecond time domain. Thus, the observed results clearly indicate that incorporation of hfa and phen-Hbzim-tpy, owing to their higher lying T_1 states, induced improvements in the photosensitization efficacy, together with enhanced luminescence characteristics of the homobimetallic lanthanide(III) complexes.

6.3.8. In-situ Generation of the Ternary Bimetallic Ln^{III} Complexes. All four complexes can also be generated *in situ* upon gradual addition of the respective

$Ln(hfa)_3(H_2O)_2$ precursor to the solution of phen-Hbzim-tpy. The progress of the reaction is monitored via absorption and emission spectroscopy. A representative titration is shown in Figure 6.10. The spectral saturation takes place upon the addition of ~2 equiv. of the lanthanide precursor in all cases, further confirming their stoichiometry to be 1:2. The spectra at saturation closely resemble their respective isolated complexes.

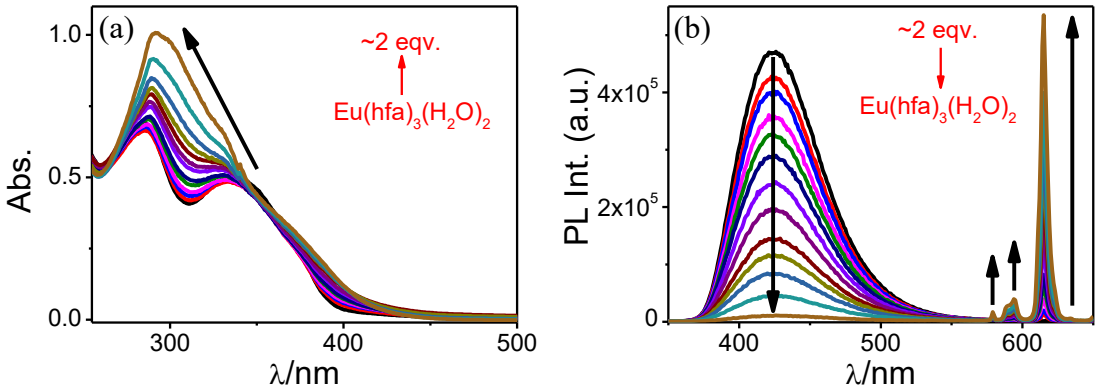

Figure 6.10. Changes in UV-vis absorption (a) and photoluminescence spectra (λ_{ex}=340nm) (b) of phen-Hbzim-tpy ligand upon incremental addition of $Eu(hfa)_3(H_2O)_2$ in dried dichloromethane at RT.

6.3.9. Thermally Activated Delayed Fluorescence (TADF)-Assisted Thermo-sensing and Thermochromic Behaviors of Complexes. After noticing the excellent luminescence responses from complexes **1**-**4**, we further tend to explore their luminescence thermometric prospects. Both steady-state and time-resolved luminescence measurements of all four complexes are performed in MeCN upon varying the temperature between 273 K and 353 K. In each case, a systematic rise in the ligand-centered emission signal takes place upon gradual increase in temperature. Based on our previous observation regarding the free phen-Hbzim-tpy ligand, we believe that this is the thermally activated delayed fluorescence (TADF) phenomenon. The successive luminescence spectra pass through an iso-emissive point in case of the La^{III} complex, whereas systematic diminution of the Ln^{III}-centered emission peaks is also noticed for the other three complexes upon the rise in temperature. Consequently, all four complexes display remarkable thermochromism. The steady-state and time-resolved emission spectral profiles of complex **2**, as the representative one, are shown in Figure 6.11. The emitting color, as depicted in the corresponding Commission Internationale de l'Éclairage (CIE) plots, switches from blue (at 273 K) to green (at 353 K) for La^{III} (**1**) and Tb^{III} (**4**) complexes; from red (at 273 K) to violet (at 313 K) to blue (at 353 K) in case of Eu^{III}

(**2**); while from green (at 273 K) to yellow (at 353 K) for Sm^{III} (**3**). In accordance with their steady-state behaviors, the lifetime of the Ln^{III}-centered emissions also decreases for all the complexes upon gradual increase in temperature, albeit to different extent, viz. 692.3 μs (273K)→268.4 μs (353K) for **2**; 34.6 μs (273K)→22.5 μs (353K) for **3**; and 10.9 μs (273K)→0.6 μs (353K) for **4**. On the other hand, the lifetime of the ligand-centered emission is found to systematically increase in all four cases, albeit to a limited extent, with rising temperature, viz., 2.09 ns (273K)→2.39 ns (353K) for **1**; 2.09 ns (273K)→2.36 ns (353K) for **2**; 2.25 ns (273K)→2.44 ns (353K) for **3**; and 2.25 ns (273K)→2.42 ns (353K) for **4** (Figure 6.12). It is also noteworthy to mention that in each case the lifetime values remain practically unaltered on going from 273K to RT. Just after crossing the RT, systematic enhancement of lifetime takes place up to 353 K. Hence, overall, the observed trend of enhancement in lifetime upon increasing the temperature is the testimony to the possible occurrence of TADF event.

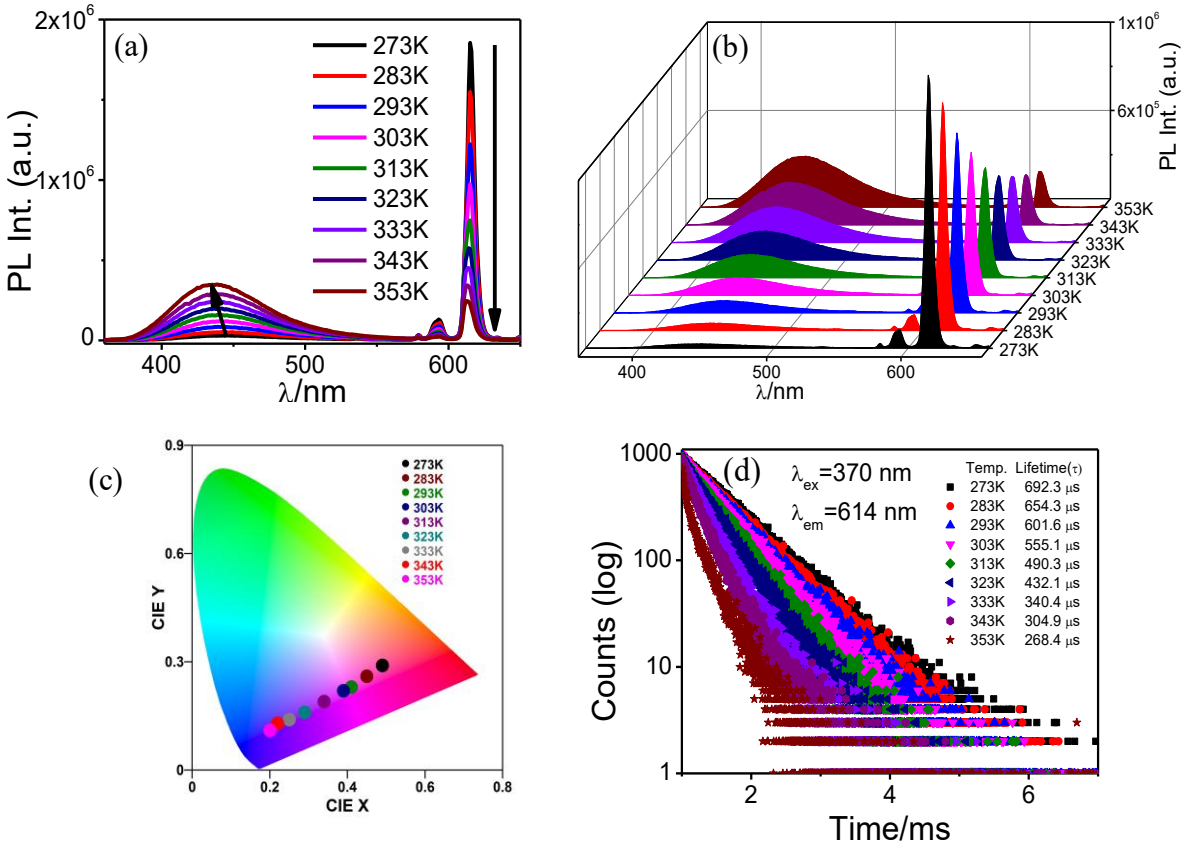

Figure 6.11. Changes in photoluminescence (λ_{ex}=330 nm) of **2** in MeCN upon varying temperature in 2D (a) and 3D (b) representation; corresponding chromaticity diagram (c) and changes in lifetime at λ_{em}=614 nm (d) upon varying temperature.

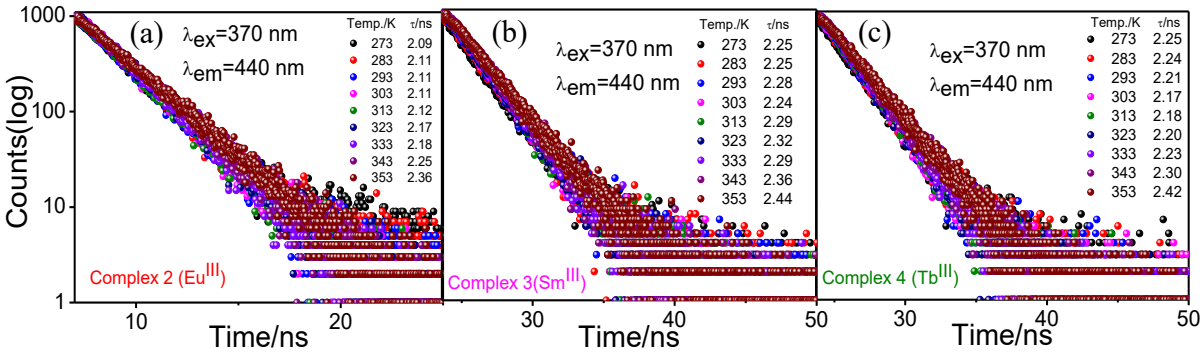

Figure 6.12. Changes in lifetime of the ligand center for Complex **2** (a), **3** (b), and **4** (c) upon varying temperature in MeCN.

6.3.10. Measurement of Delayed Fluorescence and Lifetime. To confirm the occurrence of TADF phenomena, we further recorded the delayed fluorescence spectra (Figure 6.13) as well as the delayed lifetimes (Figure 6.14) of all the four complexes in MeCN at RT. During the course of the measurement, we kept the gate at 40-60 μs to eradicate any prompt fluorescence signal.

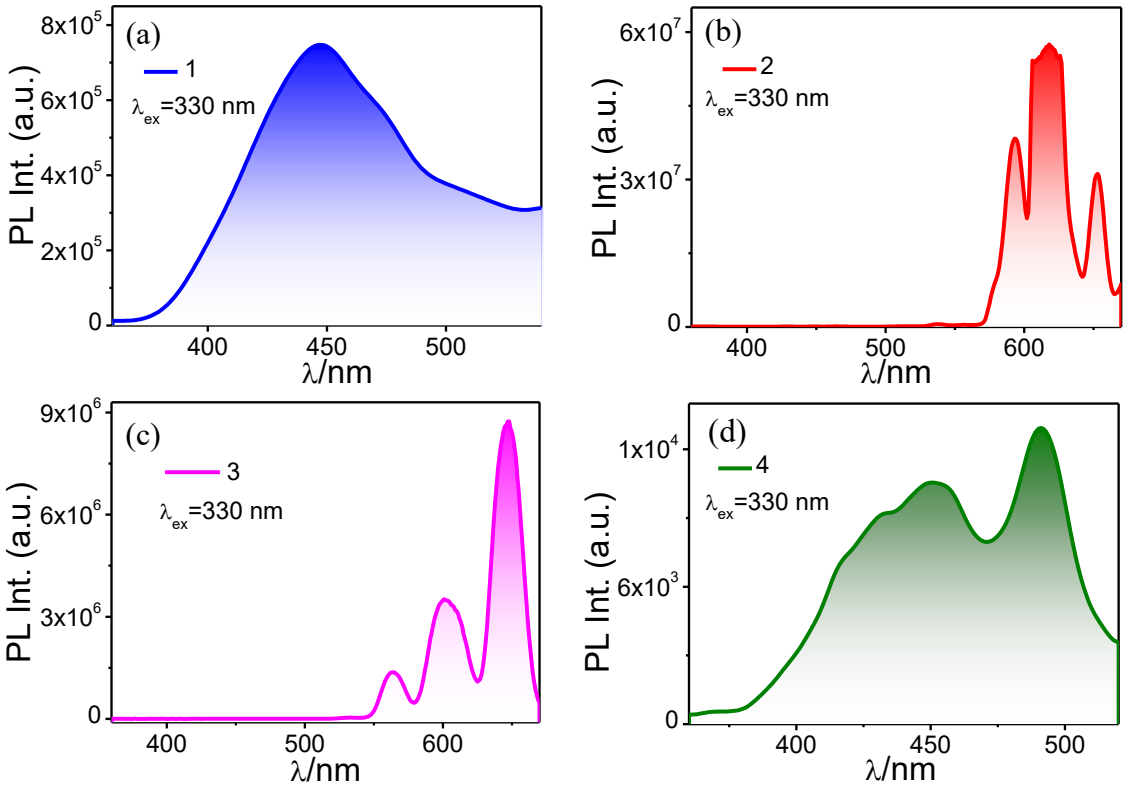

Figure 6.13. Gated emission spectra of all four complexes (λ_{ex}=330 nm) in MeCN at RT.

Previously, we have noticed a bi-exponential delayed decay for the free phen-Hbzim-tpy ligand upon monitoring at 440 nm.[29] The reason behind this alteration from its mono-exponential nature in usual TCSPC measurement, on maintaining the same conditions, is not very clear to us. We surmise herein that the ligand undergoes a twist at elevated temperature, resulting in the formation of both planar and twisted conformations, which in turn could gives rise to two components of its lifetime. A recent report also suggests that such twisting of molecules may result in displaying TADF.[74]

All four complexes also exhibit bi-exponential decay in delayed lifetime measurements upon monitoring at 440 nm. The lifetime values for the La complex are 5.8 μs and 44.1 μs, which are comparable to those of the free phen-Hbzim-tpy ligand (5.9 μs and 50.6 μs). On the other hand, it is 187.7 μs and 622.8 μs for Eu complex, 35.4 μs and 94.6 μs for Sm complex, while 4.9 μs and 44.6 μs for Tb complex. We do not know the actual reason behind the bi-exponential nature of the decays. But we believe that the excited states of the hfa ligand (S_1 and T_1) may also assist in repopulating the S_1 state of phen-Hbzim-tpy, which in turn results in the evolution of another component in their lifetime profiles.

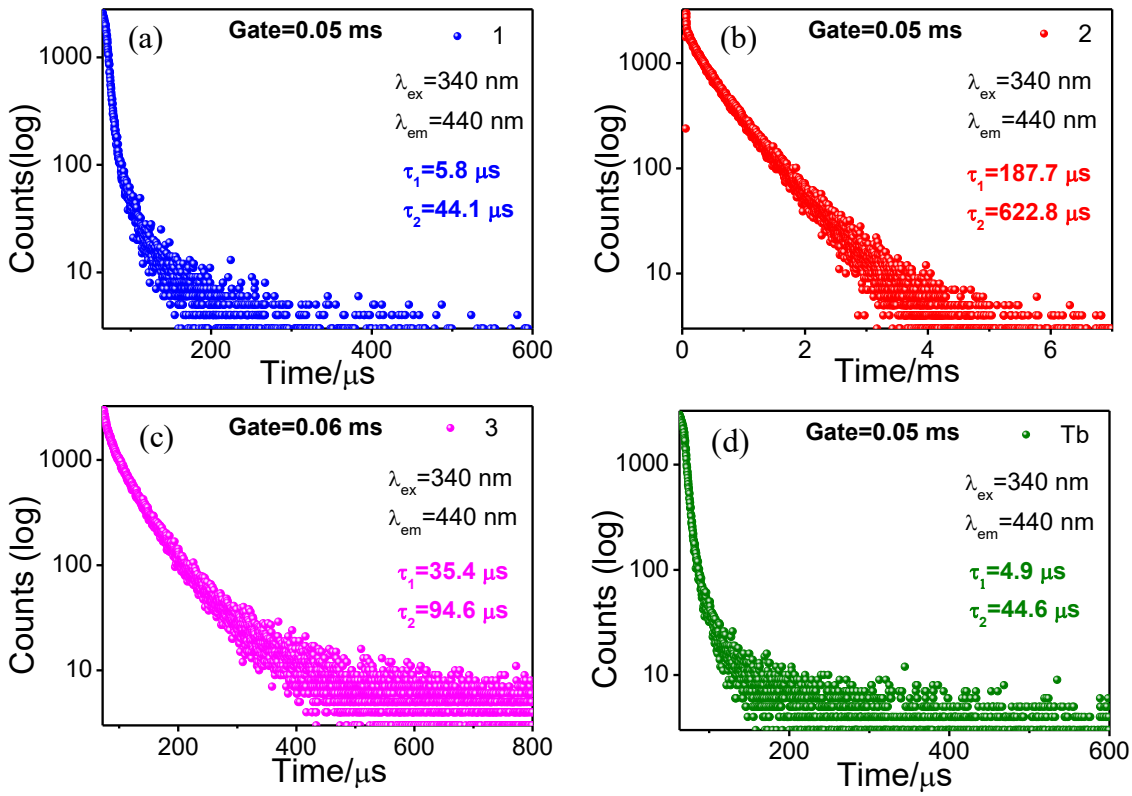

Figure 6.14. Delayed lifetime profiles for all four complexes (λ_{ex}=340 nm) in MeCN at RT.

6.3.11. Assessment of Thermosensing Efficacy of the Complexes. We are also interested in assessing the thermosensing efficacy of the complexes. In order to do so, four temperature-dependent parameters (Δ) have been employed, viz. two types of luminescence intensity ratios (I_{ED}/I_{MD} and I_{ED}/I_{ligand}) and lifetime (τ), together with our newly proposed parameter $\{I_{ligand}(T)/\tau_{ligand}(T)\}$. The latest thermometric parameter is directly related to the TADF-assisted luminescence behaviors and has been utilized in our previous work. The first two parameters, viz., I_{ED}/I_{MD} and $I_{ED}/I_{ligand,}$ are not applicable for La^{III}, Sm^{III}, and Tb^{III} complexes. It is because La^{III} ion does not possess any Ln^{III}-centered emission peak, whereas the intensities of the electric dipole transition peak for Sm^{III} and Tb^{III} ions are noticed to get overshadowed by the remarkable enhancement of the ligand-centered broad peak upon the temperature rise. In each case, the relative thermosensitivity (S_r) and temperature resolution or uncertainty (δT) have been estimated. The best S_r and δT values obtained from four complexes are presented in Table 6.5. The highest S_r values are determined to be 4.35, 10.06,

Table 6.5. Thermometric and Thermosensing Efficacy Parameters for All Four Thermosensor Complexes (1-4) in the Temperature Domain of 273-353 K

Complex	LIR (I_{ED}/I_{MD})		LIR (I_{ED}/I_{ligand})		Lifetime		I_{ligand}/τ_{ligand}	
	S_m (%K^{-1})	T_m	S_m (%K^{-1})	T_m	S_m (%K^{-1})	T_m	S_m (%K^{-1})	T_m
1	-	-	-	-	0.41	353 K	**4.35**	273 K
2	1.46	353 K	6.19	273 K	2.39	353 K	**10.06**	273 K
3	-	-	-	-	0.81	273 K	**8.52**	353 K
4	-	-	-	-	1.65	333 K	**5.02**	353 K

8.52, and 5.02, for complexes **1**, **2**, **3,** and **4**, respectively. Notably, all of these high values are based upon monitoring the newly proposed parameter, i.e., $\{I_{ligand}(T)/\tau_{ligand}(T)\}$. In order to be considered an efficient thermosensor, the S_r value should be >1% K^{-1}, while the δT value should be as low as possible than 1 K. Interestingly, all four complexes satisfactorily fulfil those criteria and thereby can be considered as efficient thermosensors within the temperature range of 273-353 K. The performance of the Eu^{III} complex (**2**) is found to be the best, followed by Sm^{III} (**3**), Tb^{III} (**4**), and La^{III} (**1**) complexes, respectively. Moreover, the thermosensing efficacies of these present complexes are found to be much better than the

earlier reported Ln^{III}-based discrete luminescent thermosensors, including their tta-based analogues[29], as revealed from Table 6.6.

Table 6.6. Comparison of Some Earlier Reported Ln^{III}-Based Discrete Thermosensors

Complex	S_m ($\%K^{-1}$)	ΔT (K)	T_m (K)	Optical Parameter	Ref.
Mononuclear Discrete Thermosensors					
$Eu(DBM)_3L$-mCF_3; HDBM=Dibenzoylmethane L=imidazo-bipyidyl ligand	4.9	303–460	323	Intensity ratio	45
$Eu(bzac)_3(H_2O)_2$; Hbzac= 1-phenyl-1,3-butanedione	5.25	83–303	303	Area	46
$Eu(CPDK_{3\text{-}5})_3$phen; $CPDK_{3\text{-}5}$=1-(4-(4-propylcyclohexyl)phenyl)octane-1,3-dione and phen=1,10-phenathroline)	1.2	298-348	298	Lifetime	47
$Eu(tta)_3$(pyphen); tta= 2-thenoyltrifluoroacetonate and pyphen= pyrazino[2,3-f][1,10]phenanthroline	1.98	83–303	323	Lifetime	48
$(Eu(HL)_2Cl$ Eu(L)(HL); H_2L=2-(tosylamino)-benzylidene-N-benzoylhydrazone	5.1 7.7	77-298 80-260	185 85	Intensity ratio	49
$Sm(fod)_3$bath; fod=anion of 6,6,7,7,8,8,8- heptafluoro-2,2-dimethyl-3,5-octanedione bath=4,7-diphenyl-1,10-phenanthroline	1.14	50-350	60	Intensity	51
$Eu(tta)_3$(tpy-HImzphen); Htta=2-thenoyltrifluoroacetone tpy-HImzphen= 2-(4-[2,2':6',2''] terpyridin-4'-yl-phenyl)-1H-phenanthro[9,10-d]imidazole)	5.78 3.36	273–343 273–333	343 333	Intensity ratio, Lifetime	52
$Eu(hfa)_3$(tpy-HImzphen); Hhfa=hexafluoroacetylacetone tpy-HImzphen= 2-(4-[2,2':6',2''] terpyridin-4'-yl-phenyl)-1H-phenanthro[9,10-d]imidazole)	12.52	273–353	353	I_{ED}/τ_{ED}	28
Dinuclear Discrete Thermosensors					
$Eu_2(tta)_6(pyrzMO)_2$	7.1	223-373	353	Area	50
$Eu_2(dbm)_6(pyrzMO)_2$	4.9		373		
$Eu_2(bta)_6(pyrzMO)_2$	7.4		373		
$Eu_2(hfa)_6(pyrzMO)_2$	4.1		363		
$Eu_2(tta)_6(bipyMO)_2$	4.8		363		
$Eu_2(dbm)_6(bipyMO)_2$	4.9		343		
$Eu_2(bta)_6(bipyMO)_2$	3.4		373		
$Eu_2(hfa)_6(bipyMO)_2$	3.2		373		
$La_2(tta)_6$(phen-Hbzim-tpy)	1.01	273-353	353	I_{ligand}/τ_{ligand}	29
$Eu_2(tta)_6$(phen-Hbzim-tpy)	3.2		313		
$Sm_2(tta)_6$(phen-Hbzim-tpy)	7.2		343		
$Tb_2(tta)_6$(phen-Hbzim-tpy)	2.16		353		
$Eu_2(tta)_6$(phen-Hbzim-tpy)	11.9	273-353	343	I_{ED}/I_{ligand}	29
$Sm_2(tta)_6$(phen-Hbzim-tpy)	4.6		323		
$La_2(hfa)_6$(phen-Hbzim-tpy)	4.35	273-353	273	I_{ligand}/τ_{ligand}	This work
$Eu_2(hfa)_6$(phen-Hbzim-tpy)	10.06		273		
$Sm_2(hfa)_6$(phen-Hbzim-tpy)	8.52		273		
$Tb_2(hfa)_6$(phen-Hbzim-tpy)	5.02		273		

It is of particular interest to note that in most of the earlier reported cases, only the Ln^{III}-centered emission responses have been adopted to showcase their thermosensing behaviors. But, simultaneous monitoring of the luminescence response for the ancillary ligand could also shed some light on elucidating the mechanistic aspect of the temperature-dependent energy transfer processes. Herein, the luminescence responses of both phen-Hbzim-tpy ligand as well as respective Ln^{III}-centres are taken into consideration for this purpose. Moreover, the literature reveals that the thermosensing ability of Eu^{III} complexes has been mostly explored among the lanthanides, followed by that of the Tb^{III} complexes. But, the present Sm^{III} and La^{III} complexes are also capable of displaying thermosensing behaviors, which, to the best of our knowledge, are quite unprecedented in the literature.

6.3.12. Solvatochromic Behaviors of Complexes. We further tend to investigate the potential solvent effect on the photoluminescence spectral behaviors of the complexes. Taking advantage of their adequate solubility in a wide variety of solvents, we recorded the photoluminescence spectral responses of all four complexes in toluene, chloroform, acetone, ethyl acetoacetate, dimethylsulphoxide, acetonitrile, ethanol, and methanol, covering a wide range of polarities. We monitored the alteration of both ligand-centered as well as characteristic lanthanide-centered sharp emission peaks, upon variation of the solvents. The emitting color of the complexes is found to stretch within a wide domain, primarily because of the interplay of both ligand- and Ln-centered emissions. Even the La^{III} complex (**1**), possessing no lanthanide-centered emission, displays various emitting colors like blue, indigo, cyan, green, and yellow. The Eu^{III} complex, on the other hand, exhibits violet, blue, indigo, and greenish-yellow along with its characteristic red color (Figure 6.15). The Sm^{III} complex emits blue, indigo, and green colors apart from its characteristic orange emission; while the Tb^{III} complex displays blue, indigo, and yellow emission together with its characteristic green region. The observed solvatochromic behaviors of the complexes probably arise due to dipole-dipole interaction between the phen-Hbzim-tpy framework and solvent molecules[75], which in turn leads to alteration of position and intensity of the ligand-centered peak. At the same time, the Ln^{III}-centered emission peaks can also undergo alteration in their intensities depending upon the coordination possibility of the associated solvent. Both these factors seem to contribute to the observed photoluminescence spectral outcomes of the complexes.

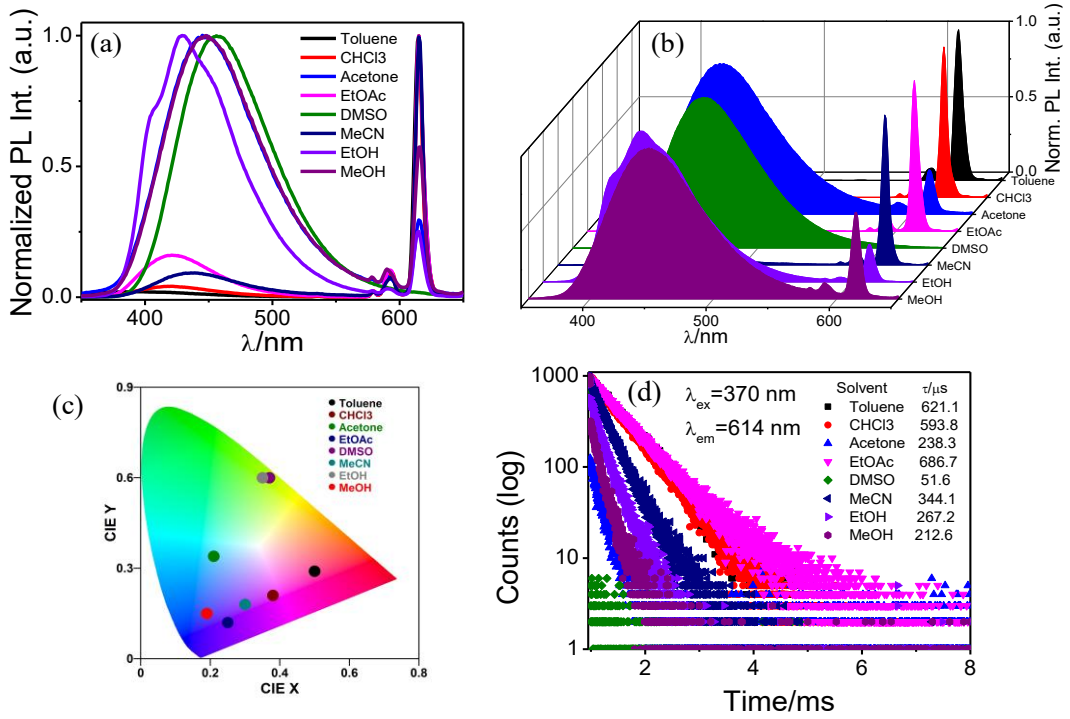

Figure 6.15. Photoluminescence spectral profiles of **2** in various solvents in 2D (a) and 3D (b) representation; corresponding chromaticity diagram (c) and changes in lifetime at λ_{em}=614 nm.

6.3.13. Excitation Wavelength Dependent Luminescence Spectral Behaviors of the Complexes. We are also curious to see the dependence of excitation wavelength on the photoluminescence behaviors of the complexes. To this end, the emission spectra of the four complexes are acquired upon varying the excitation wavelength within the domain of 320-380 nm (Figure 6.16a, c, e, and g), and associated CIE plots are presented in Figure 6.16b, d, f, and h. The emission color of La^{III} complex (**1**) is found to vary from blue to green region, while that of the Eu^{III} complex (**2**) remains almost unperturbed upon variation of excitation wavelength, probably because of its very intense emission peak at ~614 nm. The observation with regard to Sm^{III} complex (**3**) is worth noting. While it exhibits its characteristic orange emission within 320-330 nm, it offers white light emission upon exciting within the wavelength domain of 350-370 nm. The emitting color of the Tb^{III} complex (**4**) also varies, from blue to near-white light region.

6.3.14. Accomplishment of VIBGYOR and White Light Emission via Interplay of Three External Stimuli. From the foregoing observations, it is quite evident that the luminescence spectral characteristics, especially the steady-state behaviors, of all four

complexes are well-dependent on various stimuli like temperature, solvent, and excitation wavelength. Consequently, all of them emit a bunch of emission colors, under appropriate

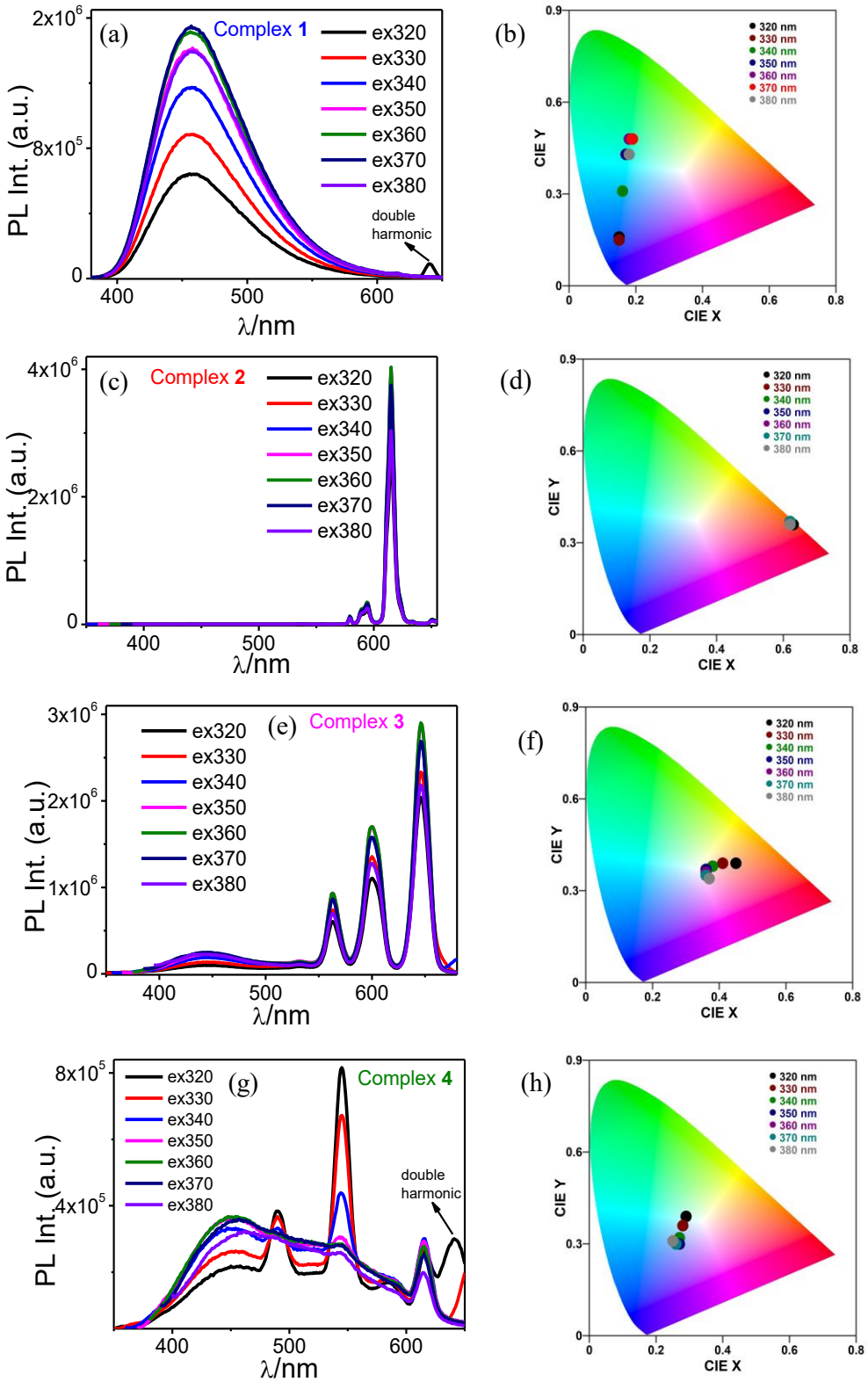

Figure 6.16. Changes in photoluminescence spectral profiles of **1**-**4** (a, c, e, g) and their corresponding chromaticity diagrams (b, d, f, h) upon varying excitation wavelength.

interplay of the said three stimuli. For example, complex **1** (La^{III}) and **4** (Tb^{III}) generate four colors, viz., blue, indigo, green, and yellow, while complex **2** (Eu^{III}) produces five colors, viz., violet, blue, indigo, yellow, and red. More intriguingly, complex **3** (Sm^{III}) can yield as many as six colors (except red) of the VIBGYOR spectrum. Additionally, the Sm^{III} complex is capable of displaying white light emission at RT upon varying the excitation wavelength between 350 and 370 nm. Table 6.7 presents concise information regarding the emitting colors of all the four complexes under the influence of different stimuli. A CIE chromaticity diagram is also presented, showing under which conditions all of these emitting colors in VIBGYOR spectrum together with white light emission are accomplished from the four complexes (Figure 6.17).

Table 6.7. Cumulative Presentation of All the Conditions to Achieve the Seven Colors of VIBGYOR along with White Light

	1	2	3	4
Violet	-	λ_{ex}=330 nm, 293-303 K; λ_{ex}=330 nm, $CHCl_3$.	λ_{ex}=380 nm, RT.	-
Indigo	λ_{ex}=350, 380 nm, RT; λ_{ex}=330 nm, 313 K; λ_{ex}=330 nm, Toluene, MeCN.	λ_{ex}=330 nm, Acetone.	λ_{ex}=330 nm, MeCN.	λ_{ex}=320-330 nm, RT; λ_{ex}=330 nm, 333 K; λ_{ex}=330 nm, Acetone.
Blue	λ_{ex}=320-340 nm, RT; λ_{ex}=330 nm, 273-293 K; λ_{ex}=330 nm, $CHCl_3$, EtOAc, MeOH.	λ_{ex}=330 nm, 323-353 K; λ_{ex}=330 nm, EtOAc, MeCN, MeOH.	λ_{ex}=330 nm, Toluene, $CHCl_3$, EtOAc.	λ_{ex}=370-380 nm, RT; λ_{ex}=330 nm, 273-323 K; λ_{ex}=330 nm, Toluene, $CHCl_3$, EtOAc.
Green	λ_{ex}=360, 370 nm, RT; λ_{ex}=330 nm, 333-353 K; λ_{ex}=330 nm, Acetone, DMSO.	-	λ_{ex}=330 nm, 273-293 K; λ_{ex}=330 nm, Acetone, EtOH, MeOH.	λ_{ex}=330 nm, 343-353 K; λ_{ex}=330 nm, 77 K; λ_{ex}=330 nm, MeCN, EtOH, MeOH.
Yellow	λ_{ex}=330 nm, EtOH.	λ_{ex}=330 nm, DMSO, EtOH.	λ_{ex}=330 nm, 343-353 K.	λ_{ex}=330 nm, DMSO.

Orange	-	-	λ_{ex}=320-330 nm, RT; λ_{ex}=330 nm, DMSO.	-
Red	-	λ_{ex}=320-380 nm, RT; λ_{ex}=330 nm, 273 K; λ_{ex}=330 nm, Toluene.	-	-
White	-	-	λ_{ex}=350-370 nm, RT.	-

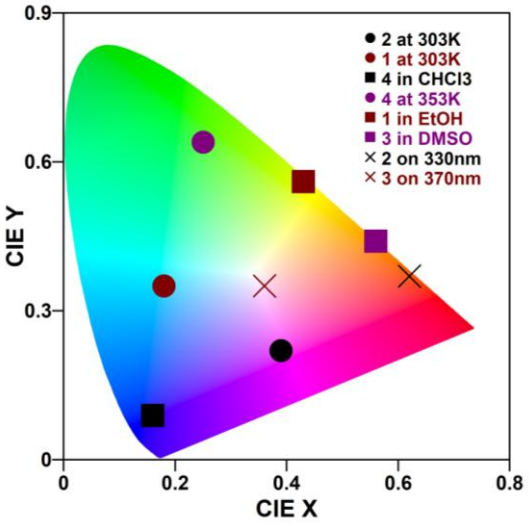

Figure 6.17. Exhibition of all seven colors of the VIBGYOR spectra along with white light emission upon application of appropriate stimuli on four complexes.

6.3.15. Elucidation of the Luminescence Spectral Behaviors and TADF-assisted Thermosensing Features of the Complexes. The antenna effect in the Ln^{III}-based sensitizers could be operative via "Dexter exchange" pathway,[76] if the position of lowest triplet energy level (T_1) of the sensitizer is at ~2500-4000 cm^{-1} higher than that of the lowest emissive state of respective Ln^{III} ($*Ln^{III}$), according to Reinhoudt's empirical rule.[62] On the other hand, if the said energy gap (between the T_1 and $*Ln^{III}$) happens to be <1800 cm^{-1}, back energy transfer to the sensitizer occurs, instead of a fruitful lanthanide(III) sensitization, according to Latva's empirical rule.[25] Now, the lowest-lying emitting excited level ($*Ln^{III}$) of Eu^{III} ($^5D_0$), Sm^{III} ($^4G_{5/2}$), and Tb^{III} ($^5D_4$) is located at ~17300, ~17900, and ~20500 cm^{-1}, respectively. In our previous set of works regarding mononuclear complexes with tpy-HImzphen, the

energetic position for the T_1 state of the ancillary ligand (~20534 cm^{-1})[27,28,52,] was lower than that of the T_1 states of both tta[27,52] (~21000 cm^{-1}) and hfa[28,40] (~22000 cm^{-1}), thereby closest to the $^*Tb^{III}$, followed by $^*Sm^{III}$ and $^*Eu^{III}$. As a result, the extent of energy transfer was found to be very poor for Sm^{III}, while in case of Tb^{III}, the energy transfer takes place in the reverse direction, yielding only the ligand-centered emission. Even after replacing the ancillary ligand with a terpyridine-bipyridine-based bridging ligand (whose T_1 state resides at ~24570 cm^{-1}), the problems regarding Sm^{III} and Tb^{III} ions remained unresolved in their dinuclear complexes containing tta as the antenna ligand. The low-lying T_1 state of the tta ligand seemed responsible for this, which could act as a quencher state. But, in the present work, both the hfa and phen-Hbzim-tpy are expected not to induce any detrimental impact on the efficient energy transfer process due to their much higher T_1 level positions. Rather, phen-Hbzim-tpy works as an additional antenna together with hfa for effective sensitization. Thus, the cumulative influences of ancillary and antenna ligands, together with the doubling of Ln-hfa moieties, are responsible for the substantial improvement of the absorption, as well as sensitized emission characteristics in the resulting dinuclear complexes. However, it should be mentioned that, although the sensitized luminescence from the present dinuclear Tb^{III} complex is better than its tta-based analogue[29], it is not as efficient as one can anticipate from the suitable energy differences. This may be attributed to the predominance of thermally-assisted back energy transfer to the ligand, which seems to be outplayed by its sensitized luminescence outcomes at 77 K.

The energy transfer pathways, based on which all four complexes exhibit multichannel thermosensing and thermochromism are worth discussing. In our latest report on the tta-based analogous dinuclear series, we noticed that the ancillary ligand can display thermally activated delayed fluorescence (TADF) via reverse intersystem crossing (RISC) pathway, which is supported by the small difference between its S_1 and T_1 state (~750 cm^{-1}). The said gap for phen-Hbzim-tpy was estimated from the absorption spectrum (for S_1)[77,78] and steady-state emission spectrum at 77K (for T_1) of a complex with $Gd^{III}Cl_3.6H_2O$ or $Gd^{III}(NO_3)_3.6H_2O$ precursors.[6,15,63,78-80] The delayed lifetime profile was bi-exponential in nature, which we surmised to be an effect of possible molecular twisting. However, in case of La^{III} complex, the low-lying T_1 state of tta seemed to have prohibited the TADF phenomenon. But, herein, the higher position of the T_1 state of hfa drives all four complexes to sustain the TADF event. As a result, systematic intensification of the ligand-centered broad emission peak is noticed for all complexes. Moreover, the delayed lifetimes of all the four

cases are bi-exponential in nature, with their values in the microsecond domain. Interestingly, the second components of the lifetime values are found to be comparable to the observed values in time-resolved MCS measurements. We do not know the actual reason for this shift from mono-exponential to bi-exponential delayed decay. But we surmise that the S_1 state of phen-Hbzim-tpy could be populated in two ways during the delayed fluorescence event. One is via the RISC pathway. The other one involves the involvement of the hfa T_1 or S_1 state-mediated energy transfer to the S_1 state of phen-Hbzim-tpy. Before reaching a concluding remark on this, further investigations regarding excited-state dynamics via transient absorption and emission spectroscopy are required. However, the systematic rise in the ligand-peak intensity yielding from TADF, together with the gradual diminution of Ln^{III}-centered peaks, results in the exhibition of remarkable thermochromism upon inspection within the temperature domain of 273 K- 353 K. It is also noteworthy to mention that the quenching of Eu^{III}-centered emission in complex **2** may very well associated with the low-lying ligand-to-metal charge transfer (LMCT) state, as the involvement of the LMCT state is quite common in Eu^{III}-complexes owing to very low Eu^{III}/Eu^{II} reduction potential (-0.35 V).[18,52,81-83] Hence, this involvement of LMCT acts as the x-factor for the Eu^{III}-complex along with TADF, which makes it superior to the rest three thermosensor complexes here. This is also reflected in their corresponding S_m and δT values. A tentative energy level diagram is also proposed below to understand the improved sensitized emission efficiency along with the feasibility for the occurrence of TADF (Scheme 6.3).

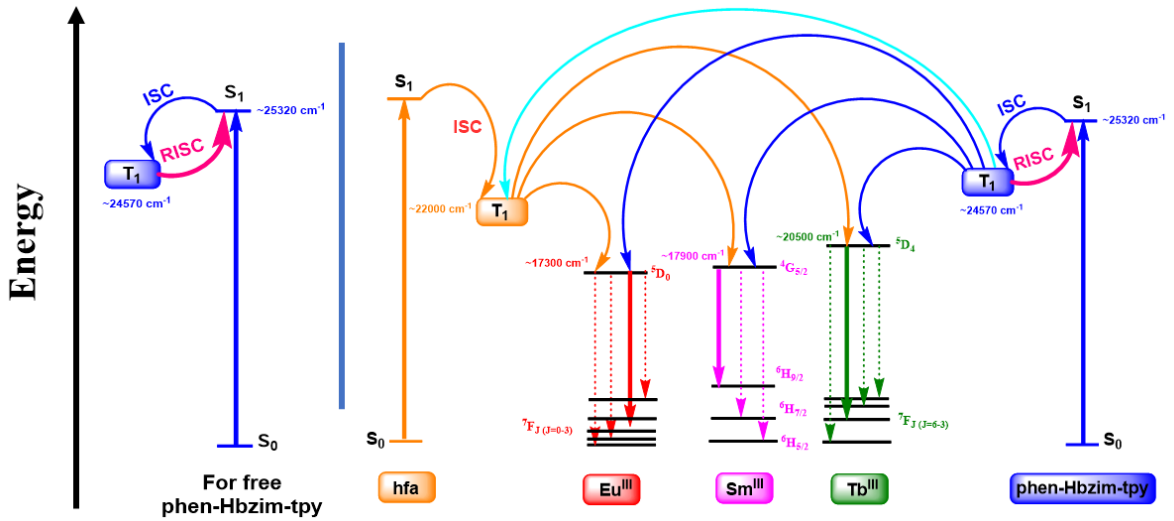

Scheme 6.3. Plausible Energy Transfer Phenomena Operating in the Complexes Counting the RISC Process

6.4. Conclusion

Synthesis, thorough characterization, and detailed investigations on the stimuli-responsive luminescence spectral behaviors of a new array of four dimeric lanthanide(III) complexes comprising a heteroditopic phenanthroline-terpyridine type bridging ancillary ligand and hexafluoroacetylacetonate as the capping antenna ligands, have been undertaken in this work. Contrary to most of the earlier reported systems wherein the absorption spectral window usually remains in the UV region, the present bimetallic lanthanide(III) complexes display absorptions stretching up to the visible region. Additionally, by virtue of the presence of two Ln-tris(hfa) units, the resulting complexes are capable of absorbing more light as reflected by their enhanced molar extinction coefficient parameters. The luminescence spectral characteristics (quantum yield and lifetime) of the complexes are also found to be substantially enhanced relative to their analogous monometallic complexes. The cumulative extent of ligand-to-metal energy transfer in the dinuclear complexes has also been improved by judicious choice of bridging ancillary ligand as well as fluorinated antenna ligand, possessing high-lying T_1 states. The sensitization effect is found to be much better than their related mononuclear complexes as well as dinuclear analogues. The elevated position of T_1 state of the hfa ligand seemed to have encouraged the TADF-assisted thermosensing and thermochromic responses of the complexes, which mainly originates from the phen-Hbzim-tpy ligand itself. We hardly found any other earlier instance in the literature wherein TADF has been utilized in luminescence thermometry from Ln^{III}-based discrete molecules. The luminescence properties of the complexes are also found to be responsive towards solvent and excitation wavelength. Finally, the luminescence responses of all four complexes were also employed to achieve all of the seven colors of the VIBGYOR spectrum, along with single-component white light emission upon appropriate introduction of the said three stimuli.

6.5. References

1. Bünzli, J.-C. G. On the Design of Highly Luminescent Lanthanide Complexes. *Coord. Chem. Rev.* **2015**, *293*, 19–47.
2. Hasegawa, Y.; Wada, Y.; Yanagida, S. Strategies for the Design of Luminescent Lanthanide(III) Complexes and Their Photonic Applications. *J. Photochem. Photobiol., C* **2004**, *5*, 183–202.

3. Armelao, L.; Quici, S.; Barigelletti, F.; Accorsi, G.; Bottaro, G.; Cavazzini, M.; Tondello, E. Design of Luminescent Lanthanide Complexes: From Molecules to Highly Efficient Photo-Emitting Materials. *Coord. Chem. Rev.* **2010**, *254*, 487–505.
4. Parker, D.; Fradgley, J. D.; Wong, K.-L. The Design of Responsive Luminescent Lanthanide Probes and Sensors. *Chem. Soc. Rev.* **2021**, *50*, 8193–8213.
5. Swavey, S.; Swavey, R. Dinuclear and Polynuclear Lanthanide Coordination Complexes Containing Polyazine Ligands: Synthesis and Luminescent Properties. *Coord. Chem. Rev.* **2009**, *253*, 2627–2638.
6. Feng, J.; Zhang, H. Hybrid Materials Based on Lanthanide Organic Complexes: A Review. *Chem. Soc. Rev.* **2013**, *42*, 387–410.
7. Reddy, M. L. P.; Sivakumar, S. Lanthanide Benzoates: A Versatile Building Block for the Construction of Efficient Light Emitting Materials. *Dalton Trans.* **2013**, *42*, 2663–2678.
8. Binnemans, K. Lanthanide-based Luminescent Hybrid Materials. *Chem. Rev.* **2009**, *109*, 4283–4374.
9. Eliseeva, S. V.; Bünzli, J.-C. G. Lanthanide Luminescence for Functional Materials and Bio-sciences. *Chem. Soc. Rev.* **2010**, 39, 189–227.
10. Li, P.; Li, H. Recent Progress in the Lanthanide-Complexes Based Luminescent Hybrid Materials. *Coord. Chem. Rev.* **2021**, *441*, 213988–214004.
11. Wei, C.; Ma, L.; Wei, H.; Liu, Z.; Bian, Z.; Huang, C. Advances in Luminescent Lanthanide Complexes and Applications. *Sci. China Technol. Sci.* **2018**, *61*, 1265–1285.
12. Montgomery, C. P.; Murray, B. S.; New, E. J.; Pal, R.; Parker, D. Cell-Penetrating Metal Complex Optical Probes: Targeted and Responsive Systems Based on Lanthanide Luminescence. *Acc. Chem. Res.* **2009**, *42*, 925–937.
13. Mahapatra, T. S.; Singh, H.; Maity, A.; Dey, A.; Pramanik, S. K.; Suresha, E.; Das, A. White-Light-Emitting Lanthanide and Lanthanide-Iridium Doped Supramolecular Gels: Modular Luminescence and Stimuli Responsive Behaviour. *J. Mater. Chem. C* **2018**, *6*, 9756-9766.
14. Nehra, K.; Dalal, A.; Hooda, A.; Bhagwan, S.; Saini, R. K.; Mari, B.; Kumar, S.; Singh, D. Lanthanides β-Diketonate Complexes as Energy-Efficient Emissive Materials: A Review. *J. Mol. Struct.* **2022**, *1249*, 131531–131555.

15. Gangan, T. U.; Sreenadh, S.; Reddy, M. L. P. Visible-Light Excitable Highly Luminescent Molecular Plastic Materials Derived from Eu^{3+}-Biphenyl Based β-Diketonate Ternary Complex and Poly(Methylmethacrylate). *J. Photochem. Photobiol., A* **2016**, *328*, 171–181.
16. Shi, J.; Hou, Y.; Chu, W.; Shi, X.; Gu, H.; Wang, B.; Sun, Z. Crystal Structure and Highly Luminescent Properties Studies of Bis-β-Diketonate Lanthanide Complexes. *Inorg. Chem.* **2013**, *52*, 5013–5022.
17. Eliseeva, S. V.; Pleshkov, D. N.; Lyssenko, K. A.; Lepnev, L. S.; Bünzli, J.-C. G.; Kuzmina, N. P.; Deciphering Three Beneficial Effects Of 2,2'-Bipyridine-N,N'-Dioxide on the Luminescence Sensitization of Lanthanide(III) Hexafluoroacetylacetonate Ternary Complexes. *Inorg. Chem.* **2011**, *50*, 5137–5144.
18. Kitagawa, Y.; Kumagai, M.; Nakanishi, T.; Fushimi, K.; Hasegawa, Y. The Role of π–f Orbital Interactions in Eu(III) Complexes for an Effective Molecular Luminescent Thermometer. *Inorg. Chem.* **2020**, *59*, 5865–5871.
19. Moudam, O.; Rowan, B. C.; Alamiry, M.; Richardson, P.; Richards, B. S.; Jones, A. C.; Robertson, N. Europium Complexes with High Total Photoluminescence Quantum Yields in Solution and in PMMA. *Chem. Commun.* **2009**, *43*, 6649–6651.
20. Khistiaeva, V. V.; Melnikov, A. S.; Slavova, S. O.; Sizov, V. V.; Starova, G. L.; Koshevoy, I. O.; Grachova, E. V. Heteroleptic β-diketonate Ln(III) Complexes Decorated with Pyridyl Substituted Pyridazine Ligands: Synthesis, Structure and Luminescence Properties. *Inorg. Chem. Front.* **2018**, *5*, 3015–3027.
21. Andreiadis, E. S.; Gauthier, N.; Imbert, D.; Demadrille, R.; Pecaut, J.; Mazzanti, M. Lanthanide Complexes Based on β-Diketonates and A Tetradentate Chromophore Highly Luminescent as Powders and in Polymers. *Inorg. Chem.* **2013**, *52*, 14382–14390.
22. He, X.; Norel, L.; Hervault, Y. M.; Métivier, R.; D'Aléo, A.; Maury, O.; Rigaut, S. Modulation of Eu (III) and Yb (III) Luminescence Using a DTE Photochromic Ligand. *Inorg. Chem.* **2016**, *55*, 12635–12643.
23. Armelao, L.; Dell'Amico, D. B.; Bellucci, L.; Bottaro, G.; Di Bari, L.; Labella, L.; Marchetti, F.; Samaritani, S.; Zinna, F. Circularly Polarized Luminescence of Silica-Grafted Europium Chiral Derivatives Prepared through a Sequential Functionalization. *Inorg. Chem.* **2017**, *56*, 7010–7018.

24. Stanley, J. M.; Zhu, X.; Yang, X.; Holliday, B. J. Europium Complexes of A Novel Ethylenedioxythiophene-Derivatized Bis(pyrazolyl)pyridine Ligand Exhibiting Efficient Lanthanide Sensitization. *Inorg. Chem.* **2010**, *49*, 2035–2037.
25. Latva, M.; Takalo, H.; Mukkala, V. M.; Matachescu, C.; Rodríguez-Ubis, J. C.; Kankare, J. Correlation Between the Lowest Triplet State Energy Level of the Ligand and Lanthanide(III) Luminescence Quantum Yield. *J. Lumin.* **1997**, *75*, 149–169.
26. Samuel, A. P.; Xu, J.; Raymond, K. N. Predicting Efficient Antenna Ligands for Tb(III) Emission. *Inorg. Chem.* **2009**, *48*, 687–698.
27. Ahmed, T.; Chakraborty, A.; Paul, A.; Baitalik, S. Synthesis, Characterization, Luminescence Properties and Deciphering the Role of Terpyridyl-Imidazole Based Ligand on Dissimilar Luminescence Sensitization of Ternary Lanthanide(III) Tris-(β-Diketonate) Complexes. *Dalton Trans*. **2023**, *52*, 14027–14038.
28. Ahmed, T.; Chakraborty, A.; Baitalik, S. Terpyridyl-Imidazole Based Ligand Coordinated to Ln(Hexafluoroacetyl acetonate)$_3$ Core: Synthesis, Structural Characterization, Luminescence Properties, and Thermosensing Behaviors in Solution and PMMA Film. *Inorg. Chem.* **2024**, *63*, 11279–11295.
29. Ahmed, T.; Baitalik, S. Thermally Activated Delayed Fluorescence-Assisted Thermosensing and Thermochromic Behaviors of Bimetallic Lanthanide(III) Complexes Based on Heteroditopic Phenanthroline-Terpyridine Ancillary Ligand. J. Photochem. Photobiol., A **2025** (doi.org/10.1016/j.jphotochem.2025.116749)
30. Zaïm, A.; Nozary, H.; Guénée, L.; Besnard, C.; Lemonnier, J. F.; Petoud, S.; Piguet, C. N-Heterocyclic Tridentate Aromatic Ligands Bound to [Ln(hexafluoroacetylacetonate)$_3$] Units: Thermodynamic, Structural, and Luminescent Properties. *Chem. Eur. J.* **2012**, *18*, 7155–7168.
31. Zhang, Z.; He, L.; Feng, J.; Liu, X.; Zhou, L.; Zhang, H. Unveiling the Relationship Between Energy Transfer and the Triplet Energy Level by Tuning Diarylethene within Europium(III) Complexes. *Inorg. Chem.* **2019**, *59*, 661–668.
32. Fioravanti, L.; Bellucci, L.; Armelao, L.; Bottaro, G.; Marchetti, F.; Pineider, F.; Poneti, G.; Samaritani, S.; Labella, L. Stoichiometrically Controlled Assembly of Lanthanide Molecular Complexes of the Heteroditopic Divergent Ligand 4′-(4-Pyridyl)-2, 2′: 6′, 2 ″-terpyridine N-Oxide in Hypodentate or Bridging Coordination Modes. Structural, Magnetic, and Photoluminescence Studies. *Inorg. Chem.* **2022**, *61*, 265–278.

33. Al-Rasbi, N. K.; Adams, H.; Suliman, F. O. Synthesis, Structure and Tunable White-Light Emission of Dinuclear Eu (III) Schiff Base Complex. *Dyes Pigm.* **2014**, *104*, 83–88.
34. Dasari, S.; Maparu, A. K.; Abbas, Z.; Kumar, P.; Birla, H.; Sivakumar, S.; Patra, A. K. Bimetallic Europium and Terbium Complexes Containing Substituted Terpyridines and the NSAID Drug Tolfenamic Acid: Structural Differences, Luminescence Properties, and Theranostic Applications. *Eur. J. Inorg. Chem.* **2020**, *2020*, 2998–3009.
35. Yadav, U.; Verma, M.; Abbas, Z.; Sivakumar, S.; Patra, A. K. An Emissive Dual-Sensitized Bimetallic Eu_2^{III}-Bioprobe: Design Strategy, Biological Interactions, and Nucleolus Staining Studies. *New J. Chem.* **2022**, *46*, 16007-16018.
36. Douib, H.; Gonzalez, J. F.; Speed, S.; Montigaud, V.; Lefeuvre, B.; Dorcet, V.; Riobé, F.; Maury, O.; Gouasmia, A.; Guennic, B. L.; Cador, O.; Pointillart, F. Modulation of the Magnetic and Photophysical Properties in 3d–4f and 4f–4f′ Heterobimetallic Complexes Involving a Tetrathiafulvalene-based Ligand. *Dalton Trans.* **2022**, *51*, 16486-16496.
37. Wang, X. D.; Wolfbeis, O. S.; Meier, R. J. Luminescent Probes and Sensors for Temperature. *Chem. Soc. Rev.* **2013**, *42*, 7834–7869.
38. Brites, C. D.; Lima, P. P.; Silva, N. J.; Millán, A.; Amaral, V. S.; Palacio, F.; Carlos, L. D. Thermometry at the Nanoscale. *Nanoscale* **2012**, *4*, 4799–4829.
39. Brites, C. D.; Marin, R.; Suta, M.; Neto, A. N. C.; Ximendes, E.; Jaque, D.; Carlos, L. D. Spotlight on Luminescence Thermometry: Basics, Challenges, and Cutting-edge Applications. **2023**, *Adv. Mater. 35*, 2302749.
40. Hasegawa, Y.; Kitagawa, Y. Thermo-sensitive Luminescence of Lanthanide Complexes, Clusters, Coordination Polymers and Metal–Organic Frameworks with Organic Photosensitizers. *J. Mater. Chem. C* **2019**, *7*, 7494–7511.
41. Bussche, F. V.; Kaczmarek, A. M.; Speybroeck, V. V.; Voort, P. V. D.; Stevens, C. V. Overview of N-Rich Antennae Investigated in Lanthanide-Based Temperature Sensing. *Chem. Eur. J.* **2021**, *27*, 7214–7230.
42. Cui, Y.; Zou, W.; Song, R.; Yu, J.; Zhang, W.; Yang, Y.; Qian, G. A Ratiometric and Colorimetric Luminescent Thermometer Over a Wide Temperature Range Based on a Lanthanide Coordination Polymer. *Chem. Commun.* **2014**, *50*, 719–721.

43. Feng, T.; Ye, Y.; Liu, X.; Cui, H.; Li, Z.; Zhang, Y.; Liang, B.; Li, H.; Chen, B. A Robust Mixed Lanthanide PolyMOF Membrane for Ratiometric Temperature Sensing. *Angew. Chem. Int. Ed.* **2020**, *59*, 21752-21757.
44. Shahi, P. K.; Singh, A. K.; Singh, S. K.; Rai, S. B.; Ullrich, B. Revelation of the Technological Versatility of the $Eu(tta)_3phen$ Complex by Demonstrating Energy Harvesting, Ultraviolet Light Detection, Temperature Sensing, and Laser Applications, *ACS Appl. Mater. Interfaces* **2015**, *7*, 18231−18239.
45. Devi, R.; Singh, K.; Vaidyanathan, S. Synergy in the Energy Transfer Between Ligands and Eu^{III} Ions in Molecular Europium Complexes: Single-Component White Light-Emitting Luminogens. *J. Mater. Chem. C* **2020**, *8*, 8643–8653.
46. Gálico, D. A.; Mazali, I. O.; Sigoli, F. A. Nanothermometer Based on Intensity Variation and Emission Lifetime of Europium(III) Benzoylacetonate Complex. *J. Lumin.* **2017**, *192*, 224–230.
47. Lapaev, D. V.; Nikiforov, V. G.; Lobkov, V. S.; Knyazev, A. A.; Galyametdinov, Y. G. Reusable Temperature-Sensitive Luminescent Material Based on Vitrified Film of Europium(III) β-Diketonate Complex. *Opt. Mater.* **2018**, *75*, 787–795.
48. Cabral, F. M.; Gálico, D. A.; Mazali, I. O.; Sigoli, F. A. Crystal Structure and Temperature Dependence of the Photophysical Properties of the $[Eu(tta)_3(pyphen)]$ Complex. *Inorg. Chem. Commun.* **2018**, *98*, 29–33.
49. Kovalenko, A. D.; Bushmarinov, I. S.; Burlov, A. S.; Lepnev, L. S.; Ilina, E. G.; Utochnikova, V. V. The Peculiarities of Complex Formation and Energy Transfer Processes in Lanthanide Complexes With 2-(Tosylamino)-Benzylidene-N-Benzoylhydrazone. *Dalton Trans.* **2018**, *47*, 4524–4533.
50. Bellucci, L.; Bottaro, G.; Labella, L.; Causin, V.; Marchetti, F.; Samaritani, S.; Dell'Amico, D. B.; Armelao, L. Composition–Thermometric Properties Correlations in Homodinuclear Eu^{3+} Luminescent Complexes. *Inorg. Chem.* **2020**, *59*, 18156–18167.
51. Ali, A.; Ahmed, Z.; Iftikhar, K.; Uddin, R. Heteroleptic Samarium Complexes with High Quantum Yields for Temperature Sensing Applications. *Dalton Trans.* **2024**, *53*, 1105–1120.
52. Ahmed, T.; Chakraborty, A.; Maity, S.; Baitalik, S. A Terpyridyl–Imidazole Based Europium Tris-(β-Diketonate) Complex as Efficient Molecular Luminescent

Thermometer and Single Component White Light Emitter via Synergy in Energy Transfer between Ligand and Eu^{3+}. *Dalton Trans*. **2024**, 53, 3065–3074.

53. Ilmi, R.; Khan, M. S.; Li, Z.; Zhou, L.; Wong, W. Y.; Marken, F.; Raithby, P. R. Utilization of Ternary Europium Complex for Organic Electroluminescent Devices and as a Sensitizer to Improve Electroluminescence of Red-Emitting Iridium Complex. *Inorg. Chem.* **2019**, *58*, 8316–8331.
54. Law, G.-L.; Wong, K.-L.; Tam, H.-L.; Cheah, K.-W.; Wong, W.-T. White OLED with a Single-Component Europium Complex. *Inorg. Chem.* **2009**, *48*, 10492–10494.
55. O'Neil, A. T.; Chalard, A.; Malmström, J.; Kitchen, J. A. White Light and Colour-Tunable Emission From A Single Component Europium-1,8-Naphthalimide Thin Film. *Dalton Trans.* **2023**, *52*, 2255–2261.
56. Shelton, A. H.; Sazanovich, I. V.; Weinstein, J. A.; Ward, M. D. Controllable Three-Component Luminescence from A 1,8-Naphthalimide/ Eu(III) Complex: White Light Emission From A Single Molecule. *Chem. Commun.* **2012**, *48*, 2749–2751.
57. Maity, D.; Bhaumik, C.; Mardanya, S.; Karmakar, S.; Baitalik, S. Light Harvesting and Directional Energy Transfer in Long-Lived Homo-and Heterotrimetallic Complexes of Fe^{II}, Ru^{II}, and Os^{II}. *Chem. Eur. J.* **2014**, *20*, 13242–13252.
58. Maity, D.; Mardanya, S.; Karmakar, S.; Baitalik, S. pH-Induced Processes in Wire-like Multichromophoric Homo-and Heterotrimetallic Complexes of Fe (II), Ru (II), and Os (II). *Dalton Trans.* **2015**, *44*, 10048–10059.
59. Maity, D.; Bhaumik, C.; Mondal, D.; Baitalik, S. Photoinduced Intramolecular Energy Transfer and Anion Sensing Studies of Isomeric $Ru^{II}Os^{II}$ Complexes Derived from An Asymmetric Phenanthroline–Terpyridine Bridge. *Dalton Trans.* **2014**, *43*, 1829–1845.
60. Maity, D.; Bhaumik, C.; Karmakar, S.; Baitalik, S. Photoinduced Electron and Energy Transfer and pH-Induced Modulation of the Photophysical Properties in Homo-and Heterobimetallic Complexes of Ruthenium(II) And Rhodium(III) Based on A Heteroditopic Phenanthroline–Terpyridine Bridge. *Inorg. Chem.* **2013**, *52*, 7933–7946.
61. Bhaumik, C.; Das, S.; Saha, D.; Dutta, S.; Baitalik, S. Synthesis, Characterization, Photophysical, and Anion-Binding Studies of Luminescent Heteroleptic Bis-Tridentate Ruthenium(II) Complexes Based on 2,6-Bis(Benzimidazole-2-yl)Pyridine and 4′-Substituted 2, 2′: 6′, 2″ Terpyridine Derivatives. *Inorg. Chem.* **2010**, *49*, 5049–5062.

62. Bünzli, J.-C. G.; Eliseeva, S. V. Basics of Lanthanide Photophysics. In Lanthanide Luminescence; Hänninen, P., Härmä, H., Eds.; Springer Series on Fluorescence, Vol. 7; Springer: Berlin, Heidelberg, 2010.
63. An, B.-L.; Gong, M.-L.; Li, M.-X.; Zhang, J.-M. Synthesis, Structure and Luminescence Properties of Samarium(III) And Dysprosium(III) Complexes with A New Tridentate Organic Ligand. *J. Mol. Struct.* **2004**, *687*, 1–6.
64. Fratini, A.; Richards, G.; Larder, E.; Swavey, S. Neodymium, Gadolinium, and Terbium Complexes Containing Hexafluoroacetylacetonate and 2, 2'-Bipyrimidine: Structural and Spectroscopic Characterization. *Inorg. Chem.* **2008**, *47*, 1030–1036.
65. Bag, P.; Rastogi, C. K.; Biswas, S.; Sivakumar, S.; Mereacre, V.; Chandrasekhar, V. Homodinuclear Lanthanide {Ln 2}(Ln= Gd, Tb, Dy, Eu) Complexes Prepared from an o-Vanillin Based Ligand: Luminescence and Single-Molecule Magnetism Behavior. *Dalton Trans.* **2015**, *44*, 4328–4340.
66. Zucchi, G.; Jeon, T.; Tondelier, D.; Aldakov, D.; Thuéry, P.; Ephritikhine, M.; Geffroy, B. White Electroluminescence of Lanthanide Complexes Resulting from Exciplex Formation. *J. Mater. Chem.* **2010**, *20*, 2114–2120.
67. Li, H.-Y.; Wu, J.; Huang, W.; Zhou, Y.-H.; Li, H.-R.; Zheng, Y.-X.; Zuo, J.-L. Synthesis and Photoluminescent Properties of Five Homodinuclear Lanthanide (Ln^{3+}=Eu^{3+}, Sm^{3+}, Er^{3+}, Yb^{3+}, Pr^{3+}) Complexes. *J. Photochem. Photobiol. A Chem.* **2009**, *208*, 110–116.
68. Armelao, L.; Dell'Amico, D. B.; Bellucci, L.; Bottaro, G.; Ciattini, S.; Labella, L.; Manfroni, G.; Marchetti, F.; Mattei, C. A.; Samaritani, S. Homodinuclear Lanthanide Complexes with the Divergent Heterotopic 4, 4′-Bipyridine N-Oxide (bipyMO) Ligand. *Eur. J. Inorg. Chem.* **2018**, *2018*, 4421–4428.
69. Wang, Z.; Liu, N.; Li, H.; Chen, P.; Yan, P. The Role of Blue-Emissive 1, 8-Naphthalimidopyridine N-Oxide in Sensitizing Eu^{III} Photoluminescence in Dimeric Hexafluoroacetylacetonate Complexes. *Eur. J. Inorg. Chem.* **2017**, *2017*, 2211–2219.
70. Natrajan, L. S.; Timmins, P. L.; Lunn, M.; Heath, S. L. Luminescent Dinuclear Lanthanide Complexes of 5-Me-HXTA. *Inorg. Chem.* **2007**, *46*, 10877–10886.
71. Shavaleev, N. M.; Pope, S. J.; Bell, Z. R.; Faulkner, S.; Ward, M. D. Visible-light Sensitisation of Near-infrared Luminescence from Yb(III), Nd(III) and Er(III) Complexes of 3, 6-Bis(2-Pyridyl)Tetrazine. *Dalton Trans.* **2003**, 808–814.

72. Jang, H.; Shin, C. H.; Jung, B. J.; Kim, D. H.; Shim, H. K.; Do, Y. Synthesis and Characterization of Dinuclear Europium Complexes Showing Pure Red Electroluminescence. *Eur. J. Inorg. Chem.* **2006**, 2006, 718–725.
73. Wang, Y.-J.; Wu, D.-F.; Gou, J.; Duan, Y.-Y.; Li, L.; Chen, H.-H.; Gao, H.-L.; Cui, J.-Z. Modulation of the Properties of Dinuclear Lanthanide Complexes Through Utilizing Different β-Diketonate Co-Ligands: Near-Infrared Luminescence and Magnetization Dynamics. *Dalton Trans.* **2020**, *49*, 2850–2861.
74. Zheng, S.-J.; Ma, J.; Su, J.; Djurovich, P. I.; Thompson, M. E.; Li, T.-Y. Simultaneous Thermally Stimulated Delayed Phosphorescence (TSDP) and Thermally Activated Delayed Fluorescence (TADF) in a Two-Coordinated Au(I) Bimetallic Complex Featuring a Tandem Carbene Structure. *J. Am. Chem. Soc.* **2024**, *146*, 19042–19049.
75. Dar, W. A.; Iftikhar, K. Phase Controlled Colour Tuning of Samarium and Europium Complexes and Excellent Photostability of Their PVA Encapsulated Materials. Structural Elucidation, Photophysical Parameters and The Energy Transfer Mechanism in the Eu^{III} Complex by Sparkle/PM3 Calculations. *Dalton Trans.* **2016**, *45*, 8956–8971.
76. Mara, M. W.; Tatum, D. S.; March, A. M.; Doumy, G.; Moore, E. G.; Raymond, K. N. Energy Transfer from Antenna Ligand to Europium(III) Followed Using Ultrafast Optical and X-Ray Spectroscopy. *J. Am. Chem. Soc.* **2019**, *141*, 11071–11081.
77. Sivakumar, S.; Reddy, M. L. P.; Bright Green Luminescent Molecular Terbium Plastic Materials Derived from 3,5-Bis(Perfluorobenzyloxy)Benzoate. *J. Mater. Chem.* **2012**, *22*, 10852–10859.
78. Teotonio, E. E.; Fett, G. M.; Brito, H. F.; Faustino, W. M.; de Sá, G. F.; Felinto, M. C. F.; Santos, R. H. Evaluation of Intramolecular Energy Transfer Process in the Lanthanide(III) Bis- and Tris-(TTA) Complexes: Photoluminescent and Triboluminescent Behavior. *J. Lumin.* **2008**, *128*, 190–198.
79. Feng, J.; Yu, J.-B.; Song, S.-Y.; Sun, L. N.; Fan, W.-Q.; Guo, X.-M.; Dang, S.; Zhang, H.-J. Near-infrared Luminescent Xerogel Materials Covalently Bonded with Ternary Lanthanide [Er(III), Nd(III), Yb(III), Sm(III)] Complexes. *Dalton Trans.* **2009**, 2406–2414.
80. Bassett, A. P.; Magennis, S. W.; Glover, P. B.; Lewis, D. J.; Spencer, N.; Parsons, S.; Williams, R. M.; De Cola, L.; Pikramenou, Z. Highly Luminescent, Triple- and

Quadruple-Stranded, Dinuclear Eu, Nd, and Sm(III) Lanthanide Complexes Based on Bis–Diketonate Ligands. *J. Am. Chem. Soc.* **2004**, *126*, 9413–9424.

81. Fu, L. M.; Ai, X. C.; Li, M. Y.; Wen, X. F.; Hao, R.; Wu, Y. S.; Wang, Y.; Zhang, J. P. Role of Ligand-To-Metal Charge Transfer State in Nontriplet Photosensitization of Luminescent Europium Complex. *J. Phys. Chem. A* **2010**, *114*, 4494–4500.
82. Berry, M. T.; May, P. S.; Xu, H. Temperature Dependence of the Eu^{3+} $^5D_0$ Lifetime in Europium Tris(2,2,6,6-tetramethyl-3,5-heptanedionato). *J. Phys. Chem.* **1996**, *100*, 9216–9222.
83. Pasatoiu, T. D.; Madalan, A. M.; Kumke, M. U.; Tiseanu, C.; Andruh, M. Temperature Switch of LMCT Role: From Quenching to Sensitization of Europium Emission in a Zn^{II}-Eu^{III} Binuclear Complex. *Inorg. Chem.* **2010**, *49*, 2310–2315.

****

List of Publications

1. **Ahmed, T**.; Chakraborty, A.; Paul, A.; Baitalik, S. Synthesis, Characterization, Luminescence Properties and Deciphering the Role of Terpyridyl-Imidazole Based Ligand on Dissimilar Luminescence Sensitization of Ternary Lanthanide(III) Tris-(β-Diketonate) Complexes. *Dalton Trans*. **2023**, *52*, 14027–14038.

2. **Ahmed, T**.; Chakraborty, A.; Maity, S.; Baitalik, S. A Terpyridyl–Imidazole Based Europium Tris-(β-Diketonate) Complex as Efficient Molecular Luminescent Thermometer and Single Component White Light Emitter via Synergy in Energy Transfer between Ligand and Eu^{3+}. *Dalton Trans*. **2024**, *53*, 3065–3074.

3. **Ahmed, T.**; Chakraborty, A.; Maity, S.; Baitalik, S. Terpyridyl-Imidazole based Ligand Coordinated to Ln(Hexafluoroacetylacetonate)3 Core: Synthesis, Structural Characterization, Luminescence Properties and Thermosensing Behaviors in Solution and PMMA Film. *Inorg. Chem.* **2024**, *63*, 11279–11295.

4. **Ahmed, T.**; Abedin, T.; Baitalik, S. Thermally Activated Delayed Fluorescence-Assisted Thermosensing and Thermochromic Behaviors of Bimetallic Lanthanide(III) Complexes Based on Heteroditopic Phenanthroline-Terpyridine Ancillary Ligand. (*Accepted for publication in the Journal of Photochemistry and Photobiology A: Chemistry, **2025**)*

5. **Ahmed, T.**; Abedin, T.; Baitalik, S. Stimuli-responsive Luminescence Behaviors of Ternary Homobimetallic LnIII-tris-hfa Complexes Comprising a TADF-active Terpyridine-Bipyridine-based Ancillary Ligand: Display of VIBGYOR and White Light Emission. *(Communicated)*

6. Pradhan, K.; Mandal, S.; **Ahmed, T.**; Rahaman, S. A.; Sepay, N.; Baitalik, S.; Jana, R. Photoexcited Nitroalkanefor the Metal-free, Reductive C-N Coupling at Ambient Temperature. *(Communicated)*

7. Paul, A.; Bar, M.; **Ahmed, T.**; Baitalik, S. Anion-Sensitive Photophysics of Luminescent Trimetallic Complexes of Fe(II), Ru(II), and Os(II) with Polarized NH Motifs. *Polyhedron*, **2020**, *190*, 114772.

8. Deb, S.; Sahoo, A.; **Ahmed, T.**; Baitalik, S. Stimuli–Responsive Molecular Switches and Logic Devices Based on Ru(II)-Terpyridyl-Imidazole Coordination Motif. *J. Phys. Chem. B* **2021**, *125*, 8919–8931.

9. Sahoo, A.; **Ahmed, T.**; Deb, S.; Baitalik, S. Neuro-Fuzzification Architecture for Modelling of Electrochemical Ion-Sensing Data of Imidazole-Dicarboxylate-Based Ru(II)-Bipyridine Complex. *Inorg. Chem*. **2022**, *61*, 10242–54.

Publications 1-5 are included in the thesis

*****